

INSITU DETERMINATION OF RESIDUAL SOIL
SHEAR STRENGTH PARAMETERS USING THE
STANDARD PENETRATION TEST WITH TORQUE

by

Marcus Allen Cottingham

A dissertation submitted to the faculty of
The University of North Carolina at Charlotte
in partial fulfillment of the requirements
for the degree of Doctor of Philosophy in
Infrastructure and Environmental Systems

Charlotte

2009

Approved by:

Dr. J. Brian Anderson

Dr. Shen-En Chen

Dr. John A. Diemer

Dr. Martha C. Eppes

Dr. Vincent O. Ogunro

Dr. Brigid A. Mullany

ABSTRACT

MARCUS ALLEN COTTINGHAM. Insitu determination of residual soil shear strength parameters using the standard penetration test with torque.
(Under the direction of DR. J. BRIAN ANDERSON)

Residual soils are found throughout the world and often behave differently than transported soils. Residual soils are identified as materials developed from the insitu weathering of rock that has remained in the location of its origin as opposed to transported soils which are developed through processes that include erosion, transport, and deposition. Geotechnical engineers rely on insitu and laboratory soil investigation techniques to determine soil properties, even though there is little within the current standard procedures to quantitatively distinguish between residual and transported soils. Due to the increasing volume of infrastructure development in areas where residual soils are present, there exists a need to better understand and quantify the properties and behaviors of residual soils.

The objective of this dissertation was to develop direct and indirect relationships between the insitu standard penetration test with torque (SPT-T) and the laboratory shear strength of residual soils. Three research sites, located in Charlotte, North Carolina near the geographic center of the Southern Piedmont region, were characterized using the SPT-T, the consolidated drained triaxial test, the dilatometer test, soil classification tests, and an interface shear test. The results suggest that a possible relationship exists between the SPT-T maximum torque ($T_{MAX(SPT)}$) and the cohesion (c'). The investigation also demonstrated that $T_{MAX(SPT)}$ can provide an assessment of triaxial shear strength (τ_{TXL}), although the relationship was largely influenced by the vertical effective stress.

Various relationships within the data set were explored and many produced low correlations, with the majority of the R^2 values below 0.4. The most promising relationship for a geotechnical engineer was $T_{MAX (SPT)}$ multiplied by the insitu water content (w_{INSITU}) versus τ_{TXL} which suggests that the insitu water content at the time of the SPT-T has an influence on the measured $T_{MAX (SPT)}$. The most promising geologic correlations were chroma versus τ_{TXL} and minor mineral percentage versus τ_{TXL} . These two trends suggest that geologic parameters can provide an assessment of triaxial shear strength. Another important result was that the undisturbed residual soils investigated did show inherent c' , which is generally neglected in design. Additionally, an exploratory investigation of remolded residual soils suggests that the cohesion (c') decreases and effective angle of internal friction (ϕ') increases due to remolding. Also, both the SPT-T and dilatometer tests provided un-conservative ϕ' values for undisturbed residual soils.

This dissertation illustrates the importance of quantitatively distinguishing between residual and transported soils. The main drawback of the study was the limited number of tests/test sites available for the research. The results clearly show the feasibility of the methods and justify further research. Ultimately, the implementation of the quick and simple torque test to a site investigation can provide valuable data for geotechnical design.

ACKNOWLEDGEMENTS

This dissertation was possible only through the influence and help of many people. I would first like to thank my advisor at the University of North Carolina at Charlotte, Dr. J. Brian Anderson. Dr. Anderson's support and guidance has been instrumental in my education and career development. I wish to thank Dr. Chen, Dr. Diemer, Dr. Eppes, Dr. Ogunro, and Dr. Mullany for taking the time to serve on my dissertation committee. I also wish to thank my parents, Ed Cottingham and Sherry Cottingham for their endless support and understanding. I would like to deeply thank my sister, Christy Caig, for everything she has given me. I would like to acknowledge my family, friends, fellow students, and professors. They all have had a great impact on my education and life.

I also would like to acknowledge the University of Florida for the use of the torque cell equipment, the NCDOT Geotechnical Testing Unit (Clint Little, Jay Stickney, Mike Smith, Chad Smith, and all of the drill rig operators) for the insitu testing support, and the NCDOT soils labs (CK Su and Randy Privette) for guidance with the triaxial testing. I would like to thank Dr. Mullany, Brian Dutterer, and Mike Moss for their fabrication support. I would like to thank George Chaloub at Texas Petrographic Inc, Dr. Eppes, Dr. Diemer, Dr. Bobbyarchick, Courtney Swanson, and the Geologic Society of America for support with the petrographic analysis. I would also like to thank the participants of the Research Experience for Undergraduate (REU) program who assisted with testing (Gabe Collier, Arezou Eslaminejad, Chantry Johnson, Ben Oliver, Jermaine Taylor, and Rebekah Vestal).

TABLE OF CONTENTS

LIST OF ABBREVIATIONS	ix
LIST OF VARIABLES	x
CHAPTER 1: INTRODUCTION	1
1.1 Problem Statement	2
1.2 Research Objectives	2
1.3 Scope of Work	2
CHAPTER 2: BACKGROUND	5
2.1 Geologic Soil Identification, Genesis, and Characteristics	5
2.2 Geotechnical Soil Properties, Testing, and Soil Mechanics	10
2.2.1 Insitu Geotechnical Testing	12
2.2.2 Laboratory Geotechnical Testing	14
2.2.3 Geotechnical Sampling	15
2.2.4 Additional Geotechnical Testing	17
2.3 Theoretical Development	18
CHAPTER 3: LITERATURE REVIEW	23
3.1 Geotechnical Testing in Residual Soil	23
3.2 Standard Penetration Test with Torque Research	26
3.3 Geologic Research in Residual Soil	29
CHAPTER 4: TESTING PROGRAM	32
4.1 Torque Testing	34
4.1.1 Torque Data Reduction	43
4.2 Triaxial Shear Testing	46

4.2.1 Triaxial Shear Data Reduction	52
4.3 Interface Shear Testing	54
4.3.1 Interface Shear Data Reduction	61
4.4 Geologic and Petrographic Analysis Testing	62
4.4.1 Geologic Data Reduction	64
CHAPTER 5: RESULTS	66
5.1 Raw Data Evaluation	67
5.1.1 Cohesion versus Adhesion	76
5.1.2 Internal Friction Angle versus Interface Friction Angle	77
5.2 Theoretical Evaluation	78
5.3 Predictive Evaluations	83
5.3.1 Torque versus Cohesion	83
5.3.2 Torque versus Effective Angle of Internal Friction	85
5.3.3 Torque versus Shear Strength	87
5.4 Additional Geotechnical Evaluations	88
5.5 Geologic Evaluations	110
5.5.1 Remolded Soil Analysis	123
CHAPTER 6: SUMMARY AND ANALYSIS	127
CHAPTER 7: CONCLUSIONS	145
CHAPTER 8: RESEARCH LIMITATIONS AND RECCOMENDATIONS	148
REFERENCES	154
APPENDIX A – Maps	160
APPENDIX B – Prosperity Church Road Site 1 Data	162

APPENDIX C – Browne Road Data	182
APPENDIX D – Prosperity Church Road Site 2 Data	205
APPENDIX E – Additional Soil Data	220
APPENDIX F – Triaxial Quick Reference List and Data sheets	223
APPENDIX G – Interface Shear Box Drawing	227
APPENDIX H – Interface Shear Box Roughness Graphs	230
APPENDIX I – Geologic Petrographic Analysis	241
APPENDIX J – PC1 Remolded Triaxial Shear Test Data	248

LIST OF ABBREVIATIONS

AASHTO	American Association of State Highway and Transportation Officials
ASTM	American Society for Testing and Materials
BR	Browne Road Site
CP	Cross Polarized Light
DMT	Dilatometer Test
DST	Direct Shear Test
FDOT	Florida Department of Transportation
INT	Interface Shear Test
NCDOT	North Carolina Department of Transportation
PC1	Prosperity Church Road Site 1
PC2	Prosperity Church Road Site 2
PP	Plain Polarized Light
REM	Remolded
RS	Residual Soil
SPT	Standard Penetration Test
SPT-T	Standard Penetration Test with Torque
STT-T	Shelby Tube Test with Torque
TXL	Consolidated Drained Triaxial Test
UNCC	University of North Carolina at Charlotte
UND	Undisturbed
USCS	Unified Soil Classification System

LIST OF VARIABLES

c'	Cohesion or drained triaxial shear strength intercept
c_a	Adhesion
C	Chroma – Geologic color dimension
E_D	Dilatometer modulus from dilatometer
e_o	Initial void ratio
H	Hue – Geologic color dimension
K	Coefficient of lateral earth pressure
K_a	Coefficient of active lateral earth pressure
K_o	At-rest coefficient of lateral earth pressure
K_D	Horizontal stress index from dilatometer
K_p	Passive coefficient of lateral earth pressure
LL	Liquid limit
I_D	Material index from dilatometer
N	Standard penetration test blow-count
N'_{60}	Corrected standard penetration test blow-count
n	Geotechnical porosity
P_a	Active lateral earth pressure force
PI	Plasticity index
Q_t	Bearing capacity
Ra	Roughness average
RF	Redness factor
R_i	Interface friction reduction factor

R_{ku}	Kurtosis of surface heights
RR	Redness ratio
R_{sk}	Skewness
R_q	Quadratic roughness
R_t	Average of peak to valley height in each cut-off length
s_u	Undrained shear strength
$T_{MAX(SPT)}$	Maximum torque – Standard penetration test with torque
$T_{SS(SPT)}$	Steady state torque – Standard penetration test with torque
$T_{MAX(STT)}$	Maximum torque – Shelby tube test with torque
$T_{SS(STT)}$	Steady state torque – Shelby tube test with torque
V	Value – Geologic color dimension
w	Water content
z	Depth
α	Adhesion factor
γ	Total unit weight
δ	Interface friction angle
ϕ'	Effective angle of internal friction
σ'_v	Effective vertical stress
σ'_h	Effective horizontal stress
τ_{TXL}	Shear strength found using triaxial shear test
τ_{END}	Shear strength at end of sampler
τ_{INT}	Shear strength found using the interface shear test
τ_{SIDE}	Shear strength along side of sampler

CHAPTER 1: INTRODUCTION

Geotechnical engineers apply soil mechanics to explain the behavior of soil as an engineering material. This behavior is determined by the composition, shearing strength, compressibility, permeability, density, and stress history of a soil mass. Geotechnical engineers can broadly divide soils into two categories: residual and transported. Residual soils are identified as materials developed from the insitu weathering of rocks that have remained in the location of their origin, while transported soils are developed by erosion, transport, and deposition. Residual soils commonly resemble the parent rock, but are friable and porous, therefore can be broken down and have the workability of a typical transported soil. This property often leads to difficulties when working with them experimentally or evaluating their design properties.

In addition, the fundamentals of classical soil mechanics are primarily based on the behavior of transported soils. The bulk of published studies, standard testing procedures, and empirical relationships were developed using transported soils. Also, there is little to distinguish residual soils from transported soils within the most widely used soil classification systems, the Unified Soil Classification System (USCS) and American Association of State Highway and Transportation Officials (AASHTO) System. Typically, geotechnical engineers use their accumulated personal knowledge and experience to guide analysis and design in residual soils. This practice often leads to conservative designs and elevated project costs.

1.1 Problem Statement

Geotechnical engineers often rely on insitu and laboratory soil investigation techniques to determine soil properties. None of the current insitu testing techniques quantitatively distinguish between residual and transported soils. Furthermore, while there are tests that can measure the shearing strength of residual soils, they are considered by most to be too costly and time consuming, therefore they are seldom used.

1.2 Research Objective

The objective of this research was to develop direct and indirect relationships between the insitu standard penetration test with torque (SPT-T) and the laboratory shear strength of residual soils. The shear strength was determined using the consolidated drained triaxial test (TXL). This research was part of a broader program at the University of North Carolina at Charlotte to improve the understanding and quantification of geotechnical behavior of residual soils. The long-term goal of this over-arching program is to develop, adapt, and refine testing procedures and methods to accurately quantify engineering properties of residual soils.

1.3 Scope of Work

This dissertation describes the methods, experiments, data, and analysis used to achieve the defined objective. The scope of the project included a comprehensive literature review, theoretical analysis, systematic testing program, detailed interpretation of the results, and future research recommendations. The tasks are outlined in the following:

- A. *Literature Review* – The comprehensive review included published literature in geology and geotechnical engineering focused on relevant insitu and laboratory testing of residual soils.
- B. *Theoretical Analysis* – The analysis of the insitu testing system was the basis of the dissertation and initial studies used to develop the project.
- C. *Testing Program* – The program incorporated the specifics of the insitu and laboratory research, operating procedures (standard and nonstandard), testing equipment, and research support partners. Various tests were performed to support the research objective, provide additional site characterization, and provide secondary shear strength measurements or correlations. The tests included the standard penetration test with torque, the consolidated drained triaxial test, the interface shear test, dilatometer, geotechnical and geologic soil classification. In addition, exploratory petrographic analyses and remolded triaxial shear tests were performed through a Geologic Society of America grant to investigate the influence of saprolite geologic on shear strength.
- D. *Results and Interpretation* – The data set included the measured parameters, intermediate calculations, and the evaluation of possible relationships. The relationships were divided between direct and indirect and are organized into three categories; raw data, theoretical, and predictive. The direct relationships are single variables used to predict single variables. The indirect relationships include single variables used to predict a multiple variable calculations and multiple variable calculations used to predict multiple variable calculations.

E. *Synthesis of Results* – This included a detailed summary of the findings, recommendations for future research, conclusions, and other considerations.

CHAPTER 2: BACKGROUND

The fields of geotechnical engineering and geology (soil science) are closely related. The primary difference between the two fields is that geology (soil science) is more involved with the soil identification and genesis, while geotechnical engineering is focused on the determination of engineering properties of soils and overall site characterization. Combining these two fields is important because any geotechnical investigation should be founded on a solid understanding of the genesis of the soil. Vaughan et al. (1988) concisely stated that “a knowledge of the way in which a soil or rock originally formed and the geologic processes to which it has since been subjected will provide many indications of its probable insitu mechanical properties and stress.”

2.1 Geologic Soil Identification, Genesis, and Characteristics

The insitu identification of residual soils is an essential and under-appreciated geologic tool. Geologists define residual soil as a soil formed, or resting on, consolidated rock of the same kind as that from which it was formed and in the same location, or a soil formed in residuum (Schaetzl and Anderson, 2005). Transported soils, also known as unconsolidated sediments, are defined as soils that have been moved from the place of their origin (McCarthy, 2002). Transported soils are broadly classified within two primary categories, coarse and fine grained. Residual soils exhibit behavior that suggests they are a mixture of these two categories making them easy to misclassify.

Some frequently encountered residual soils are tropical soils, saprolites, and decomposed granites (Mitchell, 1993). Different residual soils result due a wide range of formation rates, the types of minerals present in the bedrock, how they are affected by weathering, and the different motilities of ions that result from weathering (Schaetzl and Anderson, 2005). For a residual soil profile to develop, the rate of soil formation or weathering into the earth's crust must exceed the rate of removal of soil by erosion. The degree of weathering ranges from fresh rock to completely weathered material. The degree of weathering generally decreases from the surface down and inwards from joint surfaces and other percolation paths (Blight, 1997). Understanding the degree of weathering is further complicated by the existence of fault zones or inter-bedded lithologies that can weather preferentially (Brand, 1985).

The four main processes that contribute to weathering are physical, chemical, biological, and mineralogical. Physical processes result in the breakdown of particles, the reduction of the mean particle size, and an increase in the number of micro-fractures (Mitchell 1993). Physical processes include stress release by erosion, differential thermal strain, ice and frost formation, and salt crystallization pressures (Blight, 1997). Physical weathering can also result from wind, rain, running water, frost wedging, and tectonic forces. Chemical processes change the mineralogy of the parent material (Lee and Coop, 1995). Chemical processes result from exposure to the atmosphere, temperature changes, water and water-based solutions, and other materials (McCarthy, 2002). These processes include hydrolysis, cation exchange, and oxidation. Biological processes include both physical action (splitting by root wedging) and chemical action (bacteriological oxidation, chelation, and reduction of iron and sulphur compounds) (Blight, 1997).

The depth and amount of residual soil strongly depends on five soil-forming factors. A model developed by Hans Jenny in 1941 defined these factors as climate, organisms, relief, parent material, and time (Schaetzl and Anderson, 2005). These five factors identify the state of the system that the soil developed in, not how the conditions influence soil properties. These factors explain that given a set of conditions, a particular set of soil properties would result (Schaetzl and Anderson, 2005). Therefore, every residual soil around the world exhibits a distinctive set of properties.

Climate is the average temperature and precipitation over a period of 30 years and is the most important soil-forming factor (Schaetzl and Anderson, 2005). Hotter and more humid climates typically create deeper residual soil profiles. Climate is affected by latitude, altitude, proportion of land to water, and proximity to oceans and mountains (McCarthy, 2002). Climate is also influenced by the biotic cover that lies between the soil and the atmosphere, by slope aspect, and by snow cover (Schaetzl and Anderson, 2005). In many regions, the conditions that created the soil no longer exist. Gathering historic and current climate data of a site is important for fully characterizing the residual soil profile and understanding the history of its genesis.

Organisms, both flora and fauna, contribute to the formation of soils. Flora affects residual soil formation by retaining the products of weathering on sloping ground. For example, thick forest growth helps to retain loose soil along with ground moisture (Brand and Phillipson, 1985). Fauna soil development effects include digging and burrowing.

Relief is the relative change in elevation over a selected area and is a measure of the gravitational force available to move material downhill. Relief also influences soil

moisture, degree of oxidation within the groundwater, and vegetation differences (Schaetzl and Anderson, 2005). Relief directly impacts the amount of available water, the speed the water passes, and the rate of erosion of material from the surface. Deeper residual profiles generally are found in valleys and on gentle slopes rather than on high ground or steep slopes (Blight, 1997).

Parent material is the starting point of soil formation. Parent material influences the mineralogy, grain size distribution (texture), and layering/stratification/foliation of a soil (Schaetzl & Anderson, 2005). Residual soils can inherit anisotropy from the parent material especially from metamorphic rock with mica (Vaughan, 1990). Different parent materials develop into different residual soils in combination with the other unique soil-forming factors.

Time is also a requirement for soil formation. Pavich (1989) and Cleaves et al. (1970) reported that it takes about 1 millions years to develop 4 meters of saprolite in the Appalachian Mountains (Mitchell, 1993).

In the United States, residual soils are found in four general regions: the Southern Piedmont, the Appalachian Plateau, the Midwest, and the Northwest. The Southern Piedmont residual soils develop on bedrock composed of gneiss, schist, granite, and gabbro. Typical Appalachian Plateau lithologies consist of carbonates, sandstones, and shales. In the Midwest, the residual soils are derived from carbonates and shales. Volcanic ash and lava are the parent materials for residual soils of the Northwest (Brand and Phillipson, 1985).

The area of interest for this study is the Southern Piedmont region of North Carolina. The type of residual soil in this region is known as saprolite. Saprolite readily

develops here because of the warm, humid climate, and gently sloping topography (Vinson and Brown, 1997). Typical saprolite depths range from 20-feet to 75-feet below the ground surface (Sowers, 1963). This region is divided into approximately ten sub-regions based on parent rock and other geologic conditions. Figure 2.1 illustrates the region of interest.

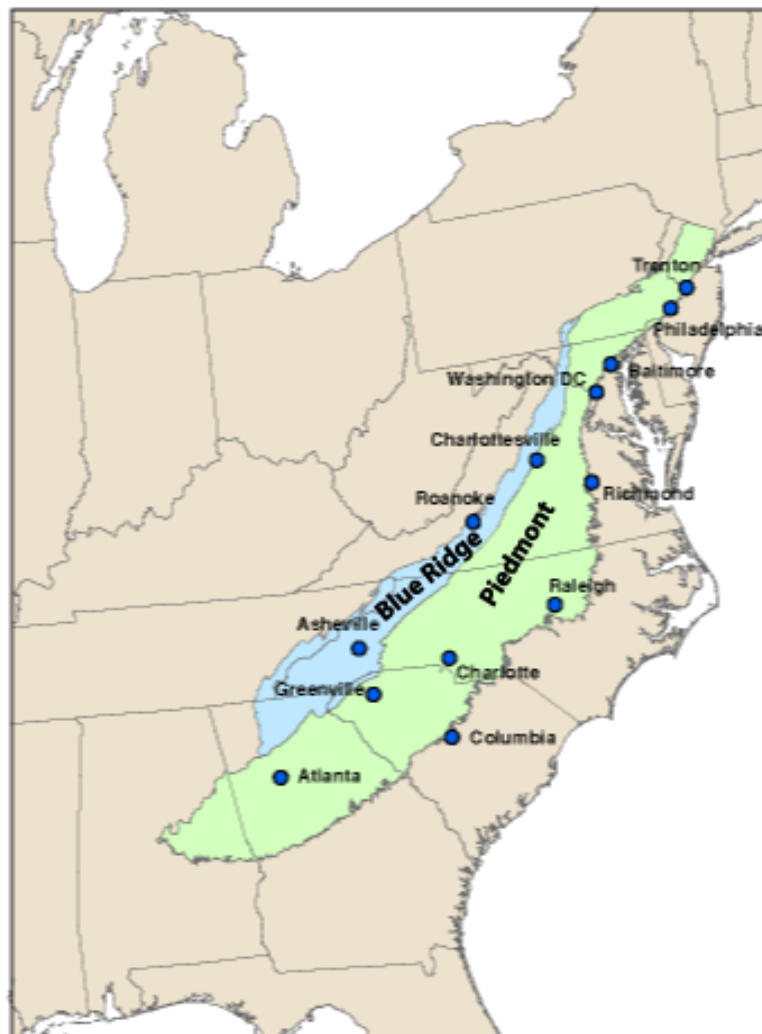


Figure 2.1 – Southern Piedmont and Blue Ridge regions (USGS, 2001)

The sub-region of the sites in this study is the Charlotte Belt and the parent material is granodiorite. The sub-region is shown in Figure 2.2. The climate zone of the area is humid subtropical, with an average annual rainfall of 43.1-inches, average January temperature of 39.3°F, average July temperature of 79.3°F, average annual temperature of 60.1°F, and elevation above sea level of 730-feet to 755-feet (City-data.com, 2009). The main criteria for choosing the research sites was the presence of a well developed residual soil profile of adequate depth.

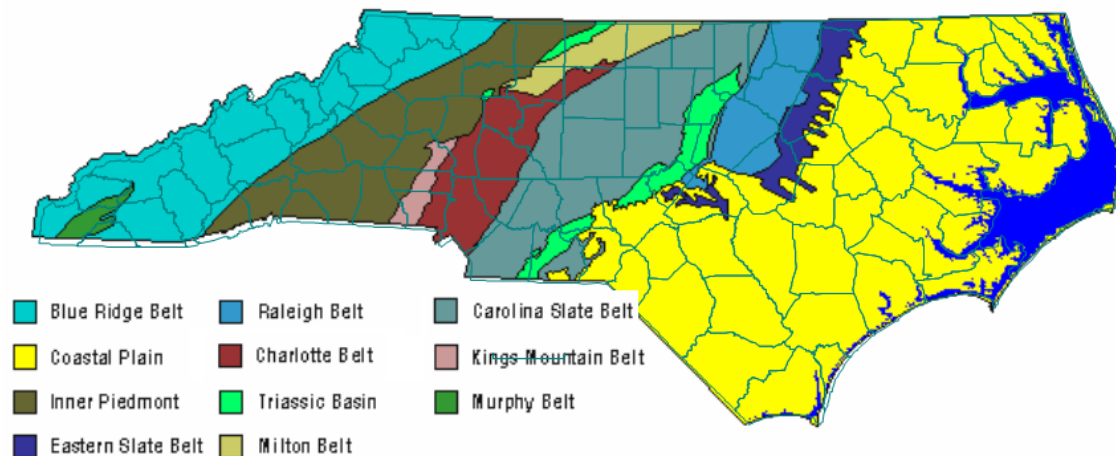


Figure 2.2 – Residual Soil Sub-regions in North Carolina (NCDENR, 2005)

2.2 Geotechnical Soil Properties, Testing, and Soil Mechanics

Geotechnical engineers characterize residual soils using terms such as heterogeneous, anisotropic, and unsaturated. Insitu soils are often stronger and stiffer than comparable transported soils. This difference in strength and stiffness is due to the characteristics of friction, cohesion, and possibly the unsaturated behavior. The concept of mean grain or particle size is not applicable to many residual soils due to the fact that

their particles consist of aggregates or crystals of weathered mineral matter that become progressively finer as the soil is manipulated. A soil that appears to be coarse sandy soil insitu may deteriorate into fine sandy silt during handling (Blight, 1997). In addition, residual soil properties also include high permeability, a drained strength envelope with a significant cohesion intercept, and a “quasi-preconsolidation pressure” or yield stress separating stiff and more compressible behavior (Vaughan, 1985; Mayne and Brown, 2003; Wang and Yan, 2006).

Residual soils also exhibit inherent shear strength and behave in a similar fashion to weakly bonded materials (Vaughan, 1985; Wang and Yan, 2006; Mohamedzein and Mohammed, 2006). The shear strength is a function of friction and cohesion. The friction component is the result of true friction and particle interlocking. The cohesion component arises from a variety of characteristics including electrostatic forces on clay minerals, matric suction, cementation, the continuous re-crystallization of minerals during weathering, and the precipitation of salts from pore water, along with the relict structures of the parent material (Mitchell and Sitar, 1982; Lee and Coop, 1995; Wang and Yan, 2006; Gan and Fredlund, 1996; Lambe and Whitman, 1969). The presence of cohesion allows soils to possess some shear strength at zero confining stress. Vaughan (1990) emphasized that a small amount of cohesion has a large effect on the behavior of geotechnical materials and that this effect is not always appreciated.

The engineering characteristics of soils can be understood using the Mohr-Coulomb theory that investigates the inter-particle contact of soil grains. This behavior is extrapolated to the soil continuum, and it is assumed that this relationship is true at the macro level. It is therefore essential that we understand these effects on the fundamental

strength and compressibility of residual soils. The following sections detail the geotechnical insitu and laboratory tests used in this research, along with the soil mechanics and mathematical theories upon which the potential correlations were based.

2.2.1 INSITU GEOTECHNICAL TESTING

Many geotechnical parameters are measured using insitu soil tests. For residual soil site characterization, insitu testing is generally preferred because good quality undisturbed samples are difficult to obtain (Mohamedzein and Mohammed, 2006). Insitu tests are more expedient and cost efficient, therefore more soils can be tested for a given budget. One can draw reasonable conclusions from insitu testing, but if the scale and frequency of the testing does not fit the degree of heterogeneity of the subsurface, the results can lead to non-representative site characterization (Brand and Phillipson, 1985). Uncertainties in site characterization can further be increased by variations in rock types or soils over relatively short distances (Failmezger et al., 1999).

The primary insitu tests used in this research were the standard penetration test (SPT), standard penetration test with torque (SPT-T), and the Shelby tube test with torque (STT-T). The SPT specifications are detailed in the ASTM International (ASTM) D 1586. The SPT is the most widely used insitu test in the United States and includes boring a hole to a set of depths, lowering a thick walled split-spoon sampler into the borehole, and hammering the sampler into the bottom of the borehole. The number of hammer blows (N) required for the sampler to penetrate the final twelve inches of each eighteen inch run are counted and correlated to geotechnical design parameters. The number of hammer blows is often corrected for overburden pressure, rod length, and hammer energy and presented as the corrected blow count (i.e. N'_{60}).

The advantages of the SPT are the ability to retrieve a disturbed soil sample and the volume of accumulated experience using the test. Many believe that the advantages do not overcome the drawbacks of operator dependency, high soil disturbance, and incongruence with the mechanics of shear strength. Nonetheless, the insitu measurements can be correlated back to the parameters needed to apply the soil mechanics equations. For example, Figure 2.3 (EPRI, 1990) and equation 2.1 present the relationship from Peck et al. (1974) to determine the angle of internal friction (ϕ') based on uncorrected N values.

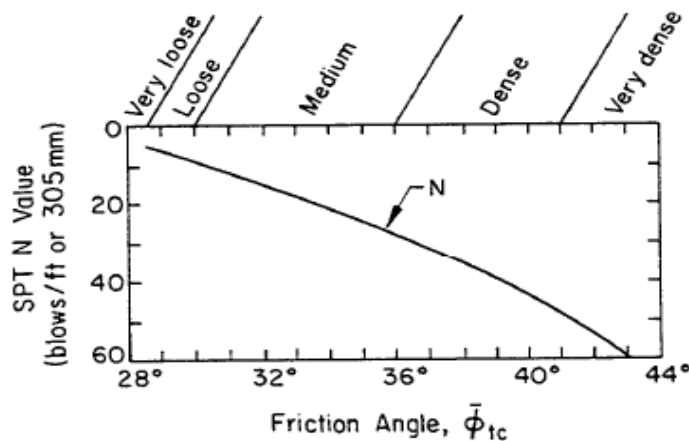


Figure 2.3 – Blow-count (N) versus angle of internal friction (ϕ') correlation

$$\phi' = 53.881 - 27.6034 * e^{-0.0147*N} \quad (2.1)$$

The SPT-T is an insitu test developed as an improvement to the SPT. There is no ASTM standard for the SPT-T; therefore the current testing procedure is based on previous test methods by Bullock and Schmertmann (2003), Winter et al. (2005), and Kelly and Lutenegger (1999). After the SPT is performed and before the sampler is removed, a torque is applied to the top of the drilling rod string. The torque required to

twist the sampler is recorded. Currently, this value can either be used to calculate the side shear friction on the sampler or to represent index parameters related to soil type (Kelly and Lutenecker, 1999; Décourt, 1998).

The Shelby tube test with torque (STT-T) is a test developed for this research and based on a combination of the SPT-T procedure and the Shelby tube sampling procedure (ASTM D 1587) used to collect undisturbed soil samples. The STT-T provides the ability to obtain both insitu torque and undisturbed laboratory shear strength on the same soil specimen. The STT-T procedure includes advancing a borehole, pushing Shelby tubes into the soil, and applying a torque to the sampler. The Shelby tube sampling procedure allows the sampler to be rotated to reduce side friction and break the soil at the end of the sampler, although the torque is not measured. As an additional measurement, the maximum force to push the sampler into the soil is also recorded for this study. This force was similar to the blow-count for the SPT in that it provides a measure of soil resistance.

2.2.2 GEOTECHNICAL SAMPLING

The friable and porous nature of residual soils leads to difficulties when sampling. Soil samples can be collected from the field for use in the laboratory to develop the resistive quantities or parameters. There are four categories of geotechnical samples including disturbed, driven, core, and block samples. The latter three are loosely described as undisturbed. Disturbed samples are difficult to use for laboratory strength and compressibility tests, but can be used for geologic analysis, to indicate soil layers passed through in boreholes, and to provide materials for index and classification tests. Disturbed samples for this research were collected using the SPT split-spoon sampler.

Samples removed from the split-spoon are typically 1.375-inches in diameter and the lengths vary depending on soil type and disturbance.

Undisturbed samples were recovered using Shelby tubes, which are considered driven samplers. Shelby tubes are thin-walled metal tubes, generally 2.8-inches in diameter and 24-inches long. Test specimens can be made to length depending on the laboratory test being performed. It is hypothesized that some inherent properties of residual soils can only be determined using undisturbed samples. Block samples are not chosen for this research based on conclusions by W. T. Hertz (1986) where little difference in experimental results was found between Shelby tubes and block samples of residual soils.

2.2.3 LABORATORY GEOTECHNICAL TESTING

The primary laboratory test used to determine the soil shear strength parameters is the consolidated drained triaxial shear test (TXL). This test allows for both detailed measurement of stresses and strains as well as rational interpretation of test results. The TXL test procedure is based on the Consolidated Undrained Triaxial Test procedure which is detailed in ASTM D 4767. For the TXL test, a cylindrical soil specimen is placed inside a pressure chamber at a uniform stress based on the insitu vertical effective stress. Inside the chamber the soil is isolated inside a rubber membrane in order to isolate the pore water pressure from the confining stress. The sample is then saturated and consolidated inside the rubber membrane. The consolidation includes applying the test stress conditions to the sample and allowing the excess pore pressure to diminish, which reduces the sample void ratio and volume. Next, a deviatoric stress is applied to the specimen at a specified strain rate. The load, deformation, pore water pressure, and

volume change are recorded and used to determine the shear strength. The only difference between the undrained and drained procedures is whether or not the pore water is allowed to drain while the deviatoric stress is applied.

The advantage of a drained test over an undrained test is that it simulates the long term behavior of soil. The drained shear strength is found by plotting the deviatoric stress versus the axial strain. From this graph, the maximum stress is determined and plotted against the confining stress. Plotting the results from two to three tests, a failure curve or envelope is evaluated. The slope and y-intercept of the curve represent the strength parameters of effective angle of internal friction (ϕ') and cohesion (c'), respectively. The cohesion is generally neglected in geotechnical design, although this may be conservative or un-conservative depending on the application and whether the long-term or short-term conditions are crucial. The reliability of the design and the risk of failure in any geotechnical application where shear strength is key must to be sufficiently addressed and the appropriate shear strength parameters measured and evaluated.

Since there is no standard test used to evaluate soil-sampler interface properties, an interface shear test (INT) procedure is utilized. The INT is based on the ASTM D 3080 direct shear test (DST). The DST is another laboratory test used to determine the shear strength, but does not simulate the same stress state as the TXL test. Generally, a specimen is placed into a box that is divided into halves. The bottom half of the box is fixed, while a load is applied to the top half of the box. The specimen is sheared along a predefined shear plane. For this research, the DST was not used to evaluate the soil shear strength. The INT is a modified version of the DST used to evaluate the shear strength at the soil-sampler interface. To perform the INT, a new shear box bottom half was

fabricated out of a metal block with similar characteristics as the split-spoon sampler and Shelby tube sampler. The new bottom half is a solid piece of metal with threads for the locking bolts that hold the two halves of the box together. To perform the test, a soil specimen is placed in the top half of the shear box and forces are applied via ASTM D 3080. Plotting the results from the tests, a failure curve or envelope is developed. The slope and y-intercept of the curve represent the shear strength parameters of adhesion (c_a) and interface friction angle (δ), respectively.

2.2.4 ADDITIONAL GEOTECHNICAL TESTING

Secondary insitu and laboratory tests are used to provide additional site characterization, support the research objective, and provide secondary shear strength measurements. The secondary tests include the classification, dilatometer (DMT), and specific gravity tests. Classification was carried out using both the Unified Soil Classification System (USCS), ASTM D 2487, and the American Association of State Highway and Transportation Officials (AASHTO) system, ASTM D 3282. The USCS and AASHTO were developed to categorize transported soils. They rely heavily on two characteristics: relative grain size fractions and the change in shear strength of the fine fraction due to wetting (Atterberg Limits). The soil classification parameters include the liquid limit (LL), plasticity index (PI), and clay fraction (less than $2\mu\text{m}$). Representative samples are passed through sieves by both mechanical agitation (coarse fractions) and washing (finer fractions). Thus, the soil is classified as an assemblage of individual particles and not a system of cemented or interlocked grains. Furthermore, there is little to distinguish residual soils from transported soils within the two soil classification

systems. The procedure used to determine the specific gravity is detailed in ASTM D 854.

The DMT specifications are specified in ASTM D 6635-01. The dilatometer tool is a flat, rectangular blade with a 2-inch round sensing disc on one side. The DMT is performed by pushing the tool into the ground stopping at 6-inch to 1-foot intervals. At each depth, gas pressure is introduced behind the disc inflating it outward into the soil. The pressures required to move the membrane 1) off the blade and 2) outward 0.043-inches are measured and used to calculate the DMT parameters of dilatometer modulus (E_D), horizontal stress index (K_D), and material index (I_D). The parameters are then used along with correlations and equations to determine the dilatometer undrained shear strength ($s_{u(DMT)}$) and effective angle of internal friction ($\phi'_{(DMT)}$). The indices and parameters are calculated using “DMT QUICKBASIC, VERSION 4.5”, a DOS program that incorporates the theories developed by Marchetti, Durgunoglu and Mitchell (GPE, 1993). The DOS program can be modified in order to present $s_{u(DMT)}$ and $\phi'_{(DMT)}$ at every depth, even though the values are not always appropriate. The main advantages of the DMT are the relatively short amount of time required for the test and the ability to get consistent data through a given depth profile. The DMT is halted at refusal.

2.3 Theoretical Development

For this research, the torque applied to a rotating sampling tool was analyzed using the free-body diagram provided in Figure 2.4, which illustrates both the maximum torque (T_{MAX}) applied to the system to cause failure, along with the shear stresses generated as the sampler rotates (τ_{SIDE} and τ_{END}).

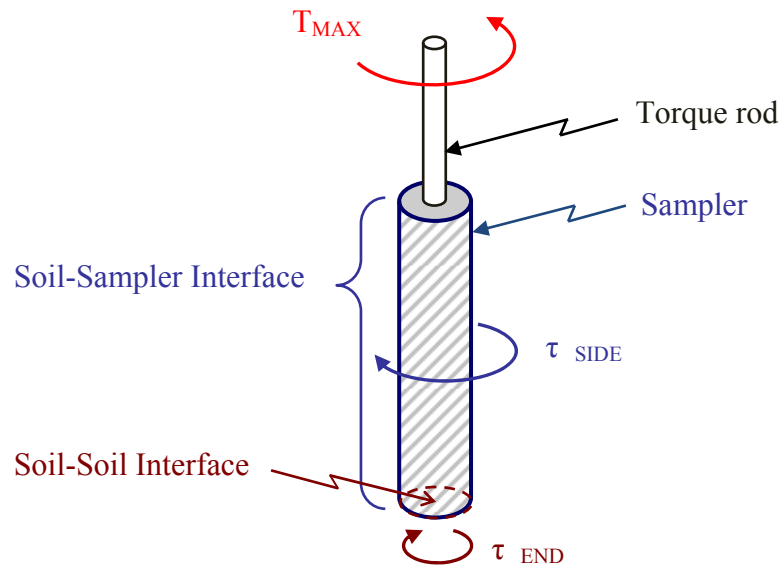


Figure 2.4 – Free-body diagram of the torque test

The applied torque rotates the sampler around the central axis and shearing stresses on the interfaces oppose rotation. The shearing stresses form along two shear surfaces; one at the interface between the soil and the side of the sampler (A_{SIDE}) and one at the soil along the bottom of the sampler (A_{END}). The stresses are described in the same manner as the vane shear test, with consideration for the soil-sampler interaction. The relationship between T_{MAX} , τ_{SIDE} , and τ_{END} is formulated in equation 2.2.

$$T_{MAX} = \tau_{SIDE} (2 \pi r_1 L) r_1 + \tau_{END} \int_0^{r_1} (2 \pi r) r dr \quad (2.2)$$

Figure 2.5 illustrates the dimensions and parameters within equation 1, where L is the length of the sampler and r_1 is the radius of the sampler.

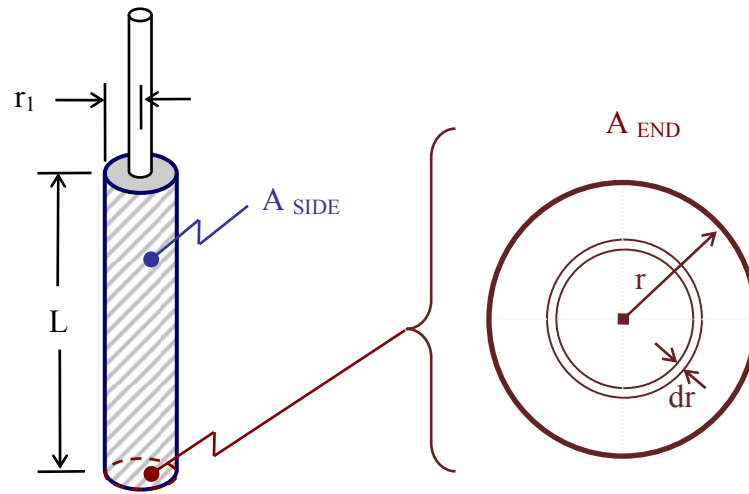


Figure 2.5 – Dimensions and parameters of the torque test

The area ratio for the SPT-T is 36:1 and for the STT-T is 33:1. At these ratios, the side shear provides the majority of the resistance. τ_{END} and τ_{SIDE} are found using equations 2.3 and 2.4, where c' is the cohesion, and ϕ' is the effective angle of internal friction, σ'_v is the effective vertical stress, c_a is the soil-sampler adhesion, σ'_h is the effective horizontal stress, and δ is the soil-sampler interface friction angle.

$$\tau_{END} = c' - \sigma'_v \tan(\phi') \quad (2.3)$$

$$\tau_{SIDE} = c_a - \sigma'_v \tan(\delta) \quad (2.4)$$

σ'_v is based on equation 2.5, where γ is the soil unit weight and z is the depth. The horizontal effective stress is found using either equations 2.6 or 2.7, based on whether at-rest or passive lateral earth pressures are developed, respectively. The actual earth pressures developed are based on the sampler used and may fall between these two conditions. K_0 is the coefficient of at-rest lateral earth pressure and K_p is the coefficient

of passive lateral earth pressure. Equations 2.8 and 2.9 present the relationships used to determine K_o and K_p .

$$\sigma'_v = \gamma z \quad (2.5)$$

$$\sigma'_h = K_o \sigma'_v \quad [\text{At-rest earth pressure}] \quad (2.6)$$

$$\sigma'_h = K_p \sigma'_v + 2c \sqrt{K_p} \quad [\text{Passive earth pressure}] \quad (2.7)$$

$$K_o = 1 - \sin(\phi') \quad (2.8)$$

$$K_p = \tan^2 \left(45 + \frac{\phi'}{2} \right) \quad (2.9)$$

Finally, integrating equation 2.2 and incorporating equations 2.3 and 2.4, T_{MAX} simplifies to equations 2.10 and 2.11.

$$T_{MAX} = \tau_{SIDE} 2 \pi r_1^2 L + \tau_{END} \frac{2}{3} \pi r_1^3 \quad (2.10)$$

$$T_{MAX} = [c_a + \sigma'_h \tan(\delta)] 2 \pi r_1^2 L + [c' + \sigma'_v \tan(\phi')] \frac{2}{3} \pi r_1^3 \quad (2.11)$$

In addition, c_a and δ are often considered functions of c' and ϕ' . Various correlations have been published and equations 2.12 and 2.13 show the most common. The adhesion factor (α) is typically 0.5. The interface friction reduction factor (R_i) is typically between 0.5 and 0.7 for smooth steel on sand or between 0.7 and 0.9 for rough steel on sand (Coduto, 1994; Bowles, 1988; McCarthy, 2007).

$$c_a = \alpha c' \quad (2.12)$$

$$\delta = R_i \phi' \quad (2.13)$$

Since τ_{END} is equivalent to the shear strength determined from the TXL and to simplify further analyses, in the remainder of this document τ_{END} will be referred to as τ_{TXL} . Since τ_{SIDE} is determined from the INT and to simplify further analyses, in the remainder of this document τ_{SIDE} will be referred to as τ_{INT} .

A parametric study was performed to determine the influence of each parameter on theoretical T_{MAX} . Table 2.1 presents the parameters and constants used. Table 2.2 presents the parameter input ranges and the output values of theoretical T_{MAX} . The behavior of T_{MAX} is more influenced by variations in ϕ' , δ , and σ'_v (which of a function of z) than c' and c_a .

Table 2.1 – Parameters and constants as single parameters varied

Parameter	Constant
z (ft)	30
c_a (psf)	0
δ (°)	25
c' (psf)	700
ϕ' (°)	25

Table 2.2 – Theoretical T_{MAX} (output) at the ranges of each parameter (input)

Input			Output : Theoretical T_{MAX} (ft-lbs)					
Parameter	Range		At-Rest			Passive		
	Min	Max	Min	Max	ΔT_{MAX}	Min	Max	ΔT_{MAX}
z (ft)	0	65	0.6	108.2	107.6	51.9	501.5	449.6
c_a (psf)	0	500	50.2	75.3	25.1	259.4	284.5	25.1
δ (°)	15	40	29.7	88.8	59.1	149.9	465.3	315.4
c' (psf)	0	1500	49.7	50.9	1.2	207.5	318.8	111.3
ϕ' (°)	15	45	63.4	28	-35.4	186.1	570.1	384

CHAPTER 3: LITERATURE REVIEW

Over the past 50 years, the understanding and knowledge of residual soils has progressed. Worldwide studies in residual soil are being established by researchers practicing in Brazil, Hong Kong, Korea, Portugal, Singapore, and Sudan, as well as in the tropics. The primary work in the United States is in the mid-Atlantic and southeastern states, primarily at sites located in North Carolina and Alabama. In addition, Wang and Yan (2006) emphasized the importance of localized research with residual soil, which justifies similar research efforts around the world.

3.1 Geotechnical Testing in Residual Soil

The earliest published geotechnical work on residual soils in the United States was by G. F. Sowers at the Georgia Institute of Technology. Between 1954 and 1963 G.F. Sowers investigated the engineering aspects, unique properties, and problems inherent in residual soils. During this period, two Masters Theses were completed at Georgia Tech dealing with Piedmont residual soils. Miller (1957) investigated the use of the vane shear test and Crowther (1963) considered SPT testing with respect to bearing capacity of shallow foundations.

During the 1980's, an extensive investigation of a single Southern Piedmont residual soil test site was documented in a doctoral dissertation by Hertz (1986) and a publication by Lambe and Hertz (1988). This work was performed on a research farm near the North Carolina State University campus, in Raleigh, North Carolina. The goal

of the research was to characterize the site by measuring the properties of compressibility, shear strength, and permeability, with special emphasis on the effects of anisotropy, mica content, stress history, suction, and sample disturbance. In addition to the work by Hertz (1986) and Lambe and Hertz (1988), additional studies at the NC State research site have been published by C. E. Wang (1995) and Wang and Borden (1996) where the weathering profile and deformation characteristics of the soils were studied.

During the 1990s, a similar comprehensive study of residual soils was conducted by Vinson and Brown (1997) at a site near Auburn University in Alabama, near the southern extent of the Southern Piedmont region. This work was intended to serve as a reference for residual soil characteristics for other research at the site and to compare different types of insitu and laboratory measurements of physical properties of the soils at the site.

Between 1988 and 2006, 13 triaxial shear test studies have been published specifically in residual soils. A summary of these studies is presented in Table 3.1. Within Table 3.1, RS represents Residual Soil, CD represents Consolidated Drained tests, CU represents Consolidated Undrained tests, and UU represents Unconsolidated Undrained tests. Selected cohesion and friction values from the triaxial tests are provided in Table 3.2.

Additional work during the 2000's in residual soils within the same region as this research has been performed by J. B. Anderson, V. O. Ogunro, and J. L. Daniels at the University of North Carolina at Charlotte (UNCC). The research by J. B. Anderson and V. O. Ogunro (2006) was entitled "Development of an Earth Pressure Model for Design

of Retaining Structures in Piedmont Residual Soils.” The objective of this study was to develop a model for earth pressure in residual soils based on commonly measured insitu or laboratory measurable soil parameters. The project included the insitu tests of the SPT, DMT, and borehole shear at research sites near Charlotte, North Carolina. Shelby tube samples were collected for laboratory tests including triaxial, consolidation, and index tests. The c' and ϕ' results from their study are provided in Table 3.2.

Table 3.1 – Comprehensive summary of published residual soils triaxial testing

Author	Date	Location	Soil Type	Test Type
Anderson and Ogunro	2008	North Carolina	Piedmont RS (Charlotte Belt and Carolina Slate Belt)	CU
Gan	1996	Hong Kong	Undisturbed completely decomposed granite and fine ash tuff (saprolite)	CD Saturated and Unsaturated
Garga	1988	Brazil	RS (“Dense” basaltic soil and “vesicular” basalt)	CU
Heartz	1986	North Carolina	Piedmont RS (Gneiss and Schist bedrock)	CD
Lambe and Heartz	1988	North Carolina	Piedmont RS	CD
Lee and Coop	1995	Korea	Decomposed granite (Compacted samples, highly organized)	CD
Mayne et al.	2000	Alabama	RS	CD; CU Disturbed and Undisturbed
Mohamedzein and Mohammed	2006	Sudan	RS (sandstone and mudstone)	UU, CIU
Rahardjo et al.	2004a	Singapore	Reconstituted RS	CD
Rahardjo et al.	2004b	Singapore	RS (2 slopes)	CD Saturated and Unsaturated

Table 3.1 – (continued)

Author	Date	Location	Soil Type	Test Type
Viana da Fonseca et al.	2006	Portugal	RS Granite (saprolite with weak relict structure)	CD
Vinson and Brown	1997	Alabama	Piedmont RS (micaceous sandy silt)	CD, CU, UU
C.E. Wang	1996	North Carolina	RS (Igneous and metamorphic rocks)	CD Unsaturated
Wang and Yan	2006	Hong Kong	2 Saprolites Weathered volcanic tuff and weathered granite	CD CU

Table 3.2 – Published cohesion and angle of internal friction results

Author	Date	Numerical Results
Anderson and Ogunro	2008	$c' > 300$ psf, $\phi' = 28^\circ$
Gan	1996	Remolded: $c' = 208.8$ psf and $\phi' = 35.5^\circ$ CDG: $c' = 439.2$ psf and $\phi' = 31^\circ$
Garga	1988	Peak CU Dense: $c' = 1228.32$ psf and $\phi' = 32^\circ$ Vesicular: $c' = 757.44$ psf and $\phi' = 23^\circ$
Mayne and Brown	2000	$c' = 355.68$ psf and $\phi' = 31^\circ$ if $c' = 0$ psf then $\phi' = 35.3^\circ$
Mohamedzein and Mohammed	2006	(Depth < 13.1ft) $c' = 0$ psf and ϕ' varies between 29-35° (Depth > 13.1ft) $c' = 0$ psf and average $\phi' = 42^\circ$
Rahardjo et al.	2004a	$\phi' = 31.5^\circ$
Rahardjo et al.	2004b	$\phi' = 41.3^\circ$ or $\phi' = 36^\circ$
Viana da Fonseca et al.	2004	$c' = 93.6$ psf and $\phi' = 45.8^\circ$
Wang, YH	2006	Weathered volcanic tuff: $\phi' = 36.6^\circ$ Weathered granite: $\phi' = 34.1^\circ$

3.2 Standard Penetration Tests with Torque Research

In 1988, S. M. Ranzine performed the initial development of the SPT-T and was the first to report test results. The measured torque was used to classify soil type and since then various authors have added to this relationship (Decourt, 1992, 1994, 1998;

Peixoto and Carvalho, 2000; Kelly and Lutenegeger, 1999). The authors argued that the torque measurement was a novel addition to the SPT which does not detract from the SPT and only requires approximately 1 minute of additional effort (Kelly and Lutenegeger, 2004). In 1994, L. Decourt recommended a soil classification based on a torque ratio of maximum torque relative to SPT blow-count (T/N) and stated that saprolites have values around 2.0. Kelly and Lutenegeger (1999) published an average T/N values for residual soils of 1.53. Various authors also published SPT-T procedures, provided examples, and presented results of testing in a variety of soils.

In New York sand, Lutenegeger and Kelly (1998) concluded that the torsional shear strength measured outside the sampler occurred in a partially remolded soil which retained much of its original fabric. They also believed that the SPT-T could provide an additional quasi-static measurement following the dynamic measurement of the split-spoon penetration that may provide a direct measurement of skin friction. In Virginia residual soils, Kelly and Lutenegeger (1999) investigated the SPT-T along with the cone penetration test (CPT) to develop relationships to internal angle of friction (ϕ'). Kelly et al. (1999) also investigated sample recovery and presented an equation for skin friction (f_s) based on the measured torque ($f_s = 2T/\pi d^2 L$). In addition, Kelly and Lutenegeger (2004) investigated the skin friction relationship in various soil types (fine-grained, coarse-grained, residual soil, glacial till) at 12 sites within the United States (TX, IL, MA, NY, VA, GA). During the study, an additional correlation was developed between the skin friction (f_s) and the SPT blow-count (N) ($f_s = \alpha_s N$).

In 1999, Peixoto et al. investigated the ability of the SPT-T to predict the ultimate bearing capacity of precast concrete piles in Brazilian unsaturated residual soil. This

study found that the SPT-T lead to good predictions of the skin friction of piles. This paper also presented adhesion values between 229.48 and 1835.0 psf. In 2007, Peixoto et al. investigated the influence of rod length on the insitu torque measurement and concluded that “the torque difference through the rod length is lower than the minimum scales of the mechanical torque meter that are used in practical engineering.”

Two additional projects were completed investigating the effects of set-up on deep foundations; one in 2003 by the Florida Department of Transportation (FDOT) and one in 2005 by the Wisconsin Department of Transportation. Soil set-up refers to an increase in skin friction with time. The FDOT tested the effects of staged SPT-T testing to develop the dimensionless pile side shear set-up factor in silty sands and shelly clays (Bullock and Schmertmann, 2003). The FDOT report concluded that the SPT-T was useful as a set-up predictor in shelly clays, but was not useful in silty sands. In conjunction with the FDOT project, J. M. Hicks (2005) completed a master’s thesis at the University of Florida entitled “Determining the effect of stage testing on the dimensionless pile side shear set-up factor.” The Wisconsin Department of Transportation investigated the ability of the SPT-T to predict pile performance, but concluded that there was no correlation between set-up values from short-term SPT-T and long-term set-up on piles (Winter et al., 2005). A similar investigation in Sweden by Axelsson and Westin (2000) concluded that torque tests on driven rods in sand were valuable for estimating set-up.

An important aspect of SPT-T testing is the shear strength at the soil-sampler interface. Published studies have evaluated the shear strength between steel and soils in Japan (Kishida and Uesugi, 1987; Subba Rao et al., 2002; Tsubakihara et al., 1993).

Subba Rao et al. (2002) presented graphs of the adhesion factor (α) in clay versus both undrained shear strength and relative steel roughness. Tsubakihara et al. (1993) developed relationships for the coefficient of friction and roughness in clay and sand-clay mixtures.

Additional soil-steel shear strength results have been published with respect to agricultural plowing at shallow soil depths (Maksoud, 2006; Soni and Salokhe, 2006). Maksoud (2006) developed relationship of soil adhesion, soil-metal friction angle, and soil shear strength (internal angle of friction and cohesion) to moisture content and bulk density. Soni and Salokhe (2006) investigated adhesion through the effects of negative pore pressure and physio-chemical adsorption on the resistance at the soil-metal interface with the goal of saving energy.

3.3 Geologic Research in Residual Soil

The geologic soil properties are used as a compliment to site investigations and are not the primary basis for engineering design. Beyond identification of soil type, geologic analyses include color, structure, gravel percent, consistence, pores, roots, texture, and clay films. The method for geologic analysis is based on guidelines published in “Soil and Geomorphology” by Birkeland (1999). The soil color is based on the Munsell Color Chart (Torrent and Barron, 1993). Munsell soil color is traditionally determined in the field by visually comparing a soil sample with a standard set of Munsell color chart chips. The Munsell color chips are defined in terms of the three dimensions of hue (H), value (V), and chroma (C). Hue is the spectral color (red, yellow, blue, etc.), value is the darkness or lightness, and chroma is the intensity of the color within a hue. Many researchers acknowledged that errors are involved in the subjective

method and stated that the Munsell system is at best semi-quantitative (Barrett, 2002; Viscarra Rossel et al., 2006; Adderley et al., 2002). In order to provide a more quantitative assessment of color, mathematical equations have been developed. A redness rating (RR) and a redness factor (RF) were developed based on the H, V, and C (Torrent and Barron, 1993; Fontes and Carvalho, 2005) and the equation 3.1 and 3.2 show the relationships.

$$RR = (10 - H) * (C/V) \quad (3.1)$$

$$RF = (10 - H) + (C/V) \quad (3.2)$$

In addition, a more microscopic geologic study can include petrographic analyses. A petrographic analysis is performed by first impregnating the soil sample with epoxy, cutting the soil into a thin slice, and polishing the slice for inspection. Using a polarizing petrographic microscope, the inspection includes point counts of grain size, mineralogy, porosity, and the nature of grain boundaries. It is hypothesized that the microscopic view afforded by petrographic analysis may provide details of mineralogy, micro-fabric, and inter-particle bonding of residual soils that influence the shear strength. This investigation may also elucidate the link between the insitu SPT-T measurements and the laboratory shear strength.

Fourteen journal articles were found on a variety of residual soils investigating the influence of mineralogy, micro-fabric, porosity, and grain boundary character on shear strength. Research in tropical Brazilian soils and weathered Anthenian Schists indicates that mineralogy has a direct influence on shear strength (Rigo et al., 2006; Myriantis and Leach, 1978). Rigo et al. (2006) also reported that the residual shear strength of tropical

soils depends on particle size distribution, effective stress, parent rock, and weathering degree. The pore volume and pore-size distribution in Singapore saprolite and Tertiary sandstone have also been shown to correlate to the amount of weathering (Rahardjo et al., 2004; Onodera et al., 1976; Jeng et al., 2004). Research investigating the role of micro-fabric or the character of grain boundaries in relation to shear strength is very limited, but a relationship has been shown in ignimbrite (Moon, 1993). No research investigating these geologic influences on shear strength was found in saprolite of the southeastern United States.

CHAPTER 4: TESTING PROGRAM

In order to achieve the research objective, three test sites were evaluated between July 2007 and July 2009. The three test sites were located in Charlotte, NC, along the future path of Interstate 485, the beltway around the city. The sites were all located within a two mile radius along Prosperity Church and Browne Roads. The sites were labeled Prosperity Church Road Site 1 (PC1), Browne Road Site (BR), and Prosperity Church Road Site 2 (PC2). Maps detailing the site locations and layout are provided in Figures A1 and A2 of APPENDIX A. The locations of the sites were dependent on the North Carolina Department of Transportation (NCDOT) Geotechnical Engineering Unit, a partner in the research.

The NCDOT supplied insitu drilling and testing assistance at no cost to the project. They performed the SPT, SPT-T, STT-T, and DMT tests in conjunction with the researchers. The laboratory tests were performed primarily by the author at the University of North Carolina Geotechnical Laboratory. Two triaxial test depths (PC1 – 9.4' and 19.4') were performed by the author with assistance at the NCDOT Soils Lab in Raleigh, NC.

Since there were no specific testing procedures for residual soils, the testing procedures used were based on the methods described previously in this dissertation. At each of the three research sites, SPT borings were performed prior to the research to verify the presence of residual soils to at least a depth of 30-feet. For this research, an

SPT-T was first performed at 5-foot intervals to a depth with relatively high blow-counts (20 to 30). From the SPT-T, disturbed split-spoon samples were field identified and preserved (collected in plastic bags) for additional tests. Based on the results from the SPT and SPT-T, the STT-T was then performed at similar 5-foot depth intervals as the SPT-T. At all three sites, a DMT was also performed at 1-foot depth intervals. A summary of the insitu and laboratory tests and the depths are provided in Table 4.1.

Table 4.1 – Summary of insitu tests

Site Location	SPT-T, STT-T, TXL, & INT		DMT
	Number of Test Depths	Total Depth (ft)	Total Depth (ft)
PC1	11	54.4	49
BR	13	65.5	44
PC2	8	39.5	30

During the insitu testing program, two types of soil samples were collected: Shelby tube and split-spoon. For each split-spoon sample collected, soil classification (geotechnical and geologic) and specific gravity tests were carried out. The Shelby tube samples were used for undisturbed TXL and INT tests. Each tube run generally provided between 20-inches and 24-inches of soil, some of which was lost to trimming and handling disturbance. Generally three 6-inch TXL specimens (18-inches total) and three 0.5-inch INT (1.5-inches total) specimens were tested. In addition, petrographic analyses were performed on six Shelby tube specimens from PC1. For possible petrographic analysis, approximately 1.5-inch soil samples were vacuum sealed and set aside from all of the Shelby tubes at each site.

4.1 Torque Testing

Table 4.2 provides the list of equipment used during the SPT-T. Photographs of the equipment and a schematic of the torque cell are provided in Figures 4.1 through 4.4.

Table 4.2 – SPT-T equipment list

Source	Equipment
North Carolina Department of Transportation	CME 550X ATV based drill rig with automatic hammer
	SPT split-spoon sampler
	SPT AW rods (5 foot and 10 foot)
University of Florida	Torque Cell (Instrumented 2 foot AW rod with 8 strain gages)
	2.5" Drive nut
	2.5" Socket
	1" Diameter rod – 4 feet long
	2 Blue data cables End 1 - Hard wired to datalogger End 2 - Quick connects to torque cell
University of North Carolina at Charlotte	Datalogger (CR1000, PS100, RS232 Cable)
	Inverter (gasoline generator) for laptop
	Laptop with Loggernet® software
Fabricated during project	Wooden centering pad



Figure 4.1 – Torque testing equipment



Figure 4.2 – Torque testing – NCDOT drill rig



Figure 4.3 – Torque testing equipment – Insitu set-up

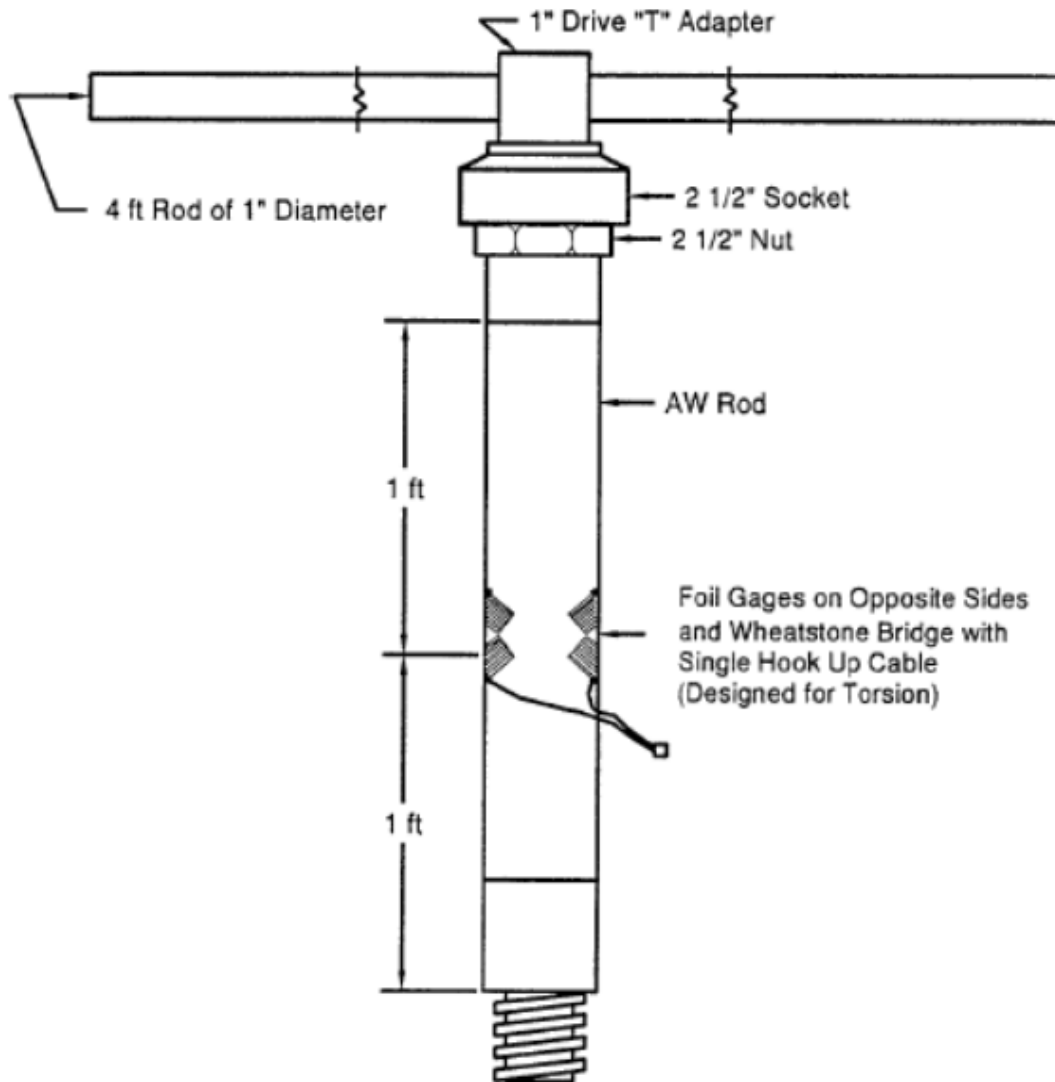


Figure 4.4– Torque cell schematic (Rausche et al., 1996)

The primary torque cell equipment was borrowed from the University of Florida and was used in their studies (Bullock and Schmertmann, 2003, and Hicks, 2005). The torque cell, a strain gage instrumented AW rod similar to that used in SPT energy testing, was fabricated and calibrated by Pile Dynamics, Inc. in 1995. Figures 4.5 and 4.6 present the two calibration sheets provided by Pile Dynamics, Inc.

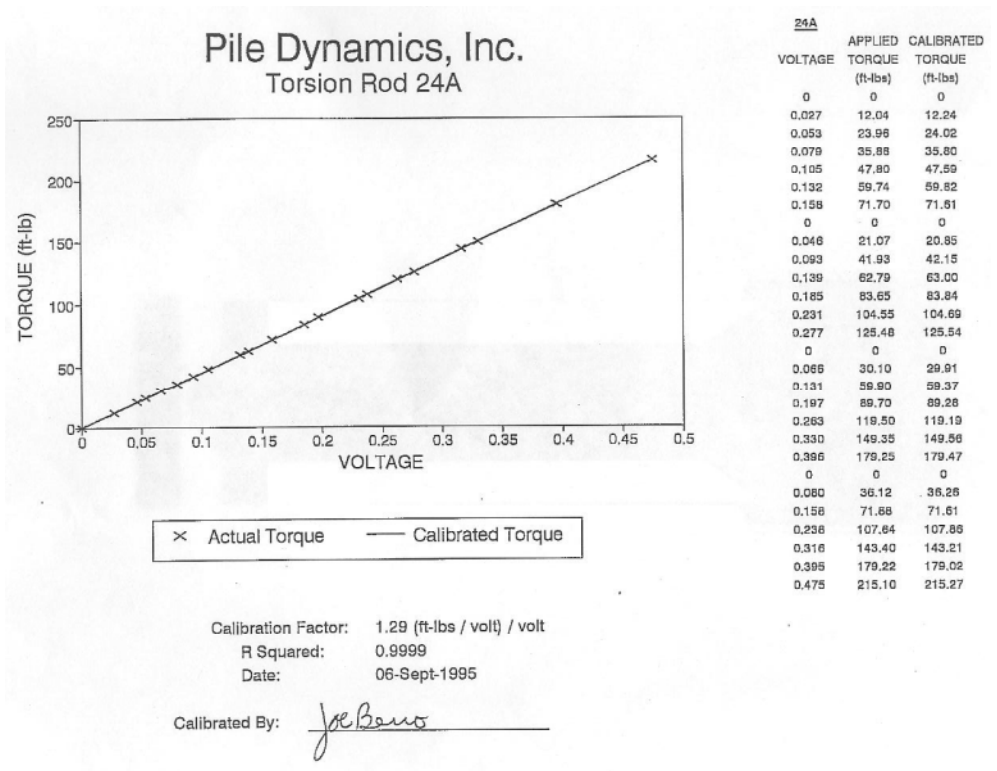


Figure 4.5 – Original Pile Dynamics, Inc. calibration graph – Torque cell 24A

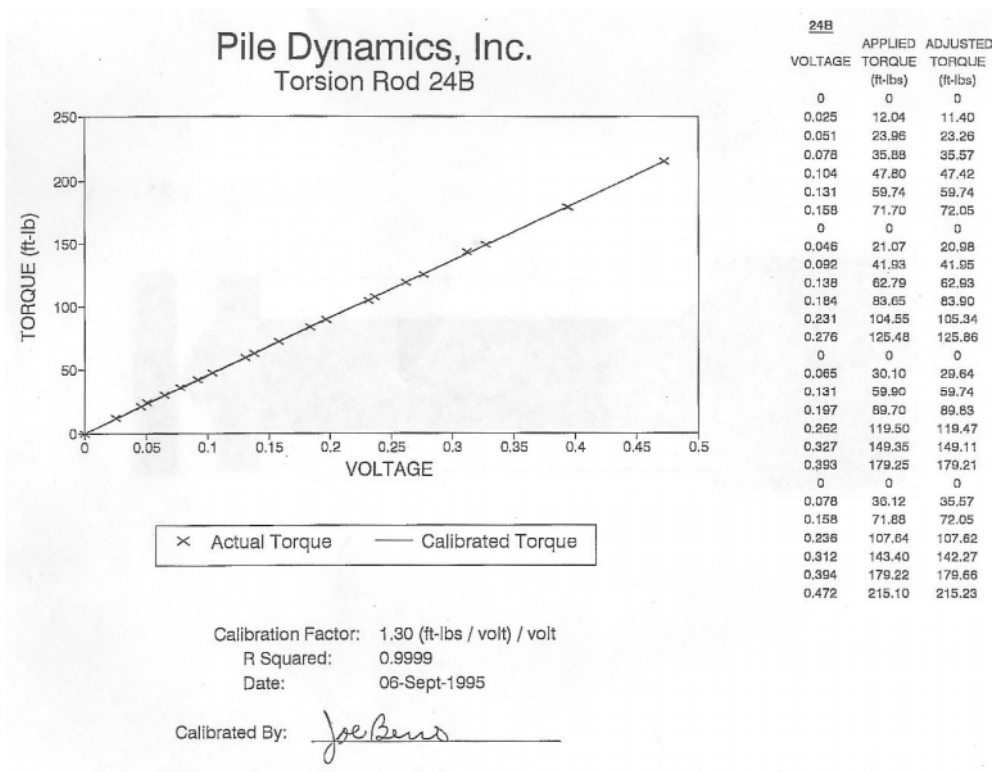


Figure 4.6 – Original Pile Dynamics, Inc. calibration graph – Torque cell 24B

The torque cell was also calibrated by the author twice during the project, July 2007 and July 2008. The procedure used to calibrate the torque cell began by clamping one end of the rod horizontally into a clamp and resting the other end on an elevated roller to allow free rotation. The 2.5-inch socket and 4-foot rod were then attached to the free end. A bucket was then attached to the 4-foot rod at a set length from the center line of rotation of the torque cell. Figure 4.7 shows the equipment set-up during laboratory calibration. Weights were then incrementally added to the bucket and the corresponding output signal was measured using the datalogger. Figures 4.8 and 4.9 show the two calibration graphs developed by the author. The specific datalogger hardware included a Campbell Scientific Inc. CR1000, PS100, and RS-232 cable. Figure 4.10 provides the wiring diagram. The software used with the datalogger hardware was Loggernet® and the program file is provided in Figure 4.11. Figure 4.12 provides a picture of the datalogger set-up in the field.



Figure 4.7 – Torque cell calibration equipment – Laboratory setup

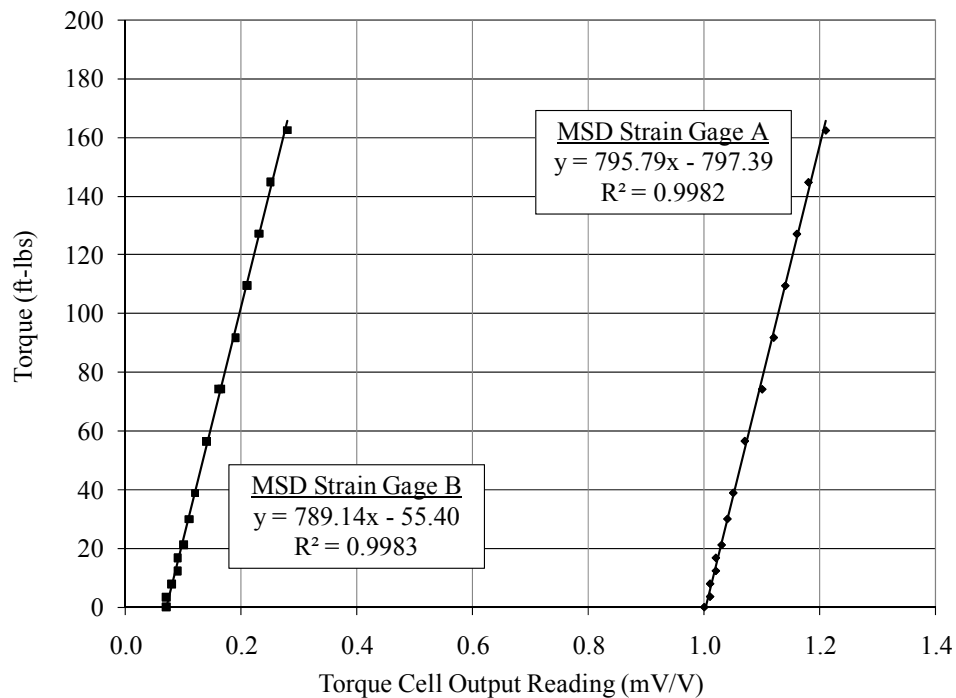


Figure 4.8 – July 2007 UNCC calibration graph

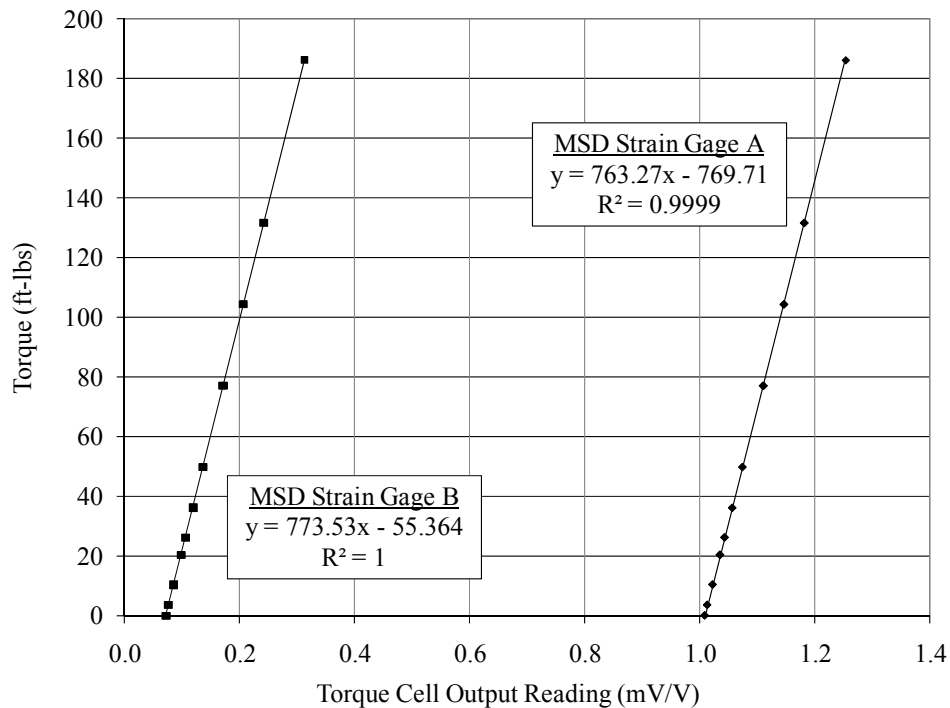


Figure 4.9 – July 2008 UNCC calibration graph

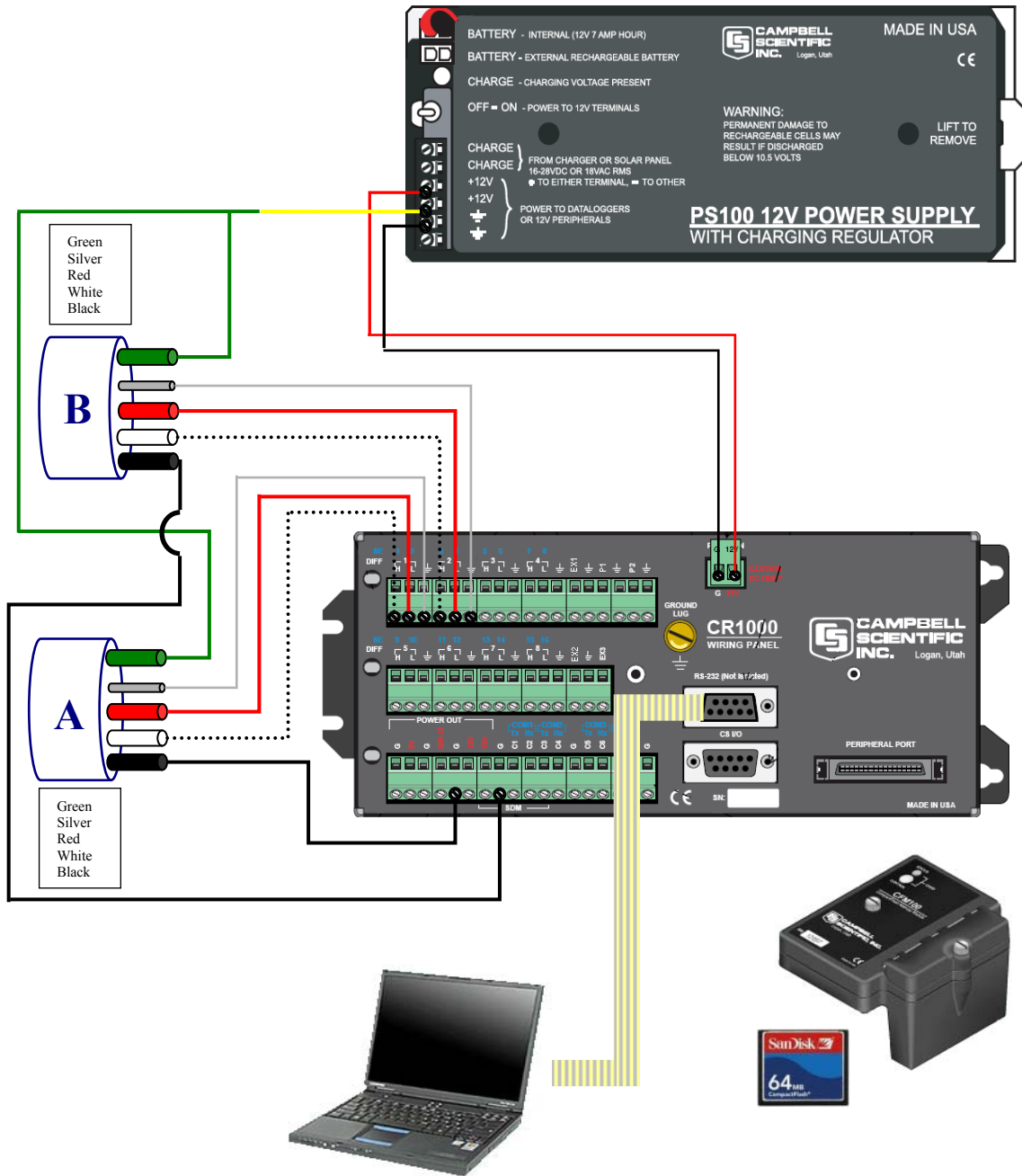


Figure 4.10 – Datalogger wiring diagram

```

'CR1000
'Created by SCWIN (2.4)
'Declare Variables and Units
Dim CSI_R
Dim CSI_1
Public Batt_Volt
Public DiffVolt(2)
Public V
Public mV
Public Msd1
Public Msd2
Public Torque1A
Public Torque2B
Units Batt_Volt=Volts
Units DiffVolt=mV

'Define Data Tables
DataTable(Torque,True,-1)
    DataInterval(0,500,msec,10)
    Sample(1,Batt_Volt,FP2)
    Sample(1,DiffVolt(1),FP2)
    Sample(1,DiffVolt(2),FP2)
    Sample(1,Torque1A,FP2)
    FieldNames("Torque1A")
    Sample(1,Torque2B,FP2)
EndTable

'Main Program
BeginProg
    Scan(500,msec,1,0)
        'Default Datalogger Battery Voltage measurement Batt_Volt:
        Battery(Batt_Volt)
        'Generic Differential Voltage measurements DiffVolt(1):
        VoltDiff(DiffVolt(1),2,mV25,1,True,0,_60Hz,1.0,0.0)
        'User Entered Calculation
        Msd1=DiffVolt(1)/Batt_Volt
        'User Entered Calculation
        Msd2=DiffVolt(2)/Batt_Volt
        'User Entered Calculation
        Torque1A=795.78625185*Msd1-797.387251555
        'User Entered Calculation
        Torque2B=789.136453689*Msd2-55.4043152551
        'Call Data Tables and Store Data
        CallTable(Torque)
    NextScan
EndProg

```

Figure 4.11 – Datalogger program file



Figure 4.12 – Torque testing datalogger – Field set-up

The datalogger was wired, prepared, and tested prior to going to the field. On the day of the test, the equipment was brought to the field and laid out as the drill rig was set up by the NCDOT. The datalogger program was started approximately 30 seconds before force was applied and stopped 30 seconds after force ceased. The author was the primary person to apply torque throughout the study. However, multiple people were needed to apply force at the two or three deepest tests at every borehole. The force was applied at a radius of approximately 4-feet from centerline of the hole and at a height of approximately 3-feet above the ground surface (approximately at the author's chest height). The total amount of torque applied was based on applying a steady force at a steady rate. The author attempted a steady addition of force throughout. In order to eliminate slipping and ensure stable footing, 1-inch diameter sticks were placed on the

ground for use as steps since the ground was slick from constant trampling and field conditions.

The author completed 180 degrees of rotation for each test and was limited by the test set-up and drill rig. The time to complete the rotation was approximately 1 to 2 minutes and based on applying a steady force at a steady rate. At the end of the test, the datalogger file was renamed and moved to a new folder on the laptop, since the program appends to old data files making it difficult to distinguish between tests.

4.1.1 TORQUE DATA REDUCTION

The torque during 180 degrees of rotation was measured. Figure 4.13 presents an example of un-adjusted insitu torque measured during a representative SPT-T at the Browne Road site. Data was recorded every 0.5 seconds. The torque was plotted versus record number to provide a reference to the point of application of the initial torque.

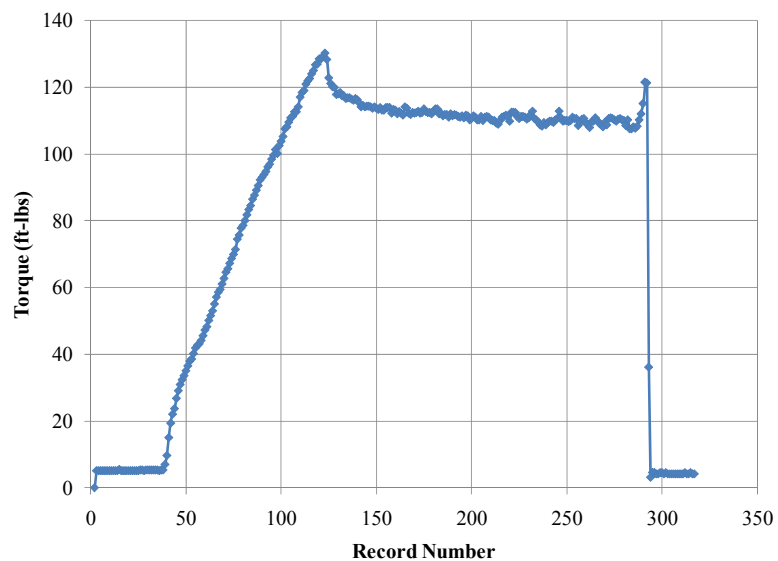


Figure 4.13 – Typical un-adjusted SPT-T torque plot – BR 55.5'

The data in Figure 4.13 was adjusted by zeroing the time and removing the extra data at the beginning and end of the file. A final adjusted torque data curve is presented in Figure 4.14.

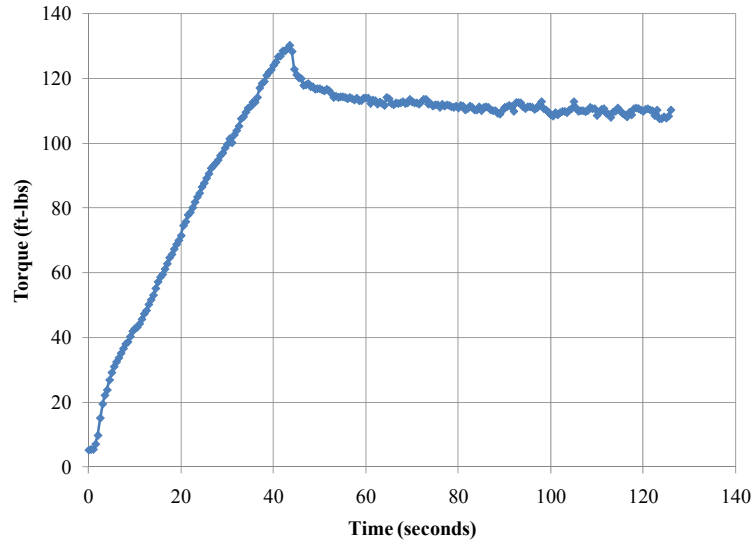


Figure 4.14 – Typical adjusted SPT-T torque plot – BR 55.5’

In addition to the maximum torque (T_{MAX}) evaluated in previous studies, this study also evaluated the steady state torque (T_{SS}). T_{MAX} was considered the initial peak in Figure 4.14 and T_{SS} was the average of a representative number of points along the horizontal portion of the curve after the peak. T_{MAX} is considered the combined failure of the shearing stresses at the two interfaces of the system. The T_{SS} is considered the residual resistance along the two interfaces. The final peak in Figure 4.13 was produced by the author rapidly pushing the torque cell at the end of the test. This peak was not analyzed during this research since there was no true measurement of the angular velocity (ω) at the time.

The STT-T used the same equipment as the SPT-T, with the addition of the items listed in TABLE 4.3.

TABLE 4.3 – STT-T equipment list

Source	Equipment
North Carolina Department of Transportation	Shelby tube connector
	Shelby tube recovery device
University of North Carolina at Charlotte	Propane torch
	Heat gloves
	Duct tape
	Acker Shelby tubes
	Acker Shelby tube caps
	Acker wax to seal ends
Fabricated during project	Wooden tube stands

Shelby tubes samples are not standard practice when investigating Piedmont soils. Thus, due to field conditions, soil type, and technique, a few Shelby tube samples were not recovered. Finesse by the drill rig operators when removing the tube from hole was essential. Impacts needed to be kept to a minimum, especially at deeper depth because more time was needed to get the sample to the surface and also time and work were required to remove SPT rods. To facilitate sample removal, a special Shelby tube recovery device was used when necessitated. This tool provided suction to the top of the soil sample. When using this tool, there were two instances (BR 40.5' and BR 45.5') where the Shelby tubes would not easily come free from this device. A large chain clamp was attached to the Shelby tube and a hammer was used to force the tube off. The impacts may have had an effect on the lab results. Coincidentally, these samples were taken at the water table which was at 42.6-feet.

After removal of the Shelby tube from the ground, a tube cap was applied to the bottom and the tube was placed into a wooden storage frame. Approximately 2-inches of wax were melted into the top end of the Shelby tube using a propane torch. After the wax cooled, the remaining void space inside the tube was filled with waste paper or soil. At PC1, the Shelby tubes were flipped, one inch of soil was removed from the bottom, and wax added to seal it. The bottoms of the tubes were not waxed at BR or PC2 to provide more soil for the laboratory tests. Both ends of the tubes were then sealed using plastic caps and duct tape. The tube was then labeled with a black marker. In order to improve organization during lab testing, the test depth was labeled along the entire length of the tube.

The Shelby tubes were transported vertically inside the same cardboard boxes in which the empty tubes were stored. Extreme care was taken during the 20 minute transport from the test sites to the UNCC soil laboratory by driving slowly and wedging the boxes to reduce movement. At the University, the tubes were stored vertically in the author's office in wooden frames. The time between field collection and lab testing is provided in Tables E1, E2, and E3 of APPENDIX E. The STT-T torque data analysis was the exactly the same as SPT-T.

4.2 Triaxial Shear Testing

To create TXL samples, a Shelby tube cutter frame was fabricated. This frame consisted of a rigid frame supporting two tube clamps. The overall frame dimensions were 35-inches high, 36.5-inches long, and 14.5-inches wide. The clamp dimensions were 6-inches long, 3-inches inside diameter, and 0.25-inch wall thickness. The two tube

clamps were separated by a 2.2-inch gap. Figures 4.15, 4.16, and 4.17 provide photos of the cutter frame.



Figure 4.15 – Shelby tube cutter frame – Profile View



Figure 4.16 – Shelby tube cutter frame – Shelby tube clamps



Figure 4.17 – Shelby tube cutter frame – End View

Within the gap between the two clamps, a 3-inch pipe cutter was used to cut the Shelby tube to a desired length. After the tube was cut, the sample was extruded vertically using a hydraulic extruder. Initially a metal lip was created on the inside diameter of the Shelby tube during cutting. This lip caused scarring and deformation of the samples as they were extruded. To address this concern, the rate and force of the pipe cutter was lowered as it approached the center of the tube wall. Using less force allowed for a slower, less intrusive cut. In addition, another solution to this concern was to not apply locking pressure to one tube clamp until the pipe cutter started to penetrate the tube. This allowed the forces of the pipe cutter to expand the Shelby tube metal lengthwise rather than radially.

Once the samples were extruded, they were placed into a pressure chamber for the TXL test. Table 4.4 provides a detailed list of the laboratory equipment used. Figures 4.18 and 4.19 provide photographs of the laboratory equipment setup. Early in the project, the TXL volume change was measured using the burettes on the pressure boards. During the project, two volume change devices were incorporated into the data acquisition system. The data acquisition system incorporated Labview[®] software and the main interactive screen developed is provided in Figure 4.20. The data acquisition hardware, pressure transducers, displacement potentiometers, and water de-aerator were also upgraded during the project.

TABLE 4.4 – Triaxial test equipment list

Equipment Type	Manufacturer	Part Number
2 Load cells – 2000lb	ARTECH Industries, Inc.	20210-2K [SN 232999; 223636]
2 Displacement potentiometers	Omega Engineering, Inc.	LP802-50 [SN 070737 7; 070737 14]
2 Pressure transducers	Durham Geo Slope Indicator	E-124 [SN 1274, 1276; 1277]
2 Load frames	ELE International	Digital Tritest
3 Pressure boards	ELE International	1 Master Control Panel 2 Auxiliary Control Panels
Water DeAerator	Nold	
2 Volume change devices	Humbolt	HM-2315
Computer with data acquisition system (Labview [®])		
Data acquisition card	National Instruments	PCI-6024E
Data acquisition module	National Instruments	USB-6210
3-inch pipe cutter	Ridge Tool Company	RIGID No. 30
Fabricated during project	Shelby tube cutter frame	
	6-inch long, 2.5-inch diameter piece of wood	
	0.5-inch thick, 2.8-inch diameter clear piece of plastic	



Figure 4.18 – Triaxial laboratory equipment setup

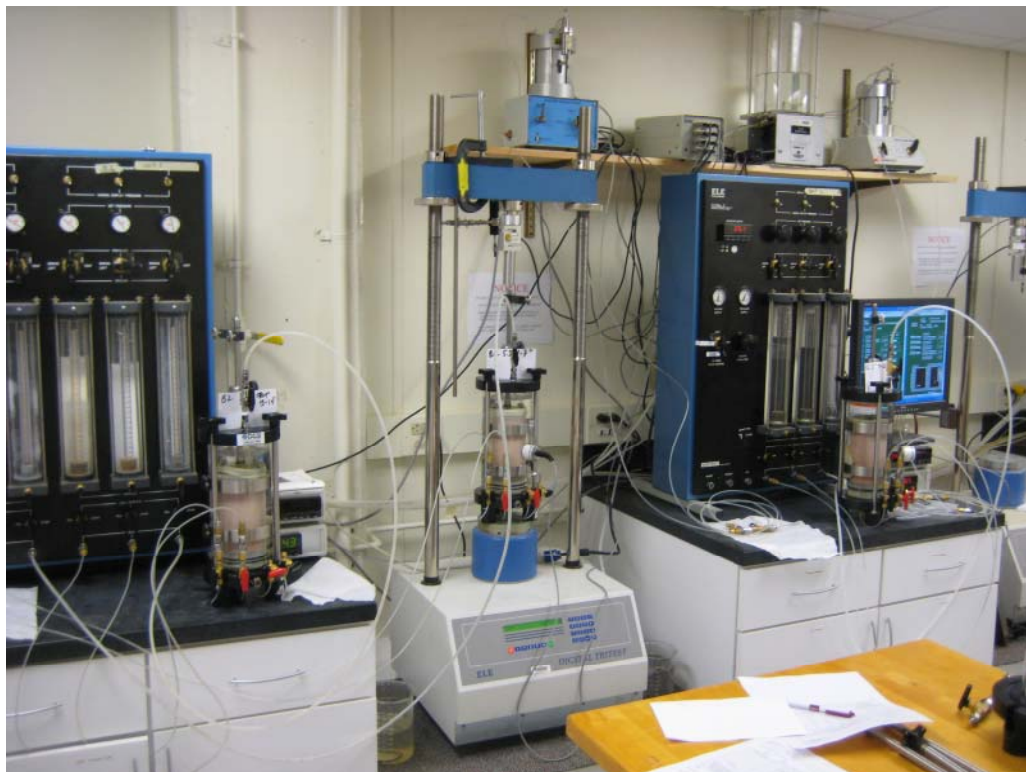


Figure 4.19 – Triaxial laboratory equipment setup with pressure chambers

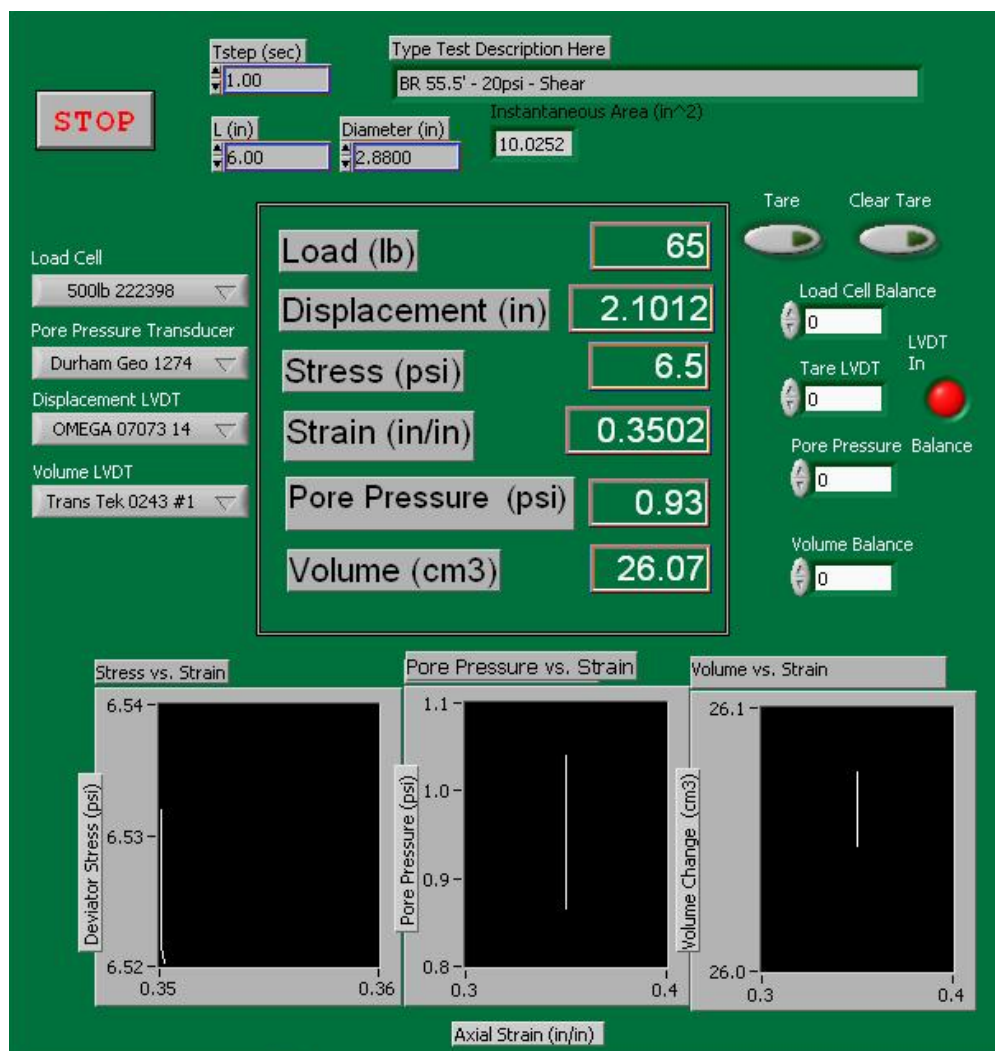


Figure 4.20 – Main Labview[®] input/output screen

During the TXL set-up, the sample height, diameter, and weight were measured. After the set-up, a bottom to top vacuum saturation was performed for approximately 30 minutes. The chamber and back pressures were then raised to test conditions incrementally by 10 psi every 30 minutes and based on the B-value procedure of ASTM D 4767. Once the test conditions were met, the pressures were maintained for a minimum of 12 hours to back-pressure saturate the sample. The final saturation was evaluated based on achieving a B-Value greater than 0.90. The consolidation portion was

then performed and evaluated to confirm completion of primary consolidation. The TXL strain rate was evaluated for each test based on the time factor for 50% triaxial consolidation (t_{50}), the consolidated undrained triaxial shear ASTM D 4787, and consolidation drained triaxial shear work by Bishop and Henkel (1957). Although the tests could technically have been run faster, the strain rate for every test was 0.01 inches per minute based on a maximum strain rate of 10% strain per hour.

Generally, the tests were run to failure based on deviator stress versus axial strain results or a minimum of 15% axial strain. As the research developed, some tests were run to a displacement of 16% strain. The additional data was recorded to evaluate the post failure behavior. After failure, the samples were removed from the pressure chamber, weighed wet, dried in a convection oven, and weighed dry. The samples were then stored in plastic bags for possible future use. Generally, two TXL tests were run simultaneously. APPENDIX F provides the reference checklist used during the research and the blank datasheet used.

4.2.1 TRIAXIAL SHEAR DATA REDUCTION

To simplify the data reduction, a semi-automated spreadsheet was created to take the data acquisition output and produce useful plots with minimal data adjustment. The main data adjustment was zeroing the piston load cell output by removing the uplift pressure. The amount removed was based on the cross sectional area of the piston and the individual test chamber pressure.

The final TXL graph was effective normal stress versus shear stress. Figures 4.21 and 4.22 present the graph for the 19.4-foot and 49.4-foot depths, respectively. The Mohr-Coulomb failure envelope is the tangent to the failure circles for three TXL tests.

The slope and y-intercept of this line correlate to the effective angle of internal friction (ϕ') and cohesion (c'), respectively. ϕ' and c' are labeled in Figure 4.22.

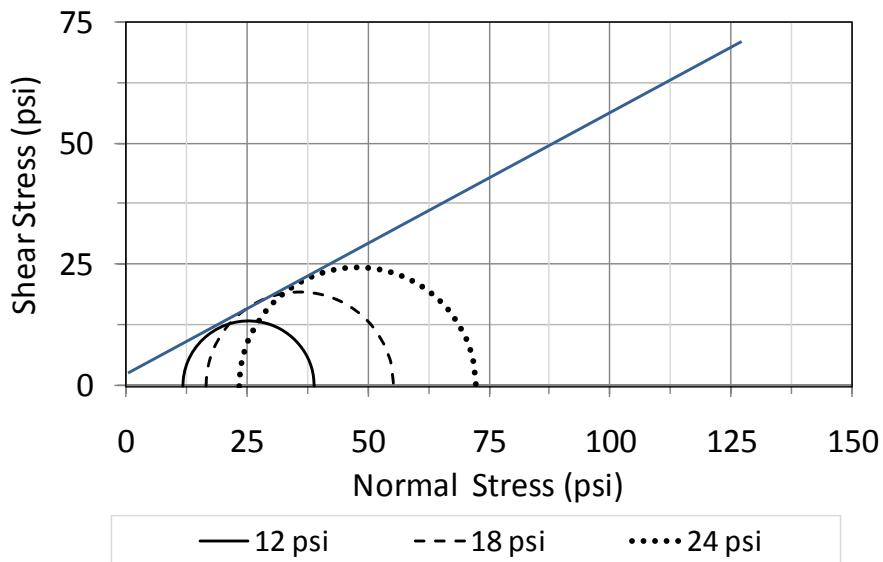


Figure 4.21 – Triaxial shear test data at PC1 19.4'

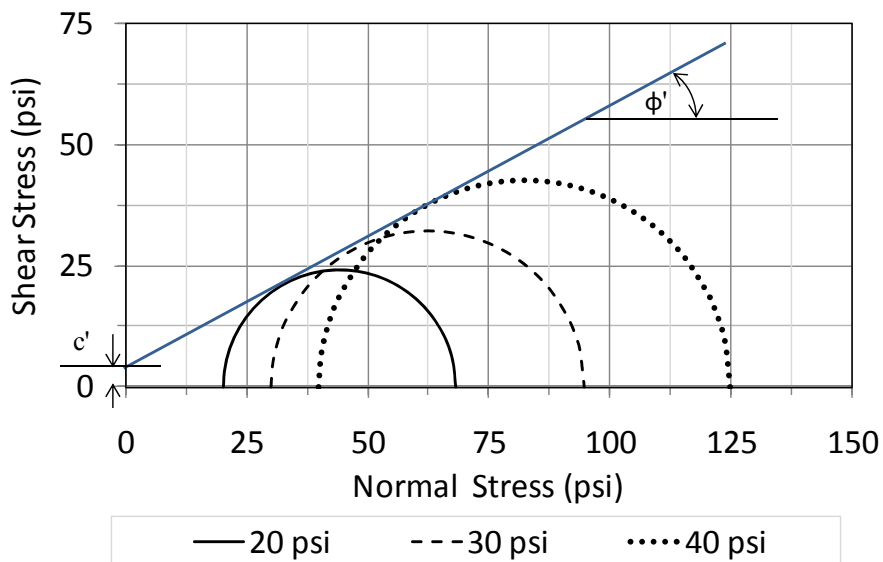


Figure 4.22 – Triaxial shear test data at PC1 49.4'

4.3 Interface Shear Testing

The specific INT procedure details were finalized during the study. The INT tests were conducted with a GeoTac direct shear machine with a shear box fabricated specifically for the research. The outside dimensions (length, width, and height) of the shear box were based on the requirements of the GeoTac load system. The inside diameter of the top half of the shear box was built to hold an undisturbed sample directly out of the Shelby tube. The bottom half of the shear box was built to mimic the surface roughness of the SPT split-spoon and Shelby tube samplers. The drawings used to fabricate the shear box are provided in Figures G1 through G5 of APPENDIX G.

An integral part of the shear box fabrication was to measure the surface roughness of the samplers. Two shear box bottom halves were fabricated, one to mimic the split-spoon sampler and one to mimic the Shelby tube sampler. The roughness of four surfaces was measured; SPT split-spoon sampler, Shelby tube sampler, steel block, and galvanized sheet metal. The surface roughness was evaluated in the Mechanical Engineering Precision Lab at UNCC. The equipment used to measure roughness was a Taylor-Hobson Form Talysurf 120L and is shown in Figure 4.23. Photos of the test set-up for the SPT-T split-spoon sampler are shown in Figures 4.24 and 4.25. Only the SPT split-spoon sampler and steel block surfaces were used in this study. The Shelby tube and galvanized sheet metal surfaces were measured for possible future tests.



Figure 4.23 – Taylor-Hobson Form Talysurf 120L



Figure 4.24 – SPT-T split-spoon sampler test set-up – Overall view

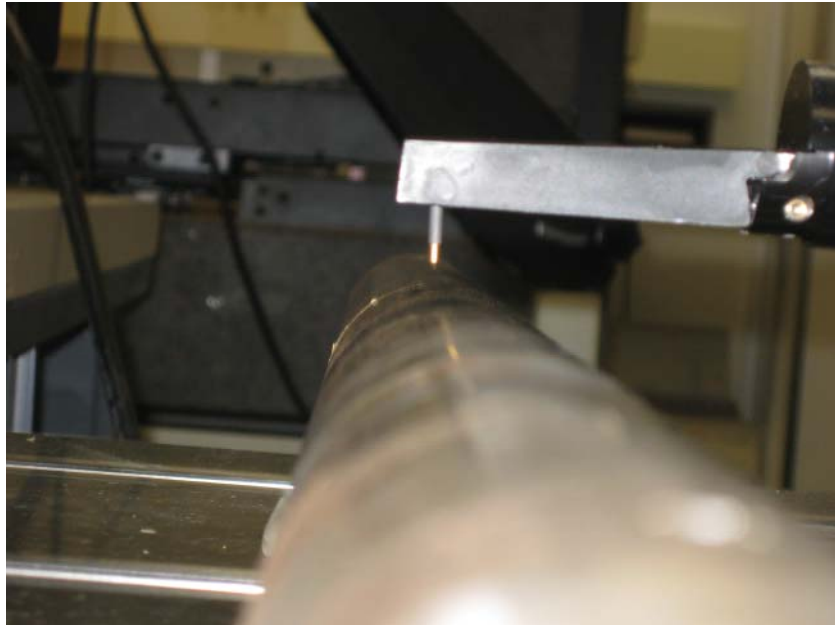


Figure 4.25 – SPT-T split-spoon sampler test set-up – Measurement tip

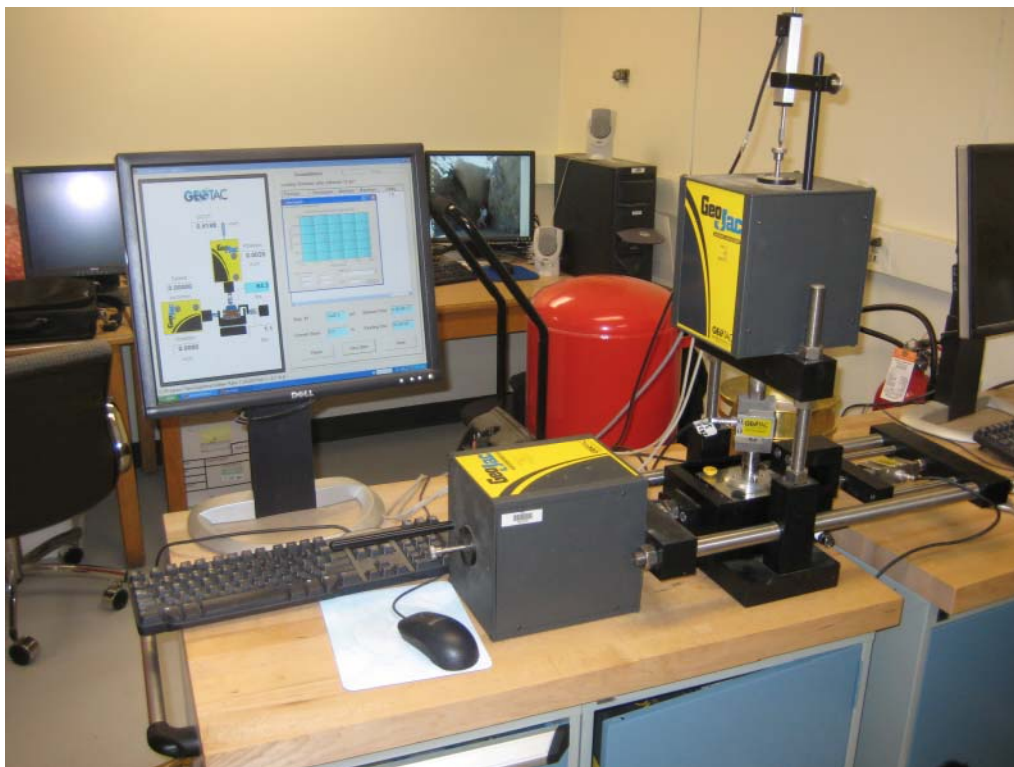
The details of the roughness test equipment were a 2 micrometer tip radius, 1 mN tip force, 5 millimeter scan length (4 millimeter minus 0.5 millimeter removed at beginning and end), 0.5 mm/sec scan rate, circle form adjustment for samplers, and tilt removal for flat surfaces. The main evaluated outputs were the roughness average (R_a) and the quadratic roughness (R_q). Additional measurements of roughness included skewness (R_{sk}), kurtosis of surface heights (R_{ku}), and average of peak to valley height in each cut-off length (R_t).

The split-spoon sampler and steel block surfaces were measured at 10 random locations. The results are provided in Table 4.5 and the output graphs from the testing are provided in Figures H1 through H22 of APPENDIX H. Tests were performed on the Shelby tube and galvanized sheet metal surfaces, but no INT tests were performed on them. The steel block roughness fell between the two extremes; therefore it was deemed an accurate representative of the split-spoon sampler.

Table 4.5 – SPT-T Roughness Data

Surface	Direction of Roughness	Number of Data Points	Ra (μm)		Rq (μm)	
			Average	StDev	Average	StDev
NEW Split-spoon Sampler	Circumference	3	2.69	1.04	3.59	1.21
USED Split-spoon Sampler	Circumference	10	5.94	1.73	6.58	2.93
Steel Block - Side 1	Parallel to INT	10	3.25	1.18	3.99	1.41

The fabricated shear box was then placed into the GeoTac testing system. The testing system consisted of two load frames (vertical and horizontal) along with associated load cell and displacement gages. Figure 4.26 shows the GeoTac testing system.

**Figure 4.26 – GeoTac load system**

To develop the specific details of the INT test, three factors needed to be finalized which included sample preparation, sample thickness, and interface shear rate. To develop the final test conditions, numerous preliminary tests were performed on back-up soil samples collected at the field sites. Figure 4.27 shows the results used to establish the sample thickness of the final tests and Table 4.6 provide the trend lines. The thickness tests were run at a shear rate of 0.01 inches per minute. The INT was finalized to be 0.5-inches thick.

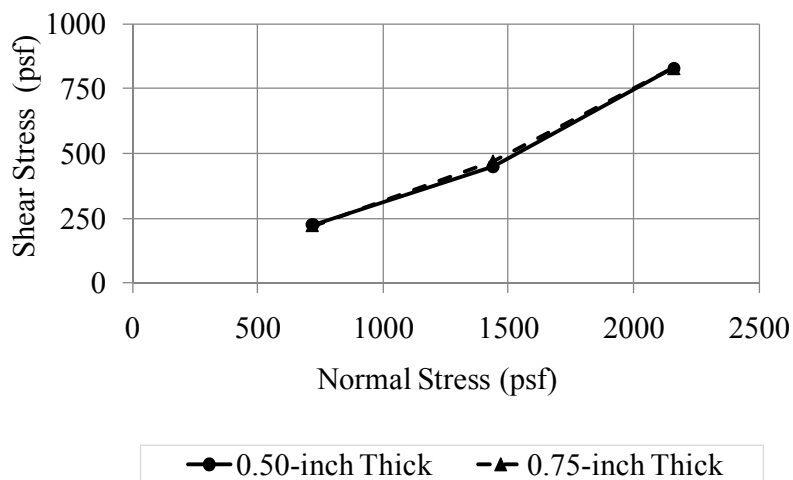


Figure 4.27 – INT thickness development results – Sand

Table 4.6 – INT thickness development trend lines– Sand

Test	Trend line equation	c_a (psf)	δ (°)
0.50-inch Thickness	$y = 0.4194x - 102.0$	- 102.0	25.55
0.75-inch Thickness	$y = 0.4229x - 102.7$	- 102.7	25.79

Figure 4.28 provides the results used to establish the shearing rate of 0.01 inches per minute. The residual soil rate tests were performed on an extra Shelby tube collected

at the Browne Road site at a depth of 12-feet. The 0.01 inches per minute rate was also chosen since it matched the TXL shearing rate. Table 4.7 provides the rate analysis trend lines.

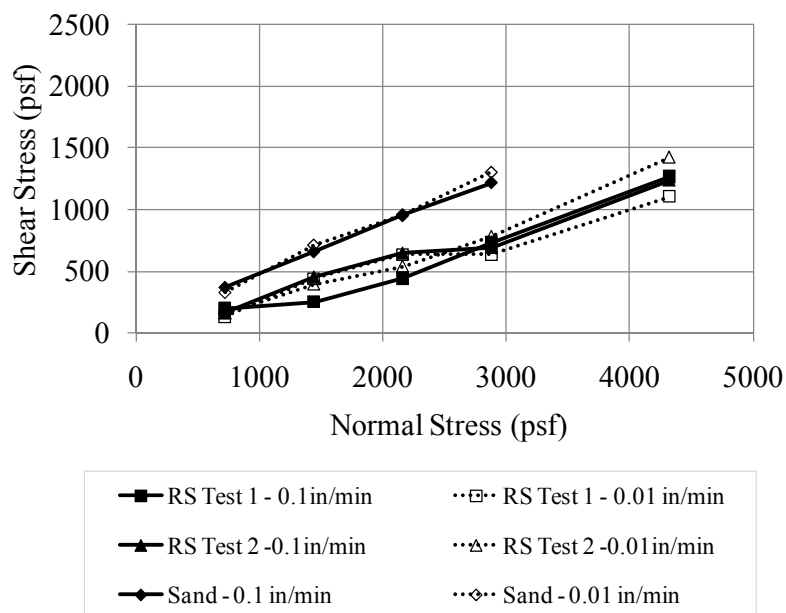


Figure 4.28 – INT rate development results

Table 4.7 – INT rate development results

Test	Trend line equation	c_a (psf)	δ ($^\circ$)
RS Test 1 - 0.1in/min	$y = 0.3109x - 138.2$	- 138.2	18.41
RS Test 1 - 0.01 in/min	$y = 0.2499x + 14.1$	14.1	14.62
RS Test 2 -0.1in/min	$y = 0.279x - 3.3$	- 3.3	16.41
RS Test 2 -0.01in/min	$y = 0.3457x - 138.7$	- 138.7	20.64
All Residual Soil Data	$y = 0.3546x - 90.5$	- 90.5	21.21
Sand - 0.1 in/min	$y = 0.3931x + 92.5$	92.5	23.76
Sand - 0.01 in/min	$y = 0.4394x + 35.0$	35.0	26.93

To prepare the sample, a 3-inch section of the Shelby tube was cut using the same method used for the TXL sample preparation. Generally, the samples were hand extruded out of the 3-inch section into a 0.5-inch Shelby tube section using a 1-inch long,

2.8-inch diameter piece of plastic along with a 6-inch long, 2.5-inch diameter piece of wood. A 6-inch by 6-inch piece of sheet metal was placed on top of the sample as it was extruded. A small weight was also added on top of the sheet metal to apply a confining pressure to the top of the sample. All of the tools were used to confine the sample and to keep the sample from deforming or cracking. Once 0.5-inches of the sample were extruded, a wire saw was used to cut the sample between the two Shelby tube sections. Another 6-inch by 6-inch piece of sheet metal was pressed into the gap cut by the wire saw. The sample was transported inside the 0.5-inch section, between the two pieces of sheet metal. One piece of sheet metal was removed at a time in order to inspect the surface and to perform any treatment. Next, the sample was extruded out of the 0.5-inch section and elevated on top of the 2.8-inch piece of plastic and with a 6-inch long, 2.5-inch diameter piece of wood. The complete connected shear box was flipped over and lowered over the soil sample, inserting the sample into the shear box. Care was taken to ensure that the proper side of the soil sample was in contact with the shear box interface surface.

A piece of filter paper and porous stone were then added into the shear box. The height and diameter of the sample were measured during the set-up. Next the shear box was placed into the GeoTac loading system and the test was initiated. As the vertical (normal) load was applied, water was introduced into the system and the shear box was submerged. A five minute consolidation was performed based on instantaneous time-deformation curves and soil data collected during the TXL test. After the consolidation step, a shear force was applied to the top half of the shear box. The tests were generally

stopped when the horizontal displacement versus shear stress curve leveled off, or at 0.25-inches of displacement.

4.3.1 INTERFACE SHEAR DATA REDUCTION

Every interface shear test had a similar trend as the insitu torque tests. Figure 4.29 provides an example of the INT shear stress versus horizontal displacement results.

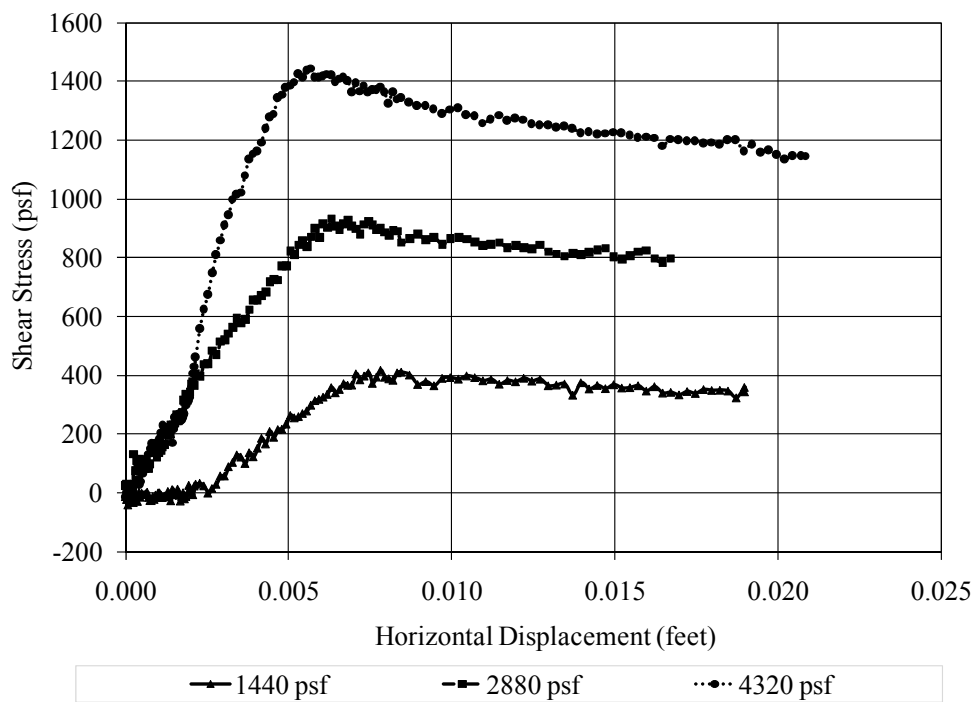


Figure 4.29 – INT GeoTac output results example for BR 60.5’

The shear stress data was zeroed based on assuming that there was no shear force at the beginning of test. The peak and steady state values were determined from the raw data. The normal stress and peak shear stress values were then plotted and an example is

provided in Figure 4.30. The slope and y-intercept were determined using a spreadsheet and corresponded to the interface friction angle (δ) and adhesion (α), respectively.

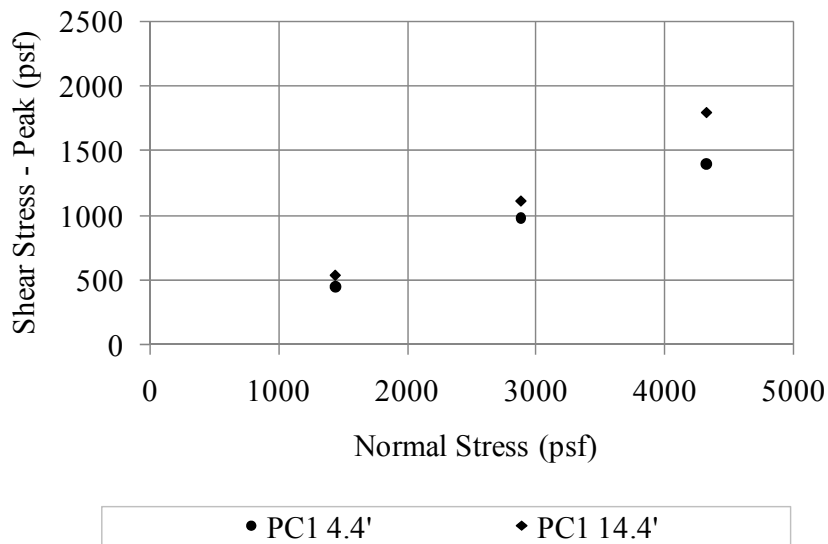


Figure 4.30 – INT intermediate results example – PC1 4.4' and 14.4'

4.4 Geologic Analyses

The geologic analyses included wet and dry color, gravel percent, consistence (stickiness and plasticity), and texture. A complement to the research came from a Geologic Society of America grant supporting petrographic analysis. The objective of the grant was to investigate the influence of saprolite geology on shear strength. Through the grant, nine thin sections were fabricated and analyzed. Six thin sections (PC1 4.4', 14.4', 24.4', 34.4', 44.4', and 54.4') were undisturbed soil and three thin sections (PC1 4.4', 24.4', and 54.4') were remolded soil.

The thin section slides were fabricated by Texas Petrographic Services, Inc. Due to the friable nature of residual soils, extreme care was used to prepare and ship the

undisturbed soil samples to the thin section fabricator. For all nine of the thin sections, 0.5-inch segments of a new Shelby tube were cut and polished. The undisturbed soil samples were manually extruded from the insitu Shelby tubes into the 0.5-inch segments. Once the soil completely filled the segment, the soil was cut using a wire saw. The remolded soil samples were also compacted inside the 0.5-inch Shelby tube segments to the undisturbed unit weight, water content, and void ratio. The 0.5-inch segments were then vacuum sealed inside plastic bags using a Kenmore® “Seal-n-Save” food preserver. The vacuum provided the soil with strength during shipping. After the samples were received by the thin section fabricator, the plastic bags were removed and the samples were impregnated twice with clear epoxy. The epoxy type was Epon Resin 815 C and was purchased from Miller-Stephenson Chemical. The final thin section slides were 2-inches by 3-inches.

Petrographic analysis of remolded residual soil was performed in order to investigate the different geotechnical and geologic changes induced by soil disturbance. In addition to the petrographic analysis, remolded consolidated drained triaxial tests were performed at the same three depths as the remolded thin sections (PC1 4.4’, 24.4’, and 54.4’). The remolded triaxial tests were performed according to ASTM D 4767. The triaxial samples were made to the insitu unit weight and Table 4.8 summarizes the unit weights.

Table 4.8 – Undisturbed and remolded unit weight summary

Depth feet	Unit Weight (pcf)	
	Undisturbed	Remolded
4.4	92.92	93.67
24.4	116.35	110.20
54.4	121.20	114.96

4.4.1 GEOLOGIC DATA REDUCTION

An Olympus CX31-P polarizing microscope was used to analyze a representative portion of each thin section. Figure 4.31 provides a photograph of the microscope used. Two resources were used to identify the minerals present: “Introduction to Optical Mineralogy” by W. D. Neese and “Atlas of rock-forming minerals in thin sections” by W. S. Mackenzie and C. Guilford.



Figure 4.31 - Olympus CX31-P polarizing petrographic microscope

The petrographic analysis used point counts to document mineralogy and grain characteristic. The point count categories included groundmass, clay bleb, quartz, and minor minerals. Using a mechanical stage, points were obtained at 1 mm intervals. In the event of a point lying on a large void in the slide, the point was discarded and the next

point was taken until 100 points were obtained for each slide. The large voids were believed to be created by disturbance during soil preparation and epoxy expansion during thin section fabrication.

Additionally, a total of eight photomicrographs of each slide were taken using four magnifications (2X, 4X, 10X, 20X) and two light types (cross polarized (CP) and plain polarized (PP)). The 2X photomicrographs for both CP and PP are provided for each slide in Figures I1 through I9 of APPENDIX I.

CHAPTER 5: RESULTS AND DISCUSSION

During the course of the field and laboratory testing, an array of soil parameters for residual soils was examined. Some of the parameters, which are commonly analyzed for transported soils, were blow-count (N), corrected blow-count (N'_{60}), cohesion (c'), triaxial effective angle of internal friction ($\phi'_{(TXL)}$) and insitu water content (w_{INSITU}). Additional non-typical parameters were the maximum torque ($T_{MAX(SPT)}$ and $T_{MAX(STT)}$), steady state torque ($T_{SS(SPT)}$ and $T_{SS(STT)}$), force to push Shelby tube (F_{PUSH}), adhesion (c_a), and interface friction angle (δ). Secondary parameters included total unit weight (γ_{MOIST}), liquid limit (LL), plasticity index (PI), clay fraction, initial void ratio (e_o), porosity (n), dilatometer modulus (E_D), horizontal stress index (K_D), material index (I_D), dilatometer undrained shear strength (s_u), dilatometer effective angle of internal friction ($\phi'_{(DMT)}$), and standard penetration test effective angle of internal friction ($\phi'_{(SPT)}$). The intermediate calculations included triaxial shear strength (τ_{TXL}) and interface shear strength (τ_{INT}). The geologic parameters included soil color dimensions of hue (H), value (V), and chroma (C), along with petrographic point count percentages (groundmass, clay blebs, quartz, and minor minerals). Beyond the primary research objective, the data were evaluated for secondary relationships, potential trends, and index systems for residual soils. The following evaluations are organized into three categories: raw data, theoretical, and empirical.

5.1 Raw Data Evaluation

The raw and reduced data for PC1 is provided in APPENDIX B, BR is provided in APPENDIX C, and PC2 is provided in APPENDIX D. The organization of the results in the appendices is summarized in Table 5.1, along with associated figure and table numbers. Summary graphs of the raw insitu and laboratory parameters versus depth for each site are provided in Figures 5.1 through 5.6.

Table 5.1 – Data contained in APPENDICES B, C, and D

Site Location	PC1	BR	PC2
APPENDIX	B	C	D
Figure and Table Numbers			
Torque			
Insitu SPT-T Torque versus Time Figures	B1	C1	D1
Insitu STT-T Torque versus Time Figures	B2	C2	D2
Triaxial Shear Figures			
Deviator Stress versus Axial Strain	B3 – B13	C3 – C15	D3 – D9
Volumetric Stain versus Axial Strain			
Principal Stress Ratio versus Axial Strain			
Consolidation Time-Deformation Curves			
Normal stress versus Axial Stress			
p' versus q			
Interface Shear			
Normal Stress versus Shear Stress Tables	B1	C1	D1
Normal Stress versus Shear Stress Figures	B14	C16	D10
Geotechnical Soil Classification			
Soil Classification Data Table	B2 – B3	C2 – C3	D2 – D3
Grain-size Distribution Curves	B15	C17	D11
Geologic			
Soil Color Data Tables	B4	C4	D4
Soil Classification Data Tables	B5	C5	D5
Dilatometer			
Data versus Depth Data Output Table	B6	C6	D6

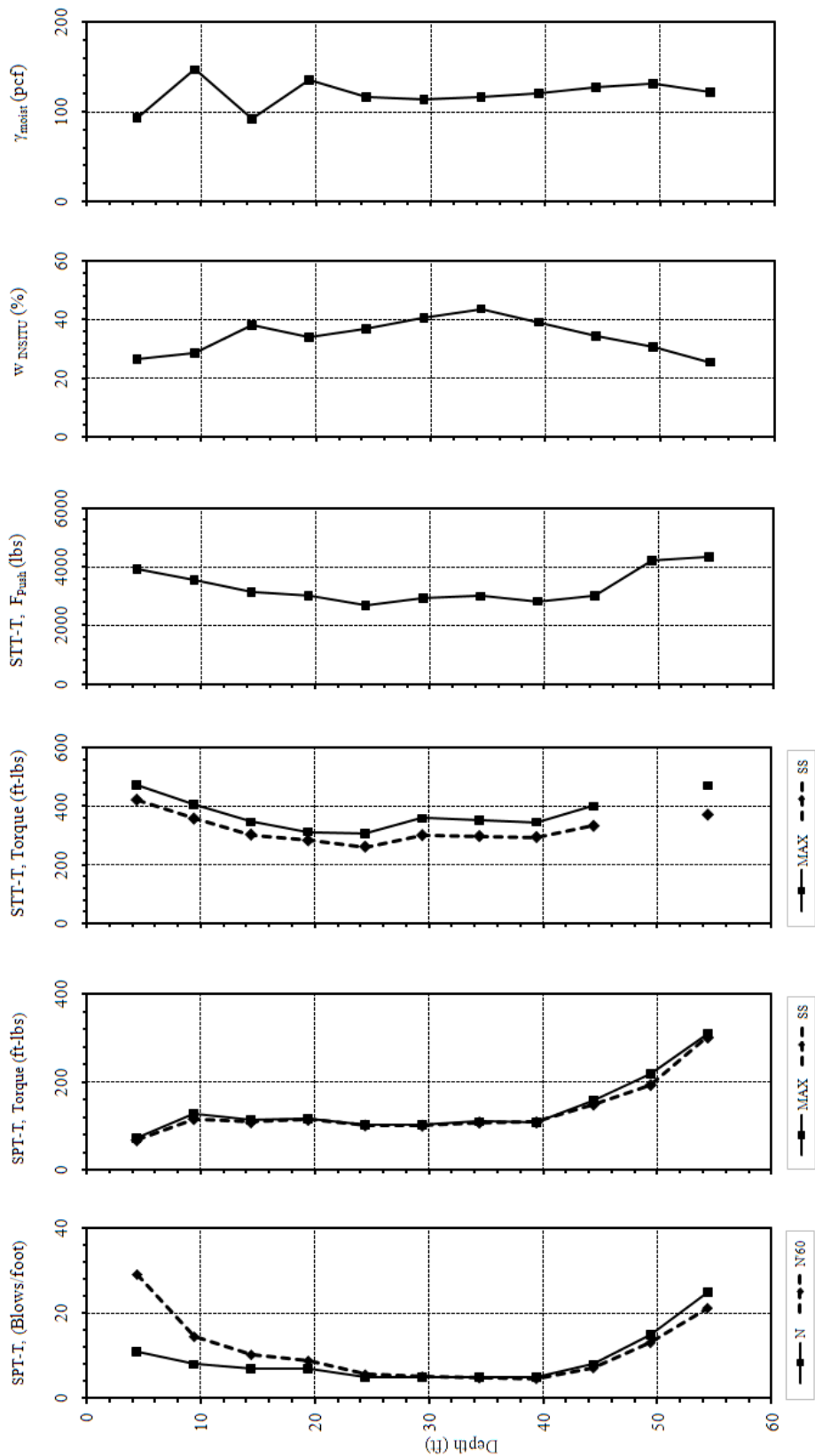


Figure 5.1 – PC1 Insitu parameters versus depth

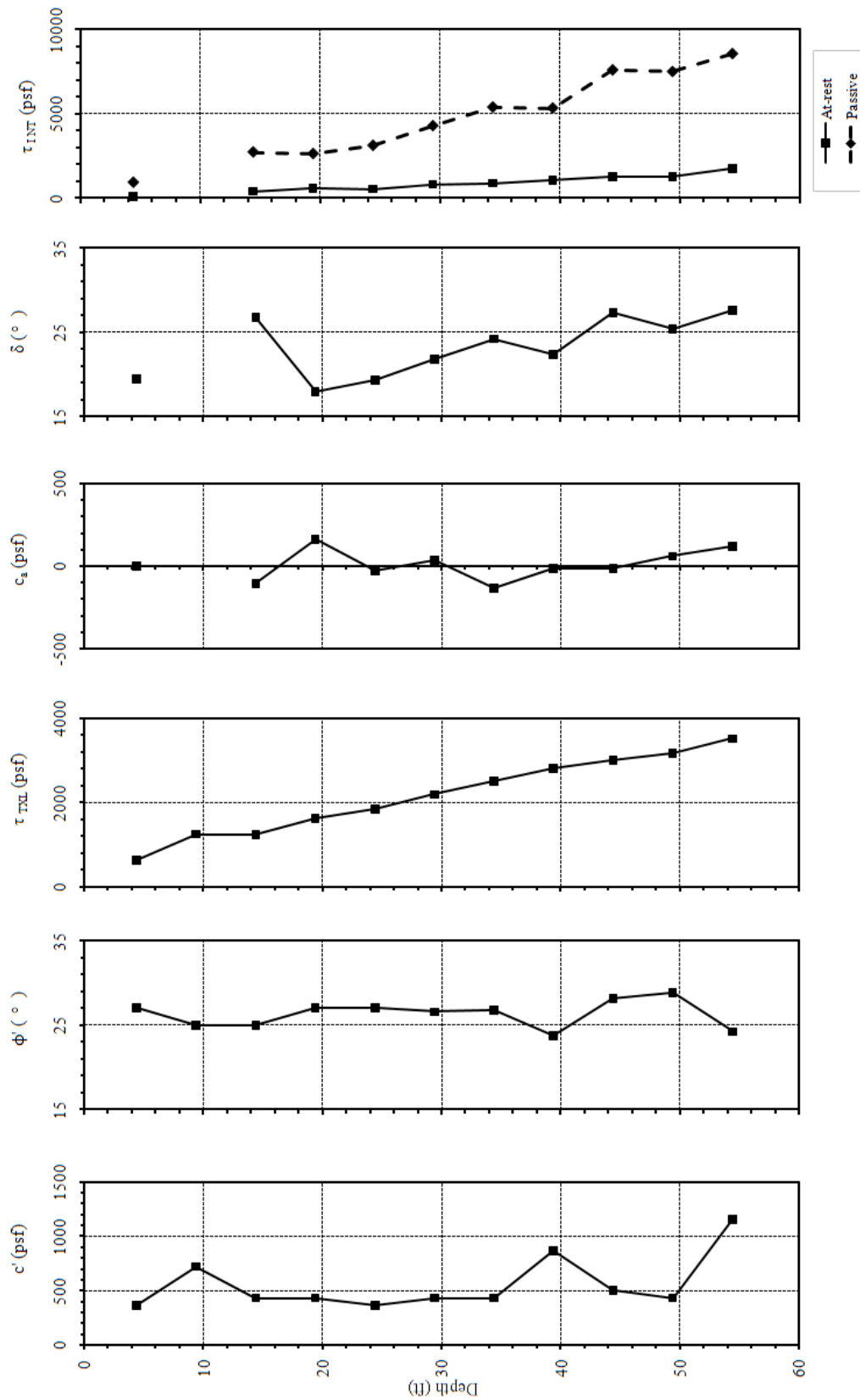


Figure 5.2 – PC1 Laboratory parameters versus depth

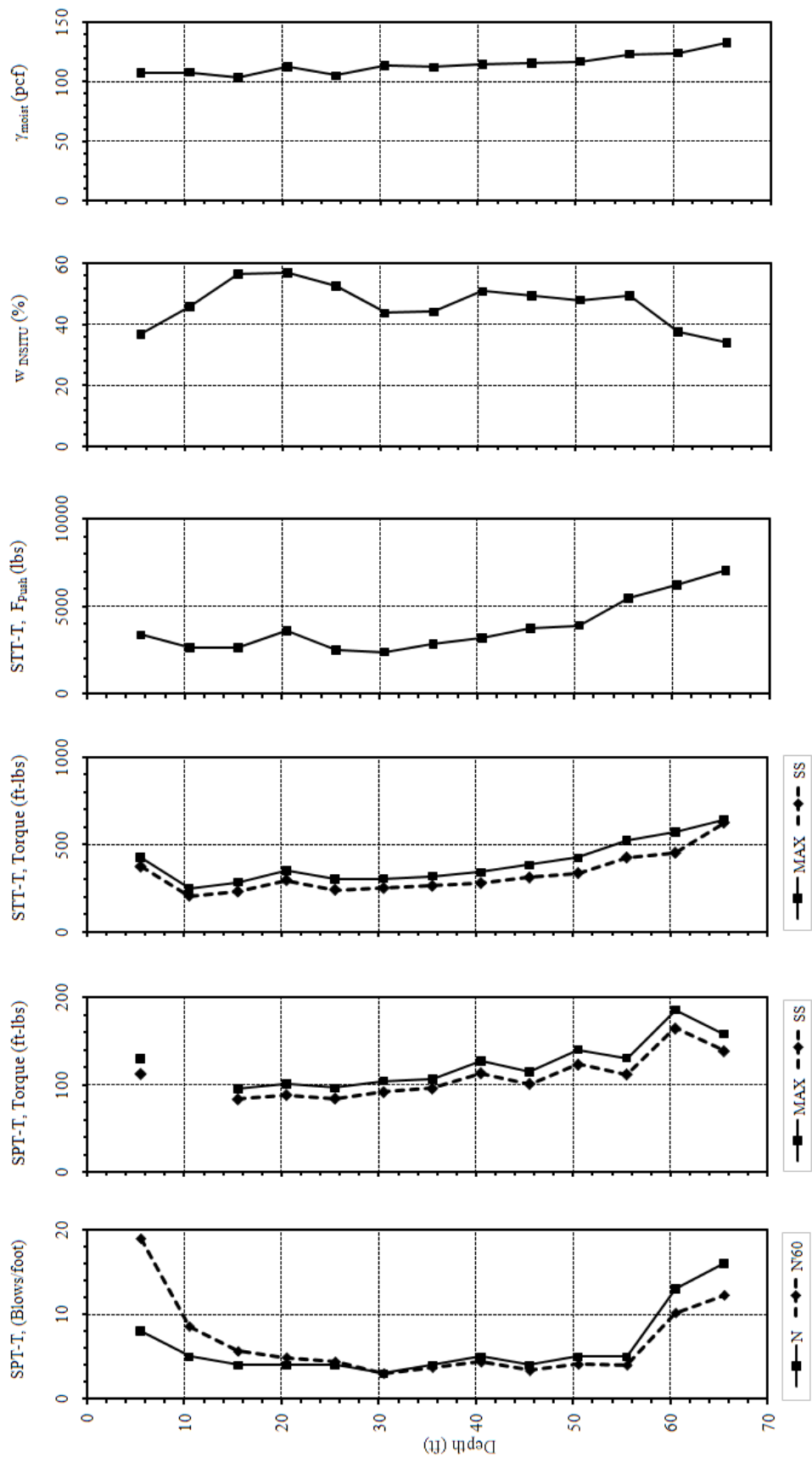


Figure 5.3 – BR Insitu parameters versus depth

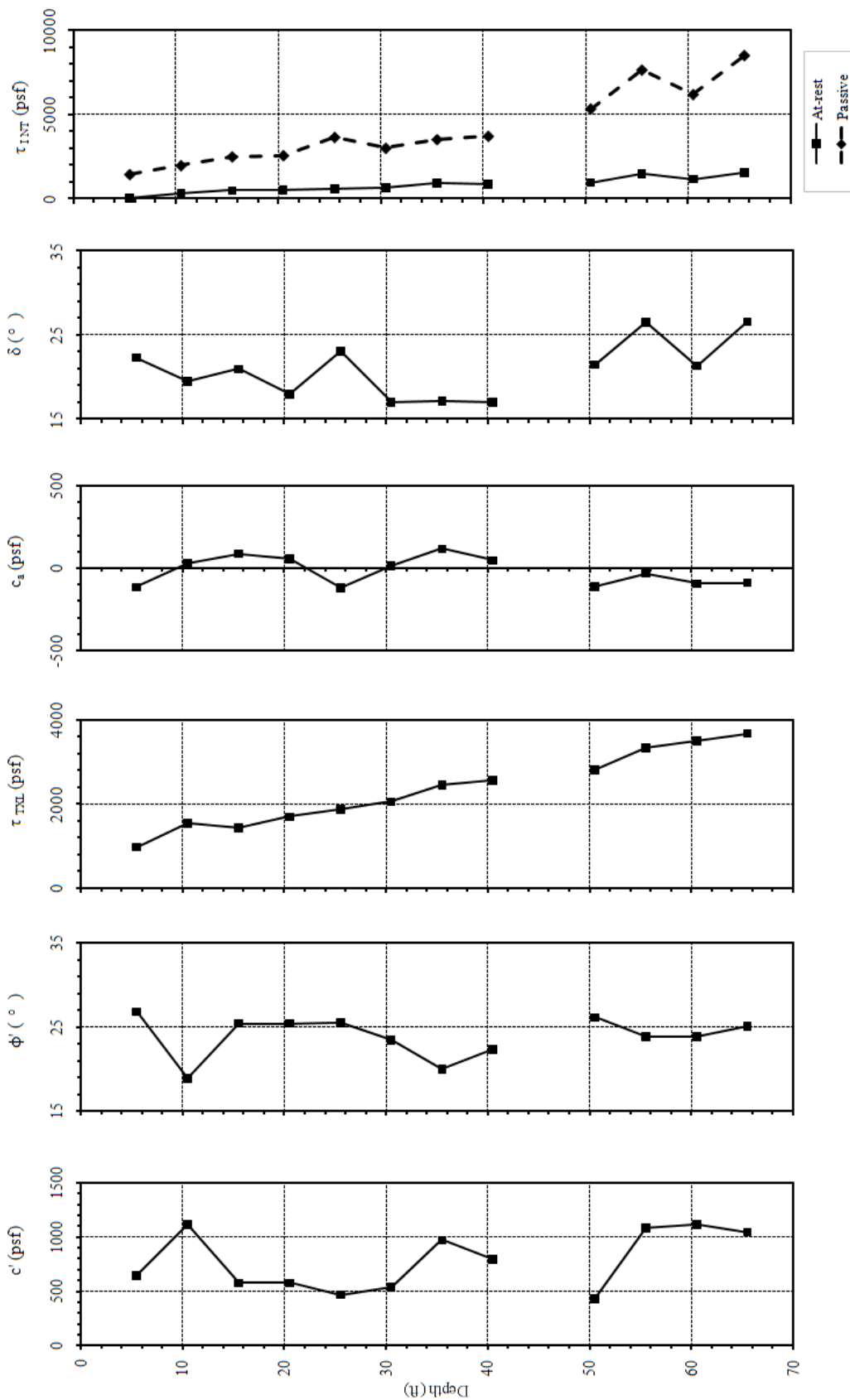


Figure 5.4 – BR Laboratory parameters versus depth

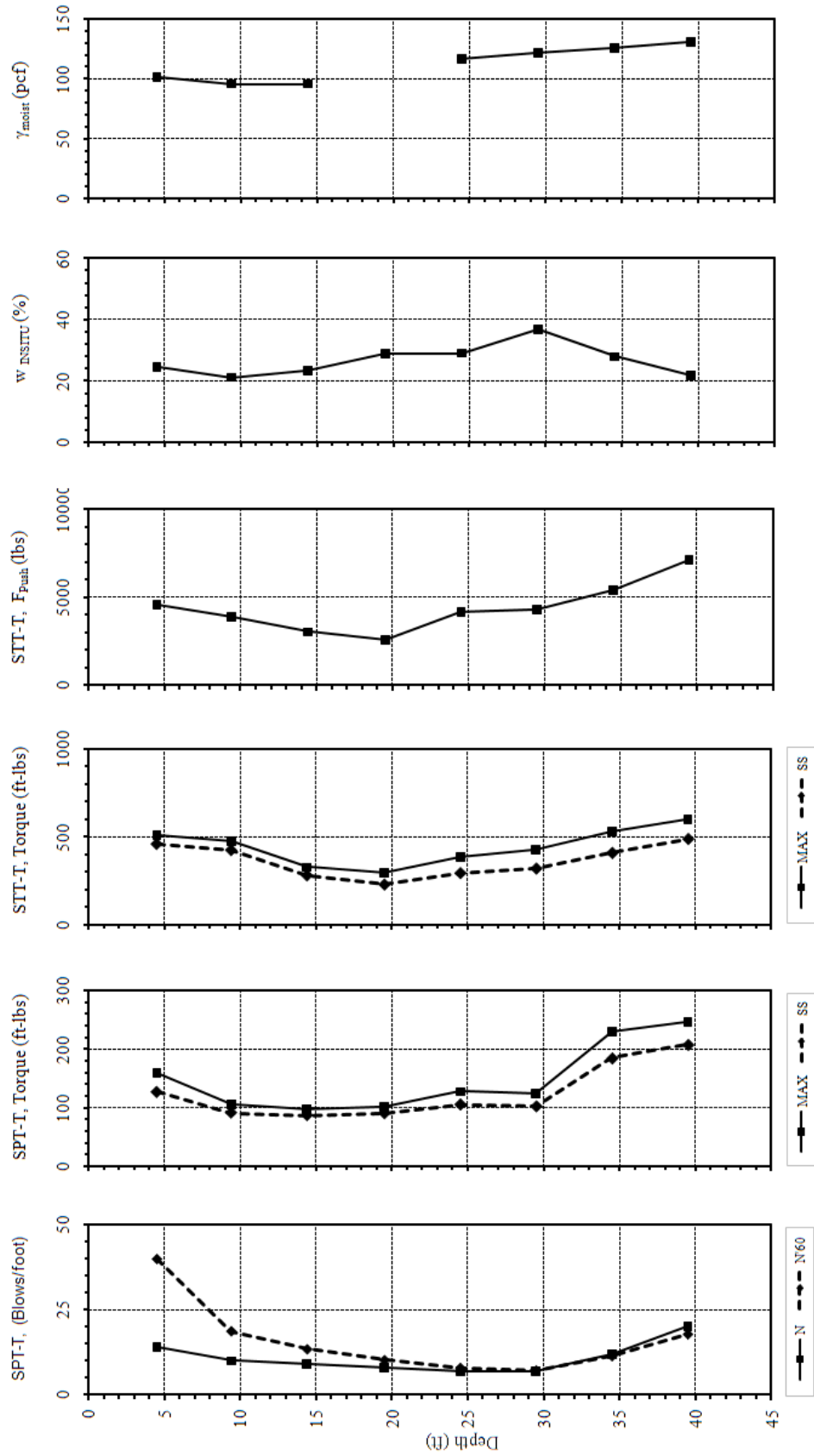


Figure 5.5 – PC2 Insitu parameters versus depth

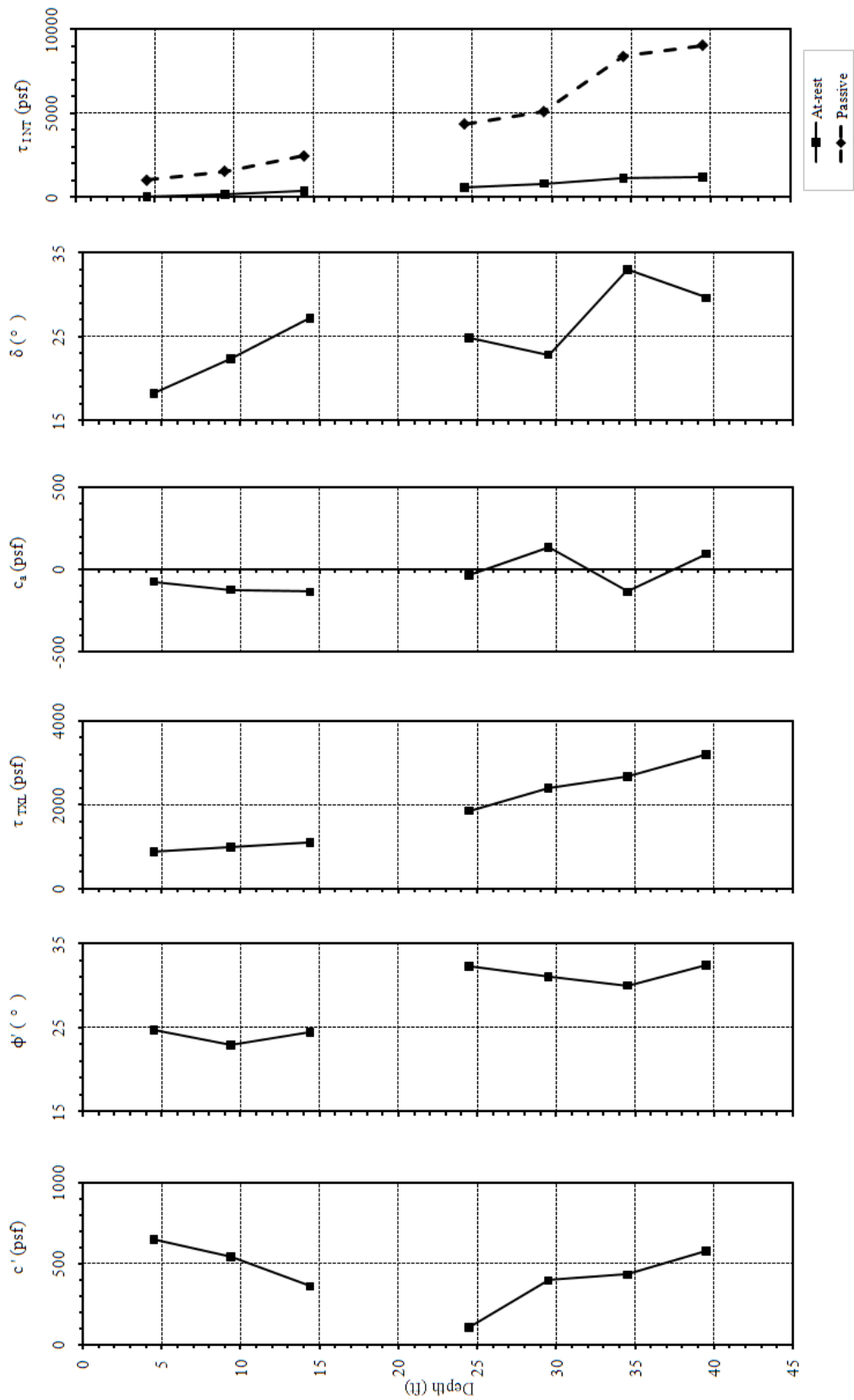


Figure 5.6 – PC2 Laboratory parameters versus depth

The groundwater table was 34.0-feet at PC1, 42.6-feet at BR, and 28.3-feet at PC2. There were various trends versus depth as illustrated in Figures 5.1 through 5.6. The insitu water content at PC1 and PC2 generally increased from the ground surface to the groundwater table depth, and then decreased (Figures 5.1 and 5.3). At BR, w was more sporadic (Figure 5.5). N'_{60} , T_{MAX} , T_{SS} , and F_{PUSH} had trends that decreased from the ground surface and then increased, with the highest values at the deepest depth (Figures 5.1, 5.3, and 5.5). These trends correlated to typical weathering profiles of residual soils.

The γ_{MOIST} , τ_{TXL} , and τ_{INT} generally increased downward from the ground surface throughout the profile (Figure 5.1 through 5.6). c' , c_a , ϕ' , and δ showed no clear trend throughout the profile (Figure 5.2, 5.4, and 5.6). In addition, the c' and ϕ' exhibited an inverse relationship. As the friction angle rose, the cohesion fell, and vice versa. However, the torque values were relatively constant with depth (between 95 and 150 ft-lbs), suggesting a limited direct relationship to vertical effective stress (Figures 5.2, 5.4, and 5.6).

Since c_a was based on only three INT tests at each depth, the confidence of the c_a results was low. Performing several (10-20) tests would improve the confidence, although performing several tests would require additional soil. The negative (below zero) c_a values were contributed partly to the limited number of tests. In addition, the INT tests appeared to be sensitive to small changes in soil type, surface cut, and water content. These soil conditions seemed to change spatially and temporally reducing the ability to evaluate a single set of soil conditions. Additionally, the INT load cells were recalibrated to confirm the results. While there were small offsets, they were not

significant. The maximum (Max), minimum (Min), average (Ave), standard deviation (StDev), and coefficient of variance (CoV) of the geotechnical parameters at each site are provided in Table 5.2. In addition, the data for the BR 45.5' depth were removed from the analysis based on insitu disturbance during sampling and poor laboratory results.

Table 5.2 – Geotechnical parameter summary by site

	Site	Max	Min	Ave	StDev	CoV
N'_{60} (blow/ft)	PC1	29.1	4.6	11.3	7.8	69.0
	BR	18.9	3.0	7.0	4.7	67.1
	PC2	39.8	7.2	15.8	10.6	67.1
$T_{MAX(SPT)}$ (ft-lbs)	PC1	309.4	71.3	139.2	67.8	48.7
	BR	185.3	94.9	124.7	28.6	22.9
	PC2	246.8	97.3	148.9	58.6	39.4
$T_{SS(SPT)}$ (ft-lbs)	PC1	300.9	67.2	133.0	64.0	48.1
	BR	164.4	82.9	109.4	25.3	23.1
	PC2	207.5	86.8	124.2	46.4	37.4
$T_{MAX(STT)}$ (ft-lbs)	PC1	470.4	307.5	376.7	58.4	15.5
	BR	640.8	246.1	393.3	124.8	31.7
	PC2	598.0	294.2	441.9	104.0	23.5
$T_{SS(STT)}$ (ft-lbs)	PC1	420.0	260.7	321.1	48.1	15.0
	BR	624.5	204.0	329.3	121.4	36.9
	PC2	484.4	226.5	359.9	93.9	26.1
w (%)	PC1	43.69	25.38	34.34	6.01	17.5
	BR	57.09	33.90	46.38	7.58	16.3
	PC2	36.91	21.13	26.72	5.16	19.3
γ_{MOIST} (pcf)	PC1	146.7	92.1	119.4	16.4	13.7
	BR	132.6	103.5	115.0	8.6	7.5
	PC2	130.6	95.7	112.4	14.6	13.0
c' (psf)	PC1	1152.0	360.0	556.4	251.7	45.2
	BR	1116.0	432.0	780.0	269.5	34.6
	PC2	648.0	108.0	437.1	178.1	40.7
ϕ' (°)	PC1	28.8	23.7	26.3	1.6	6.1
	BR	26.8	18.9	23.9	2.4	10.0
	PC2	32.4	22.9	28.3	4.1	14.5
δ (°)	PC1	27.6	17.9	23.2	3.57	15.4
	BR	26.58	16.99	20.88	3.4	16.3
	PC2	32.97	18.23	25.45	4.93	19.4

The following raw data, theoretical, and predictive evaluations are presented based on their ability to meet the objective. The trend lines, R^2 values, and Pearson r coefficients were derived using a spreadsheet. The R^2 values provided a measure of how well the trend line approximates the real data points. The Pearson r coefficient indicated the extent of a linear relationship between two data sets. The Pearson p -values indicate the significance of the Pearson r coefficient based on sample size and a two-tailed normal distribution. The p -values were determined using a statistics calculator and values less than 0.05 were considered 95% significant (Soper, 2009). All of these statistical evaluations should only be used to supplement engineering judgment. For example, a high correlation does not imply causation between the variables. In addition, a low correlation may be restricted by the sample size or masked by more pronounced relationship between other variables.

5.1.1 COHESION VERSUS ADHESION

The raw data evaluations were done to compare the collected data to published trends. Only the SPT-T split-spoon sampler data were analyzed because of the limited amount of soil. Figure 5.7 presents the cohesion (c') versus adhesion (c_a). No trend was expected due to negative (below zero) c_a values. The Pearson r was 0.145 and the two-tailed p -value was 0.222.

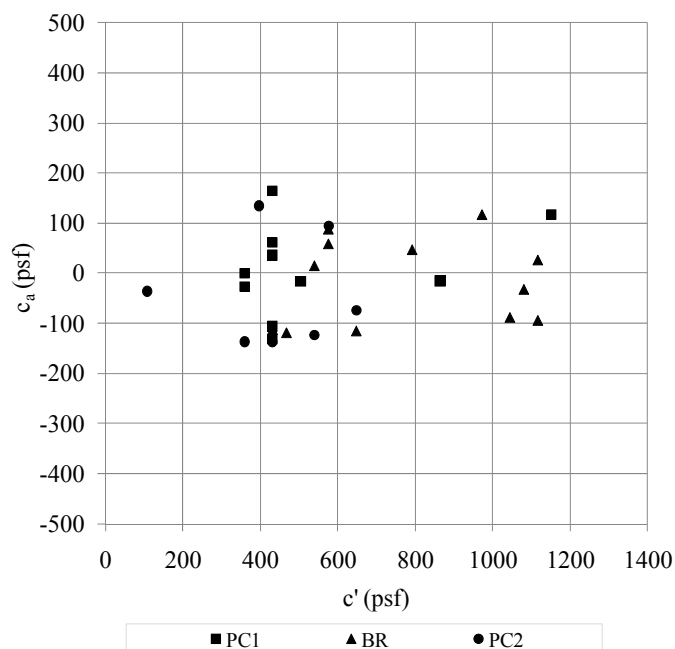


Figure 5.7 – Direct empirical correlation of cohesion (c') versus adhesion (c_a)

5.1.2 INTERNAL FRICTION ANGLE VERSUS INTERFACE FRICTION ANGLE

Figure 5.8 presents the laboratory effective angle of internal friction (ϕ') versus interface friction angle (δ). A clear relationship was observed. Based on the linear trend line, the relationship provided a 43.6 degree slope and an approximate 1:1 relationship. The Pearson r was 0.495 and two-tailed p -value was 0.003. The average interface friction reduction factor (R_i) were 0.88 at PC1, 0.89 at BR, and 0.91 at PC2,, while the published R_i values were 0.5 to 0.7 for smooth steel on sand and 0.7 to 0.9 for rough steel on sand. No interface tests have been published for residual soils. In addition, the δ values were deemed valid based on typical values of $TAN(\delta)$ such as 0.4 for rusted/rough steel pile foundation design (McCarthy, 2002). The average $TAN(\delta)$ was 0.43 at PC1, 0.38 at BR, and 0.48 at PC2.

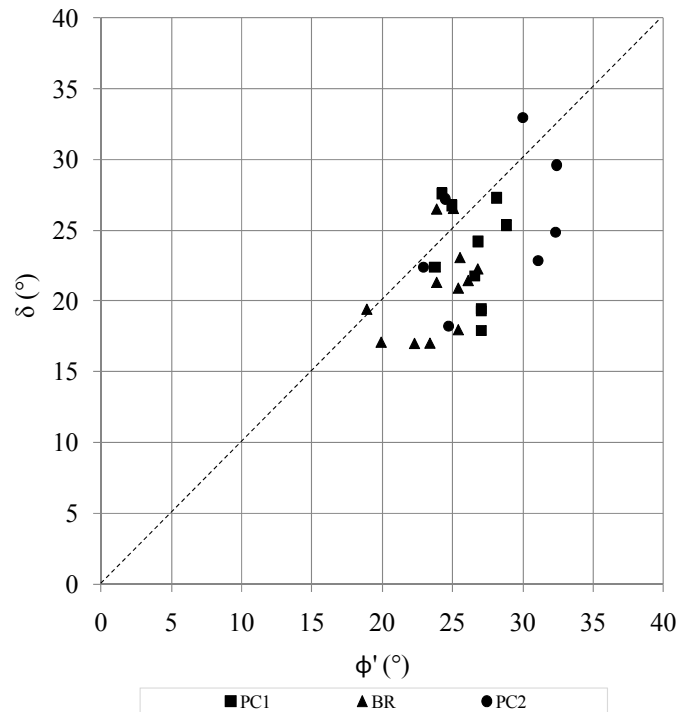


Figure 5.8 – Direct empirical correlation between ϕ' versus δ

5.2 Theoretical Evaluation

The theoretical evaluations are not predictive in nature; rather they were undertaken to determine if the developed theoretical equations and test program were accurate. Since test specimens were limited by the number of tubes collected, the evaluation was based only on the SPT-T split-spoon sampler characteristics. Figure 5.9 presents the graph of the theoretical T_{MAX} versus the T_{MAX} measured insitu. The theoretical T_{MAX} values were based on inputting the laboratory measurements from the TXL and INT tests into the developed equations. The measured adhesion (c_a) values were not used, since those values were negative (below zero) and deemed impractical. In the analysis, c_a values were estimated to be zero, which is often the case in geotechnical

design practice. The initial equations were based on the at-rest lateral earth pressure. The expected relationship was 1:1 or a 45 degree trend line. Even though the at-rest values under-predicted the insitu measurements, a trend still is evident. The linear trend line is provided in Figure 5.10.

Since the at-rest pressure evaluation under-predicts the T_{MAX} , the theoretical T_{MAX} was recomputed based on passive earth pressures. Figures 5.11 and 5.12 present the passive earth pressure evaluations. The passive earth pressure prediction over-predicted the insitu measurements. These relationships lead to the conclusion that the actual earth pressure developed during the SPT-T falls between the at-rest and passive pressure states. The earth pressure is closer to the passive pressure condition. Figure 5.13 presents both the at-rest and passive pressure conditions on the same graph. The dotted line represents the actual insitu earth pressure conditions and coefficient of lateral earth pressure (K) value. Additionally, a relationship was explored by varying c_a and K in order to better predict T_{MAX} . Ultimately, incorporating two equations ($c_a = 0.5 c'$ and $K = 0.5 K_p$, where K_p is the coefficient of passive earth pressure) provided an approximate 1:1 correlation. Figure 5.14 presents a graph of this relationship. Finally, Figure 5.15 presents the relationship incorporating two same equations without cohesion or adhesion ($c_a = 0$, $c' = 0$, and $K = 0.5 K_p$, where K_p is the coefficient of passive earth pressure).

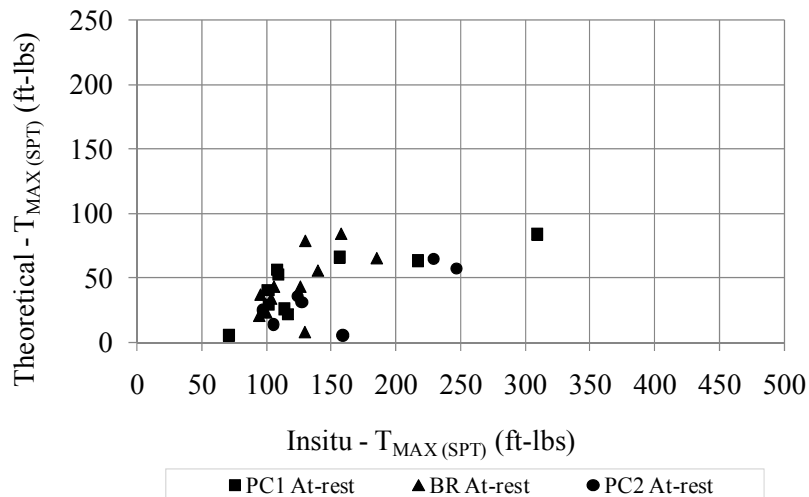


Figure 5.9 – Direct theoretical analysis between $T_{MAX(SPT)}$ [Measured Insitu] versus $T_{MAX(SPT)}$ [Theoretical based on laboratory measurements] – At-rest earth pressure

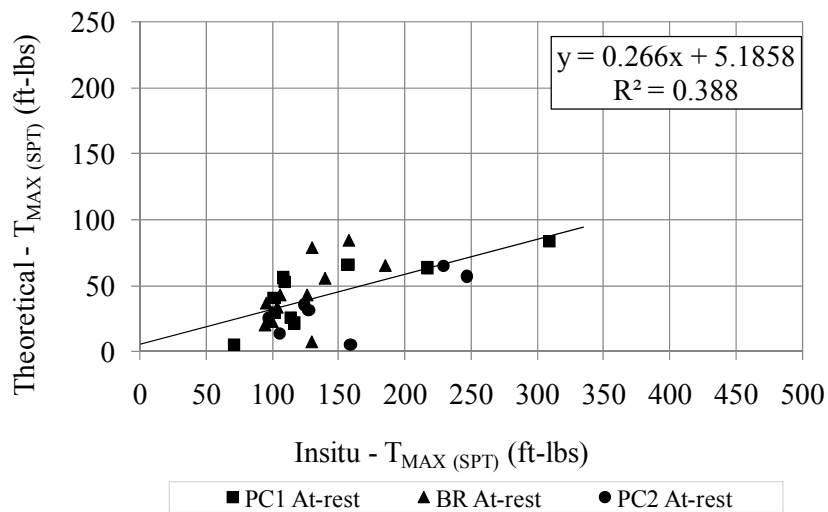


Figure 5.10 – Direct theoretical analysis between $T_{MAX(SPT)}$ [Measured Insitu] versus $T_{MAX(SPT)}$ [Theoretical based on laboratory measurements] – At-rest earth pressure – Linear trend line

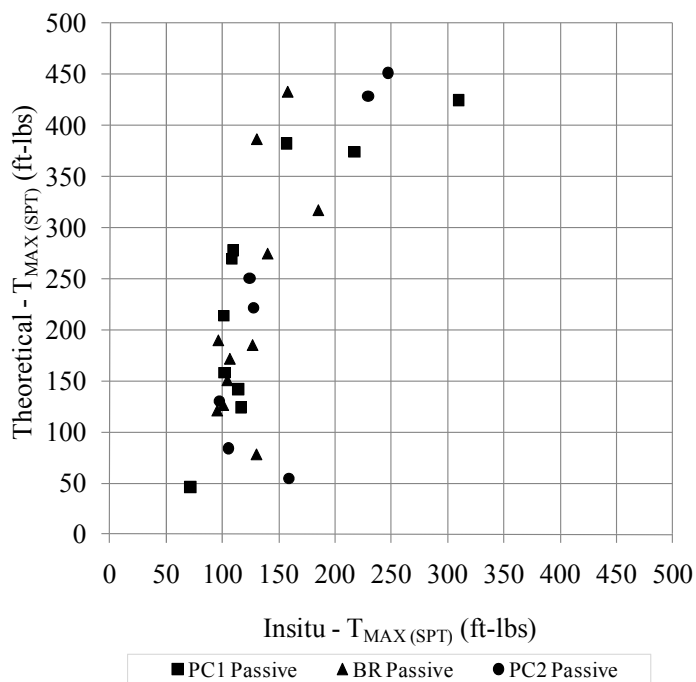


Figure 5.11 – Direct theoretical analysis between $T_{MAX(SPT)}$ [Measured Insitu] versus $T_{MAX(SPT)}$ [Theoretical based on laboratory measurements] – Passive earth pressure

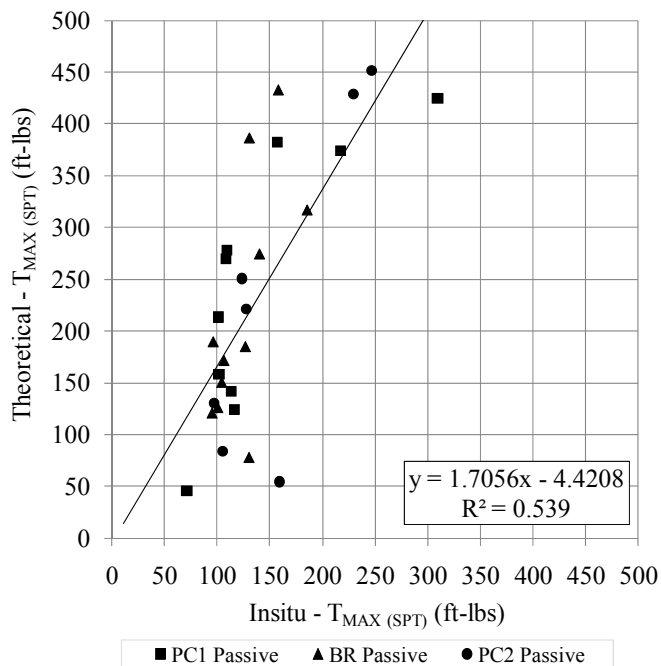


Figure 5.12 – Direct theoretical analysis between $T_{MAX(SPT)}$ [Measured Insitu] versus $T_{MAX(SPT)}$ [Theoretical based on laboratory measurements] – Passive earth pressure – Linear trend line

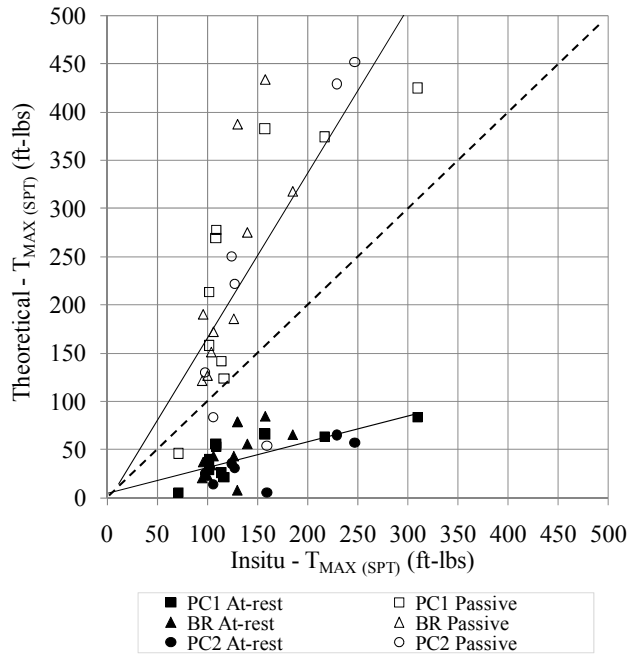


Figure 5.13 – Direct theoretical analysis between $T_{MAX(SPT)}$ [Measured Insitu] versus $T_{MAX(SPT)}$ [Theoretical based on laboratory measurements] – Both at-rest and passive pressure analyses – Linear trend lines

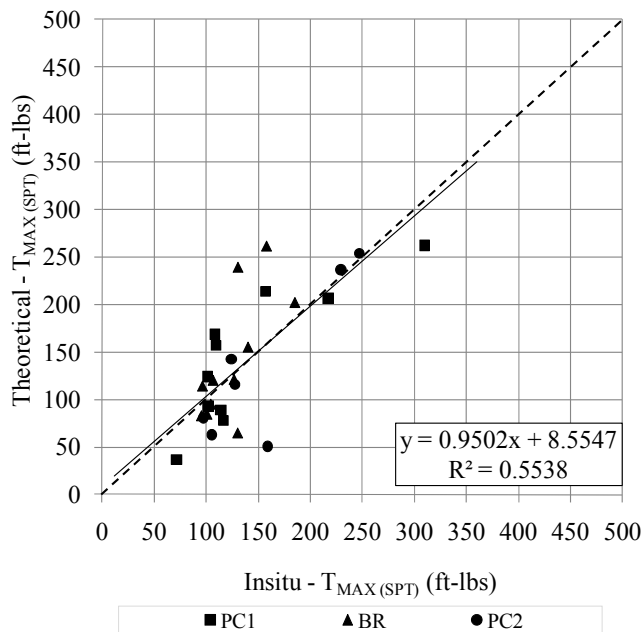


Figure 5.14 – Analysis between $T_{MAX(SPT)}$ [Measured Insitu] versus $T_{MAX(SPT)}$ [Theoretical based on laboratory measurements] – 1:1 correlation ($c_a = 0.5 c'$ and $K = 0.5 K_p$)

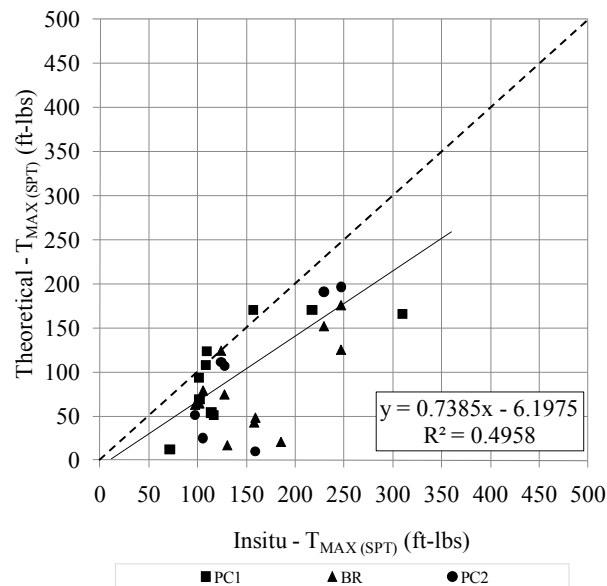


Figure 5.15 – Analysis between $T_{MAX(SPT)}$ [Measured Insitu] versus $T_{MAX(SPT)}$ [Theoretical based on laboratory measurements] – ($c_a = 0$, $c' = 0$, $K = 0.5 K_p$)

5.3 Predictive Evaluations

The predictive evaluations fell into three overall categories: 1) a single variable used to predict a single variable, 2) a single variable used to predict a multiple variable calculation, and 3) a multiple variable calculation used to predict a multiple variable calculation. The first category consists of the direct relationships and the latter two consists of the indirect relationships. Two insitu SPT-T torque values were evaluated; the maximum torque ($T_{MAX(SPT)}$) and the steady state torque ($T_{SS(SPT)}$).

5.3.1 TORQUE VERSUS COHESION

Figure 5.16 provides the graph of the insitu $T_{MAX(SPT)}$ versus the laboratory c' and Figure 5.17 shows the linear trend line. This evaluation was done to determine if the $T_{MAX(SPT)}$ would predict with confidence a value for c' . The Pearson r coefficient was

0.357 and p-value was 0.026. Figure 5.18 plots $T_{SS(SPT)}$ versus c' . No strong trends were determined from these correlations.

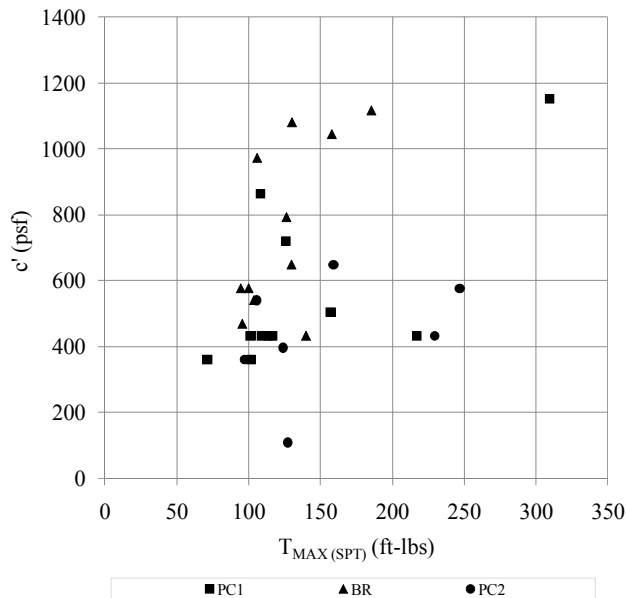


Figure 5.16 – Direct empirical correlation between $T_{MAX(SPT)}$ and c'

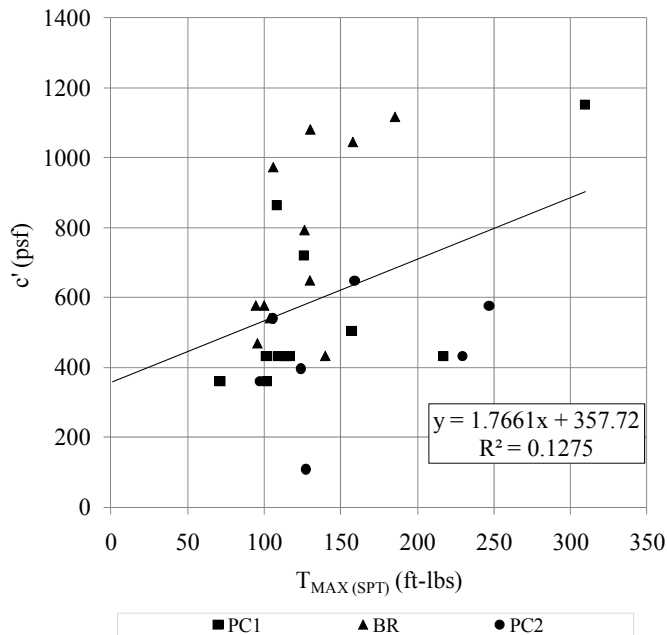


Figure 5.17 – Direct empirical correlation between $T_{MAX(SPT)}$ and c' – Linear trend line

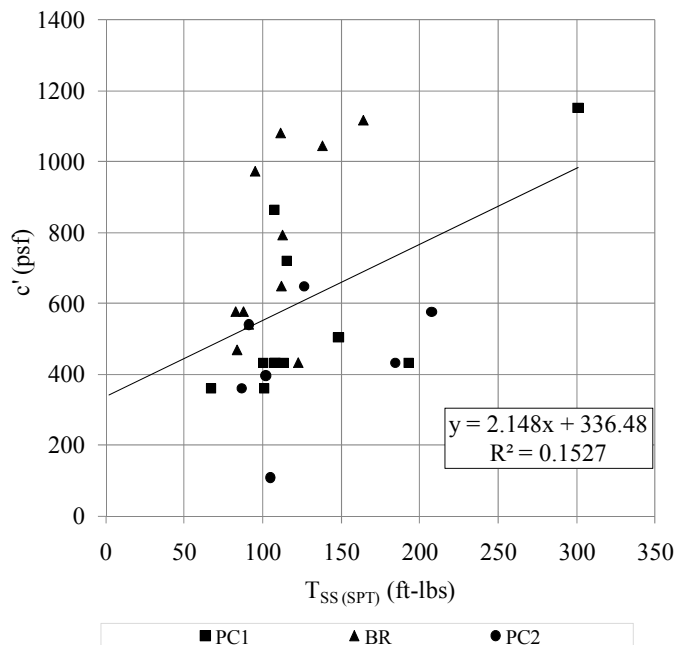


Figure 5.18 – Direct empirical correlation between $T_{SS(SPT)}$ and c'

5.3.2 TORQUE VERSUS EFFECTIVE ANGLE OF INTERNAL FRICTION

Figure 5.19 provides the correlation of T_{MAX} versus effective angle of internal friction (ϕ'). This comparison produced a cloud of data, mainly due to the relatively limited range of ϕ' values (mainly between 18.9° and 32.4°) and T_{MAX} values (mainly between 95 ft-lbs and 150 ft-lbs). The Pearson r coefficient was 0.287 and p -value was 0.062. The T_{MAX} versus ϕ' investigation showed a relationship similar to N versus ϕ' . Figures 5.20 provide the $T_{SS(SPT)}$ versus ϕ' .

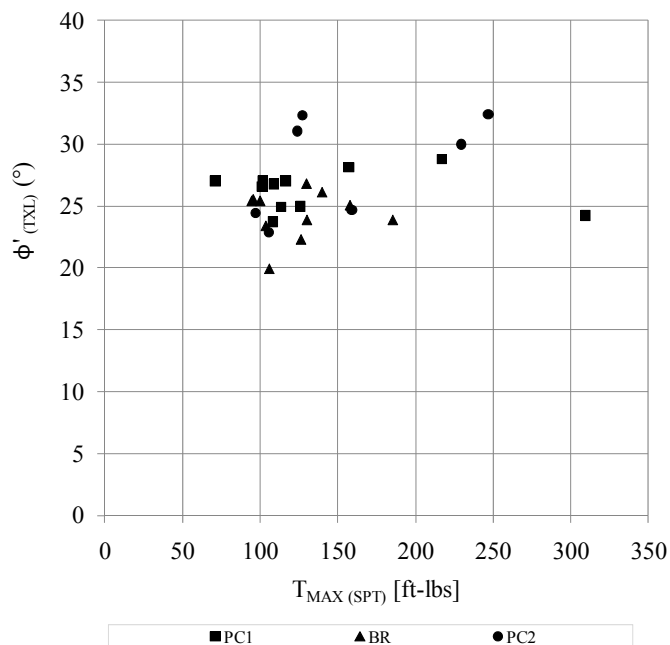


Figure 5.19 – Direct empirical correlation $T_{MAX(SPT)}$ and $\phi'_{(TXL)}$

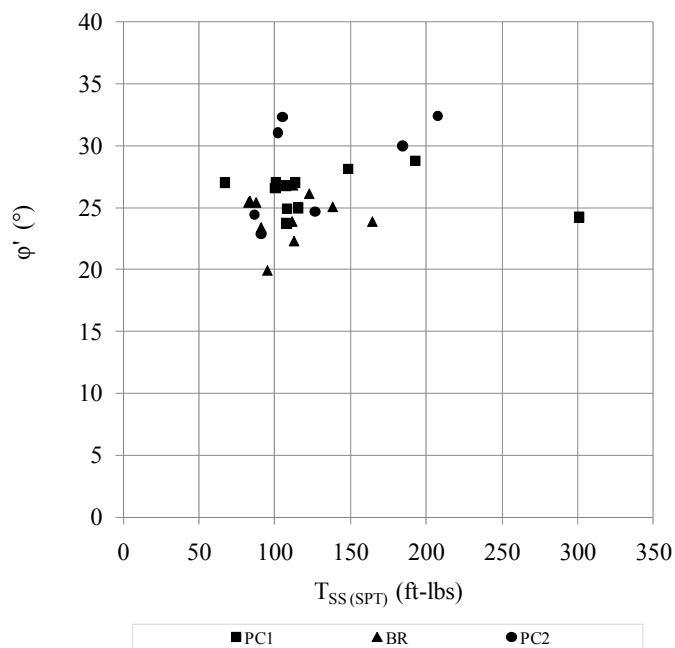


Figure 5.20 – Direct empirical correlation $T_{SS(SPT)}$ and $\phi'_{(TXL)}$

5.3.3 TORQUE VERSUS TRIAXIAL SHEAR STRENGTH

Figure 5.21 provides the correlation of T_{MAX} versus triaxial shear strength (τ_{TXL}). The Pearson r coefficient was 0.609 and p -value was 0.000. This relationship was largely dependent on depth, since a significant portion of the change in τ_{TXL} was due to the increase in vertical effective stress (σ'_v). This multi-variable indirect relationship does illustrate that visual trends do exist based on depth and through the weathering profile, although the individual parameters may not directly correlate. Figure 5.22 provides the $T_{SS(SPT)}$ versus τ_{TXL} .

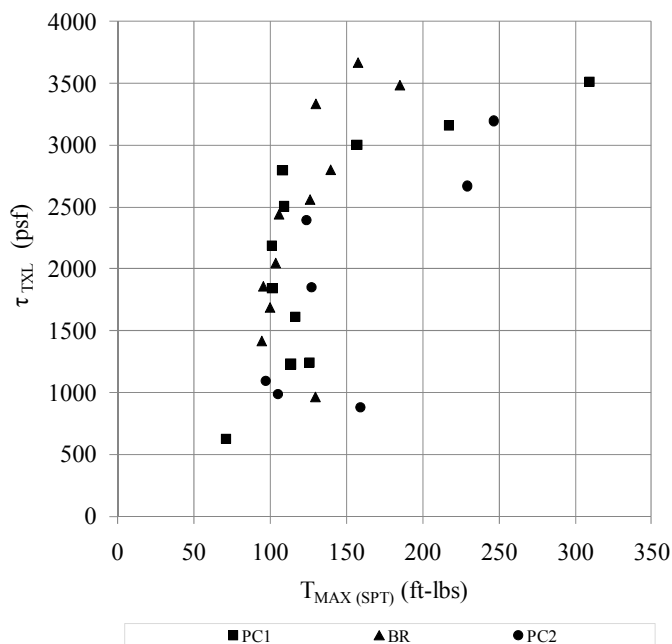


Figure 5.21 – Indirect empirical correlation between $T_{MAX(SPT)}$ and τ_{TXL}

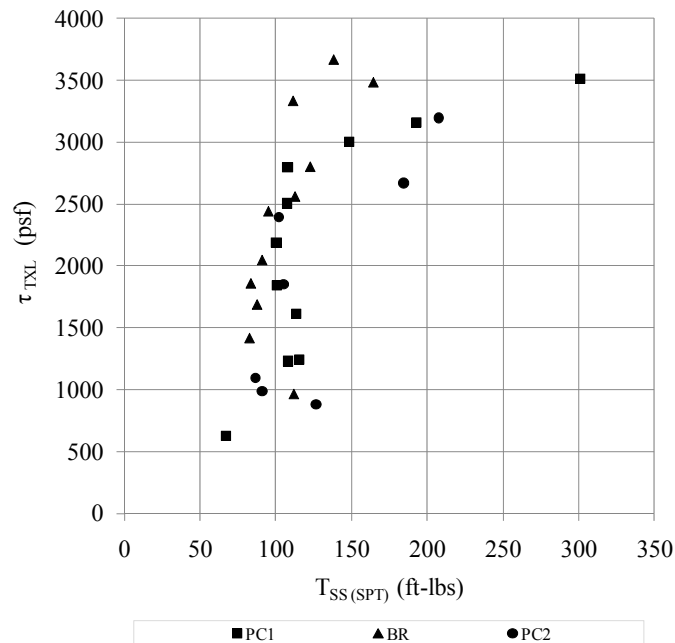


Figure 5.22 – Indirect empirical correlation between $T_{SS(SPT)}$ and τ_{TXL}

5.4 Additional Geotechnical Evaluations

During this research, a large data set was collected to provide detailed site characterizations of the three research sites. An in-depth analysis was completed to determine any secondary relationships, potential trends, and index systems for residual soils. Since the published trends were for transported soils, interpretations for this data were done with respect to residual soils. Figures 5.23 through 5.28 present the additional geotechnical and dilatometer parameters versus depth. The geotechnical parameters include the insitu water content (w_{INSITU}), liquid limit (LL), plasticity index (PI), initial void ratio (e_o), and porosity (n). The dilatometer parameters include the dilatometer modulus (E_D), horizontal stress index (K_D), material index (I_D), undrained shear strength ($s_{u(DMT)}$), and the effective angle of internal friction ($\phi'_{(DMT)}$).

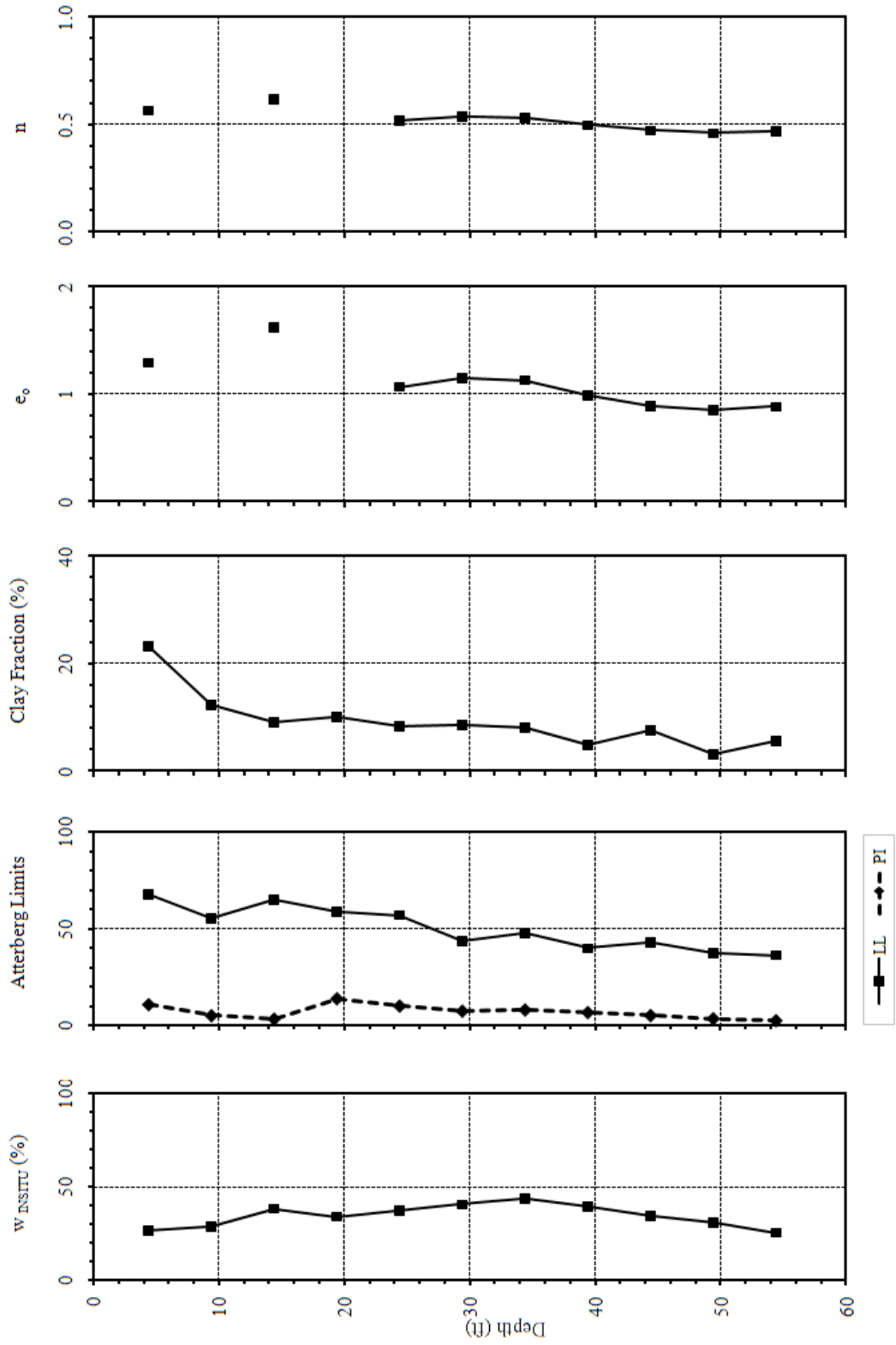


Figure 5.23 – PC1 Additional geotechnical parameters versus depth

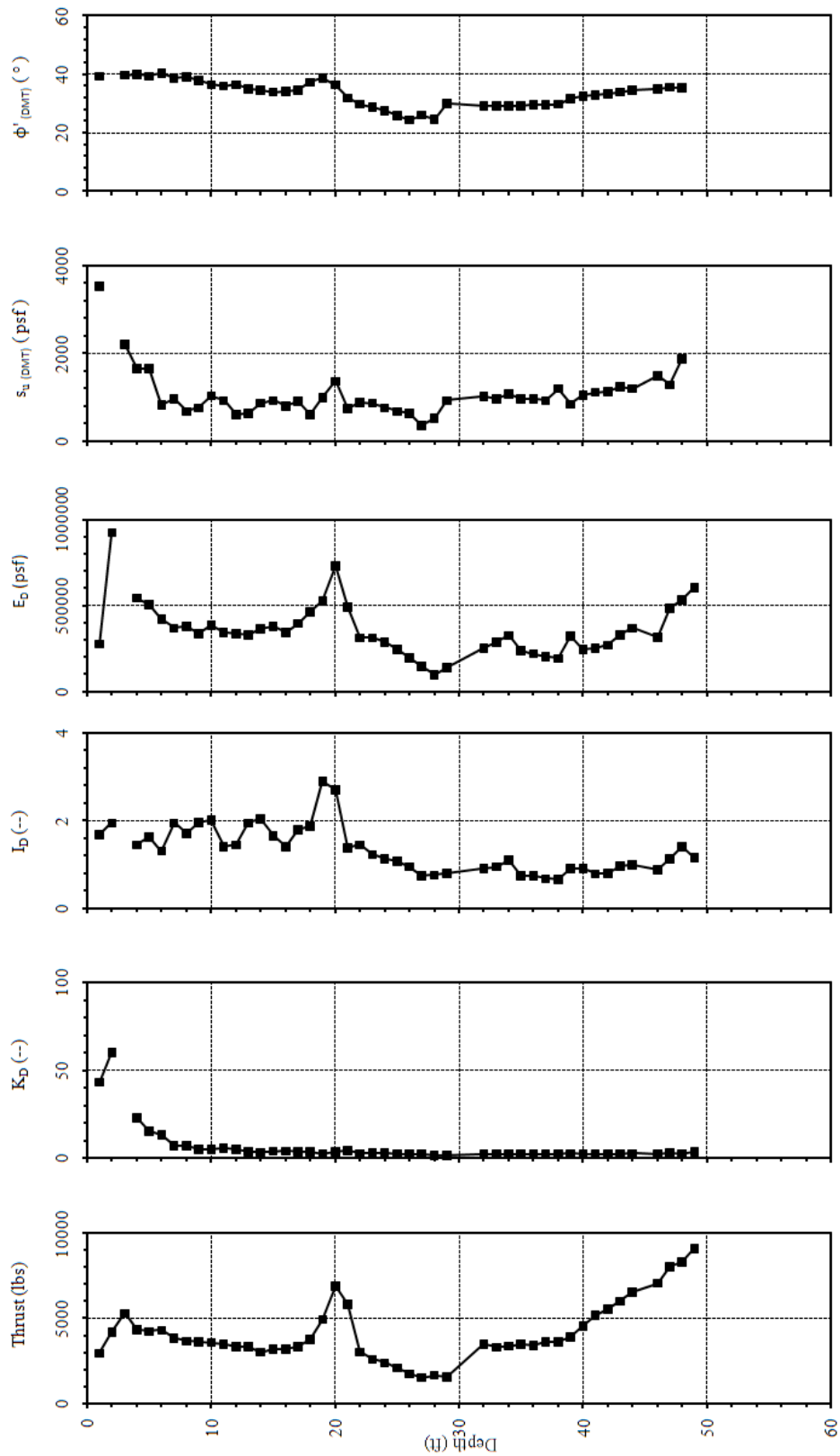


Figure 5.24 – PC1 Dilatometer parameters versus depth

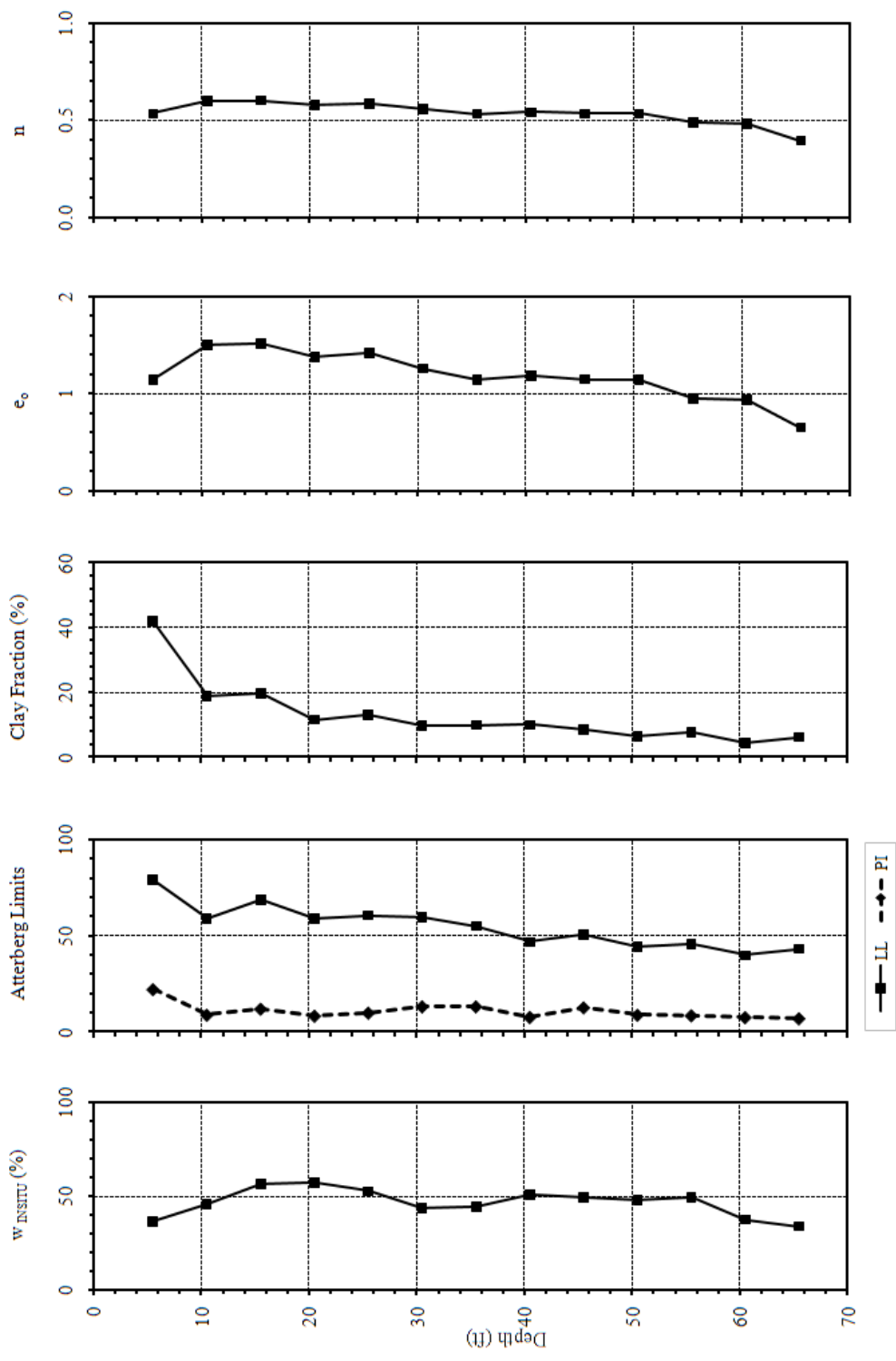


Figure 5.25 – BR Additional geotechnical parameters versus depth

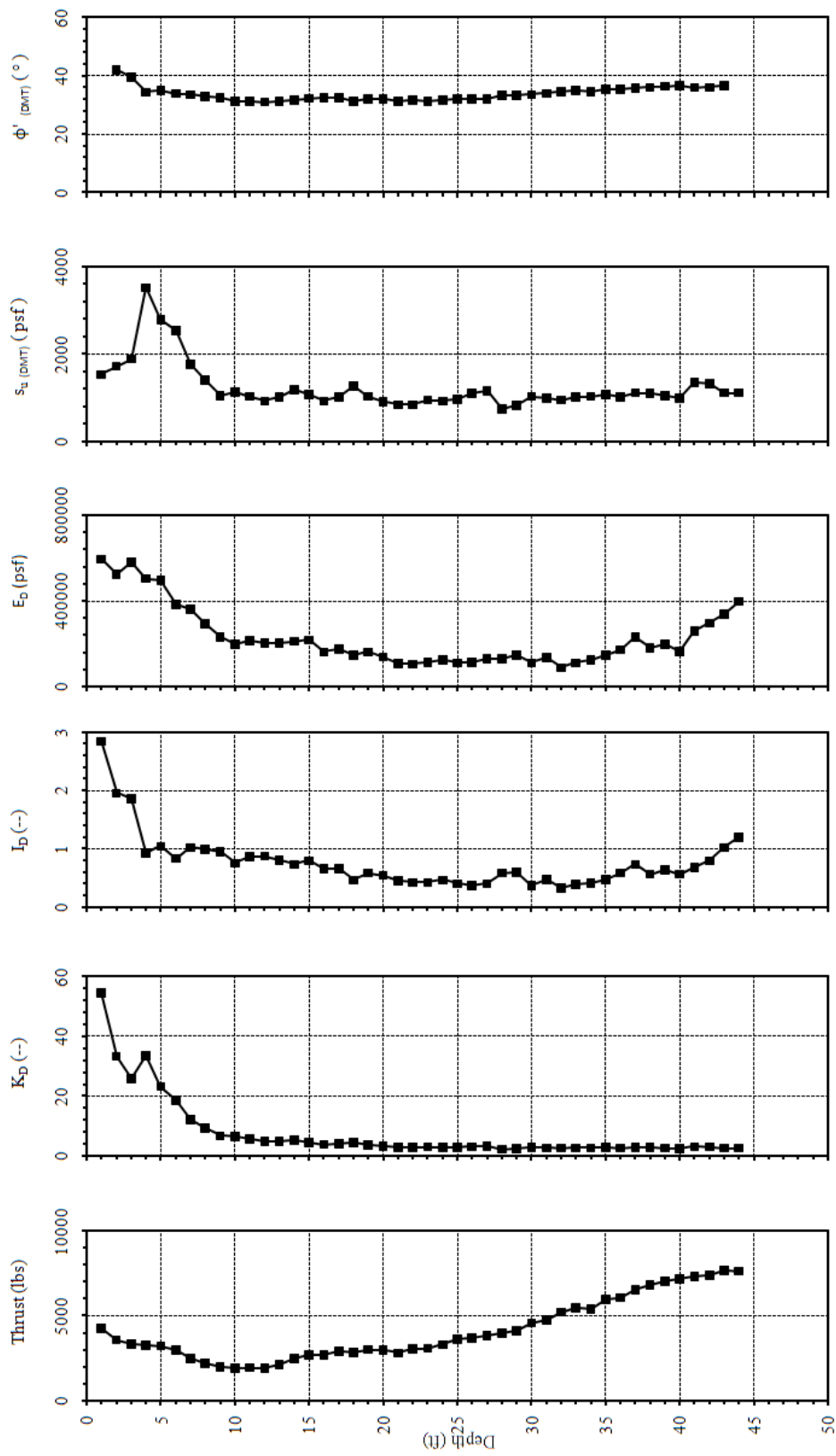


Figure 5.26 – BR Dilatometer parameters versus depth

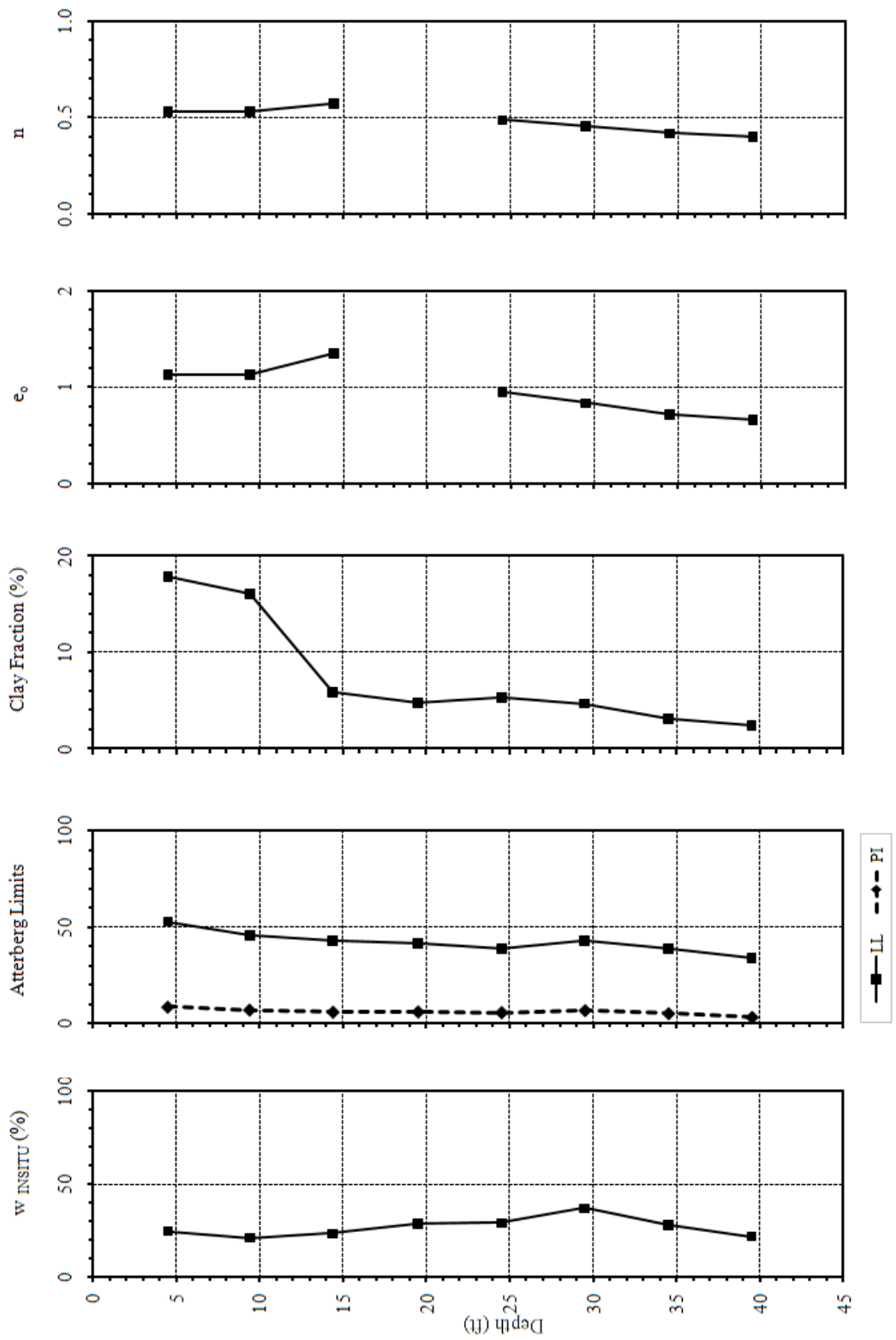


Figure 5.27 – PC2 Additional geotechnical parameters versus depth

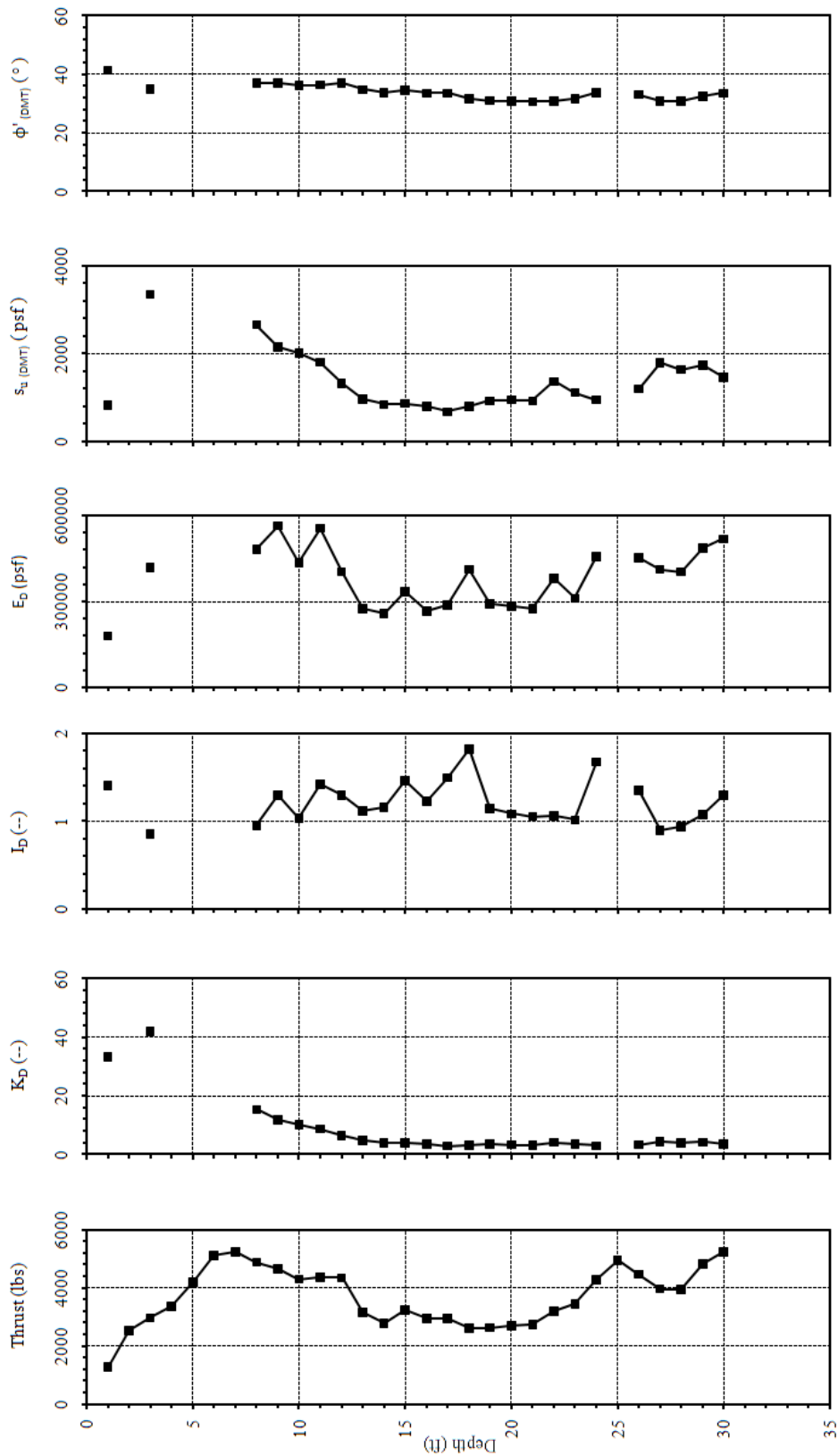


Figure 5.28 – PC2 Dilatometer parameters versus depth

The average specific gravity was determined to be 2.70 at PC1, 2.74 at BR, and 2.64 at PC2. The LL, PI, clay fraction, e_o , and n all tended to decrease with depth, with clay fraction showing the clearest trend. These parameters were investigated based on their predicted influence on other parameters and observations during the research. These parameters were also investigated to determine their influence on the SPT-T and to evaluate the ability of their measurements to predict the most desirable variables; c' , ϕ' , and, τ_{TXL} . Two additional quantities were evaluated: the torque to blow-count ratio (T/N) and torque times insitu water content ($T * w_{INSITU}$). The published T/N value was evaluated in order to compare to previous research, which used 72 percent efficiency for the corrected blow-count (N'_{72}). Decourt (1998) published T/N values of 2.0 for saprolite. Kelly and Lutenegger (1999) published comparable T/N values of 1.5 for residual soils. The comparable average T/N values were 2.53 at PC1, 3.89 at BR, and 1.88 at PC2. The $T * w_{INSITU}$ value was introduced to evaluate the influence of insitu water content on the system. A corrected torque value (T'_{MAX}) was also introduced in an attempt to correct the maximum torque value for influence of the vertical effective stress (σ'_v). The T'_{MAX} equation was based on the equation used to correct blow-counts and is provided in Equation 5.1, where σ'_v is in pounds per square foot (Liao and Whitman, 1986).

$$T'_{MAX} = T_{MAX} * \sqrt{\frac{2000}{\sigma'_v}} \quad (5.1)$$

Relationships between the SPT-T versus STT-T, DMT versus TXL, and SPT-T versus TXL measurements were explored to study the inter-relationship of the tests. Table 5.4 summarizes the additional relationships investigated and presents the corresponding figure numbers (Figures 5.29 through 5.44), trend line R^2 values for those relationships with reasonable correlations, and Pearson p-values (two-tailed).

Table 5.4 –Additional geotechnical relationships

Figure Number	X-axis	Y-axis	Pearson	
			r Coefficient	p-value (two-tailed)
5.7	c'	c_a	0.145	0.222
5.8	ϕ' (TXL)	δ	0.495	0.003
5.29	T_{MAX} (SPT)	T_{MAX} (STT)	0.620	0.000
5.30	ϕ' (TXL)	ϕ' (SPT)	0.278	0.068
5.31	ϕ' (TXL)	ϕ' (DMT)	0.013	0.477
5.32	c' (TXL)	s_u (DMT)	0.023	0.458
5.16	T_{MAX} (SPT)	c'	0.357	0.026
5.33		ϕ'	0.287	0.062
5.21		τ_{TXL}	0.609	0.000
5.33		Clay fraction	-0.339	0.033
5.34		w_{INSITU}	-0.403	0.014
5.36	T'_{MAX}	c'	0.045	0.813
		ϕ'	0.157	0.407
		τ_{TXL}	-0.309	0.096
		Clay fraction	0.406	0.026
5.35	N	c'	0.257	0.085
		ϕ'	0.267	0.077
		τ_{TXL}	0.354	0.027
		Clay fraction	-0.190	0.157
5.37	$T * w$	c'	0.500	0.003
		ϕ'	-0.003	0.494
		τ_{TXL}	0.768	0.000
		Clay fraction	-0.278	0.072

Table 5.4 – (continued)

Figure Number	X-axis	Y-axis	Pearson	
			r Coefficient	p-value (two-tailed)
5.38	T / N	c'	0.194	0.157
		ϕ'	-0.210	0.137
		τ_{TXL}	0.561	0.001
		Clay fraction	-0.380	0.021
5.39	LL	c'	-0.094	0.311
		ϕ'	-0.293	0.058
		τ_{TXL}	-0.701	0.000
		Clay fraction	0.819	0.000
5.40	PI	c'	0.016	0.467
		ϕ'	-0.243	0.098
		τ_{TXL}	-0.394	0.016
		Clay fraction	0.753	0.000
5.41	Clay fraction	c'	0.024	0.450
		ϕ'	-0.240	0.101
		τ_{TXL}	-0.659	0.000
5.42	e_o	c'	-0.139	0.232
		ϕ'	-0.505	0.002
		τ_{TXL}	-0.711	0.000
		Clay fraction	0.465	0.005
5.43	n	c'	-0.147	0.219
		ϕ'	-0.524	0.001
		τ_{TXL}	-0.718	0.000
		Clay fraction	0.481	0.004

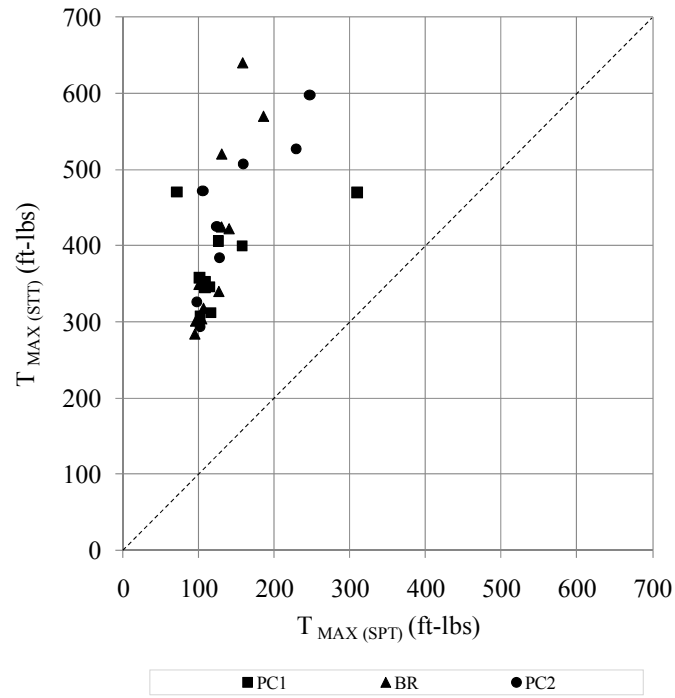


Figure 5.29 – $T_{MAX(SPT)}$ versus $T_{MAX(STT)}$

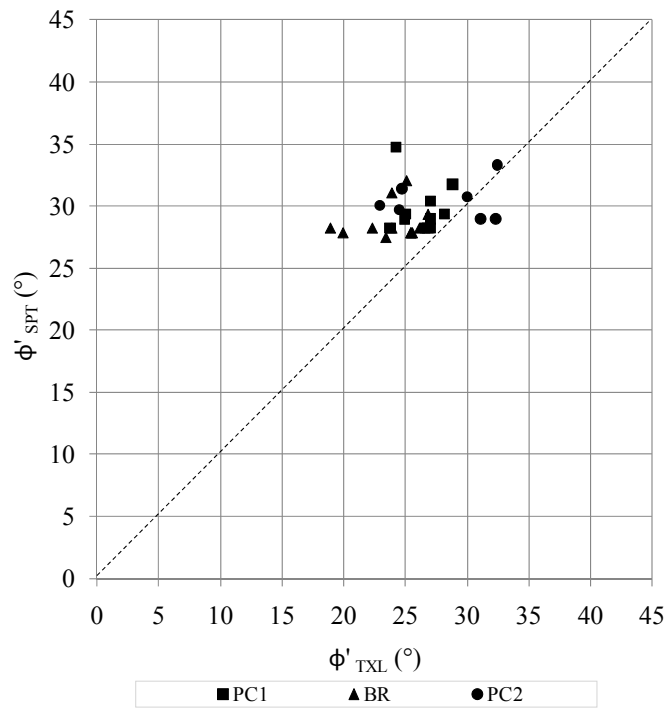


Figure 5.30 – ϕ'_{TXL} versus ϕ'_{SPT}

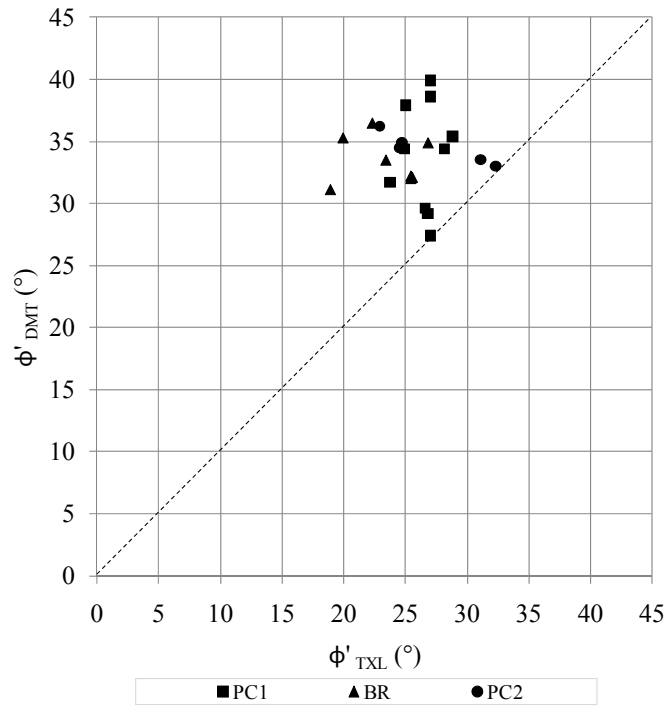


Figure 5.31 – ϕ'_{TXL} versus ϕ'_{DMT}

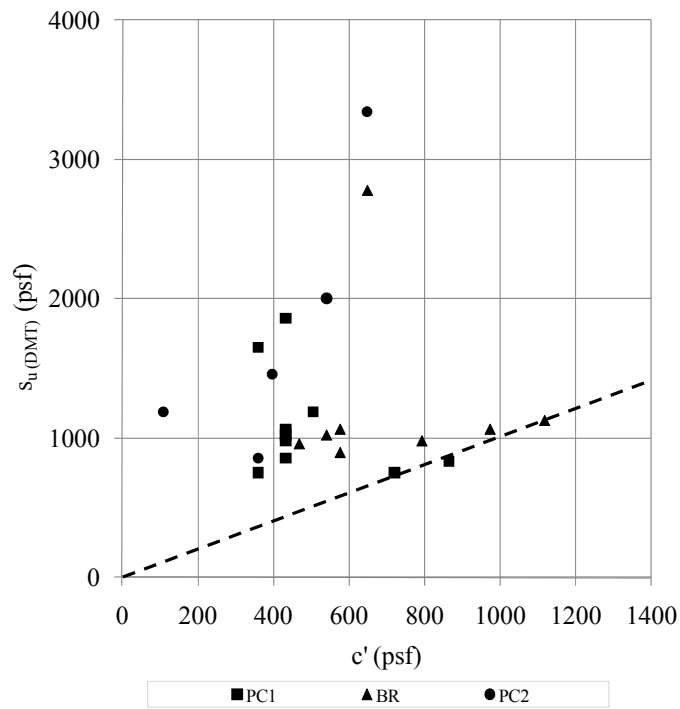


Figure 5.32 – c' versus s_u (DMT)

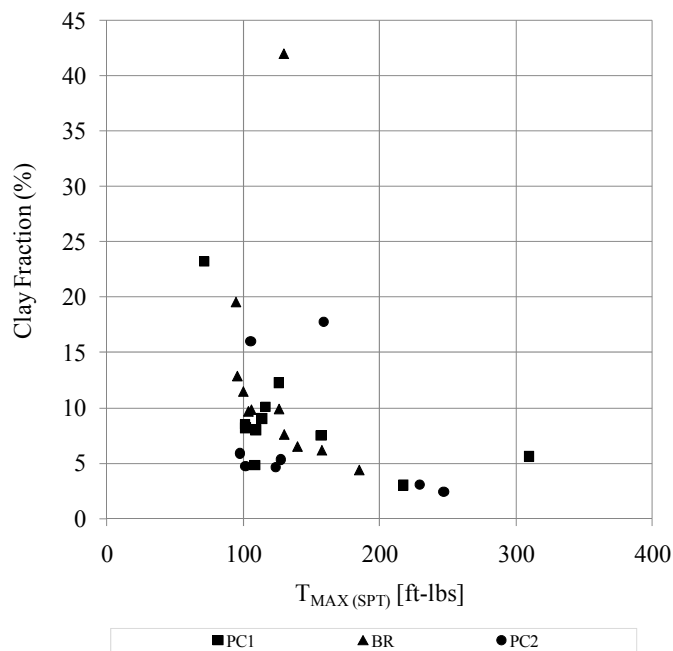


Figure 5.33 – T_{MAX(SPT)} versus clay fraction

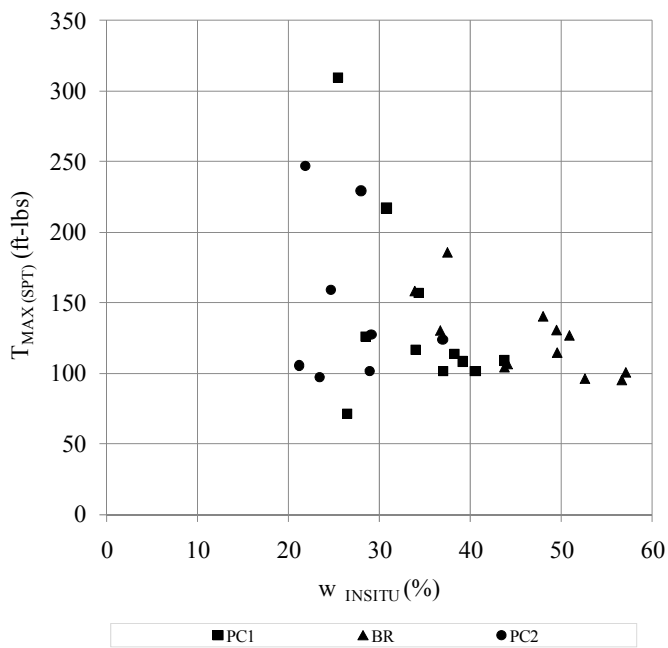


Figure 5.34 – w_{INSITU} versus T_{MAX(SPT)}

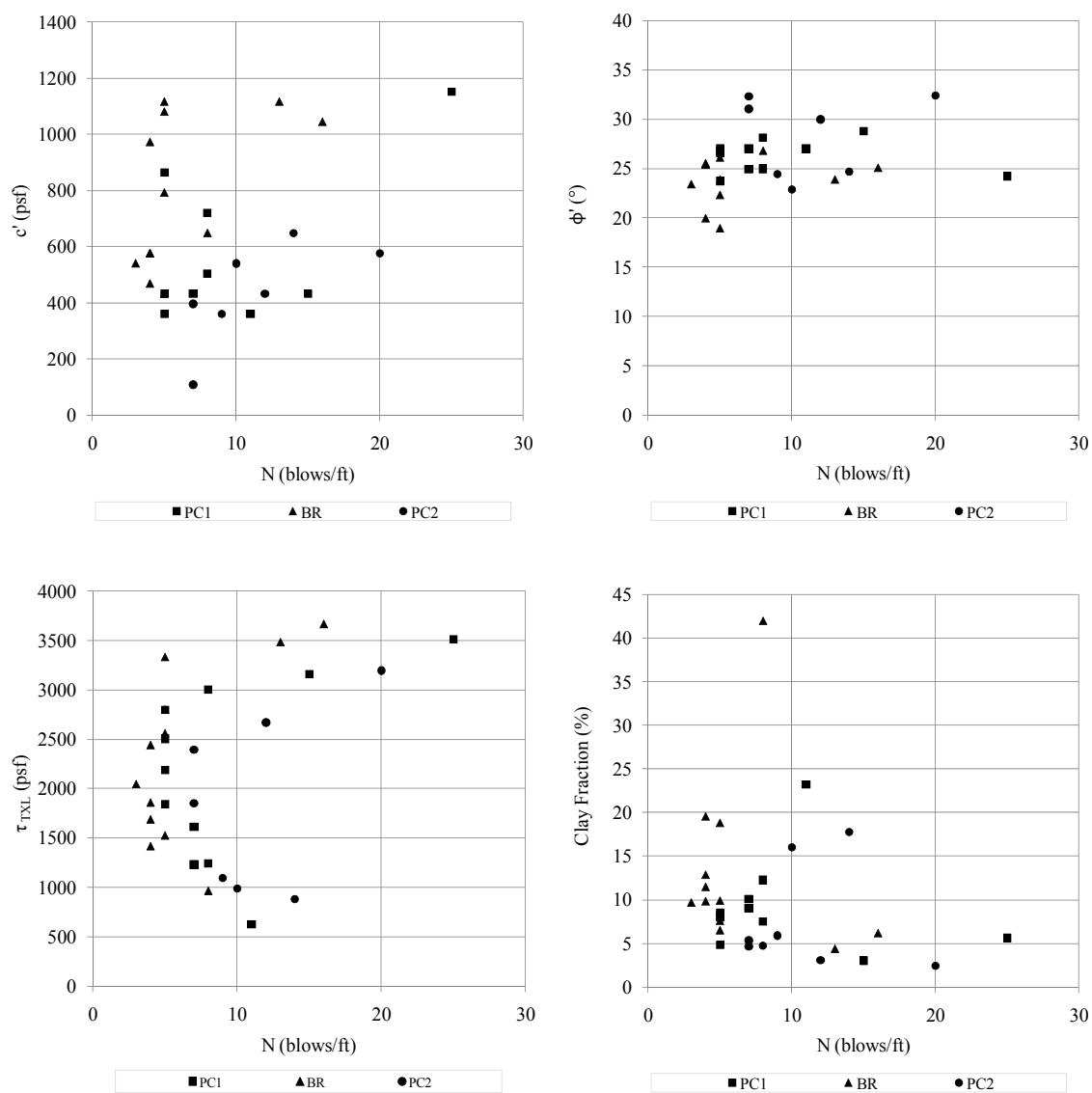


Figure 5.35 – Uncorrected blow-count (N) versus c' , ϕ' , τ_{TXL} , and clay fraction

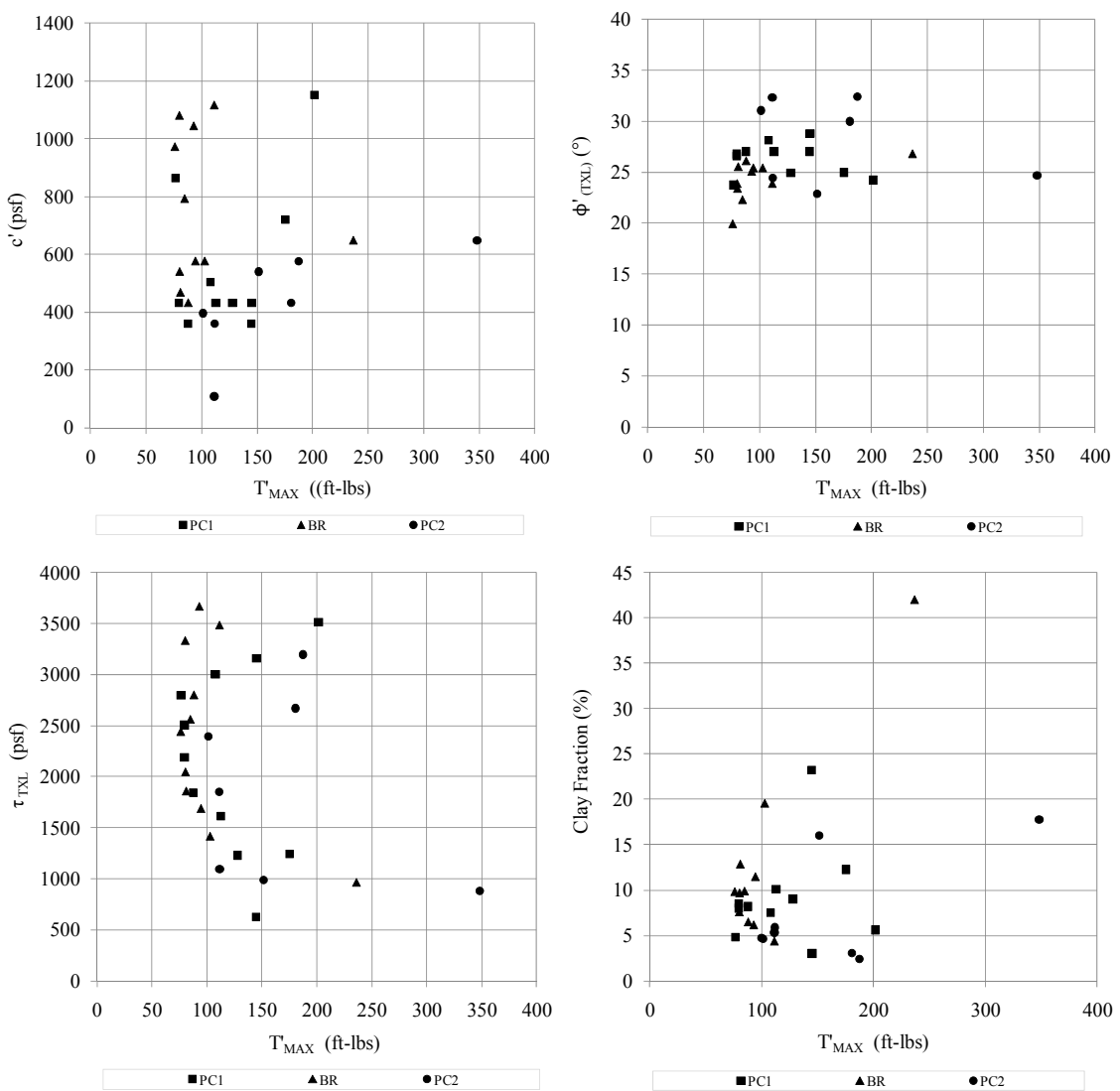


Figure 5.36 – Corrected torque (T'_{MAX}) versus c' , ϕ' , τ_{TXL} , and clay fraction

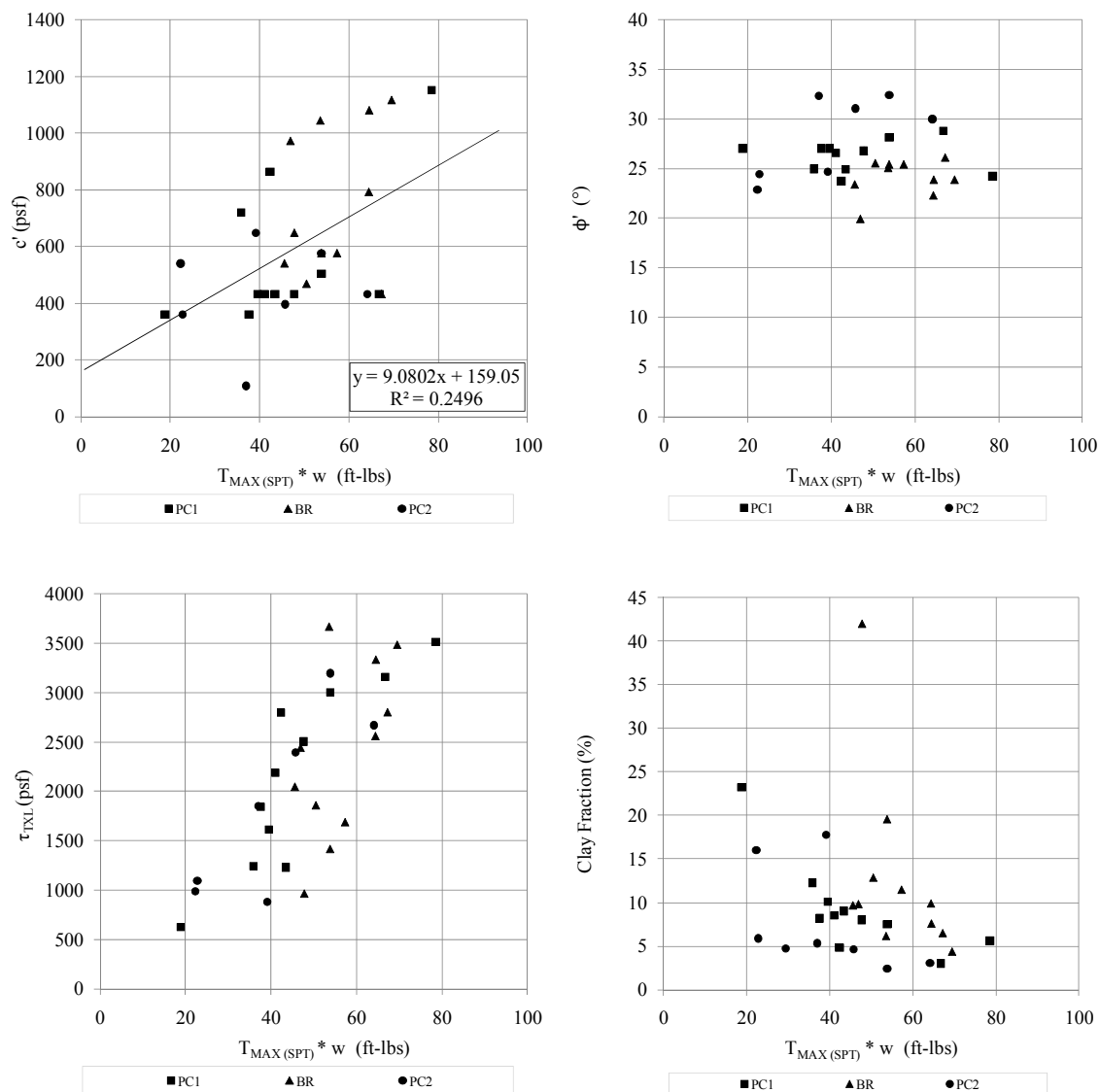


Figure 5.37 – ($T_{MAX(SPT)} * w_{INSITU}$) versus c' , ϕ' , τ_{TXL} , and clay fraction

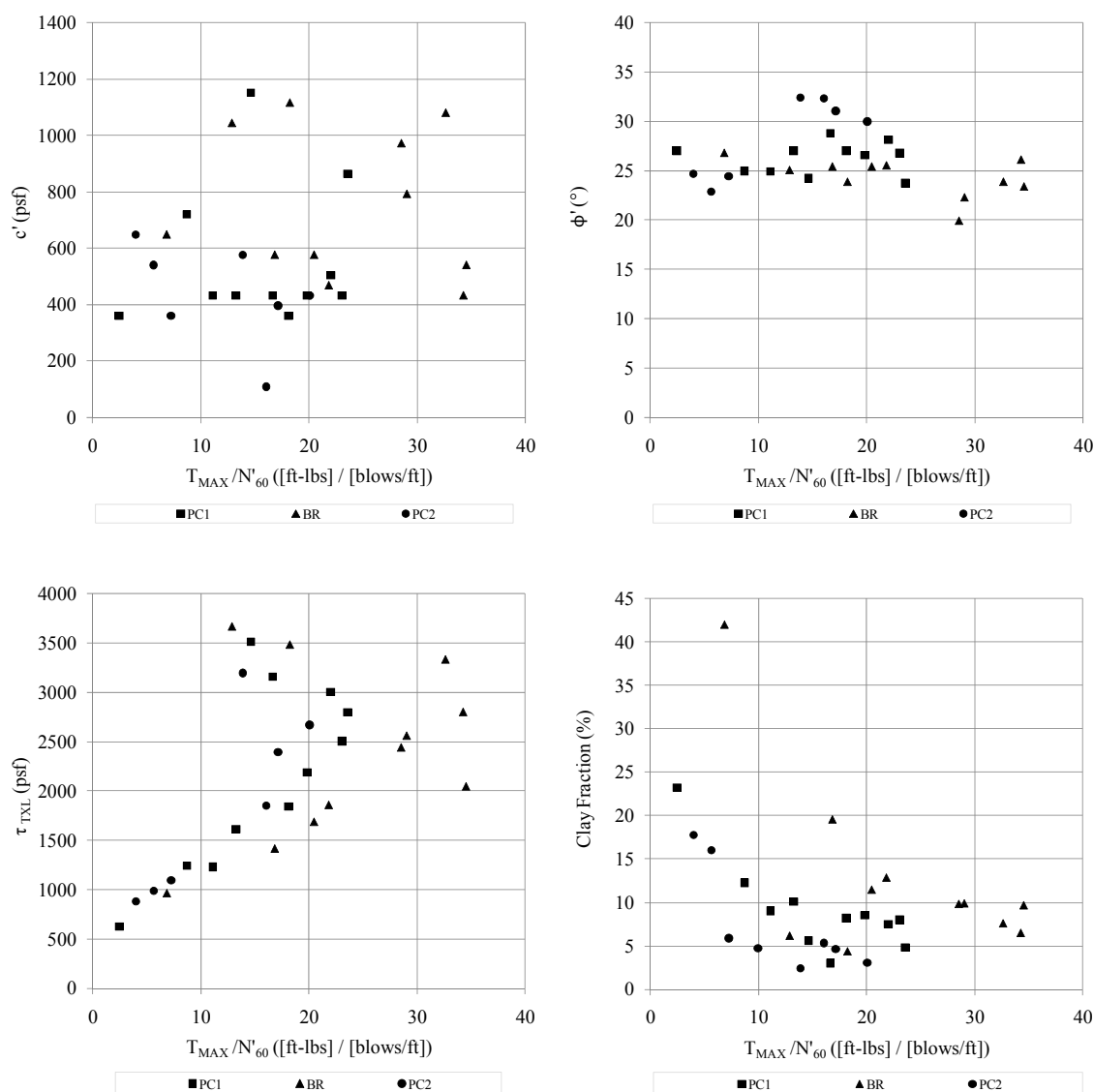


Figure 5.38 – ($T_{MAX(SPT)}/N'_{60}$) versus c' , ϕ' , τ_{TXL} , and clay fraction

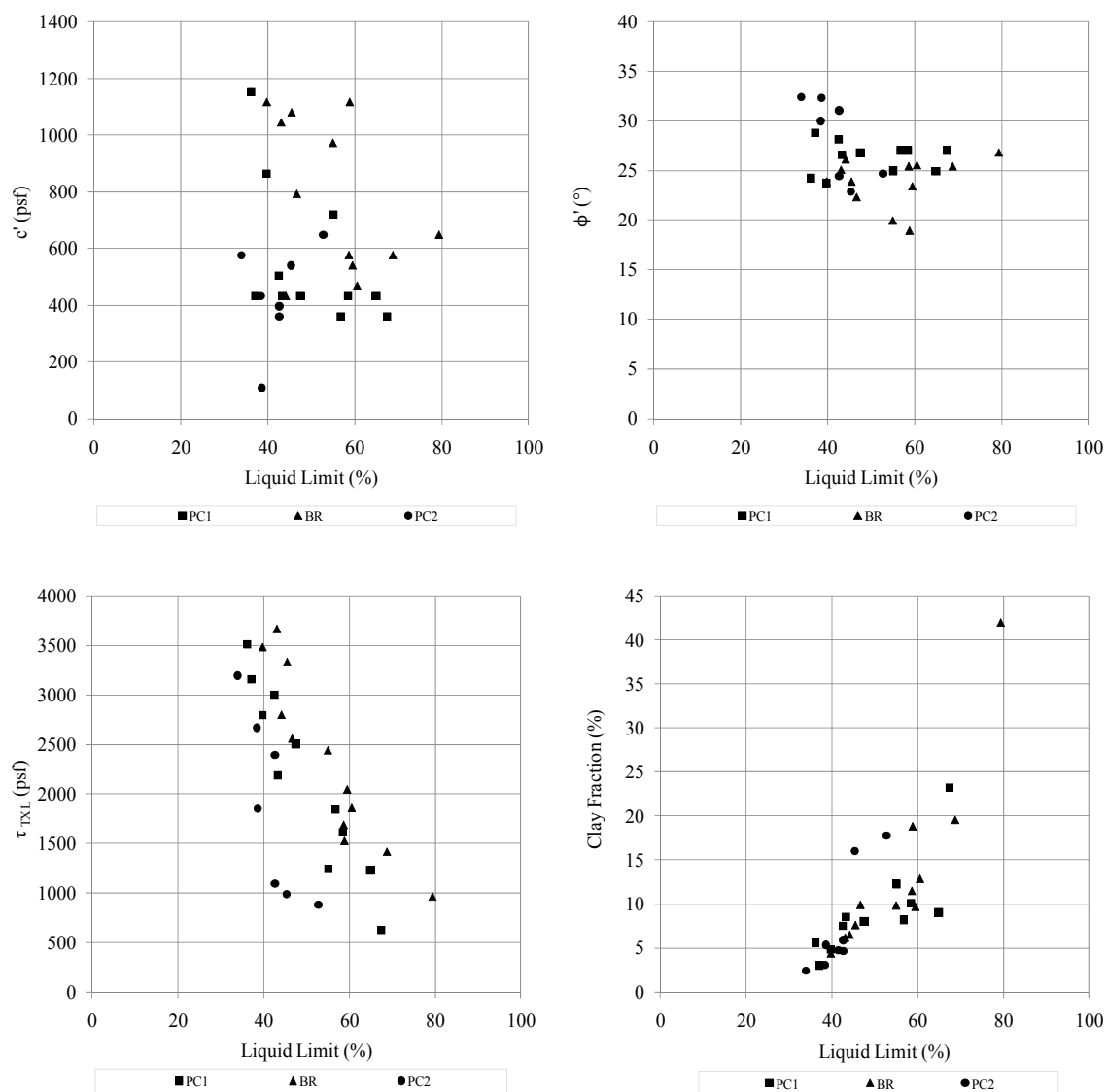


Figure 5.39 – Liquid limit (LL) versus c' , ϕ' , τ_{TXL} , and clay fraction

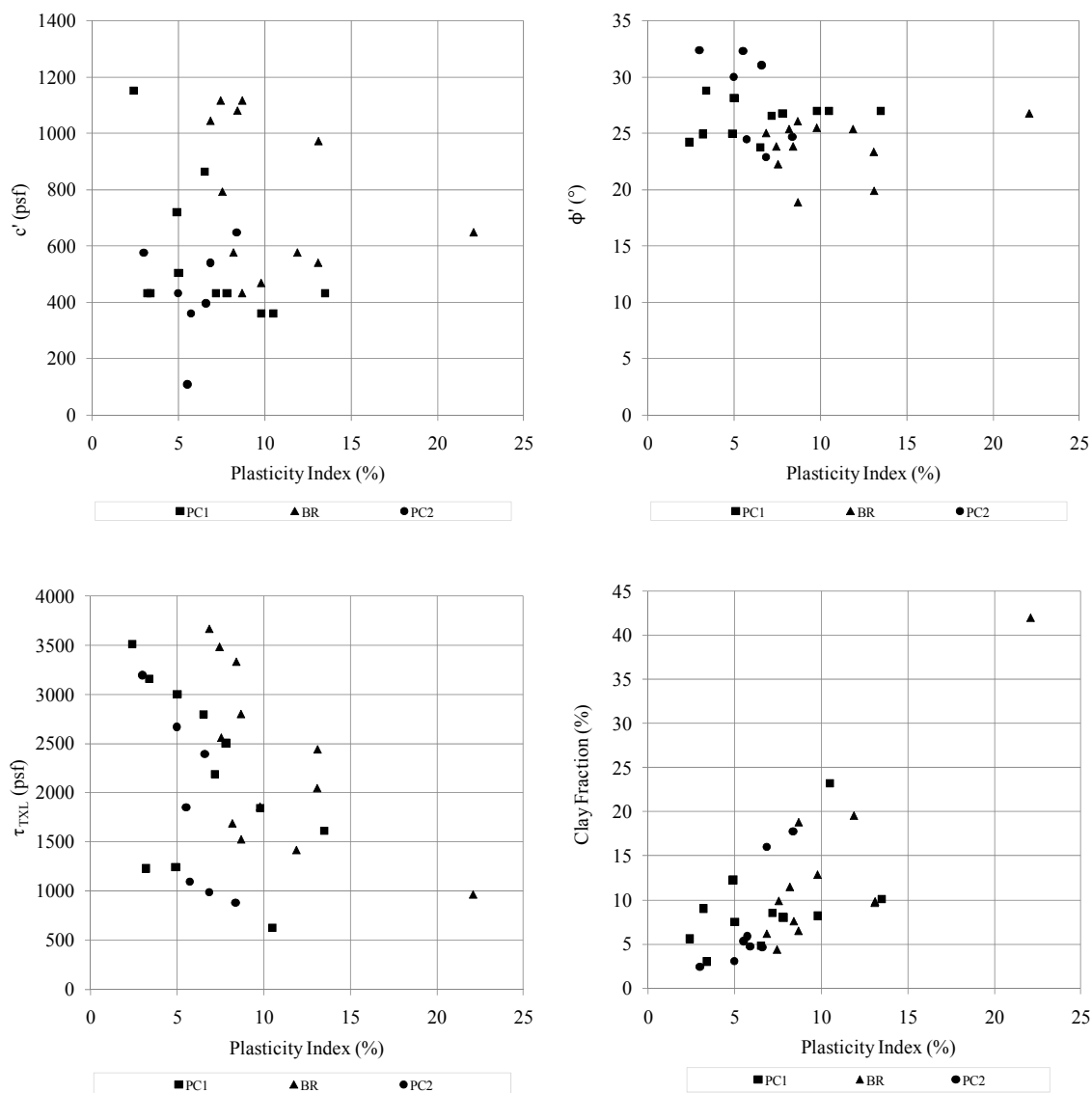


Figure 5.40 – Plasticity index (PI) versus c' , ϕ' , τ_{TXL} , and clay fraction

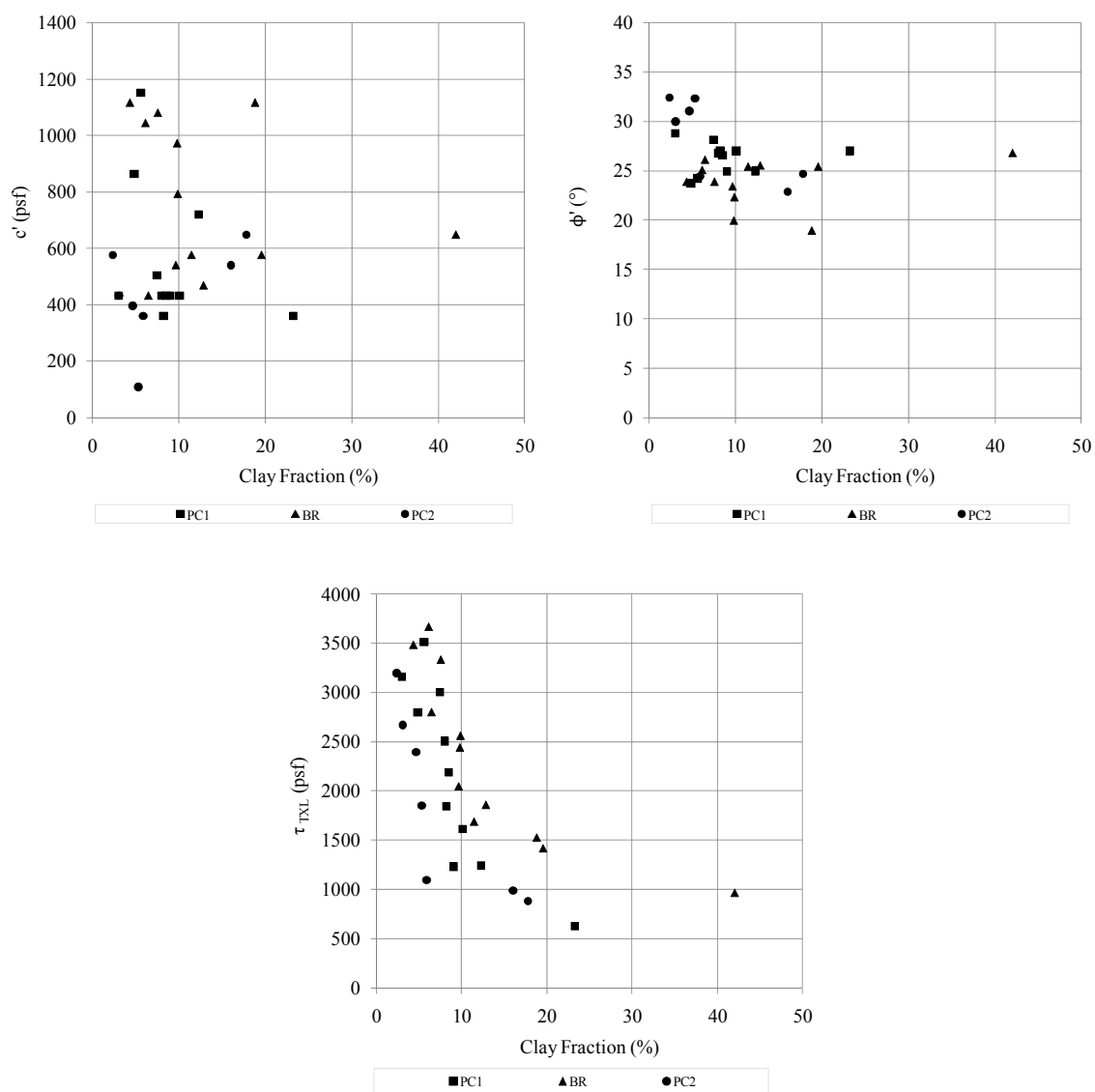


Figure 5.41 – Clay fraction versus c' , ϕ' , and τ_{TXL}

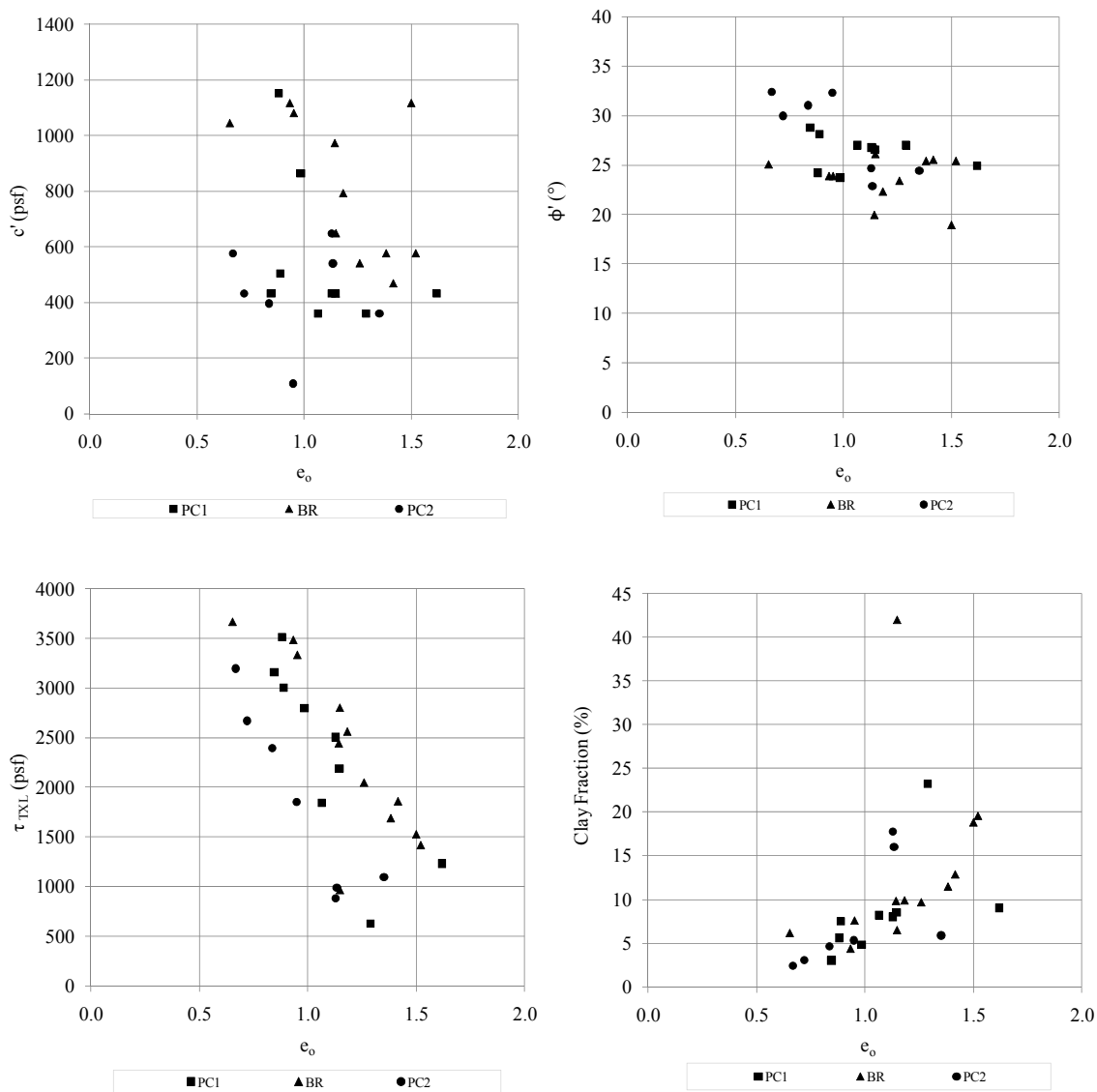


Figure 5.42 – Void Ratio (e_o) versus c' , ϕ' , τ_{TXL} , and clay fraction

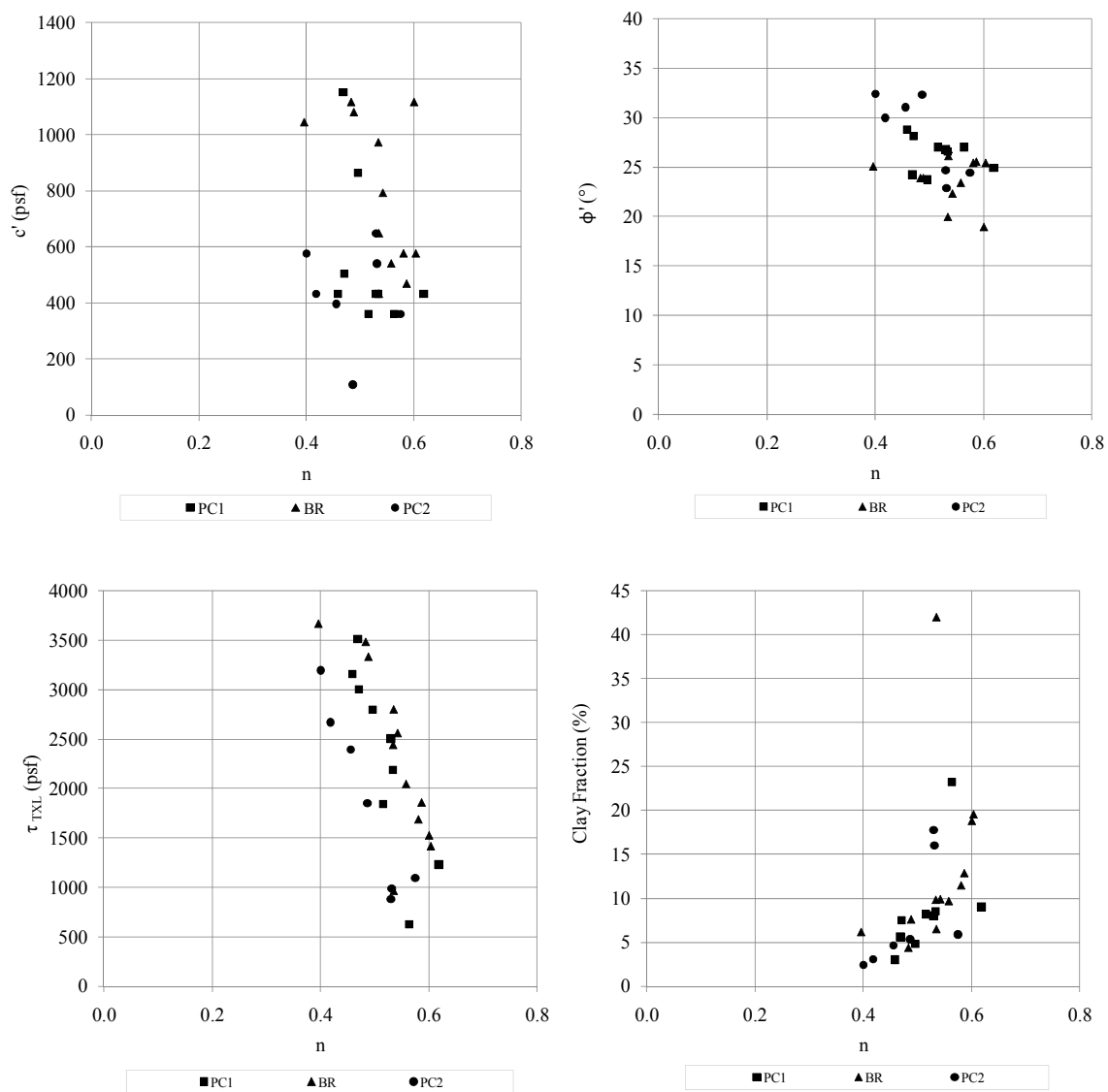


Figure 5.43 – Porosity (n) versus c' , ϕ' , τ_{TXL} , and clay fraction

5.5 Geologic Evaluations

The geologic study was undertaken to improve the site characterization and to evaluate relationships between the geotechnical and geologic parameters. Figures 5.47 through 5.49 present the soil dry color dimensions (hue (H), value (V), and chroma (C)), redness ratio (RR), redness factor (RF), point count percentages versus depth. The point count percentages included the categories of groundmass, clay bleb, quartz, and minor minerals. The porosity was difficult to estimate due the epoxy cracks developed during the thin section fabrication. The specific details and notes from the petrographic analysis are provided in Table I1 of APPENDIX I.

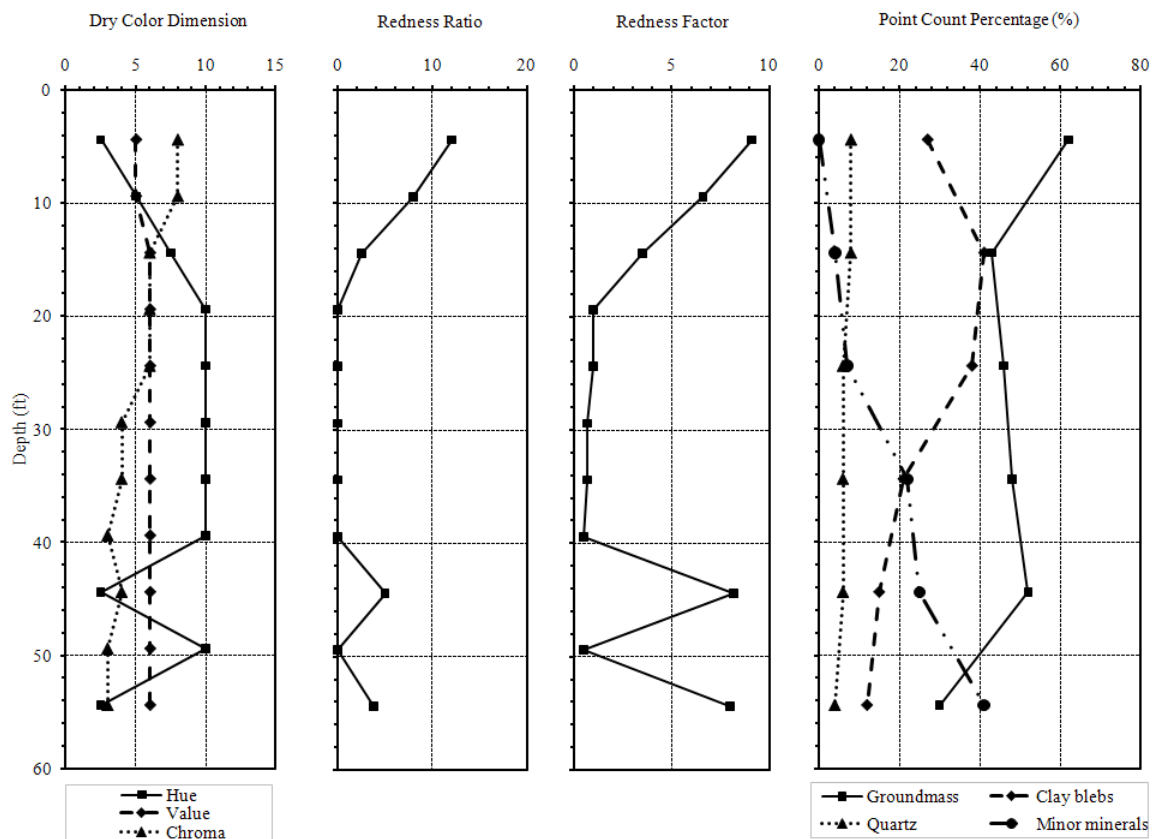


Figure 5.44 – PC1 Geologic parameters versus depth

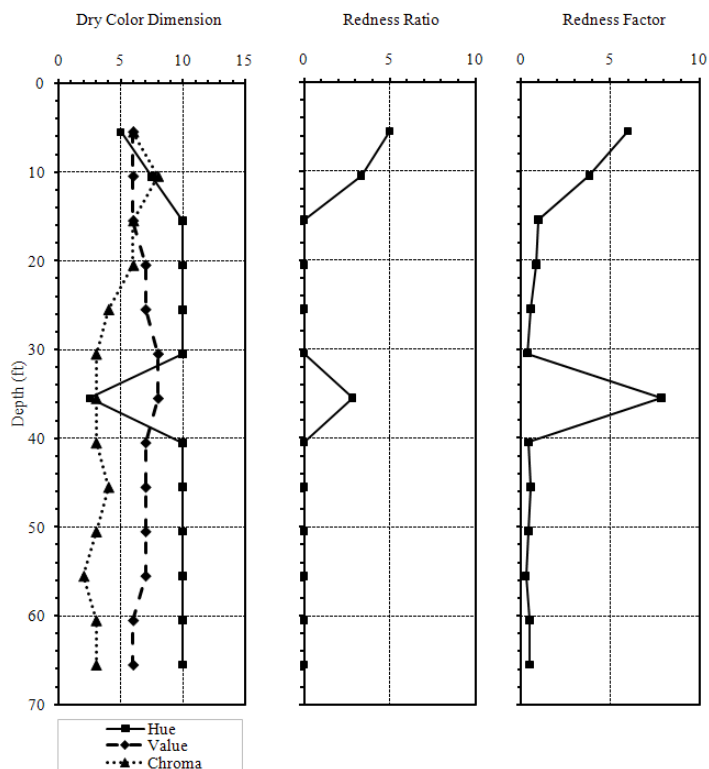


Figure 5.45 – BR Geologic parameters versus depth

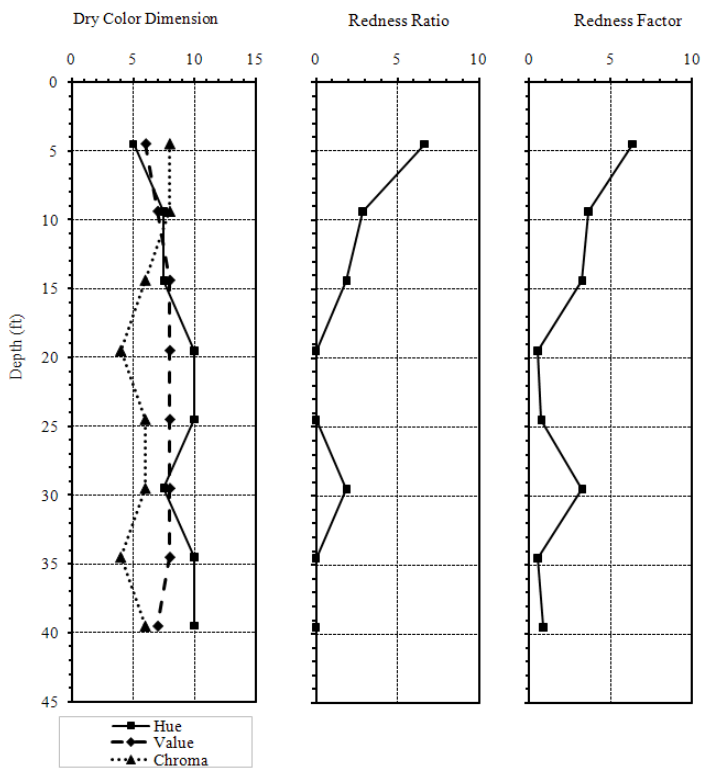


Figure 5.46 – PC2 Geologic parameters versus depth

The dry color dimensions showed steady and observable changes through the profile. Hue slightly increased, value was fairly constant, and chroma slightly decreased with depth. The hue was redder at the surface and more yellow at the deeper depths. The chroma was more intense at the surface and duller at the deeper depths. Both of these trends were typical for weathered residual soil profile and attributed to the natural processes. There was a spike in chroma around the groundwater table at each site. The groundwater table was 34.0-feet at PC1, 42.6-feet at BR, and 28.3-feet at PC2. This spike was attributed to the naturally fluctuating groundwater table and the oxidation process associated with the changing availability of oxygen. The redness ratio and redness factor both slowly decreased with depth. Since they both had the same trend, only the redness factor was used in the evaluations.

The PC1 petrographic analysis showed that the groundmass, clay bleb, and quartz percentages tended to decrease with depth, while the minor mineral percentage increased with depth. All of these trends were typical and expected for a weathered residual soil profile. The increase in minor minerals at deeper depths corresponded with less weathering, since the unweathered materials were easier to identify. The groundmass consisted of disaggregated clay minerals along with very fine grained quartz and minor minerals, including some organic material at the 4.4-foot depth. The clay blebs consisted of crystals where substitution has been complete and the original euhedral form (grains in igneous rocks with a regular crystallographic shape) is still evident. The clay blebs displayed large particles with preferred orientation of mineral grains that appeared to conform to original mineral grain boundaries. The quartz category was divided between the soils above and below 30-feet deep. Above 30-feet, the quartz grains were heavily

fractured with most showing infiltration and wedging along fractures by clay mineral. Below 30-feet, the quartz grains showed far less infiltration by clay minerals along fractures than samples from higher strata.

Various geologic investigations were completed to evaluate the ability of the geologic parameters to predict the most desirable geotechnical variables; c' , ϕ' , τ_{TXL} , and clay fraction (Figures 5.47 through 5.54). Table 5.5 summarizes the geologic relationships investigated, the corresponding figure numbers, trend line R^2 value of the relationships with reasonable correlations, the Pearson r correlation, and p-values (two-tailed). For the petrographic analysis, it is important to note that any correlation is only preliminary since the data is only based on six data points.

Table 5.5 – Geologic evaluations

Figure Number	X-axis	Y-axis	Pearson	
			r Coefficient	p-value (two-tailed)
5.47	Hue	c'	-0.184	0.165
		ϕ'	0.200	0.145
		τ_{TXL}	0.258	0.084
		Clay fraction	-0.389	0.017
5.48	Value	c'	-0.210	0.133
		ϕ'	0.128	0.250
		τ_{TXL}	0.128	0.250
		Clay fraction	-0.359	0.018
5.49	Chroma	c'	-0.326	0.039
		ϕ'	0.086	0.326
		τ_{TXL}	-0.815	0.000
		Clay fraction	0.489	0.003
5.50	Redness Factor	c'	0.148	0.218
		ϕ'	-0.189	0.159
		τ_{TXL}	-0.339	0.033
		Clay fraction	0.436	0.008
5.51	Groundmass Percentage	c'	-0.795	0.029
		ϕ'	0.780	0.034
		τ_{TXL}	-0.649	0.082
		Clay fraction	0.776	0.035
5.52	Clay Bleb Percentage	c'	-0.638	0.086
		ϕ'	-0.054	0.460
		τ_{TXL}	-0.757	0.041
		Clay fraction	0.200	0.352
5.53	Quartz Percentage	c'	0.852	0.016
		ϕ'	-0.909	0.006
		τ_{TXL}	0.286	0.291
		Clay fraction	-0.140	0.396
5.54	Minor Mineral Percentage	c'	0.845	0.017
		ϕ'	-0.297	0.284
		τ_{TXL}	0.962	0.001
		Clay fraction	-0.653	0.080

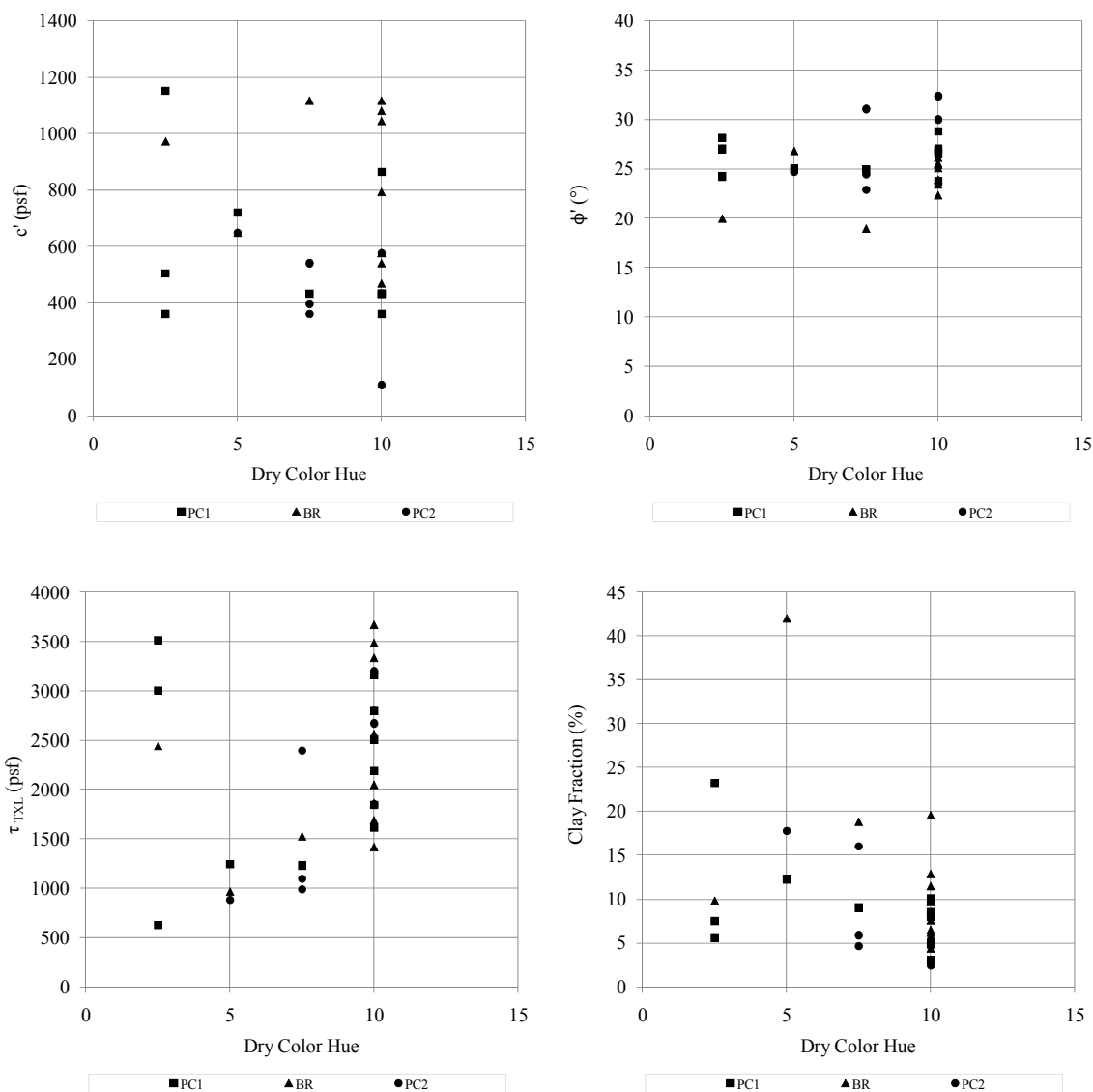


Figure 5.47 – Dry color hue versus c' , ϕ' , τ_{TXL} , and clay fraction

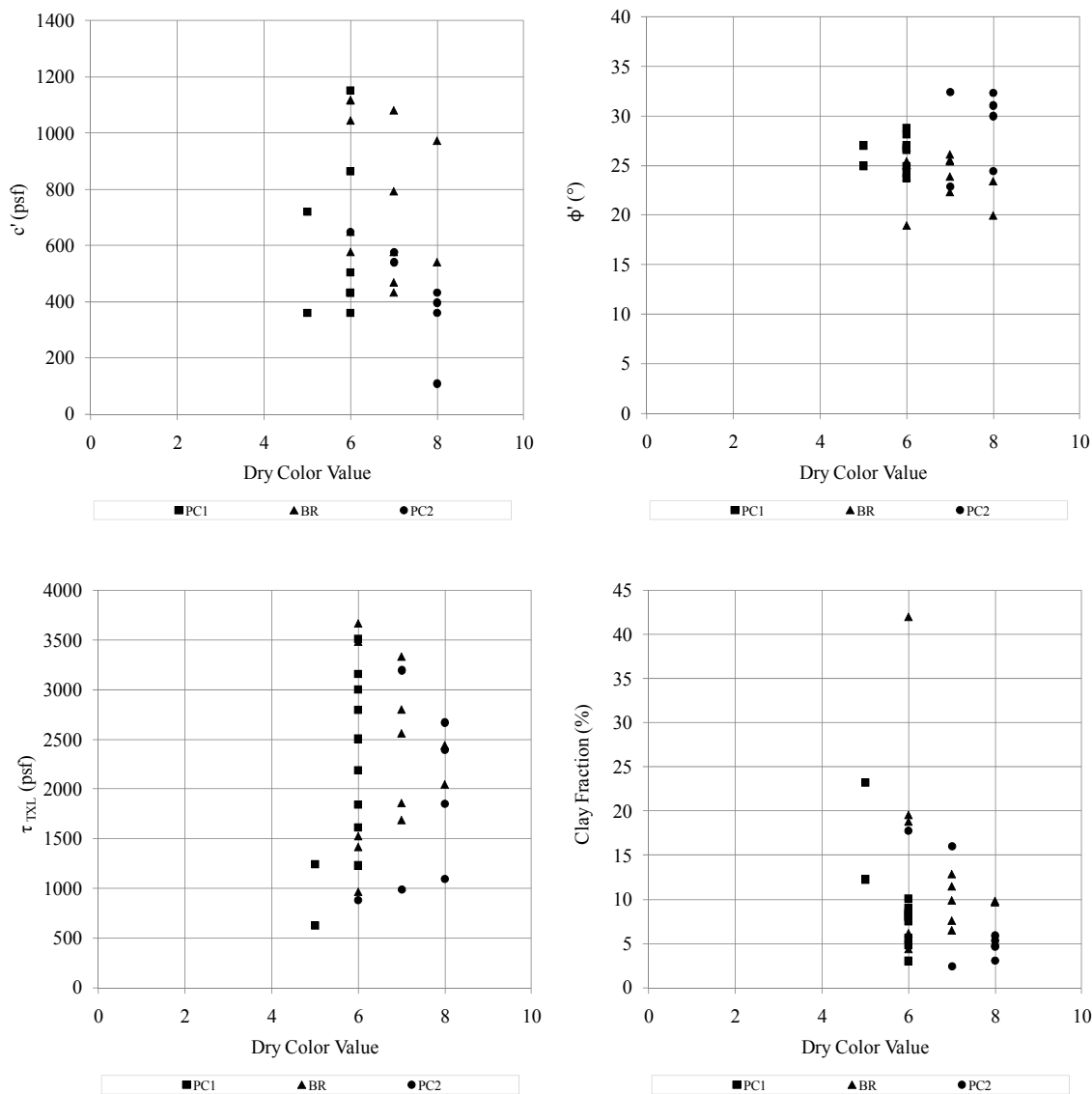


Figure 5.48 – Dry color value versus c' , ϕ' , τ_{TXL} , and clay fraction

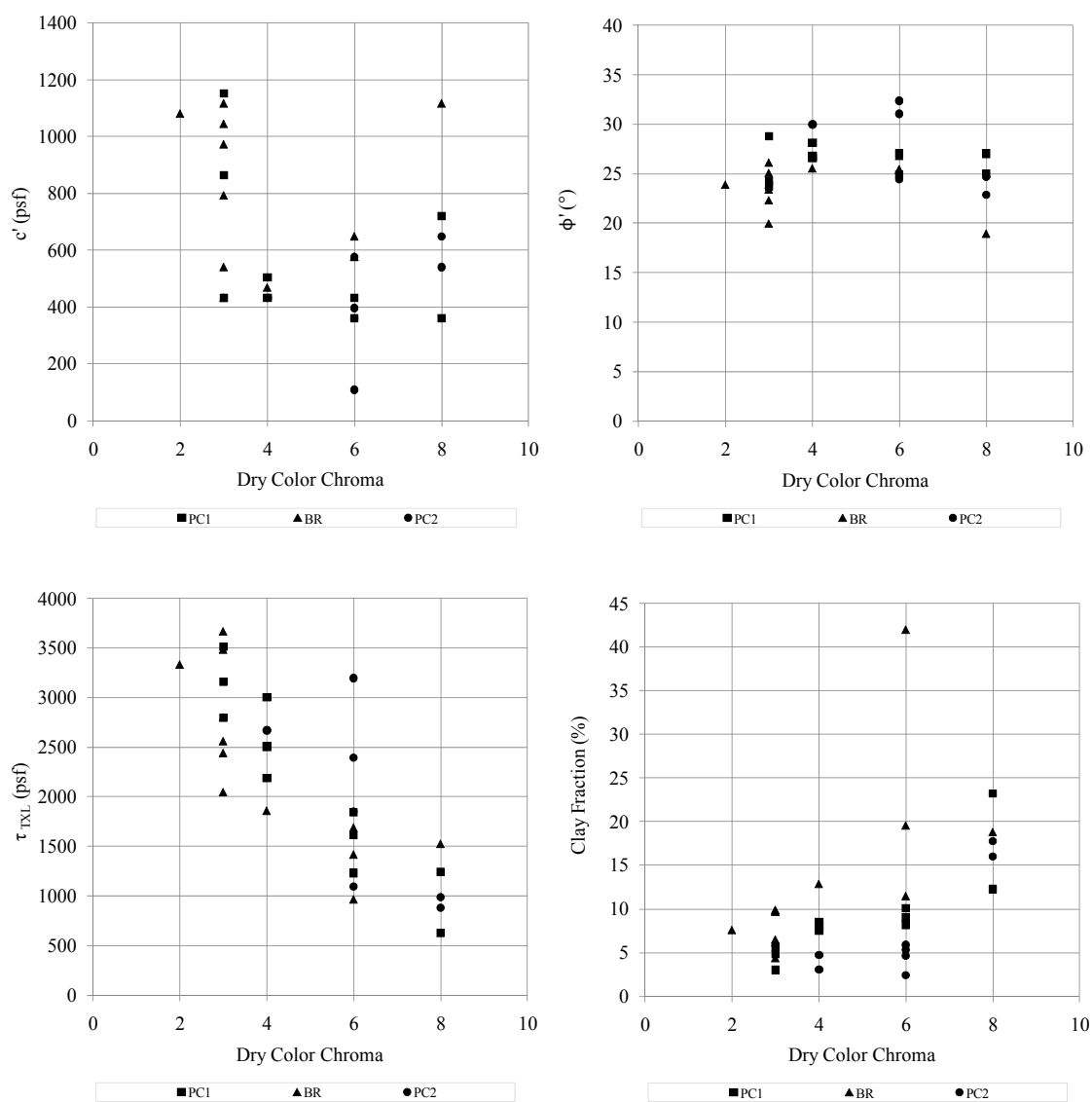


Figure 5.49 – Dry color chroma versus c' , ϕ' , τ_{TXL} , and clay fraction

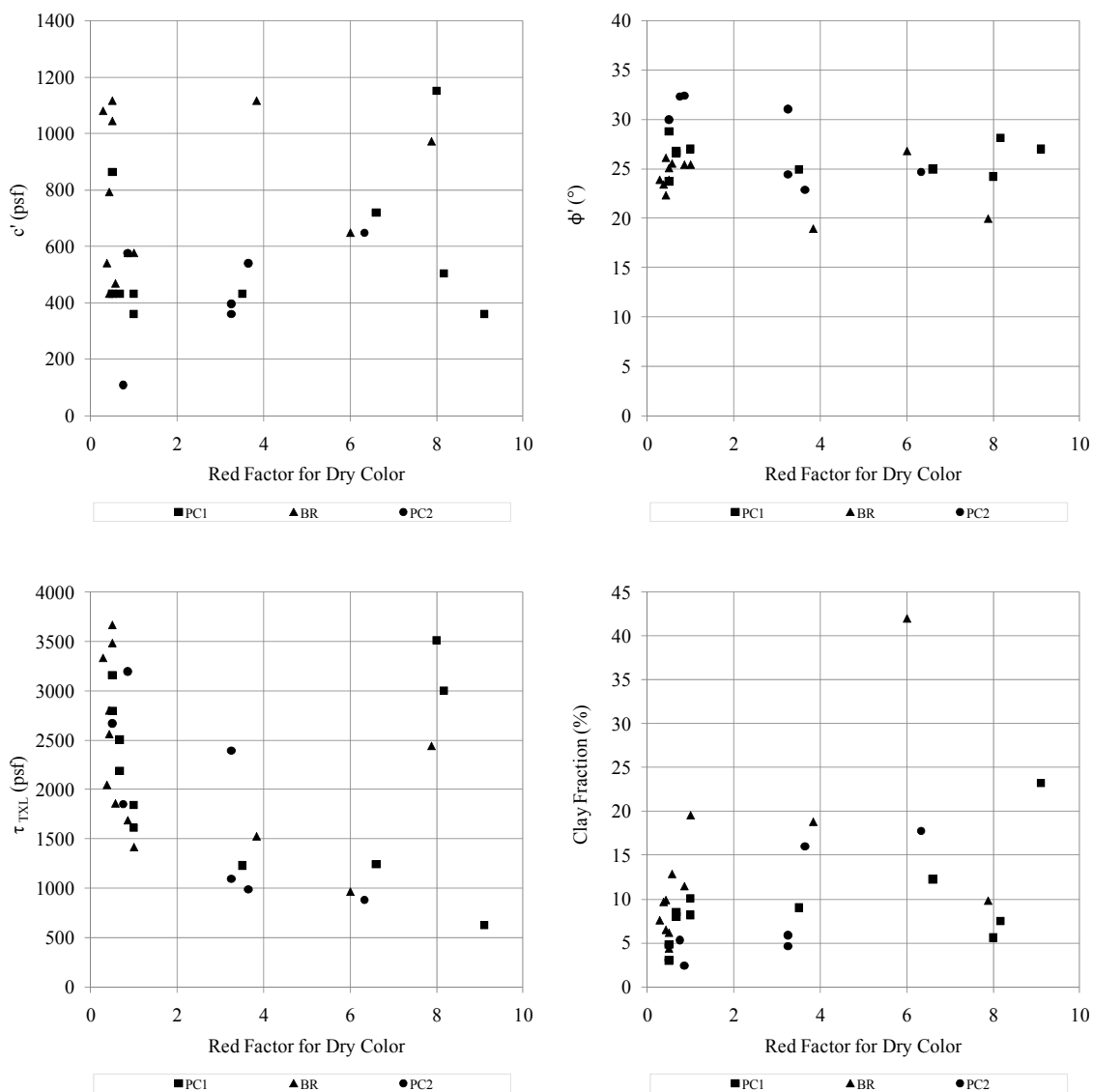


Figure 5.50 – Dry color redness factor versus c' , ϕ' , τ_{TXL} , and clay fraction

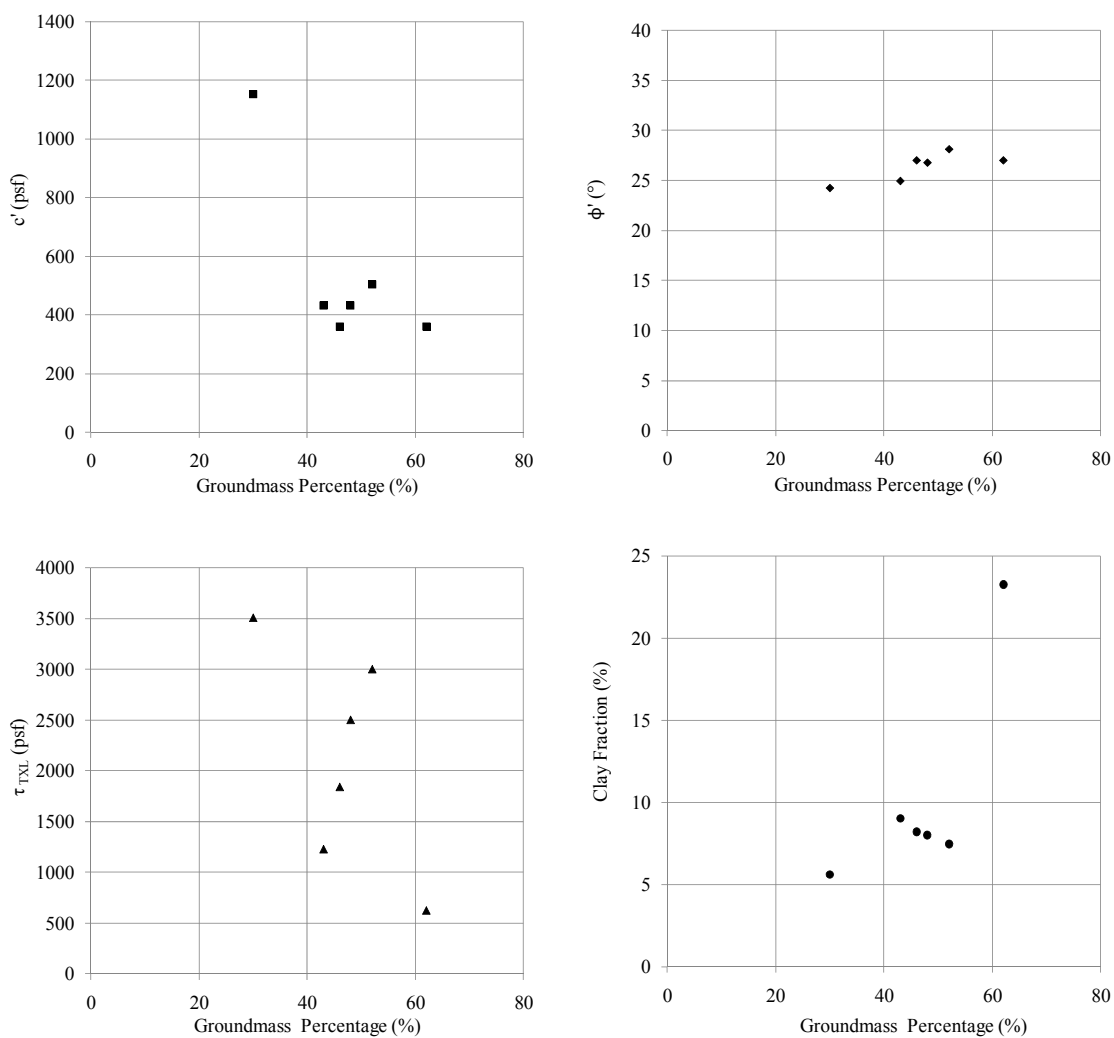


Figure 5.51 – PC1 Groundmass percentage versus c' , ϕ' , τ_{TXL} , and clay fraction

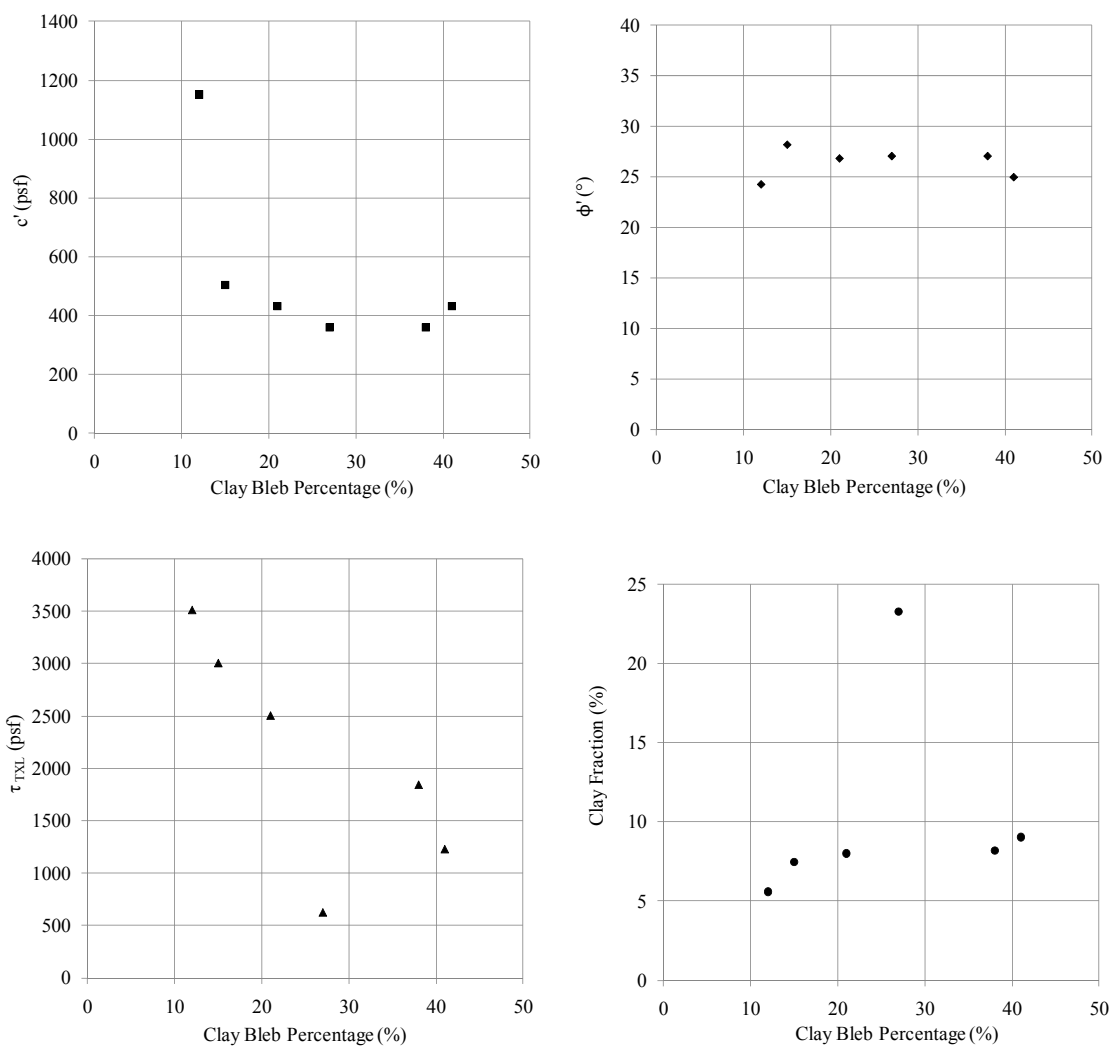


Figure 5.52 – PC1 Clay blebs percentage versus c' , ϕ' , τ_{TXL} , and clay fraction

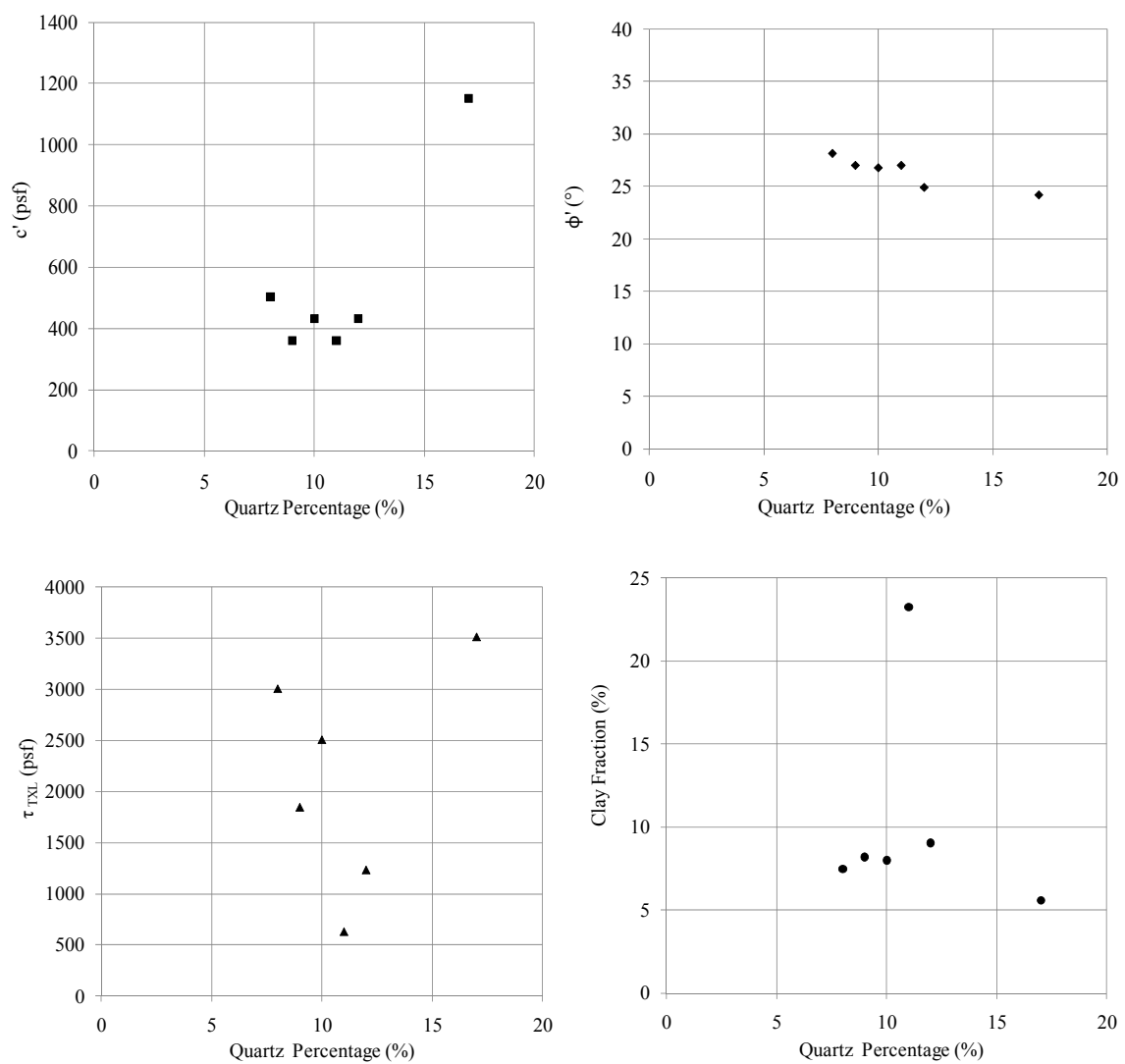


Figure 5.53 – PC1 Quartz percentage versus c' , ϕ' , τ_{TXL} , and clay fraction

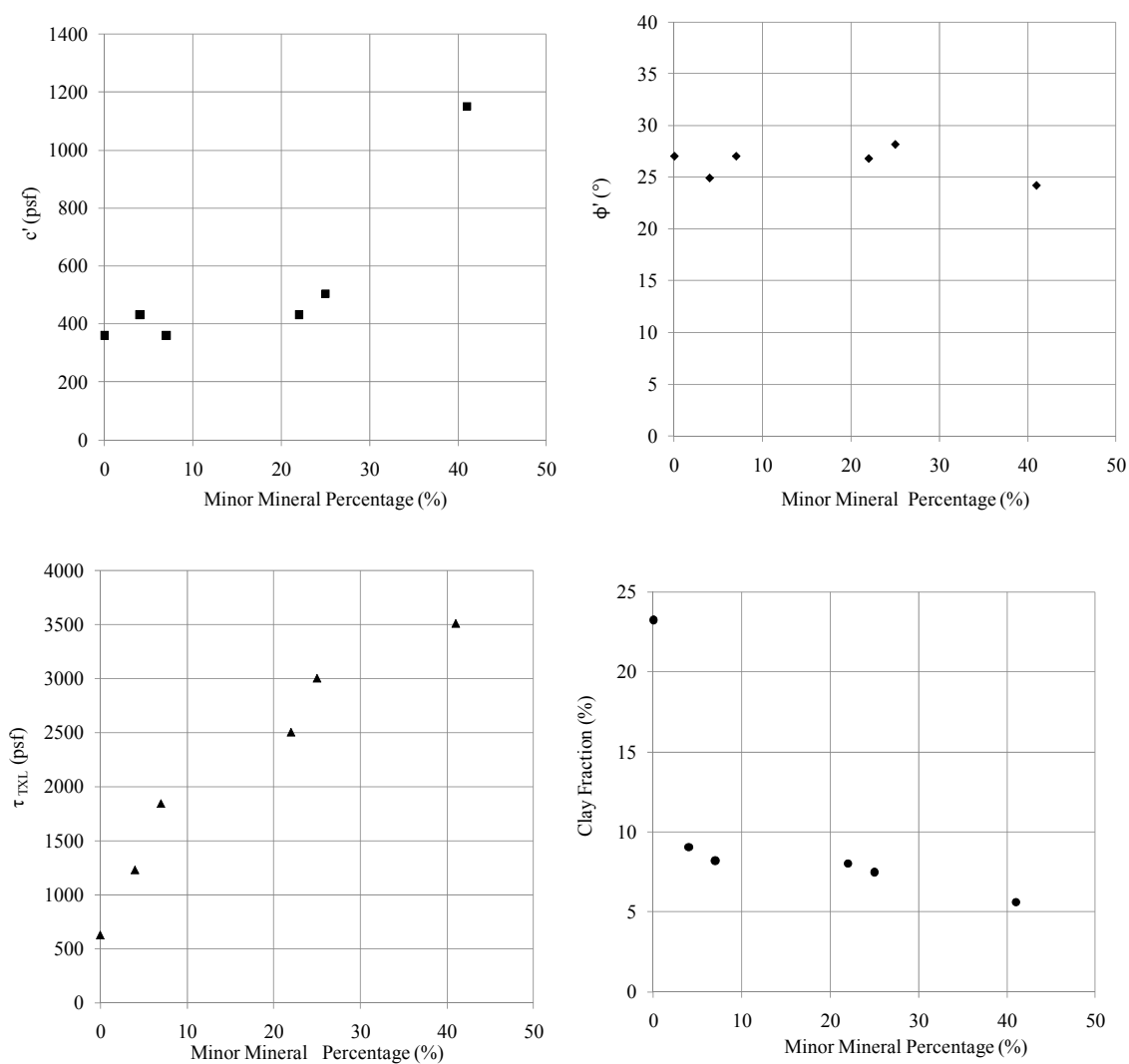


Figure 5.54 – PC1 Minor mineral percentage versus c' , ϕ' , τ_{TXL} , and clay fraction

5.5.1 REMOLDED SOIL ANALYSIS

The details from the remolded petrographic analysis are provided in Tables I2 and photomicrographs are provided in Figures I7 through I9 of APPENDIX I. Figure 5.58 presents the point count percentage versus depth for both the undisturbed (UND) and remolded (REM) residual soils. Table 5.6 presents the undisturbed and remolded point count percentage values, along with the total and percent changes.

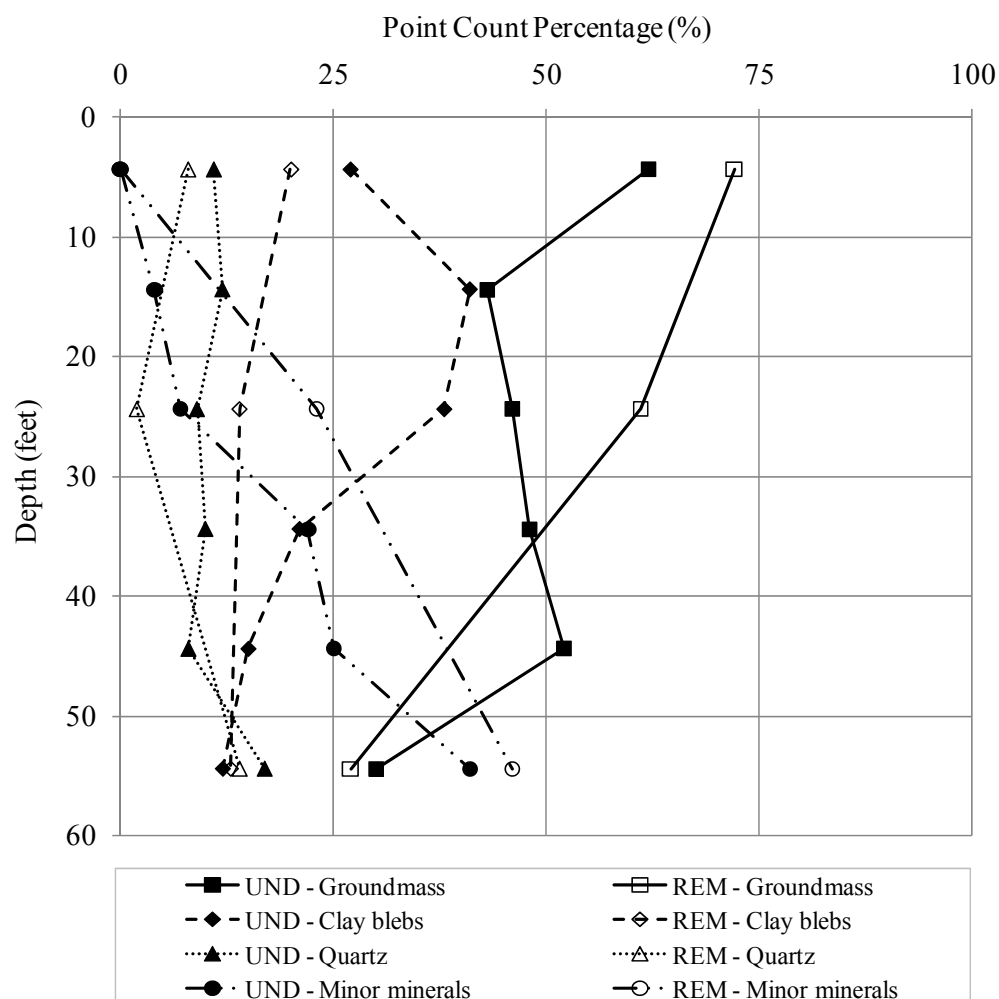


Figure 5.55 – Undisturbed and remolded point count percentages versus depth

Table 5.6 – PC1 Undisturbed and remolded petrographic point count values

Parameter	Depth (feet)	Undisturbed	Remolded	Total Change	Percent Change (%)
Groundmass (%)	4.4	62	72	+ 10	+ 16.1
	24.4	46	61	+ 15	+ 32.6
	54.4	30	27	- 3	- 10.0
Clay bleb (%)	4.4	27	20	- 7	- 25.9
	24.4	38	14	- 24	- 63.2
	54.4	12	13	+ 1	+ 8.3
Quartz (%)	4.4	11	0	- 11	- 100.0
	24.4	9	2	- 7	- 77.8
	54.4	17	14	- 3	- 17.6
Minor Minerals (%)	4.4	0	0	0	0
	24.4	7	23	+ 16	+ 228.6
	54.4	41	46	+ 5	+ 12.2

At each depth, the clay bleb and quartz point count percentages generally decreased when remolded, while the groundmass and minor mineral percentages increased. Additional petrographic observations were that clay blebs were smaller in remolded soil, the overall matrix in remolded samples was less compact and cohesive despite similar mineralogy, grain to grain relations in remolded samples were looser with more interstitial pore space, and remolded samples generally were finer grained (suggesting the clay blebs were broken down) than those of undisturbed samples. These trends clearly indicate observable microscopic effects due to disturbance.

Table 5.7 presents the undisturbed and remolded triaxial shear c' and ϕ' values, along with the total and percent changes. The data from the remolded triaxial shear tests is provided in Figures J1 through J3 of APPENDIX J. An important observation from the remolded triaxial shear tests was that longer times were needed for triaxial consolidation

(higher t_{50} values). This effect may lead to lower residual soil permeability and a need for a slower the shear rate. At each depth evaluated in this research, it is clear that residual soil c' values decreased when remolded, while residual soil ϕ' values increased.

Table 5.7 – PC1 Undisturbed and remolded triaxial c' and ϕ' values

Parameter	Depth (feet)	Undisturbed	Remolded	Total Change	Percent Change (%)
c' (psf)	4.4	403.2	0	- 403.2	- 100
	24.4	403.2	0	- 403.2	- 100
	54.4	1152.0	360.0	- 792.0	- 68.8
ϕ' (°)	4.4	27.0	30.1	+ 3.1	+ 11.5
	24.4	27.0	28.6	+ 1.6	+ 5.9
	54.4	24.2	31.6	+ 7.4	+ 30.6

To evaluate the significance on geotechnical design of the changes in c' and ϕ' , a parametric study was undertaken through a ultimate bearing capacity (Q_u) analysis of a shallow foundation based on equation 5.1, where B is the square foundation width and D is the depth of embedment. Three foundations were examined using the changing soil properties from the three test depths. The bearing capacity factors (N_c , N_q , and N_γ) were based on the friction angle (ϕ') and the other parameter were held constant at the values provided in Table 5.8.

$$Q_t = B^2 (1.3 c' N_c + \gamma_{\text{MOIST}} D N_q + 0.4 B \gamma_{\text{MOIST}} N_\gamma) \quad (5.1)$$

Table 5.8 – End bearing parametric study constants

Parameter	Constant
D (feet)	3
γ_{MOIST} (pcf)	119.4
σ'_v (psf)	3580.5
B (feet)	5

The Q_u analysis is provided in Table 5.9. Q_u decreased at all depths when the calculations were changed for the undisturbed to remolded soil properties. The combined effects of c' of ϕ' due to remolding had an overall negative effect on Q_u or reduced the bearing capacity of the shallow foundation. This analysis illustrates and confirms that current design practice for shallow foundation bearing capacity design is conservative when using remolded soil properties.

Table 5.9 – Bearing capacity parametric study

Depth of Properties (feet)	$Q_{u \text{ UND}}$ (kips)	$Q_{u \text{ REM}}$ (kips)	ΔQ_u (kips)	Percent Change (%)
4.4	594.5	319.8	- 274.7	- 46.2
24.4	594.5	261.7	- 332.8	- 56.0
54.4	1,036	890.9	- 145.1	-14.0

CHAPTER 6: SUMMARY AND ANALYSIS

Residual soil shear strength (τ) parameters are the effective angle of internal friction (ϕ') and cohesion (c'). Geotechnical engineers are more comfortable incorporating the effective angle of internal friction into their design than the cohesion. The effective angle of internal friction is widely accepted due to the large volume of work supporting it. The reluctance to use cohesion comes from the lack of strong fundamental understanding, the friable behavior of residual soils, and the fact that none of the current geotechnical testing methods quantitatively distinguish between residual and transported soil. Geotechnical engineers use transported soil techniques, only calibrated to transported soils, to characterize residual soil sites. They use their accumulated personal knowledge and experience to guide their designs in residual soils. This design practice leads to elevated project costs, conservative designs, significant design variability, and is not very sustainable.

This research began with the goal of answering two questions: 1) Do residual soils have inherent undisturbed cohesion that is generally neglected in geotechnical design? and 2) Can we consistently get undisturbed samples back to the laboratory to measure it? Even though these questions have been made by previous researchers, they were addressed as part of the foundation of this research. Once reliable insitu testing, sampling, and laboratory testing methods were established, the sampling and laboratory methods were still considered to be time consuming and costly. Therefore, the objective

of the dissertation became a study using an insitu test to provide an assessment of the shear strength parameters without having to perform the laboratory tests. In addition, the insitu test had to be a simple, cheap, and practical procedure that could easily be incorporated into currently accepted site investigations. The insitu test chosen for this research was the Standard Penetration Test with Torque (SPT-T). The insitu SPT-T parameters are the blow-count (N), maximum torque (T_{MAX}), and insitu water content (w_{INSITU}). The study utilized the consolidated drained triaxial shear test (TXL) to determine the shear strength parameters (ϕ' and c'). An interface shear test, the dilatometer test (DMT), geotechnical and geologic soil classification tests were also used to reinforce the objective and provide additional quantitative site characterization data.

The main accomplishments of this dissertation were 1) three comprehensive exploration programs for residual soil sites incorporating both insitu and laboratory testing methods, 2) a detailed investigation of direct and indirect relationships between the insitu SPT-T parameters (N , T_{MAX} , and w_{INSITU}) and the laboratory shear strength parameters (ϕ' and c') of residual soils, and 3) an exploratory evaluation of relationships within the collected data set. The raw and reduced data was first plotted versus depth and visually inspected for relationships and trends. Then direct and indirect (multi-variable quantities) empirical correlations between the insitu and laboratory parameters were plotted and the significance of any linear correlations was based on a Pearson analysis. When applicable, linear, logarithmic, and exponential trend lines were obtained and the corresponding R^2 values were examined.

Tables 5.2, 5.3, 5.5, 5.6, and 5.9 summarized the maximum, minimum, average, and standard deviation for the parameters measured during this study. These values

indicate ranges for a basic index system for residual soil. The blow-count (N), torque (T), effective angle of internal friction (ϕ'), cohesion (c'), and interface friction angle (δ) were comparable to the published residual soil values discussed in the literature review. The adhesion (c_a) investigation in relation to published results was inconclusive due to negative (below zero) value. Table 6.1 provides the average values of the shear strength parameters (c' and ϕ') at each site compared to the average and range of published values. An important observation was the undisturbed residual soils in this study showed inherent c' , which is generally neglected in design. Additionally, an exploratory investigation of remolded residual soils suggests that c' likely decreases and effective angle of internal friction (ϕ') likely increases due to remolding. Also shown in Table 6.1, both the SPT-T and dilatometer (DMT) provided un-conservative ϕ' estimates for the undisturbed residual soils at the research sites investigated.

Table 6.1 – Average Shear Strength Parameter Values

Parameter	Site	Average Values			Published Values	
		Triaxial Shear	SPT-T	Dilatometer	Average	Range
c' (psf)	PC1	556.4			483.1	0 – 1228.32
	BR	780.0				
	PC2	437.1				
ϕ' (°)	PC1	26.3	29.7	33.9	34.5	23 – 45.8
	BR	23.9	28.6	33.5		
	PC2	28.3	30.3	33.8		

In order to further compare the results from this research to published data, the coefficient of variation of was also evaluated and values are shown in Table 6.2.

Table 6.2 – Coefficient of variance results for cohesion (c') and friction angle (ϕ')

Parameter	Site	Average Values	Published Values (Harr, 1987)
c' (psf)	PC1	45.2	40.2
	BR	34.6	
	PC2	40.7	
ϕ' (°)	PC1	6.13	10.3
	BR	10.2	
	PC2	14.5	

Additionally, the torque to blow-count ratio (T/N), the interface friction reduction factor (R_i), and TAN (δ) values were compared to published research. The published T/N values were based on the maximum torque and a 72 percent efficiency for the corrected blow-count (N'_{72}). Decourt (1998) published T/N values of 2.0 for saprolite. Kelly and Lutenegeger (1999) published comparable T/N values of 1.5 for residual soils. The comparable average T/N values were 2.53 at PC1, 3.89 at BR, and 1.88 at PC2. The average coefficient of variance for T_{MAX} and T/N at each site is provided in Table 6.3.

Table 6.3 – Coefficient of variance results for torque (T_{MAX}) and torque ratio (T/N)

Parameter	Site	Average Values
T_{MAX} (ft-lbs)	PC1	48.7
	BR	22.1
	PC2	39.3
T / N	PC1	41.7
	BR	38.7
	PC2	50.0

The average interface friction reduction factor (R_i) values were 0.88 at PC1, 0.89 at BR, and 0.91 at PC2, while the published R_i values were 0.5 to 0.7 for smooth steel on sand and 0.7 to 0.9 for rough steel on sand. In addition, the average TAN (δ) was 0.43 at

PC1, 0.38 at BR, and 0.48 at PC2, which compared to published TAN (δ) values of 0.4 for rusted/rough steel pile foundation design (McCarthy, 2002). These published values were for transported soils since, no published interface tests were found for residual soils.

Additional correlations between various laboratory parameters indicated that disturbed residual soils behave similarly to transported soils. The two best correlations were the liquid limit versus clay fraction and plasticity index versus clay fraction. The graphs are provided in Figure 6.1. While these look good, they are pointing out expected relationships.

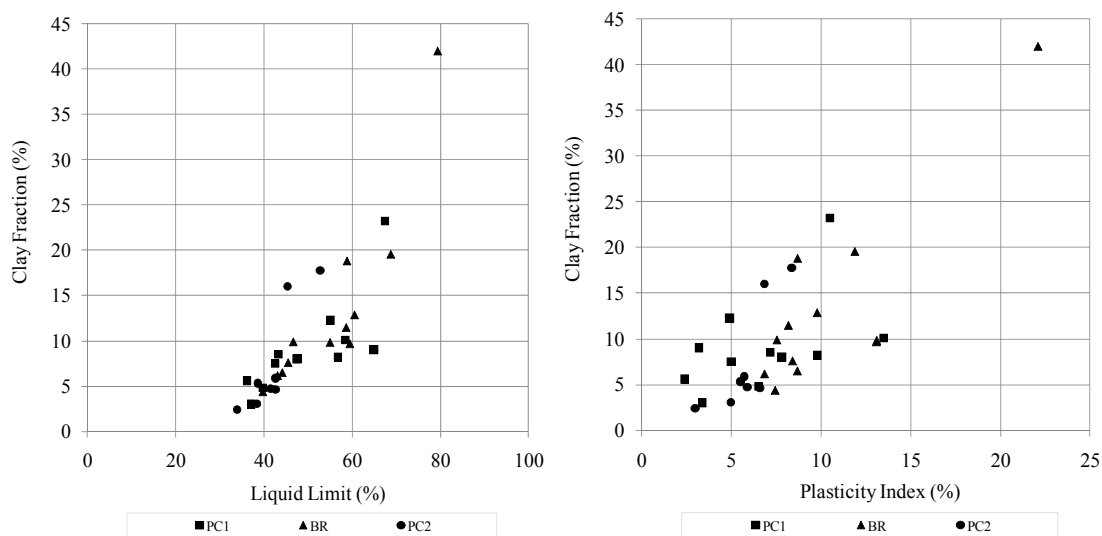


Figure 6.1 – Empirical correlations between laboratory parameters

These results illuminate the importance of quantitatively distinguishing between residual and transported soils within the current geotechnical testing methods. The theoretical evaluations confirmed the developed equations, the overall foundation for the study, and that the earth pressure developed during the SPT-T fell between the at-rest and passive conditions. Figure 6.2 illustrates the theoretical equations for the at-rest and

passive earth pressure conditions. Figure 6.3 show the relationship incorporating an earth pressure of one-half the passive earth pressure and an adhesion equal to one-half cohesion.

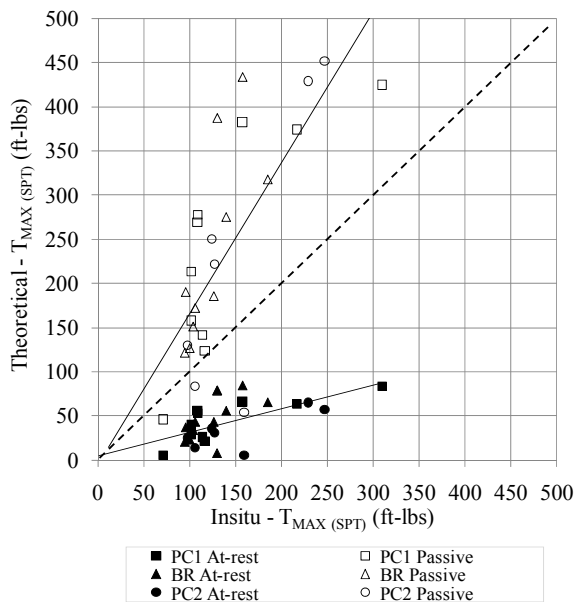


Figure 6.2 – Direct theoretical analysis between T_{MAX} (SPT) [Measured Insitu] versus T_{MAX} (SPT) [Theoretical based on laboratory measurements] – Both at-rest and passive pressure analyses – Linear trend lines

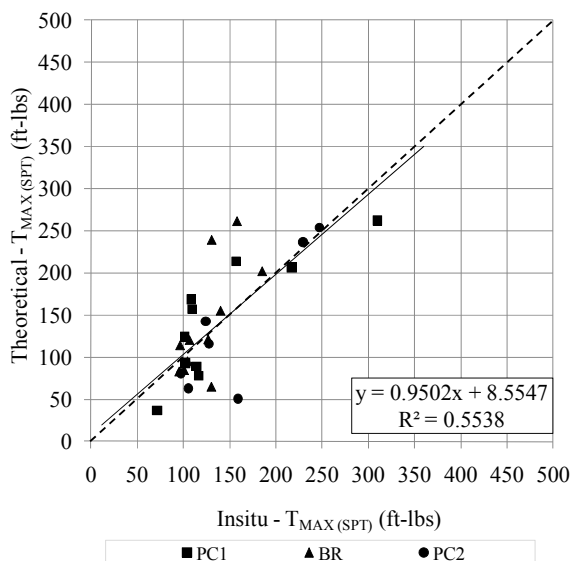


Figure 6.3 – Analysis between T_{MAX} (SPT) [Measured Insitu] versus T_{MAX} (SPT) [Theoretical based on laboratory measurements] – 1:1 correlation ($c_a = 0.5 c'$ and $K = 0.5 K_p$)

After the analysis of the raw data and theoretical justification, the study evaluated the ability of the insitu SPT-T parameters (N , T_{MAX} , and w_{INSITU}) to predict the shear strength parameters (c' and ϕ'). Evaluations were also completed versus the shear strength (τ_{TXL}), an indirect multi-variable quantity based on the c' , ϕ' , and the vertical effective stress (σ'_v). The τ_{TXL} relationship is provided in equation 6.1.

$$\tau_{TXL} = c' + \sigma'_v \tan(\phi') \quad (6.1)$$

The most desired direct predictive empirical correlation was T_{MAX} versus c' . Although an overwhelming linear relationship did not exist (linear $R^2 = 0.1275$), continued research is justified based on visual assessment of the results and the Pearson analysis ($r = 0.357$ and two-tailed p-value = 0.026). The most promising predictive correlation to c' was the indirect quantity of T_{MAX} times w_{INSITU} (linear $R^2 = 0.2496$, $r = 0.500$, and p-value = 0.003). This correlation suggests that the insitu water content at the time of the SPT-T has an influence on the measured T_{MAX} . The two correlations to cohesion are provided in Figure 6.4.

The T_{MAX} versus ϕ' investigation showed a relationship similar to N versus ϕ' . These plots exhibited a cloud of data, mainly due to the relatively limited range of ϕ' values (mainly between 18.9° and 32.4°) and T_{MAX} values (mainly between 95 ft-lbs and 150 ft-lbs). Developing a $T_{MAX} - \phi'$ equation similar to published $N - \phi'$ equations would require a larger data set. The empirical correlations to ϕ' are shown in Figure 6.5. A commonly accepted correlation graph and $N - \phi'$ equation are provided in Figure 6.6 (EPRI, 1990) and equation 6.2 (Peck et al., 1974).

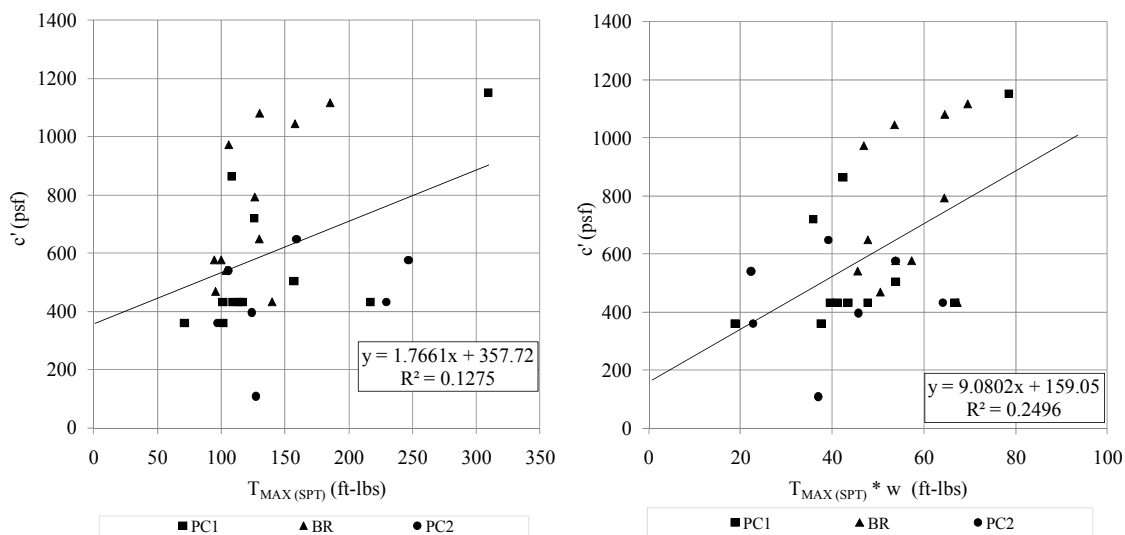


Figure 6.4 – Empirical correlations to cohesion (c')

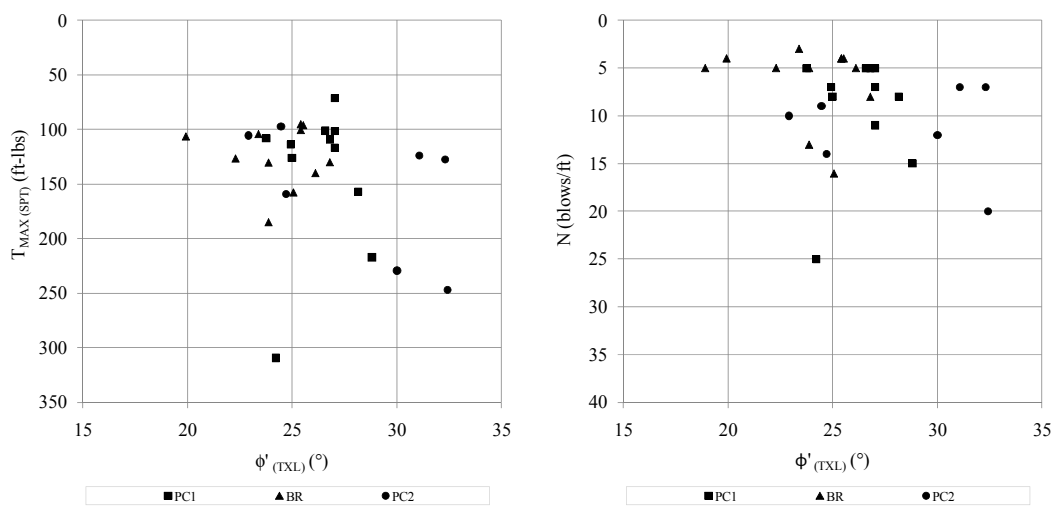


Figure 6.5 – Empirical correlations to effective angle of internal friction ($\phi'_{(TXL)}$)

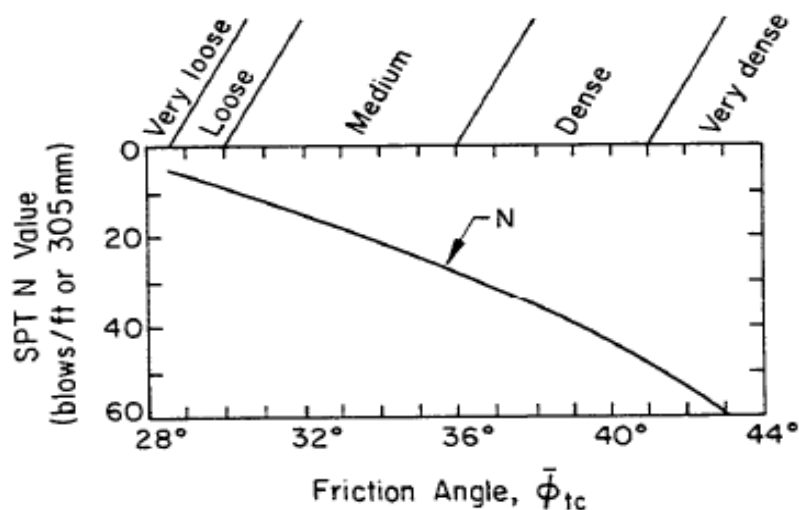


Figure 6.6 – Blow-count (N) versus friction angle (ϕ') correlation (EPRI, 1990)

$$\phi' = 53.881 - 27.6034 * e^{-0.0147*N} \quad (6.2)$$

The T_{MAX} versus τ_{TXL} correlation provided a relatively high trend line (linear $R^2 = 0.3402$, logarithmic $R^2 = 0.3847$, $r = 0.609$ and p -value = 0.000) in comparison to T_{MAX} versus c' or ϕ' . The T_{MAX} times w_{INSITU} versus τ_{TXL} ($R^2 = 0.5902$, $r = 0.768$, and p -value = 0.000) provided the best empirical correlation of geotechnical variables. The τ_{TXL} linear trend lines illustrate that a multi-variable correlation may exist, even though τ_{TXL} is an intermediate calculation largely influenced by the vertical effective stress (σ'_v). These relationships illustrate that trends do exist based on depth and through the weathering profile, although the individual parameters may not directly correlate. The two correlations to τ_{TXL} are shown in Figure 6.7.

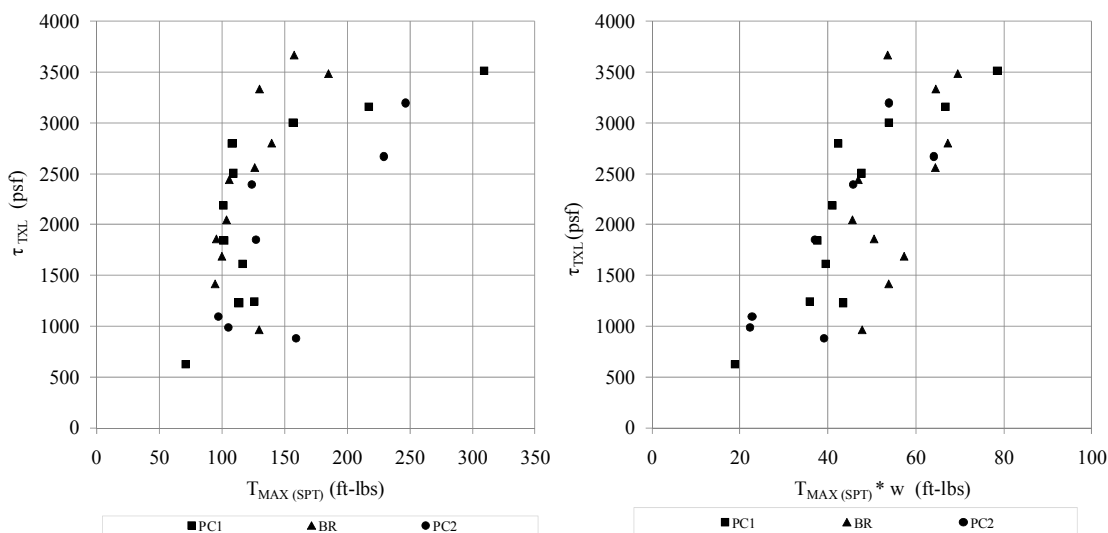


Figure 6.7 – Empirical correlation to shear strength (τ_{TXL})

Additional relationships to the shear strength and shear strength parameters were evaluated versus all of the data collected at the three research sites. Two of the best correlations were the void ratio (e_o) versus ϕ' and e_o versus τ_{TXL} , which are provided in Figure 6.8. Again, these relationships show visual trends, but only reinforce expected relationships from traditional soil mechanics. Figure 6.9 provides a published relationship between relative density and angle of internal friction, where the relative density provides a measure of void ratio and the angle of internal friction provides a measure of shear strength (EPRI, 1990).

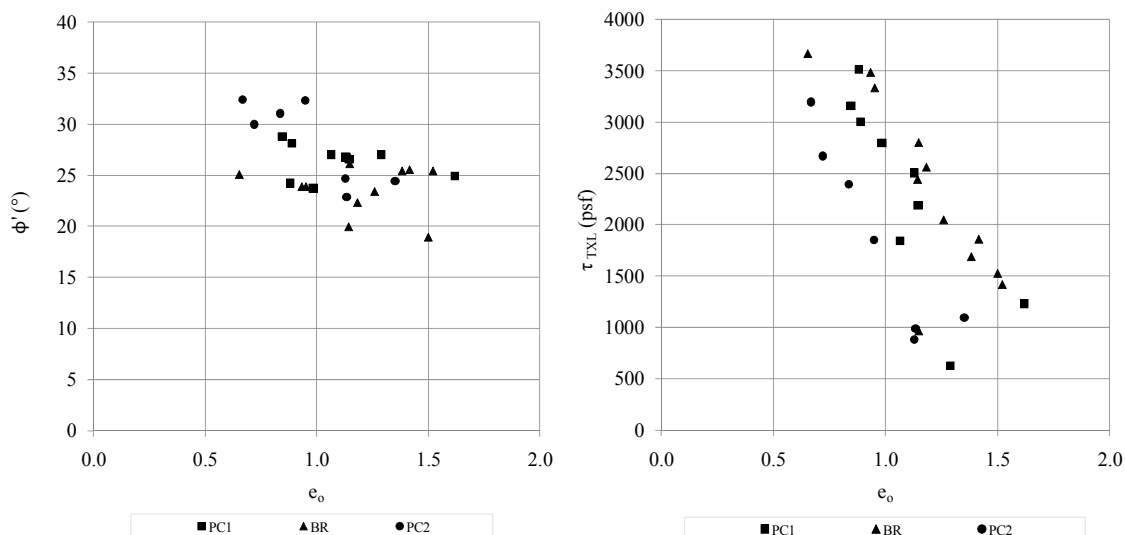


Figure 6.8 – Empirical correlation to shear strength parameters

N Value (blows/ft or 305 mm)	Relative Density	Approximate $\bar{\phi}_{tc}$ (degrees)	
		(a)	(b)
0 to 4	very loose	< 28	< 30
4 to 10	loose	28 to 30	30 to 35
10 to 30	medium	30 to 36	35 to 40
30 to 50	dense	36 to 41	40 to 45
> 50	very dense	> 41	> 45

a - Source: Peck, Hanson, and Thornburn (12), p. 310.
b - Source: Meyerhof (13), p. 17.

Figure 6.9 – Relationship between relative density and angle of internal friction

Using the measured maximum void ratio (e_{MAX}) of 1.62 and minimum void ratio (e_{MIN}) of 0.62 for residual soils in this research, the relative densities through the profiles at each site were calculated. The average relative density values were 0.54 at PC1, 0.54 at BR, and 0.67 at PC2. Figure 6.10 provides all of the data compared to the published data presented in Figure 6.9.

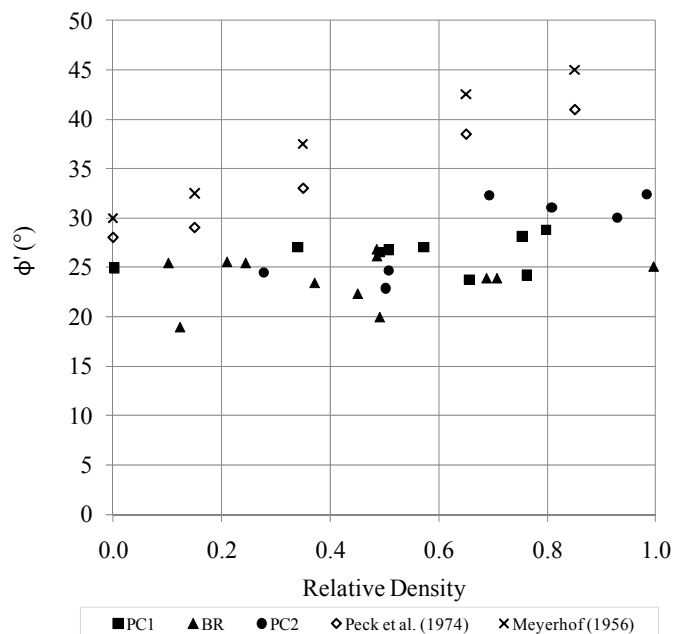


Figure 6.10 – Relative densities compared to published data

None of the geologic soil classification parameters (hue, value, chroma, or red factor) showed a high correlation to the shear strength parameters. The most promising visual geologic correlation was chroma versus shear strength (τ_{TXL}). This relationship had limited value since τ_{TXL} is an intermediate calculation largely influenced by the vertical effective stress (σ'_v). Again, this multi-variable indirect relationship does show that observable trends exist, but the two variables do not necessarily have direct causation. For example, the soil color was redder and more intense at the surface due to the associated weathering processes, but the low shear strength was largely due to the shallow depth and a lower vertical effective stress. Figure 6.11 provides the chroma versus τ_{TXL} relationship.

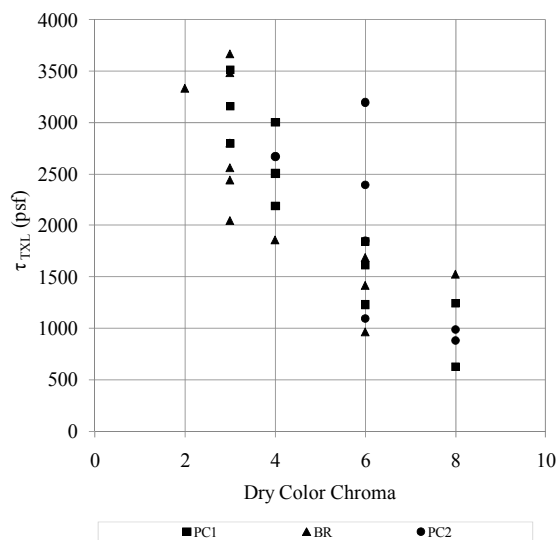


Figure 6.11 – Chroma correlation to shear strength

Beyond the visual assessment of correlations, expected theoretical links between the primary effects of weathering and the shear strength parameters were also evaluated. The two most dominant weathering processes are oxidation and hydrolysis due to the humid sub-tropic climate and the accessibility to oxygen and water. Oxidation and hydrolysis both occur throughout the soil profile but to different degrees as evident in redder hues from iron oxides, more intense chroma, and larger percentages of clay-sized minerals measured by clay fraction and groundmass, along with the percentage and type of minerals present like iron oxide and clays.

Figure 6.12 presents the cohesion, angle of internal friction, and clay fraction versus depth at the three research sites. The cohesion is generally attributed to higher electrostatic forces between clay minerals, cementation, and the relict structure of the parent material, while the friction component is attributed to pure friction and particle interlocking.

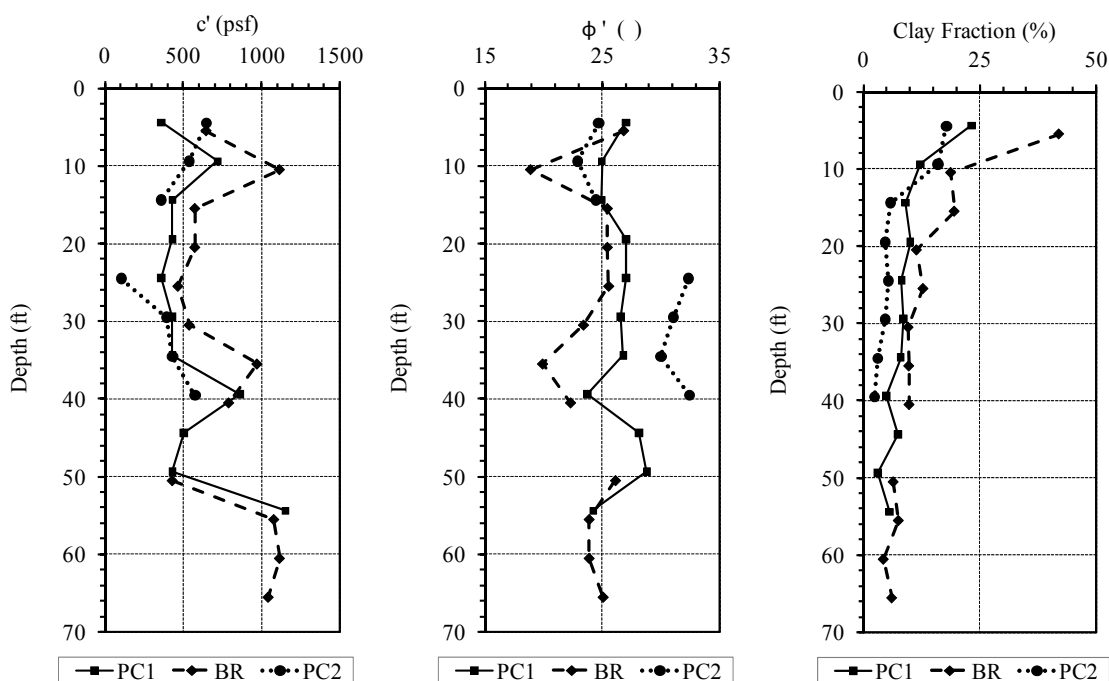


Figure 6.12 – Cohesion, friction angle, and clay fraction versus depth by site

Each of the three sites showed similar cohesion trends versus depth. There were three areas of relatively higher cohesion; 1) around the surface, 2) at the deepest depths, and 3) around the fluctuating groundwater table. At the surface, the higher cohesion correlated to redder hues from increased iron oxides, a higher clay fraction as shown in Figure 6.12, and a higher groundmass percentage, likely leading to more electrostatic forces and higher cementation. The increased amount of secondary minerals like red iron oxides may act to cement larger particles together and also as coatings to strengthen individual particles. The cohesion increases at the surface and at the groundwater table were consistent with an area of higher oxidation and hydrolysis as evidenced by a spike of intense chroma. The trend between chroma and cohesion was not evident throughout the entire soil profile since there was not an increase in chroma at the deepest depth. The

increase in cohesion at the deepest and least weathered soil could be attributed to more intact relict structure of the parent material, through stronger inherent bonds.

The angle of internal friction versus depth is also shown in Figure 6.12. Even though the angle of internal friction was relatively constant at each of the three sites, there were slight drops at the same three locations where the cohesion spiked up; 1) around the surface, 2) at the deepest depths, and 3) at the groundwater table. At these locations, the reduced friction is likely due to smoother and less angular soil particles, which ultimately reduce the pure friction and particle interlocking. Another possible explanation for the reduced angle of internal friction may be small defects created on the primary minerals that are easily propagated as stress is applied. If the products of oxidation and hydrolysis create materials that act as lubricants, the results may be to further reduce the pure friction observed at these locations. The lubrication may be related to clay minerals with weaker bonds or clay minerals with greater affinity to water, thus drawing and maintaining water along the surfaces of the larger particles.

The cohesion developed due to increased electrostatic forces should likely correlate directly to an increase in geotechnical clay fraction. No such visual relationship was found, although there was a visual trend between the angle of internal friction and clay fraction. As the percent of clay sized particles increased, the angle of internal friction slightly decreased. This trend may be attributed to smaller, smoother, and less angular particles, which ultimately results in less pure friction and less particle interlocking. These relationships are shown in Figure 6.13.

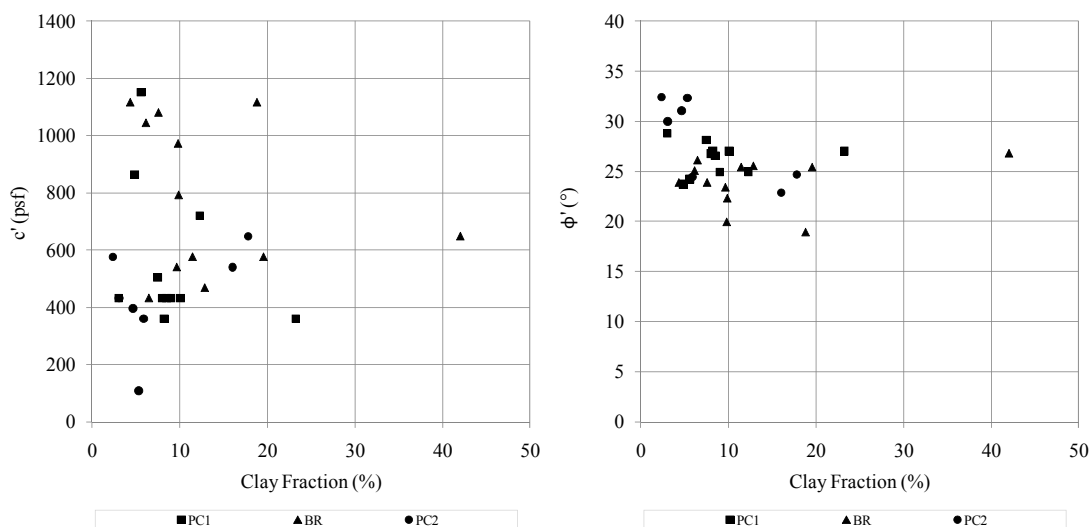


Figure 6.13 – Clay fraction versus the shear strength parameters

A similar relationship was also expected between an increase in cohesion from electrostatic forces and increase in geologic groundmass or clay bleb percentages. These relationships are provided in Figure 6.14. Since the groundmass is a direct indication of amounts of unidentifiable clay-sized particles. An increase in cohesion was expected with more groundmass, but no trend between groundmass and either shear strength parameter was evident. Therefore, the other factors like clay minerals acting to lubricate or retain water may play a role in this relationship. For clay bleb percentage, higher cohesion would have been expected if clay bleb percentage was a direct measure of clay-sized particles, but the clay bleb category only accounted for identifiable clay minerals not size. Every category within the mineralogical analysis had some amount of clay-sized particles within them. The relationship between cohesion and clay bleb percentage showed no trend.

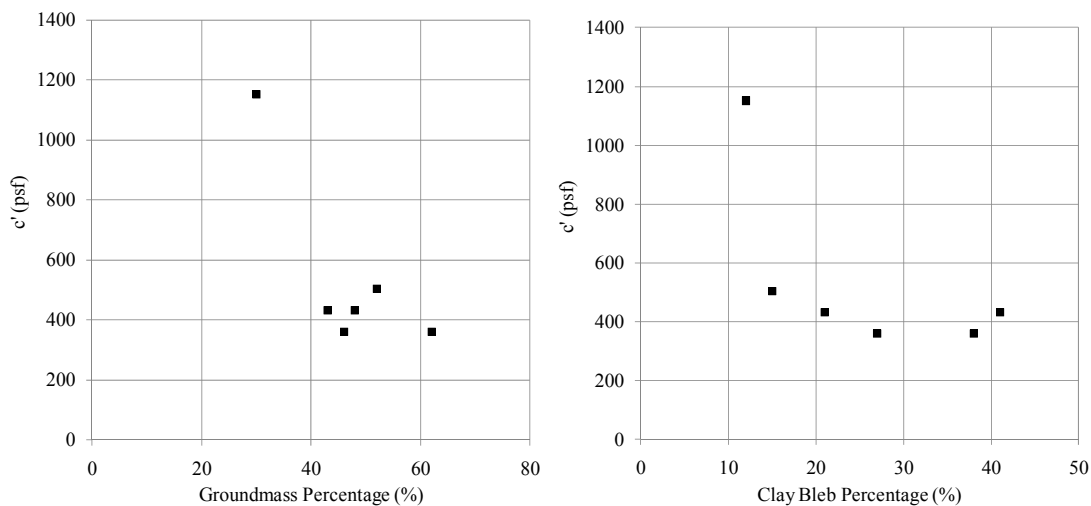


Figure 6.14 – Groundmass or clay bleb percentage versus cohesion

Any mineralogical relationship to the shear strength parameters is also highly dependent on the individual strength of the minerals present. Since quartz is a relatively strong mineral that resist weathering, a correlation between higher quartz percentage and higher angle of internal friction was expected but not found. Although, there was a slight trend indicating less friction as quartz percentage increased. This may be attributed to smaller, smoother, and less angular quartz particles, which ultimately results in less pure friction and less particle interlocking or an increase in minor defects on the quartz minerals. The relationships between quartz percentage and the shear strength parameters are provided in Figure 6.15.

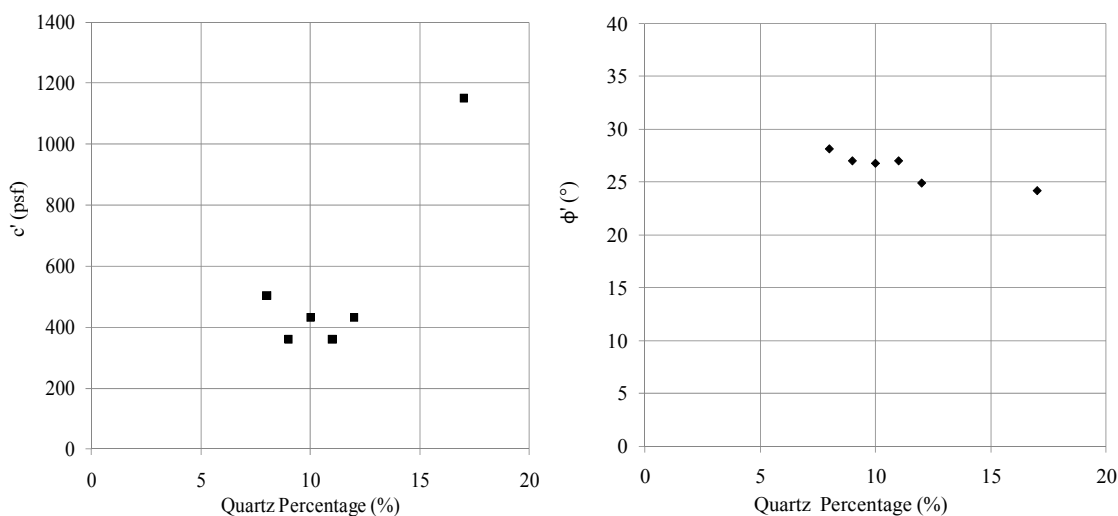


Figure 6.15 - Quartz versus shear strength parameters

It is important to also note that the effects from mineralogy are a relative measurement. The overall effects of one mineral may be masked by the more pronounced effects of other minerals. For example, as quartz percentage is going down reducing friction, other minerals that provide an interlocking structure may be going up increasing friction. A more in-depth analysis of the types of particles present, their strength properties, angularity, roundness, and structural relationship to one another may provide more detailed relationships to the shear strength parameters, but was not completed as part of this dissertation.

CHAPTER 7: CONCLUSIONS

The main findings of this study were:

- 1) The insitu standard penetration test with torque (SPT-T) parameters (N , T_{MAX} , and w_{INSITU}) did not provide clear direct or indirect empirical correlations to the laboratory shear strength parameters (ϕ' and c'). The empirical insitu torque versus cohesion relationship developed is provided in Figure 7.1.

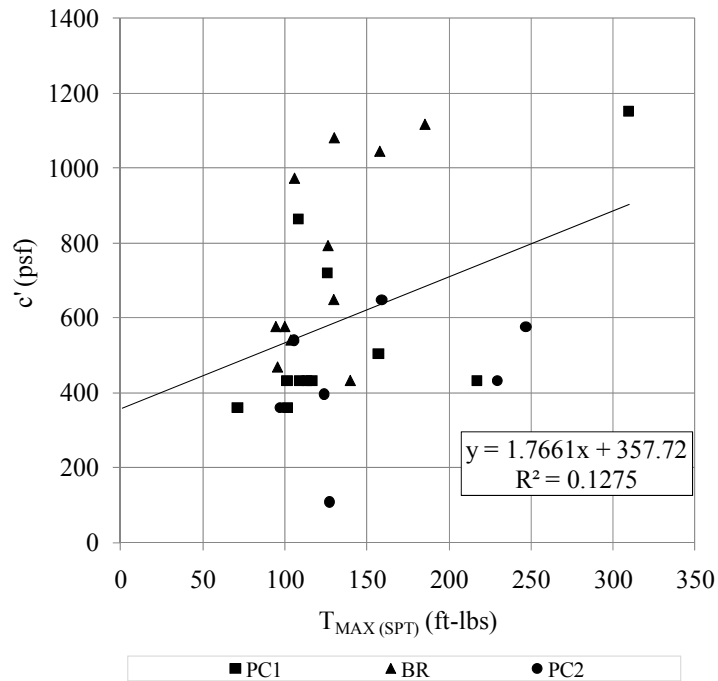


Figure 7.1 – Torque versus cohesion (c')

- 2) No overwhelming statistically significant trends were found within the larger data set, including to the geologic parameters, although some visual trends were evident.
- 3) The undisturbed residual soils tested in this work showed inherent cohesion (c').
- 4) The SPT-T and dilatometer (DMT) tests provided un-conservative estimates of undisturbed residual soil effective angle of internal friction (ϕ').
- 5) Three remolded residual soil triaxial shear tests suggest that c' likely decreases and effective angle of internal friction (ϕ') likely increases due to remolding.

This dissertation described the methods, experiments, data, and analysis used to achieve the defined objective. The project included a comprehensive literature review, theoretical analysis, systematic testing program, detailed interpretation of the results, and future research recommendations. Based on the conclusions, additional work to create a larger data set could lead to valuable geotechnical and geologic relationships. Understanding the relationships between torque and shear strength parameters can improve the fundamental understanding of residual soil behavior.

Ultimately, if the SPT-T is ever put into practice, the implementation of a procedure to measure torque during an SPT site investigation would be relatively simple. The tests would be easy to perform, require limited training, and need only a couple of additional minutes per test depth. A hand-held removable torque cell could easily be added in-line for each test by the drill rig operators. Another option could be to develop a correlation curve between the drill rig hydraulic pressures used to apply the torque and the torque. With this curve, the operator would simply need to read and report the pressure during the applied torque.

Based on the results of this study, the SPT-T may eventually provide an assessment of soil properties including shear strength. The main drawback of this study was the limited number of tests used in the correlations, but this study does provide reasonable justification for further research. The results do not significantly conclude that the SPT-T is better than current methods. Ultimately, the implementation of a quick and simple torque test to a site investigation may provide valuable data for geotechnical design.

Based on the results of this study, the SPT-T can provide an assessment of soil properties including shear strength. The main drawback of this study was the limited number of tests used in the correlations, but this study does provide reasonable justification for further research. Ultimately, the implementation of a quick and simple torque test to a site investigation may provide valuable data for geotechnical design. The possibilities are evident.

CHAPTER 8: RESEARCH LIMITATIONS AND RECOMMENDATIONS

The main limitations of the research were funding and the dependence on limited insitu testing assistance by the NCDOT. The timeline, depth, and breadth of the study were confined by these limitations. A larger data set would have increased the confidence and value of this investigation. Compared to published research, the time, and the cost to perform the testing methods, the 30 test depths at three research sites were significant to provide a reasonable exploratory evaluation of trends and correlations. At two of the research sites, more depths were tested than originally proposed. Also, the laboratory testing was strategically chosen based on the limited number of undisturbed soil samples.

Secondary research sites, additional laboratory tests, and the fabrication of a Shelby tube pusher were considered, but not included within the final project. All of the sites in this research were in a similar residual soil of granitic parent material within the Charlotte Belt. Testing in a single soil type had the advantage of a larger data set of similar soil, although all of the data may have been clouded within a range of this particular soil type investigated. In other words, if various soil types (residual soils outside the Charlotte Belt or transported soils) were examined, there may have been more of a macro trend between the insitu parameters and the laboratory shear strength parameters. The Shelby tube pusher would have allowed for more independent insitu soil

testing. Another limitation was the undetermined sensitivity of the SPT-T to field conditions and operator variability.

The future path of this research should focus on the development and standardization of the standard penetration tests with torque (SPT-T) and the interface shear test (INT). The two testing methods are still in their early stages of development and only a larger data set can define the best procedure and increase confidence in their results. An exhaustive set of tests could show that these tests are valuable, statistically significant, reliable, and repeatable. Additionally, the tests should be done on a variety of transported and residual soils. Even with the limited number of tests performed during this study, the results clearly demonstrate the feasibility of the methods and the value of further research.

Based on the vertical stress, depth influence, and that T_{MAX} was relatively constant with depth (between 95 ft-lbs and 150 ft-lbs), a more comprehensive corrected torque value than the one presented in this research (T'_{MAX}) may be a valuable path of investigation. Corrections for the depth, vertical stress, angular velocity, water content, soil classification, or sampler conditions may provide a better empirical correlation. In addition, using a normalization constant into another multi-variable quantity similar to the shear strength (τ_{TXL}) may provide additional data analysis tool.

Since the conditions at the time of the insitu SPT-T testing was not exactly the same as the conditions during the laboratory triaxial shear testing, there is significant justification to study the fundamental behavior of the residual soil at various conditions and along various stress paths. For example, the insitu SPT-T was likely performed at an undrained, disturbed, passive earth pressure condition, while the triaxial shear tests were

performed at a drained, less disturbed condition than the SPT-T. Determining the conditions and stress history of each test could lead to a less empirical correlation than was determined during this research, along with a better fundamental understanding of residual soil behavior. Even though the SPT-T and triaxial shear tests were at slightly different soil conditions, the soil properties are closely related.

If the SPT-T became an accepted insitu test, the limited flexibility in the procedure would dictate the insitu conditions at the time of the tests. The conditions of a residual soil site may be considered drained or undrained depending on the depth of the test, whether sufficient time is given after the insertion of the sampler, and the angular velocity of the test. Based on the triaxial consolidation results at the research sites in this study, one minute would be sufficient time to wait between sampler insertion and torque application for the residual soil. For a drained torque test, the required angular velocity of the test would need to be slow enough to not allow the excess pore pressure to build. The angular velocity was not evaluated during this research.

Additionally, the stress history of the triaxial shear test samples may affect the results determined. Adjusting the triaxial shear test conditions may provide a better comparison between insitu and laboratory shear strength properties. This more fundamental comparison would be valuable, even though the shear strength properties needed would depend on the requirements of the design. Additionally, neglecting the cohesion or assuming undisturbed parameters may provide conservative or unconservative designs depending on the application and the whether the long-term or short-term parameters are required. The drained shear strength parameters were investigated in this research because they simulates the long term behavior of soil and, in

general, slope stability and retaining structures are governed by the long-term parameters. Even though the drained shear strength parameters were examined, a complete geotechnical design must incorporate numerous variables. The soil type, stress history, and loading characteristics (type, size, and duration), along with site characteristic like groundwater are crucial to evaluate.

Another recommendation is to return to the insitu test sites and collect additional STT-T data and Shelby tubes. The STT-T should be performed to evaluate the repeatability of the torque measurement on exactly the same soil. The soil samples could then be used to perform additional geotechnical tests including direct shear, consolidation, permeability, and undrained triaxial shear tests. The comparison between the drained and undrained triaxial shear tests would be valuable to evaluate which triaxial shear procedure is more applicable and appropriate for residual soils. Another recommendation would be to perform numerous insitu tests at a single depth in a homogeneous soil type. In conjunction with numerous undisturbed laboratory tests, this approach could investigate the repeatability of the tests. Another suggestion is to perform SPT-T at transported soil control sites to see if there is any fundamental difference between SPT-T in sands, clays, and residual soils.

Due to the low confidence in the INT results, a recommendation is to perform more INT tests focused on the accuracy and precision of the test. In addition, the INT tests should be performed on a wider range of normal stresses to establish a relevant stress range for the test. The tests would presumably verify a straight failure line at all normal stresses or show a failure curve similar to the triaxial Mohr-Coulomb failure

curve. The tests may also define the influence of normal stress on adhesion (c_a) and interface friction angle (δ).

The INT tests should also include analysis of the Shelby tube sampler used in the Shelby tube test with torque (STT-T) and the influence of water on the soil-sampler interface. These analyses could improve the fundamental understanding of the test system. The STT-T study could provide an additional link between the at-rest and passive earth pressure conditions developed during sampling and testing. Since water affects the interface friction between many surfaces, the study should focus on the influence of water as a lubricant on the soil-sampler interface along with the role of excess pore pressure on the interface shear strength measurements, c_a and δ . A set of both dry and wet INT tests would help to address this concern.

Based on the results of the three remolded triaxial tests and the distinctive characteristics of residual soils, another recommendation is to perform a suite of remolded geotechnical tests on the same soils as this research has already characterized. It is important to continue to examine and quantify the difference between undisturbed and remolded residual soil properties. The tests could specifically address the question of whether residual soils have structure or fabric properties that lead to inherent cohesion or shear strength. The tests could include remolded triaxial shear (drained and undrained), direct shear, interface shear, consolidation, permeability, and compaction. All of the soil tested during this study was stored in plastic bags for future testing and analysis. A summary of the soil samples collected and remaining are provided in Tables E4, E5, and E6 of APPENDIX E.

Based on the petrographic study, a final recommendation would be to develop a quantifiable measurement of interlocking that could be evaluated during the point count analysis. For example, every time the point count lands on a grain that is larger than a predetermined size, the total percent of surface area adjacent to other grains could be estimated. The quantification of interlocking could lead to better and more accepted geotechnical correlations.

REFERENCES

- Adderley, W., Simpson, I., and Davidson, D. (2002). "Colour description and quantification in mosaic images of soil thin sections." *Geoderma*, 108(3-4), 181-195.
- Anderson, J. B., Ogunro, V. O., Detwiler, J. M., and Starnes, J. R., (2006). "DMT testing for the estimation of lateral earth pressure in Piedmont residual soils." *Proc., Second International Conference on the Flat Dilatometer*, Washington, D.C., 184-189.
- Axelsson, G. and Westin, A. (2000). "Torque Tests on Driven rods for prediction of pile set-up." *Geotechnical Special Publication no. 100*, 297-311.
- Barrett, L. (2002). "Spectrophotometric color measurement in situ in well drained sandy soils." *Geoderma*, 108(1-2), 49-77.
- Blight, G. E. (1997). *Mechanics of Residual Soils: A guide to the formation, classification, and geotechnical properties of residual soils, with advice for geotechnical design*, Balkema Publishers, Rotterdam, Netherlands.
- Bishop, A. W. and Henkel, D. J. (1957). *The Triaxial Test*. William Clowes 7 Sons, London.
- Birkeland, P.W., (1999). *Soil and Geomorphology*. 3rd ed. New York, Oxford University Press.
- Bowles, J. E. (1988). *Foundation Analysis and Design*. McGraw Hill, Inc., New York.
- Brand, E. W., and Phillipson, H. B. (1985). *Sampling and Testing of Residual Soils: A Review of International Practice*, Southeast Asian Geotechnical Society, Scorpion Press, Hong Kong.
- Bullock, P. J., Schmertmann, J. H., McVay, M. C., and Townsend, F. C. (2005). "Side shear setup. II: Results from Florida test piles." *Journal of Geotechnical and Geoenvironmental Engineering*, 131(3), March, 301-310.
- Bullock, P. J., and Schmertmann, J.H. (2003). "Determining the effects of stage testing on the dimensionless pile side shear setup factor." Submitted to the Florida Department of Transportation by University of Florida, Final Report Contract #BC354 RPWO #27, February.
- Charlotte Chamber of Commerce (2009). www.Charlottechamber.com
- City-data.com (2009).
<http://www.city-data.com/us-cities/The-South/Charlotte-Geography-and-Climate.html>

- Coduto, D. P. (1994). *Foundation Design: Principles and Practices*. Prentice Hall, Inc., New Jersey.
- Crowther, C. L. (1963). "The design, construction, and use of a static penetrometer in micaceous silts of the southern Piedmont region." MS Thesis, Georgia Institute of Technology, Atlanta, GA.
- Decourt, L. (1998). "A more rational utilization of some old in situ tests." *Proc. First Intl Conf. on Site Characterization ISC '98*, Atlanta, A. A. Balkema, 913-918.
- EPRI EL-6800 (1990). "Manual on Estimating Soil Properties for Foundation Design." Final Report, Project 1493-6, Cornell University, Ithaca, New York.
- Failmezger, R. A., Rom, D., and Ziegler, S. B. (1999). "SPT? - A better approach to site characterization of residual soils using other insitu tests." *Behavioral Characteristics of Residual Soils, Geotechnical Special Publication No. 92*, ASCE, 158-175.
- Fontes, M., and Carvalho Jr., I. (2005). "Color attributes and mineralogical characteristics, evaluated by radiometry, of highly weathered tropical soils." *Soil Science Society of America Journal*, 69(4), 1162-1172.
- Gan, J. K. M., and Fredlund, D.G. (1996). "Shear strength characteristics of two saprolitic soils." *Journal Canadian Geotechnical*, 33(4), 595-609.
- Garga, V. K. (1988). "Effect of Sample Size on Shear Strength of Basaltic Residual Soils." *Canadian Geotechnical Journal*, 25(3), August, 478-487.
- Google maps (2009). www.google.com/maps
- GPE, Inc. (1993). "Marchetti Dilatometer – Data Reduction "DMT" Basic Program." April 3, 1993.
- Harr, Milton E. (1987). *Reliability-based Design in Civil Engineering*. Dover Publications, Inc., Mineola, New York.
- Heartz, W. T. (1986). "Properties of a Piedmont residual soil." PhD Dissertation, North Carolina State University, Raleigh, NC.
- Hicks, J. M. (2001). "Determining the effect of stage testing on the dimensionless pile side shear setup factor." MS Thesis, University of Florida, FL.
- Jeng, F. S., Weng, M. C., Lin, M. L., and Huang, T. H. (2004). "Influence of petrographic parameters on geotechnical properties of tertiary sandstones from Taiwan." *Engineering Geology*, 73, 71-91.

- Kelly, S. P., and Lutenegeger, A. J. (2004). "Unit Skin Friction from the Standard Penetration Test Supplemented with the Measurement of Torque." *Journal of Geotechnical and Geoenvironmental Engineering*, 130(5), 540-543.
- Kelly, S. P., and Lutenegeger, A. J. (1999). "Enhanced Site Characterization in Residual Soils Using the SPT-T and Drive Cone Tests." *Behavioral Characteristics of Residual Soils, Geotechnical Special Publication No. 92*, ASCE, 88-100.
- Kishida, H., and Uesugi, M. (1987). "Tests Of The Interface Between Sand And Steel In The Simple Shear Apparatus." *Geotechnique*, 37(1), 45-52.
- Lambe, P. C., and Hertz, W. T. (1988). "Consolidated drained triaxial testing of Piedmont residual soil." *Advanced Triaxial Testing of Soil and Rock, ASTM STP 977*, 311-320.
- Lambe, T. W., and Whitman, R. V. (1969). *Soil Mechanics*, John Wiley and Sons, New York.
- Lee, I. K., and Coop, M. R. (1995). "Intrinsic behaviour of a decomposed granite soil." *Geotechnique*, 45(1), 117-130.
- Liao, S. S. C., and Whitman, R. V. (1986). "Overburden correction factors for SPT in Sand." *Journal of Geotechnical Engineering Division, ASCE*, 112(3).
- Lutenegeger, A. J., and Kelly, S. P. (1998). "Standard penetration tests with torque measurement." *Geotechnical site characterization, Robertson and Mayne, eds.*, 939-945.
- Mackenzie, W. S. and Guilford, C. (1980). *Atlas of rock-forming mineral in thin sections*, Halsted Press, John Wiley & Sons, New York, New York.
- Maksoud, M. A. F. (2006). "Laboratory determining of soil strength parameters in calcareous soils and their effect on chiseling draft prediction." *Balkin Agricultural Engineering Review*, 9, 1-13.
- Mayne, P.W., and Brown, D.A. (2003). "Site Characterization of Piedmont residuum of North America." *Characterization and Engineering Properties of Natural Soils*, 2, 1323-1339.
- Mayne, P. W., Brown, D. A., Vinson, J. L., Schneider, J. A., and Finke, K. A. (2000). "Site Characterization of Piedmont Residual Soils at the NGES, Opelika, Alabama." *National Geotechnical Experimentation Sites, ASCE GSP No. 93*, 160 -185.
- McCarthy, D. F. (2002). *Essentials of Soil Mechanics and Foundations Basic Geotechnics*, 6th ed., Prentice Hall, Upper Saddle River, New Jersey.

Miller, E. T. (1957). "A study of shear characteristics of the soils of the Piedmont region determined by rotating vanes." MS Thesis, Georgia Institute of Technology, Atlanta, GA.

Mitchell, J. K., (1993). *Fundamentals of Soils Behavior*, Wiley, New York.

Mitchell, J. K., and Sitar, N. (1982). "Engineering properties of tropical residual soils." Proceedings of the ASCE Geotechnical Engineering Division Specialty Conference: Engineering and Construction in Tropical and Residual Soils, Honolulu, HI, 30-57.

Mitchell, J. K., and Soga, K. (2005). *Fundamentals of Soil Behavior*, John Wiley and Sons, Hoboken, New Jersey.

Mohamedzein, Y., and Mohammed H. A. (2006). "Compressibility and shear strength of a residual soil." *Geotechnical and Geological Engineering*, 24, 1385 -1401.

Moon, V. G. (1993). "Microstructural controls on the geomechanical behaviour of ignimbrite." *Engineering Geology*, 35(1-2), 19-31.

Myerhoff, G. G. (1956) "Penetration tests and bearing capacity of cohesionless soils." Journal of Soil Mechanics and Foundation Division. ASCE, 82(SM1), 1-19.

Myrianthis, M. L. and Leach, B. (1978). "Basic geotechnical and mineralogical properties of the weathered Athenian schist." *Rock Mech Felsmech Mec Roches*, 10(3), 151-164.

NCDENR, North Carolina Department of Environment and Natural Resources (2005). <http://www.enr.state.nc.us/>

Neese, W. D. (1986). *Introduction to Optical Mineralogy*, Oxford University Press, New York, New York.

Onodera, T., Masanobu, O., and Minami, K. (1976). "Shear Strength of Undisturbed Sample of Decomposed Granite Soil." *Soils and Foundations*, 16(1), 17-26.

Peck, R. B., Hanson, W. E., and Thornburn, T. H. (1974). *Foundation Engineering*, John Wiley and Sons, New York.

Peixoto, A. S. P., de Albuquerque, P. J. R., and de Carvalho, D. (2000). "Utilization of SPT-T, CPT and DMT tests to predict the ultimate bearing capacity of precast concrete pile in Brazilian unsaturated residual soil." *Geotechnical Special Publication no. 99*, 32-39.

Peixoto, A. S. P, Antenor, V. B., Ramos, T. M., and David, R. (2007). "Rod length influence in torque measurement of SPT-T test." *Geotechnical Special Publication, no. 162, Proceedings of Sessions of Geo-Denver 2007 Congress: Problematic Soils and Rocks and In Situ Characterization*, 14.

- Rahardjo, H., Aung, K. K., Leong, E. C., and Rezaur, R. B. (2004a). "Characteristics of Residual Soils in Singapore as formed by weathering." *Engineering Geology*, 73, 157-169.
- Rahardjo, H., Ong, B. H., and Leong E. C. (2004b). "Shear strength of a compacted residual soil from consolidated drained and constant water content triaxial tests." *Canadian Geotechnical Journal*, 41(3), 421-436.
- Rausche, F., Thendean, G., Abou-matar, H., Likin, G. E., and Goble, G. G. (1996). "Determination of Pile Drivability and Capacity for Penetration Tests, Volume 1: Final Report." FHWA-RD-96-179. Federal Highway Administration, McLean, VA.
- Rigo, M. L., Pinheiro, R. J. B., Bressani, L. A., Bica, A. V. S., and de Silveira, R. M. (2004). "The residual shear strength of tropical soils." *Canadian Geotechnical Journal*, 43, 431-447.
- Schaetzl, R. J., and Anderson, S. (2005). *Soils: Genesis and Geomorphology*. Cambridge University Press, New York.
- Soni, P., and Salokhe, V. (2006). "Theoretical Analysis of Microscopic Forces at the Soil-tool interfaces: A Review." *Agricultural Engineering International: the CIGR Ejournal*. Manuscript PM 06 010, 7, 1-25.
- Soper, D. (2009). <http://www.danielsoper.com/statcalc/calc44.aspx>
- Sowers, G. F. (1963). "Engineering properties of residual soils derived from igneous and metamorphic rocks." *Proc., 2nd Panamerican Conf. on Soil Mech. and Found. Engrg.*, Sao Paulo, Brazil.
- Subba Rao, K. S., Allam, M. M., and Robinson, R. G. (2002). "An apparatus for evaluating adhesion between soils and solid surfaces." *Journal of Testing and Evaluation*, 20(1), 27-36.
- Taylor, D. W. (1948). *Fundamentals of Soil Mechanics*, John Wiley and Sons, New York.
- Terzaghi, K., and Peck, R. B. (1948). *Soil Mechanics in Engineering Practice*, John Wiley and Sons, New York.
- Torrent, J. and Barron, V. (1993). "Laboratory Measurements of Soil Color: Theory and Practice." Soil Science Society of America Inc. Special Publications, 31. Soil Color. Proceedings symposium, San Antonio. 21-33.
- Tsubakihara, Y., Kishida, H., and Nishiyama, T. (1993). "Friction between cohesive soils and steel." *Soils and Foundations*, 33(2), 145-156.

USGS, United State Geologic Survey (2001).
<http://va.water.usgs.gov/PiedWkshop/map.htm>

Vaughan, P. R., and Kwan, C. W. (1984). "Weathering, structure, and insitu stress in residual soils." *Geotechnique*, 34(1), 43-59.

Vaughan, P. R. (1985). "Mechanical and Hydraulic Properties of In-situ Residual Soils." *First International Conference in Geomechanics in Tropical Lateritic and Saprolitic Soils- General Report, Dept Civil Engineering – Imperial College, London*, 32.

Vaughan, P. R., Maccarini, M., and Mokhtar, S. M. (1988). "Indexing the engineering properties of residual soil." *Quarterly Journal of Engineering Geology*, London, 21, 69-84.

Vaughan, P. R. (1990). "Keynote paper: Characterizing the mechanical properties of in-situ residual soils." *Geomechanics in Tropical Soils, Proc. Of the Second International Conference in Geomechanics in Tropical Soils*, 469-487.

Viana da Fonseca, A., Carvalho, J., Ferreira, C., Santos, J. A., Almeida, F., Pereira, E., Feliciano, J., Grade, J., and Oliveira, A. (2006). "Characterization of a profile of residual soil from granite combining geological, geophysical, and mechanical testing techniques." *Geotechnical and Geological Engineering*, 24, 1307-1348.

Vinson, J. L., and Brown, D. A. (1997). "Site characterization of the Spring Villa geotechnical test site and a comparison of strength and stiffness parameters for a Piedmont residual soil." *Report No. IR-97-04, Highway Research Center, Harbert Engineering Center, Auburn University, AL*, 385.

Viscarra Rossel, R., McBratney, A., Minasny, B., and Roudier, P. (2006). "Colour space models for soil science." *Geoderma*, 133(3-4), 320-337.

Wang, C. E. (1995). "Deformation characteristics and elastic settlement of piedmont residual soils." MS Thesis, North Carolina State University, Raleigh, NC.

Wang, C. E., and Borden, R. H. (1996). "Deformation characteristics of Piedmont residual soils." *ASCE Journal of Geotechnical Engineering*, 122(10), 822-830.

Wang, Y. H., and Yan, W. M. (2006). "Laboratory studies of two common saprolitic soils in Hong Kong." *Journal of Geotechnical and Geoenvironmental Engineering*, 132(7), 923-930.

Winter, C. J., Wagner, A. B., and Kormurka, V. E. (2005). "Investigation of Standard Penetration Torque Testing (SPT-T) to Predict Pile Performance." Submitted to the Wisconsin Department of Transportation. Wisconsin Highway Research Program #0092-04-09.

APPENDIX A – Maps

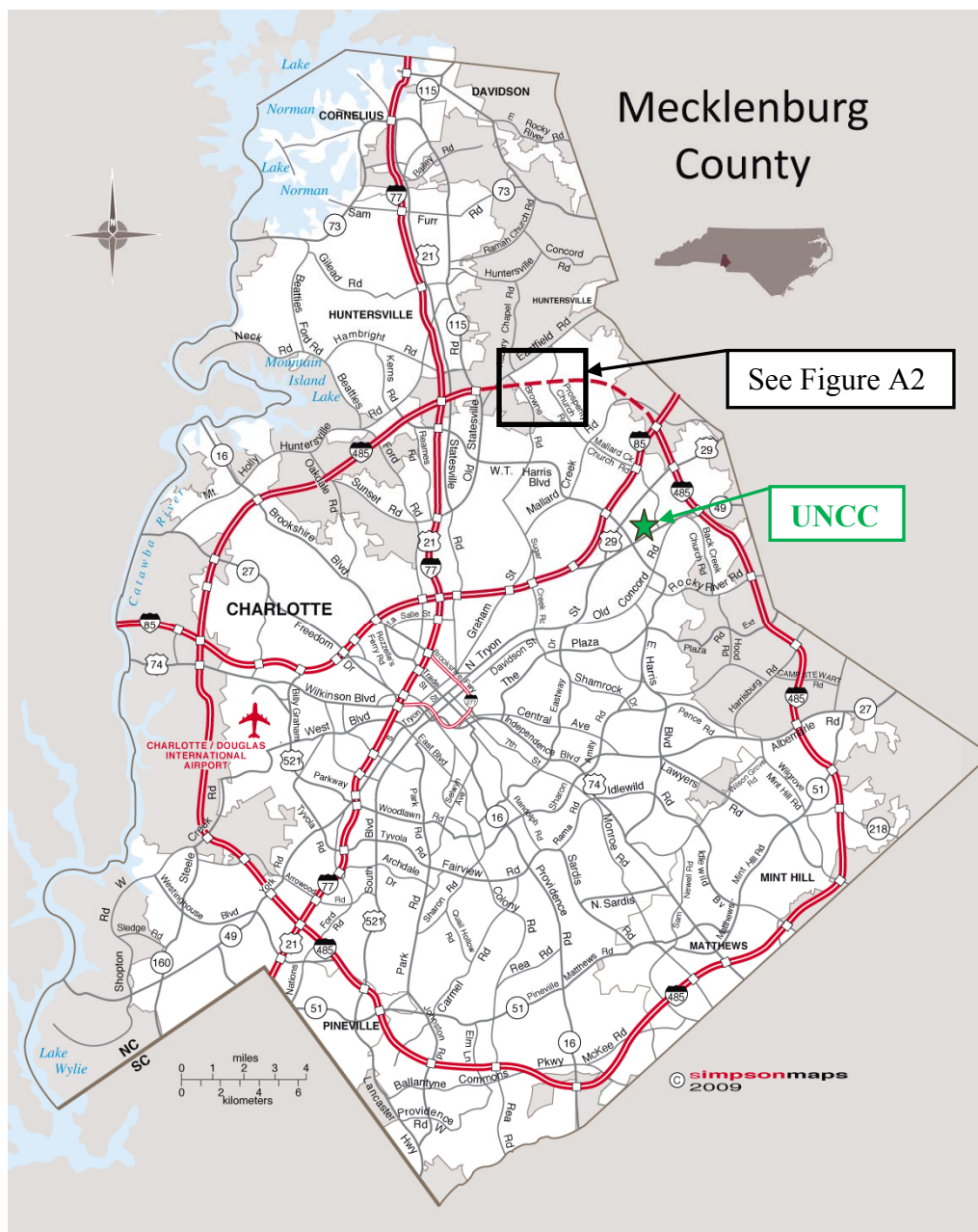


Figure A1 – Research area map – (Charlotte Chamber of Commerce, 2009)



Figure A2 – Research local map – Scale 1000ft (Google maps, 2009)

APPENDIX B – Prosperity Church Road Site 1 Data

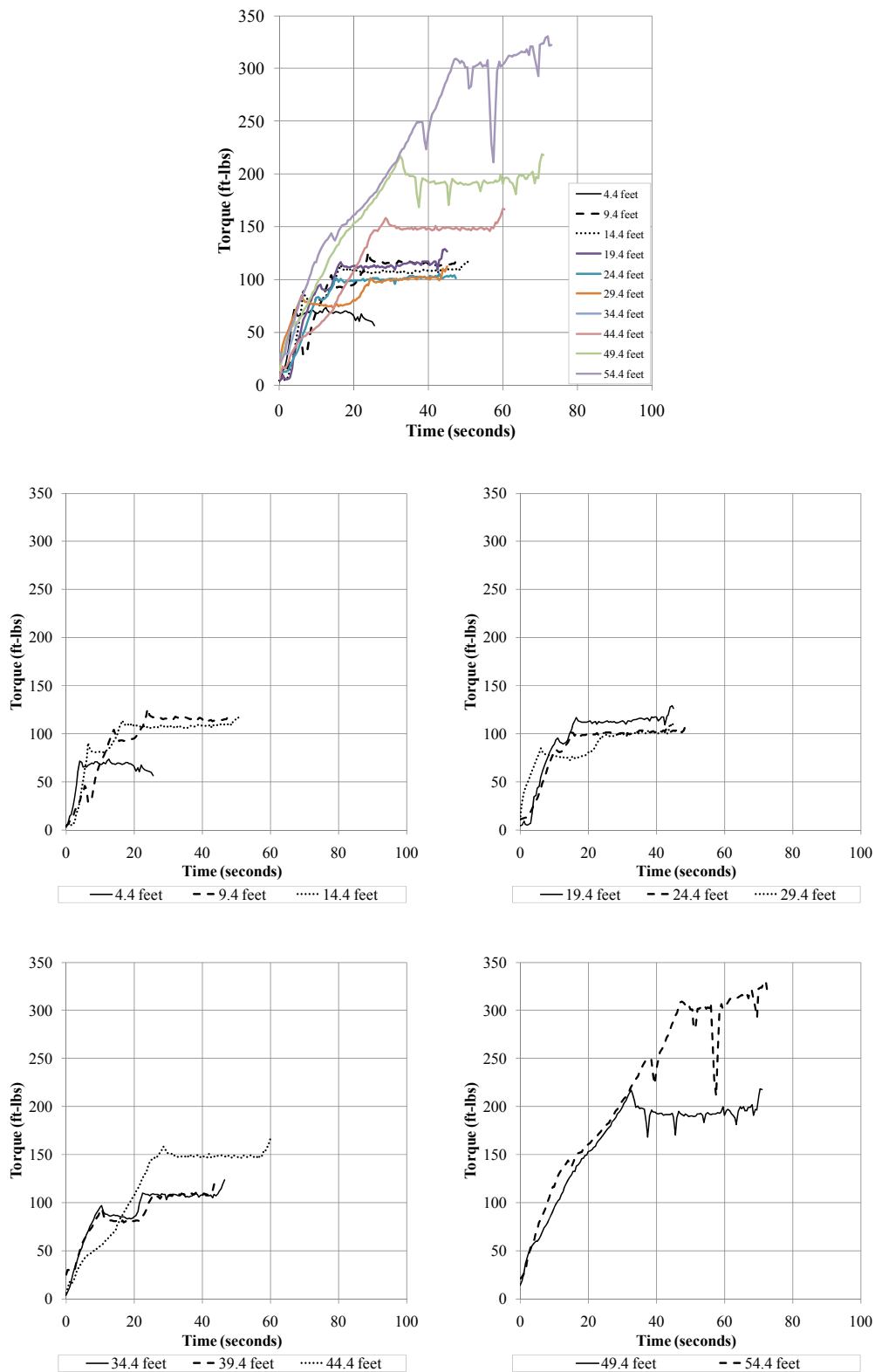


Figure B1 – PC1 – SPT-T Torque data 1

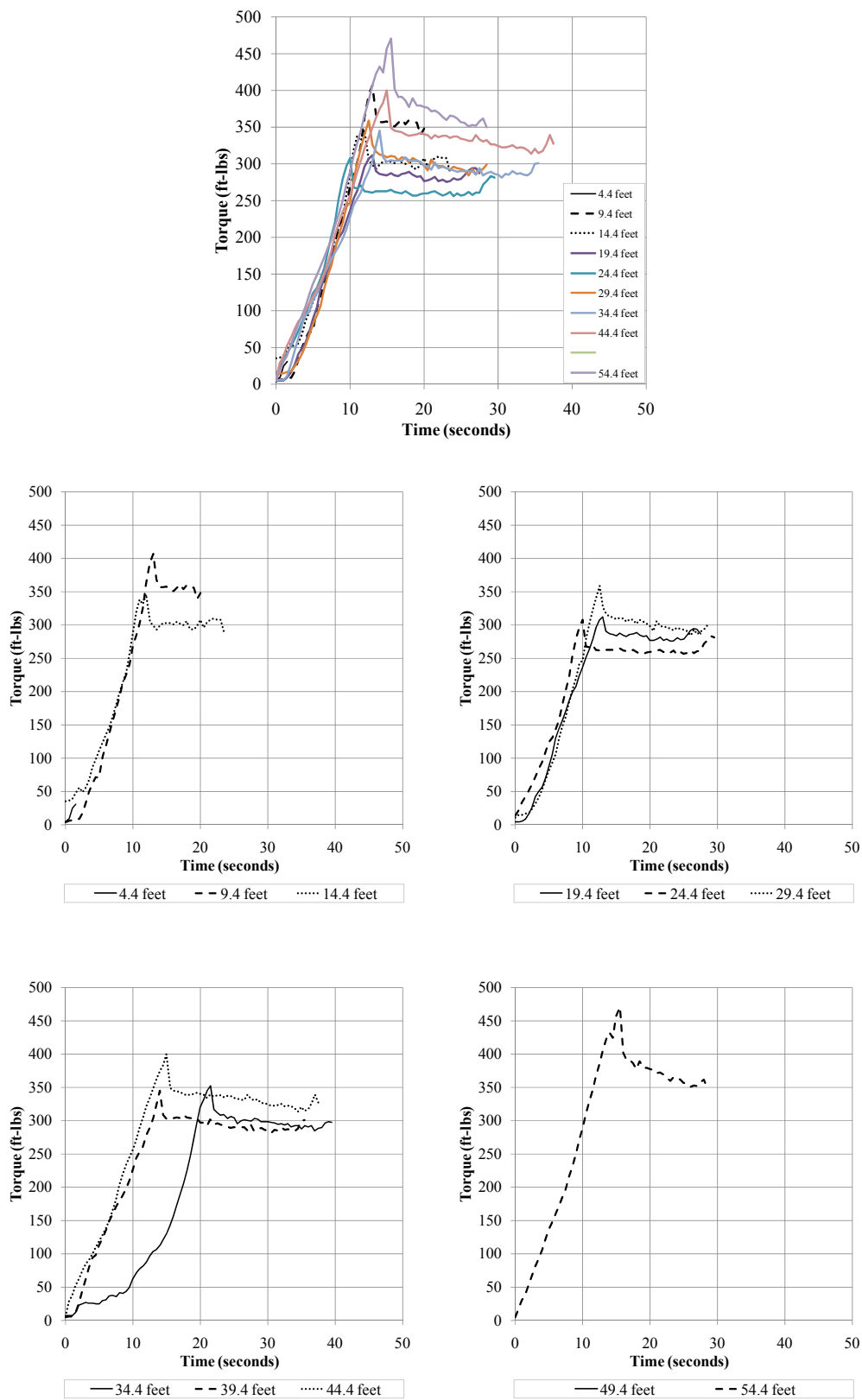


Figure B2 – PC1 – STT-T Torque data 1

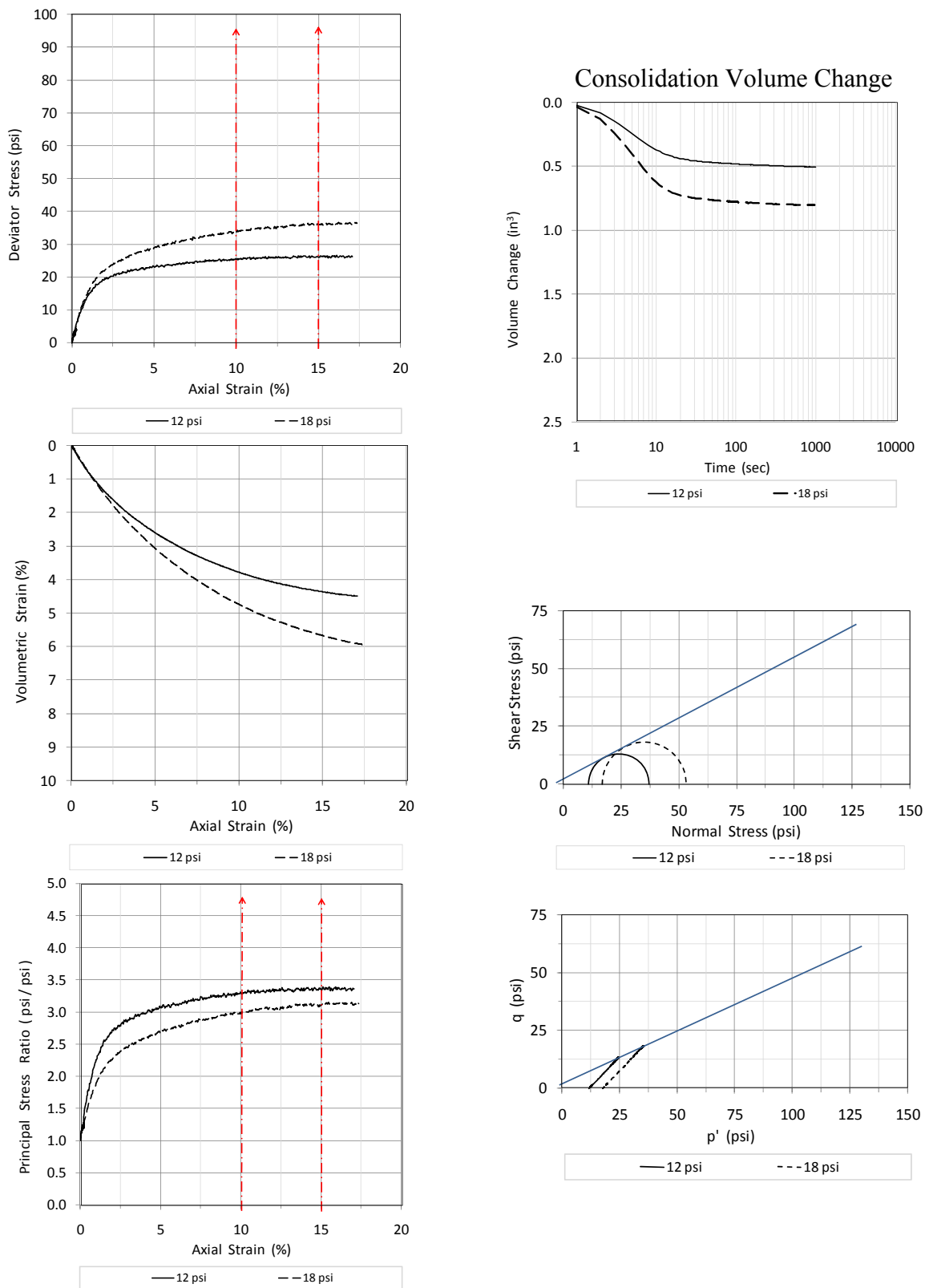


Figure B3 – PC1 4.4' Triaxial data

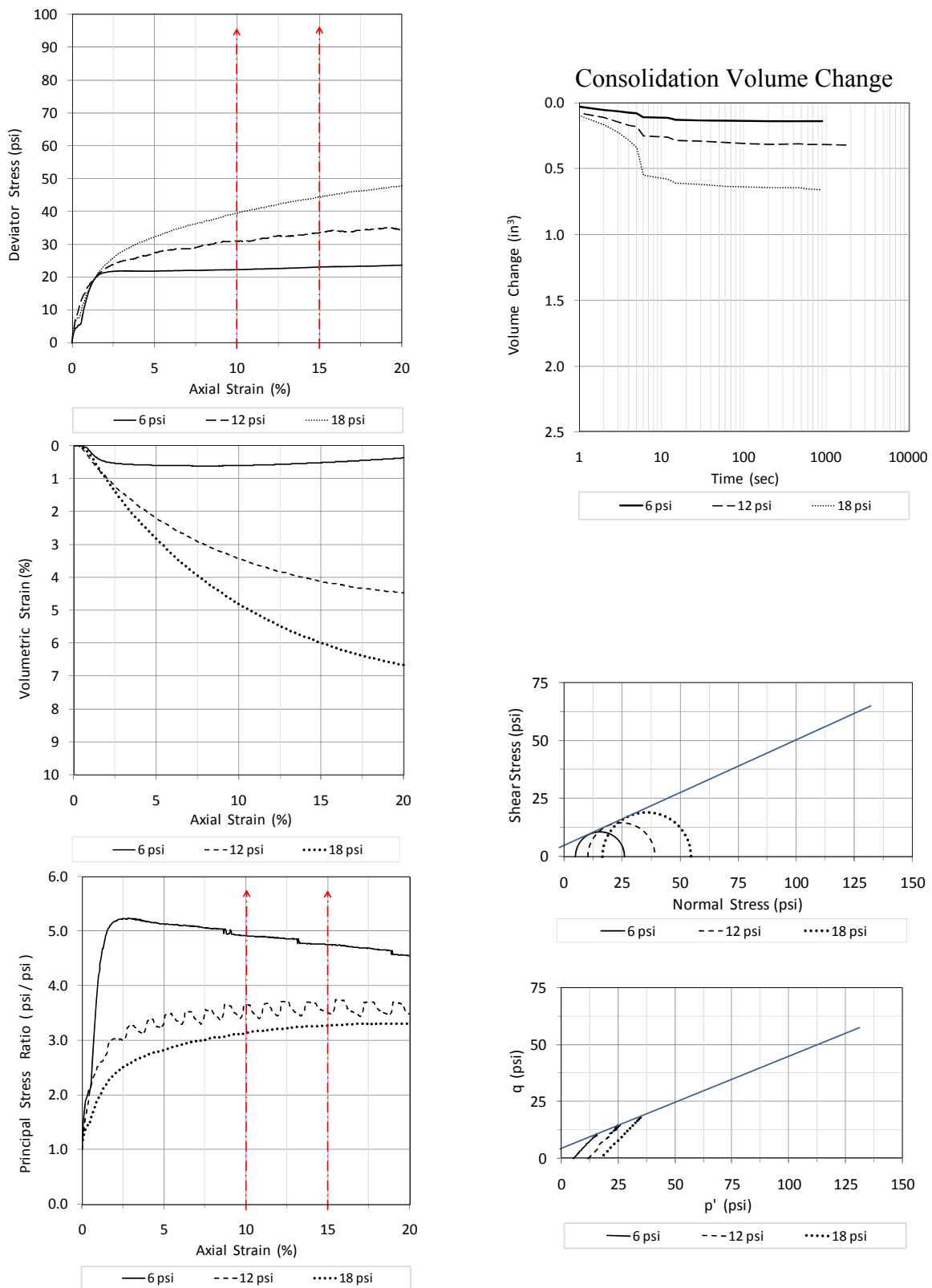


Figure B4 – PC1 9.4' Triaxial data – NCDOT B3

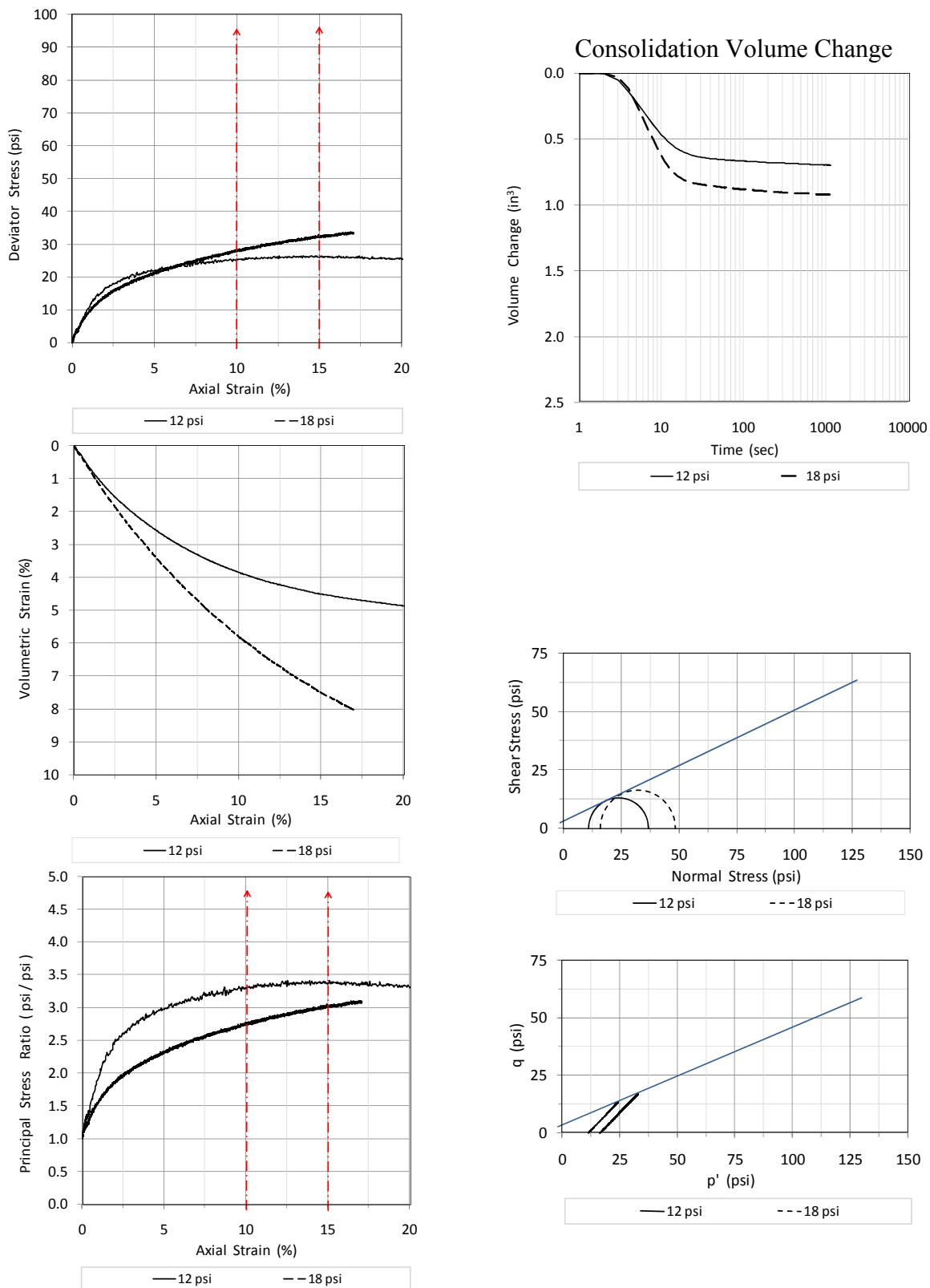


Figure B5 – PC1 14.4' Triaxial data

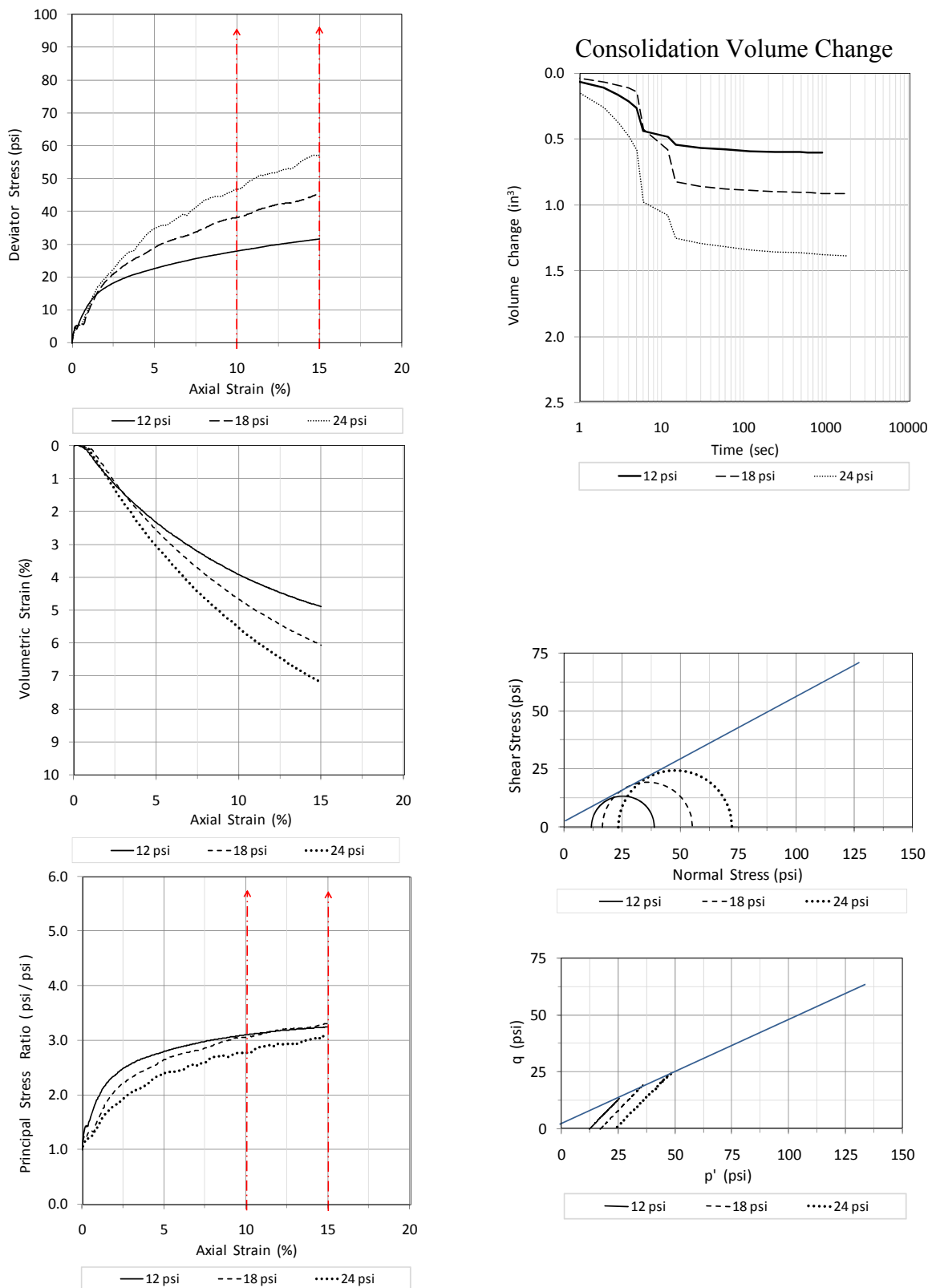


Figure B6 – PC1 19.4' Triaxial data – NCDOT B3

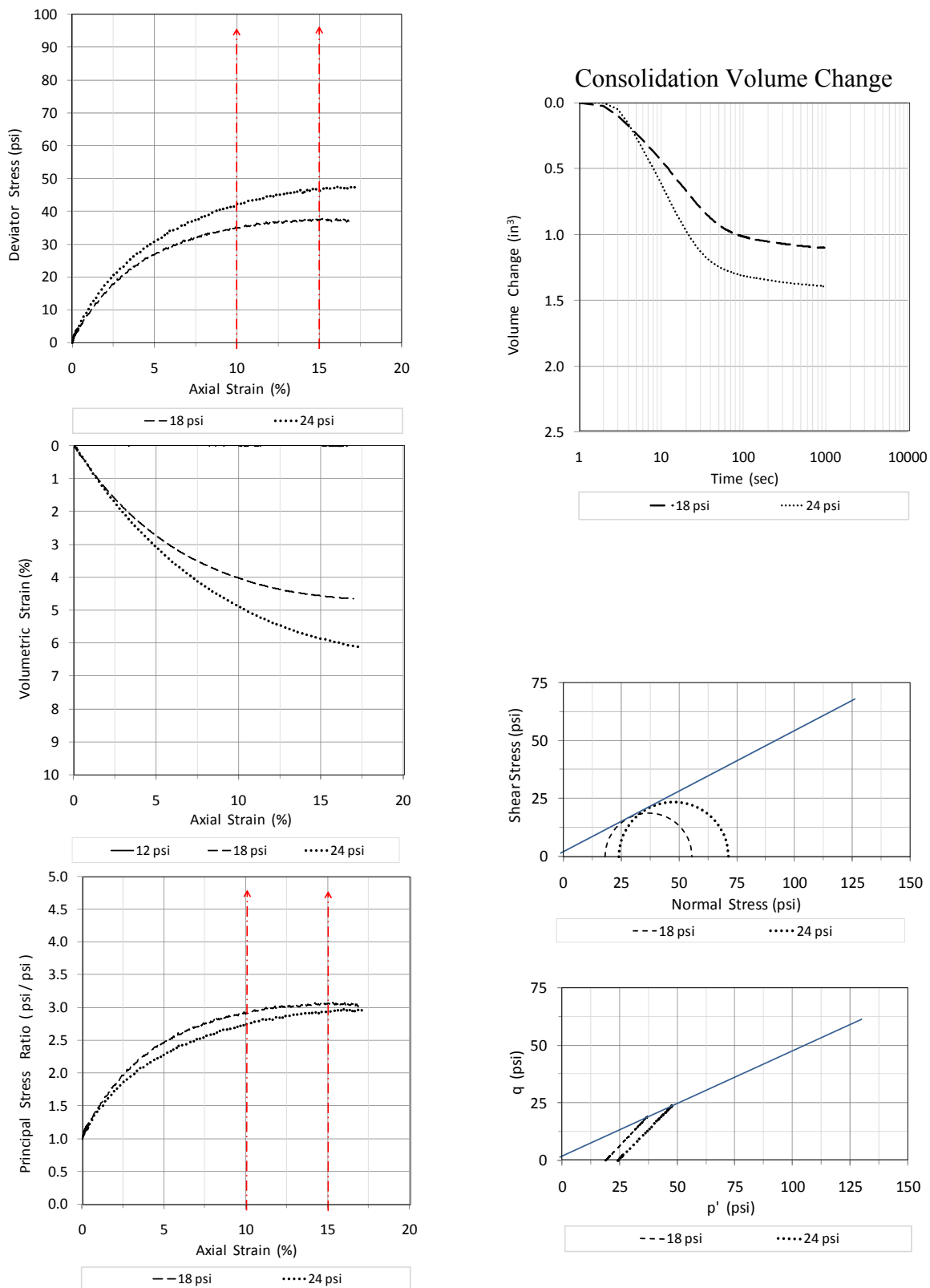


Figure B7 – PC1 24.4' Triaxial data

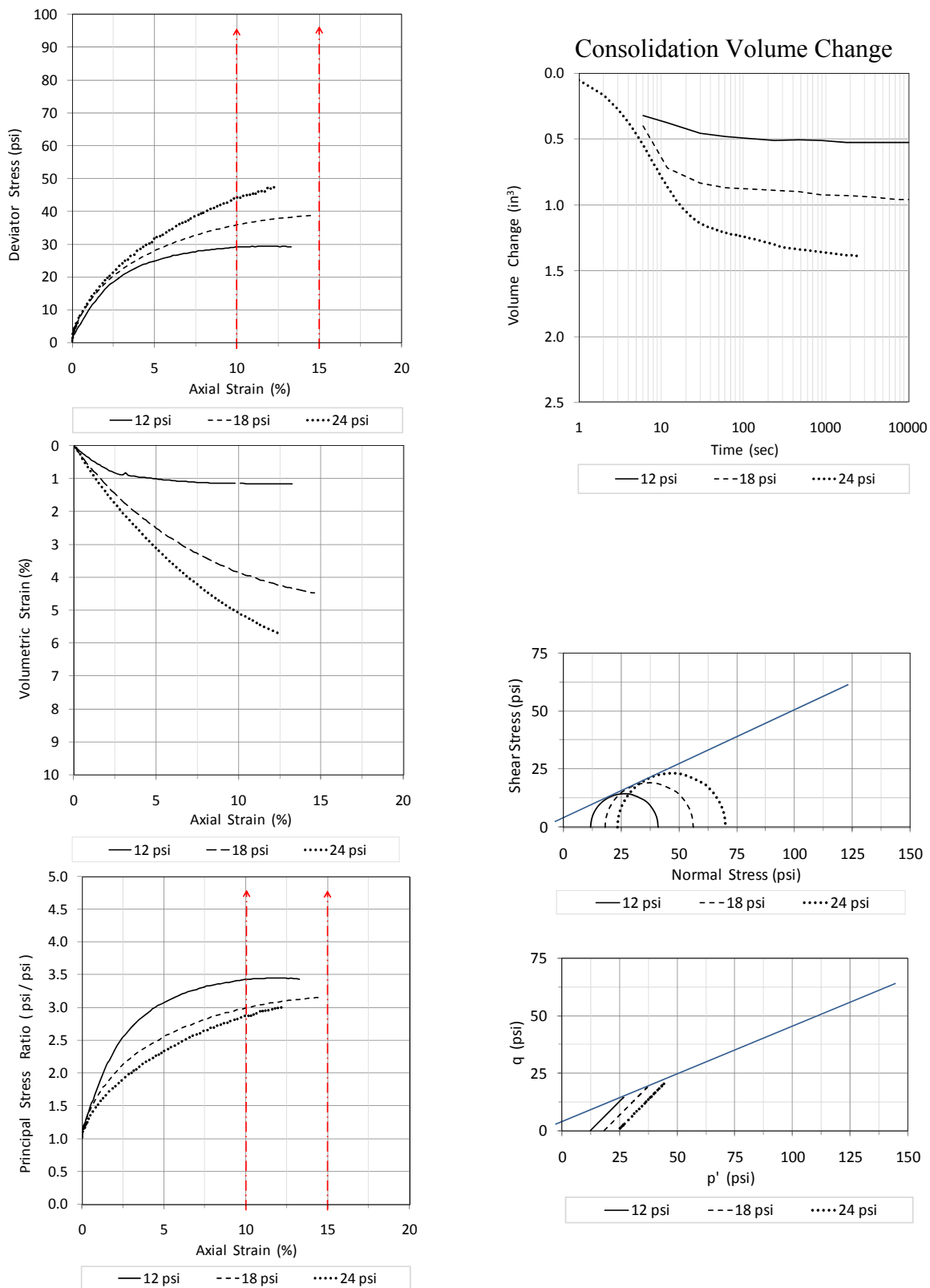


Figure B8 – PC1 29.4' Triaxial data

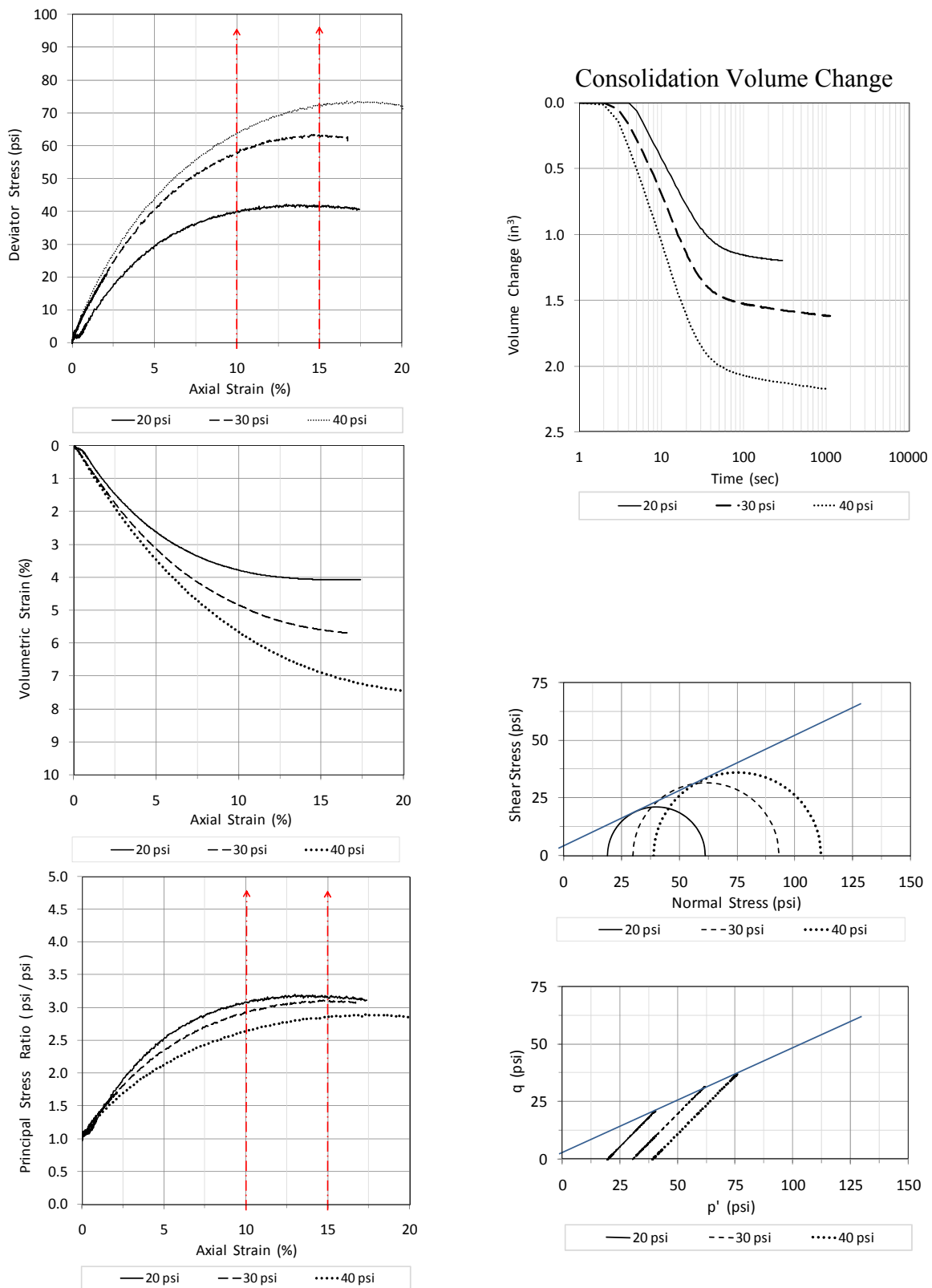


Figure B9 – PC1 34.4' Triaxial data

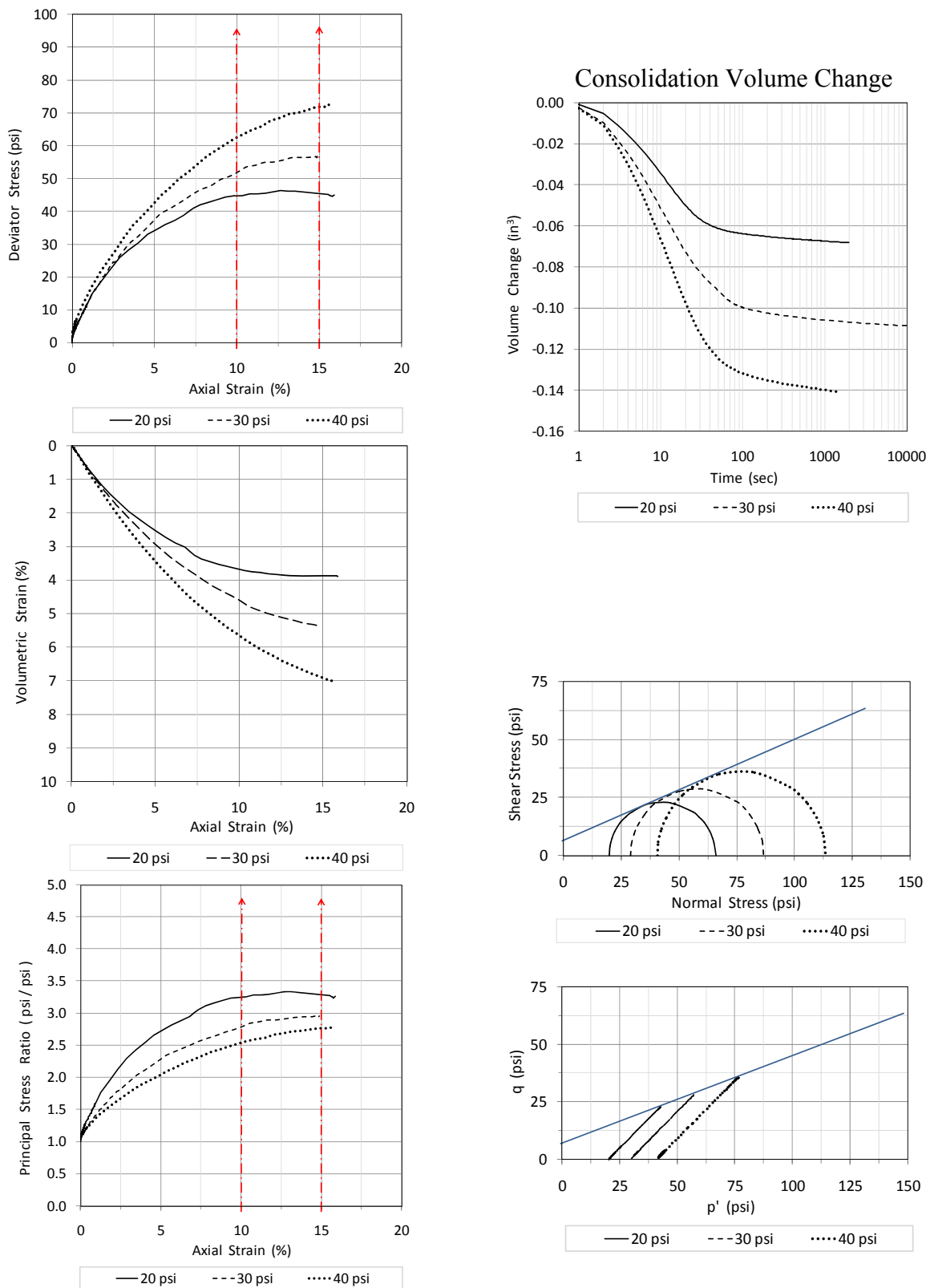


Figure B10 – PC1 39.4' Triaxial data

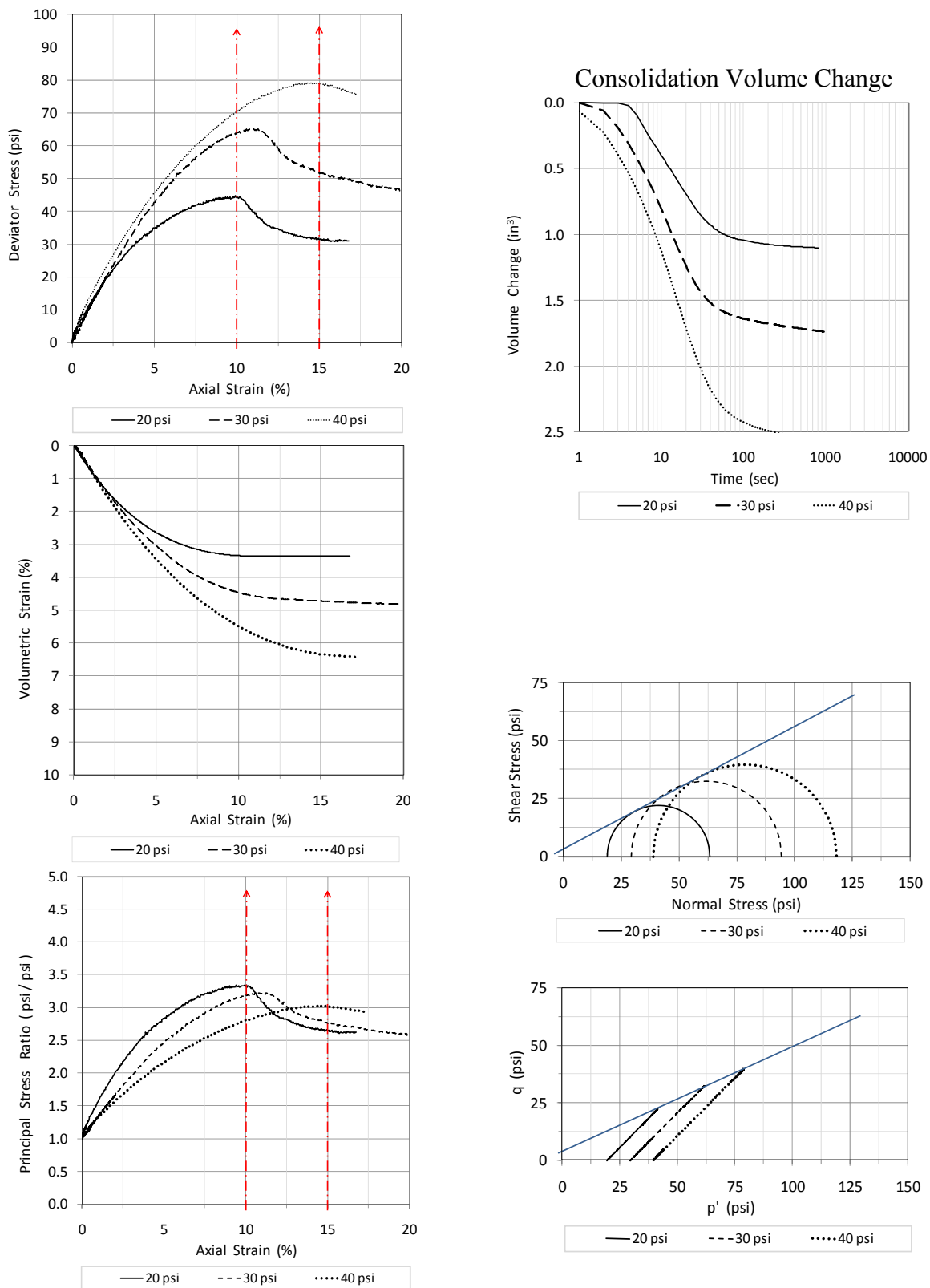


Figure B11 – PC1 44.4' Triaxial data

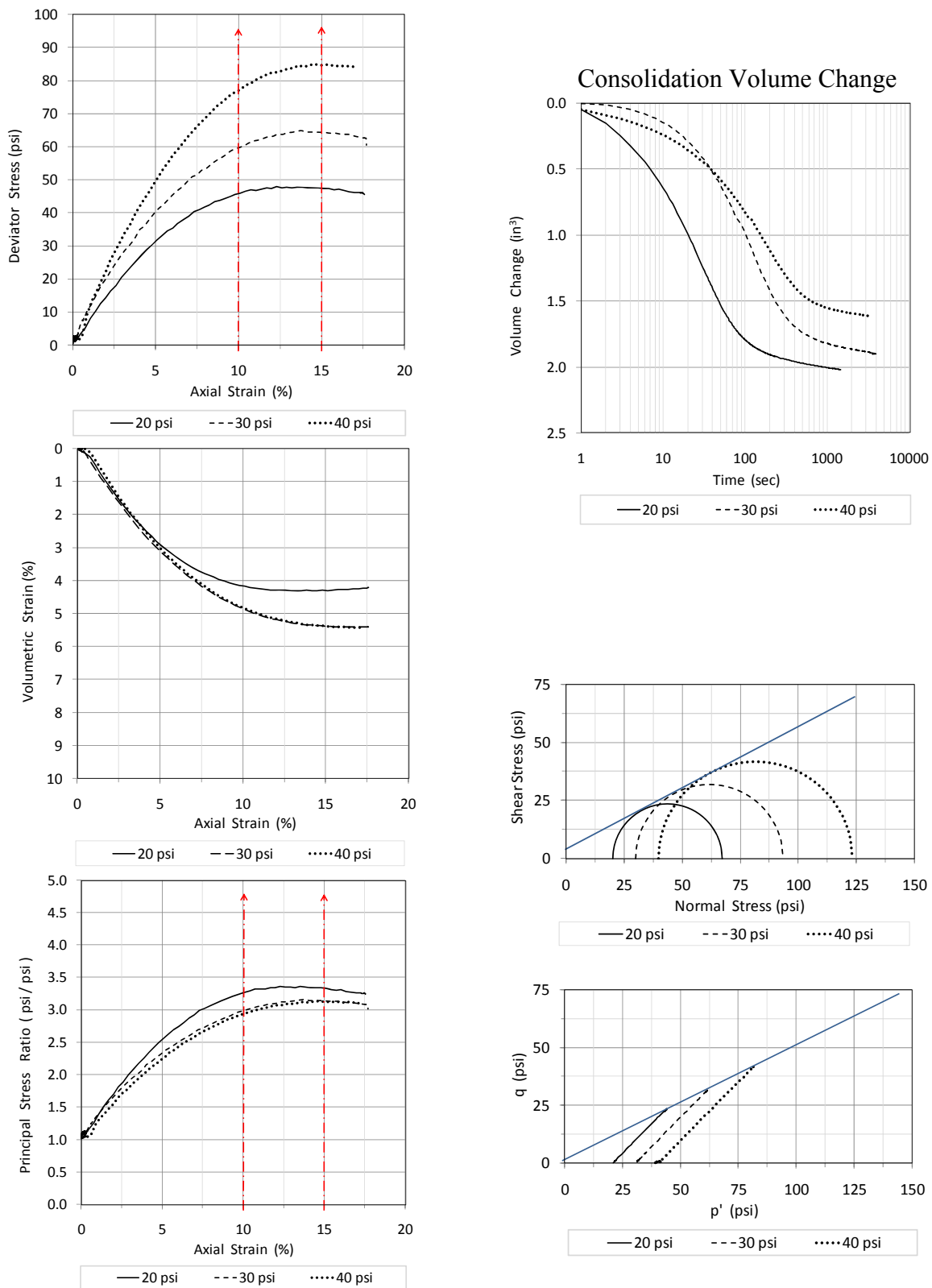


Figure B12 – PC1 49.4' Triaxial data

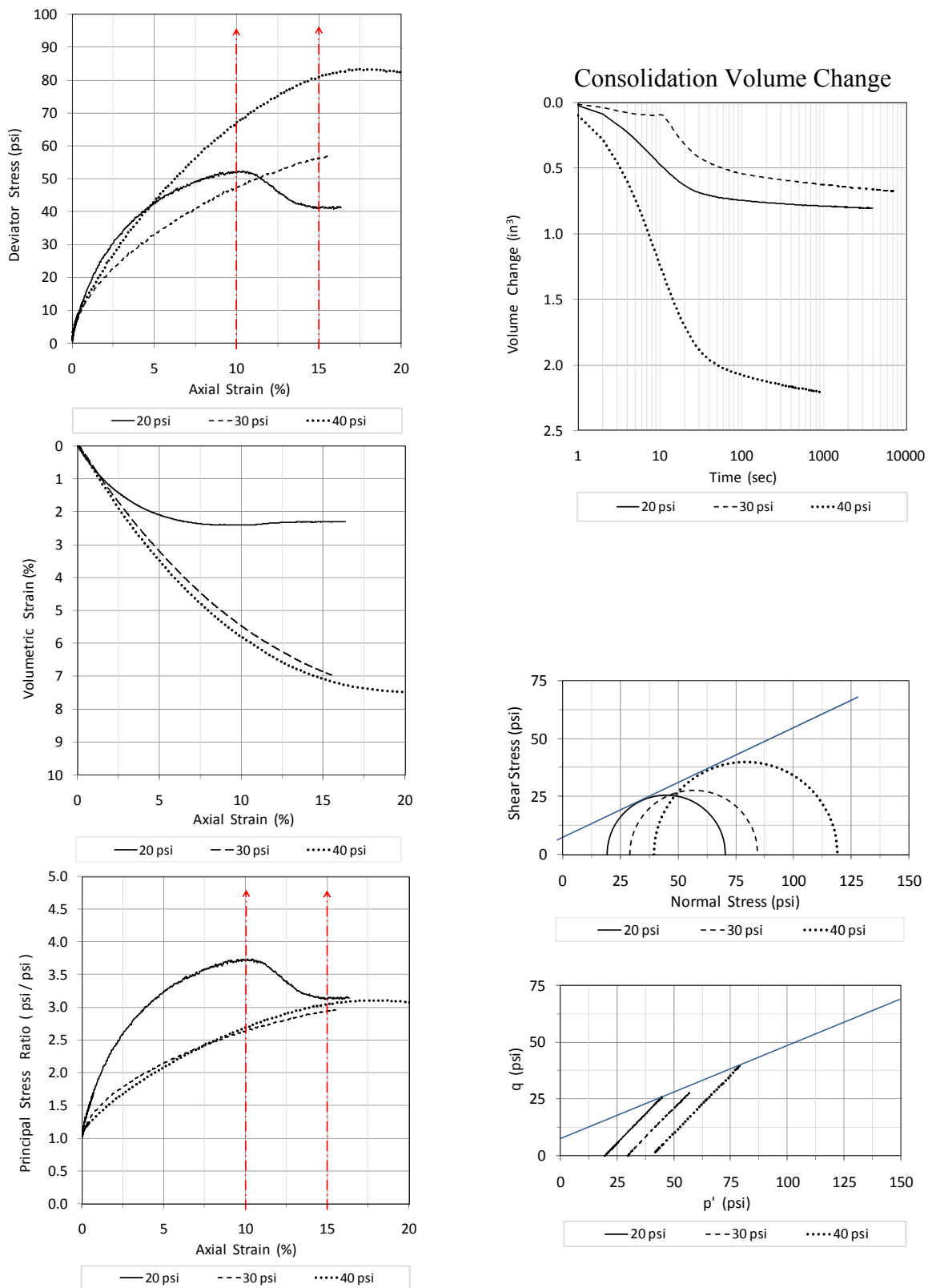


Figure B13 – PC1 54.4' Triaxial data

Table B1 – PC1 Interface shear test data

Depth	4.4 feet	14.4 feet	19.4 feet	24.4 feet	29.4 feet
Normal Stress (psi)	Shear Stress (psi)				
10	3.139	3.757	4.208	2.917	4.160
20	6.806	7.743	7.111	6.590	6.958
30	9.688	12.493	10.264	9.410	11.424

Table B1 – (continued)

Depth	34.4 feet	39.4 feet	44.4 feet	49.4 feet	54.4 feet
Normal Stress (psi)	Shear Stress (psi)				
10	3.139	3.486	4.347	4.333	5.208
20	6.951	7.590	8.743	9.271	9.993
30	11.132	10.931	13.236	12.667	14.188

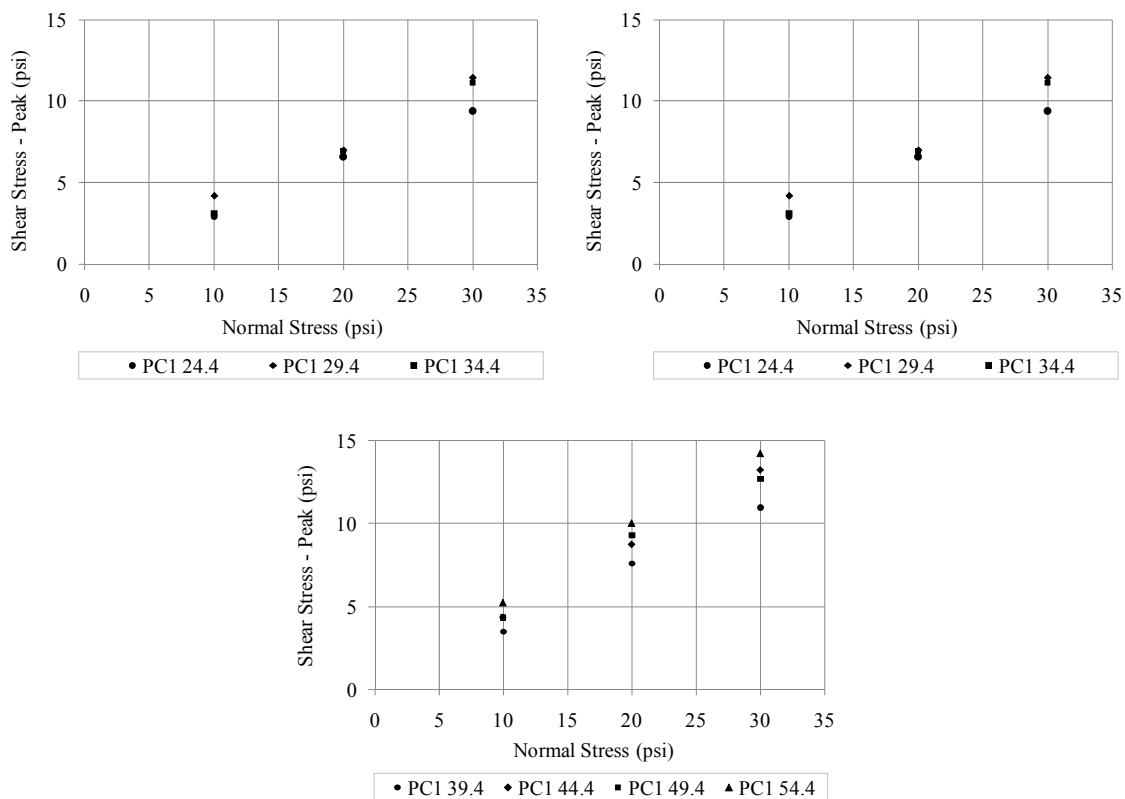


Figure B14 – PC1 Interface shear test data graph

Tables B2 – PC1 Geotechnical soil classification data

Depth	AASHTO	USCS	LL	PL	PI	Clay Fraction
feet	Class	Class	%	%	%	% < 2 μ m
4.4	A-7-6	MH	67.4	56.9	10.5	29.5
9.4	A-5	MH	55.1	50.2	4.9	19.5
14.4	A-5	MH	64.9	61.7	3.2	19.3
19.4	A-7-6	MH	58.5	45.0	13.5	17.8
24.4	A-5	MH	56.8	47.1	9.8	14.0
29.4	A-5	ML	43.4	36.2	7.2	16.3
34.4	A-5	ML	47.5	39.7	7.8	13.7
39.4	A-4	ML	39.7	33.2	6.5	12.0
44.4	A-5	ML	42.6	37.6	5.0	13.0
49.4	A-4	SM	37.2	33.8	3.4	6.4
54.4	A-4	SM	36.2	33.7	2.4	10.1
<p>MH - Inorganic silts, micaceous or diatomaceous fine sandy or silty soils, elastic silts</p> <p>ML - Inorganic silt and very fine sands, rocks flour, silty or clayey fine sands or clayey silts with slight plasticity</p> <p>SM - Silty-Sands, sand-silt mixtures – Non-plastic fines or fines with low plasticity</p>						

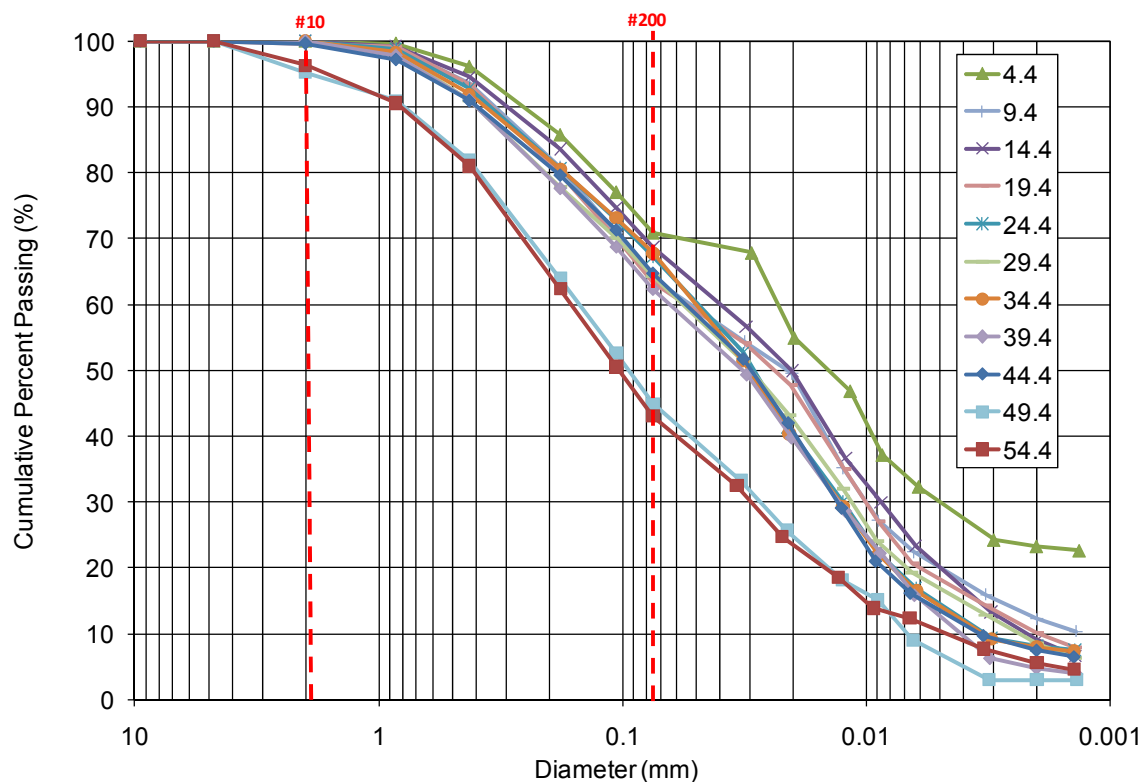
**Figure B15 – PC1 Grain-size distribution curve**

Table B3 – PC1 Soil classification data – grain-size distribution

PC1 4.4'		PC1 9.4'		PC1 14.4'	
Cumulative Percent Passing	D (mm)	Cumulative Percent Passing	D (mm)	Cumulative Percent Passing	D (mm)
100.00	9.5000	100.00	9.500	100.00	9.500
100.00	4.7500	100.00	4.750	100.00	4.750
100.00	2.0000	100.00	2.000	100.00	2.000
99.62	0.8500	98.90	0.850	99.22	0.850
96.09	0.4250	93.57	0.425	94.52	0.425
85.74	0.1800	80.87	0.180	83.64	0.180
77.03	0.1060	70.81	0.106	74.74	0.106
70.85	0.0750	63.98	0.075	68.68	0.075
67.80	0.0295	54.36	0.031	56.65	0.031
54.88	0.0197	49.56	0.020	49.98	0.020
46.81	0.0116	35.18	0.012	36.65	0.012
37.13	0.0086	27.18	0.009	29.99	0.009
32.28	0.0061	22.38	0.006	23.33	0.006
24.21	0.0030	15.99	0.003	13.33	0.003
23.25	0.0020	12.27	0.002	9.04	0.002
22.60	0.0013	10.39	0.001	6.66	0.001

Table B3 – (continued)

PC1 19.4'		PC1 24.4'		PC1 29.4'	
Cumulative Percent Passing	D (mm)	Cumulative Percent Passing	D (mm)	Cumulative Percent Passing	D (mm)
100.00	9.500	100.00	9.500	100.00	9.500
100.00	4.750	100.00	4.750	100.00	4.750
99.60	2.000	100.00	2.000	100.00	2.000
99.08	0.850	98.84	0.850	98.26	0.850
93.47	0.425	92.81	0.425	90.92	0.425
79.84	0.180	80.68	0.180	77.87	0.180
70.14	0.106	72.79	0.106	70.17	0.106
63.23	0.075	67.25	0.075	64.39	0.075
54.21	0.031	52.66	0.032	51.28	0.032
47.83	0.020	41.37	0.021	43.27	0.021
35.07	0.012	30.09	0.012	32.05	0.012
27.10	0.009	22.57	0.009	24.04	0.009
20.73	0.006	16.93	0.006	19.23	0.007
14.35	0.003	9.40	0.003	12.82	0.003
10.07	0.002	8.20	0.002	8.50	0.002
7.97	0.001	7.52	0.001	6.41	0.001

Table B3 – (continued)

PC1 34.4'		PC1 39.4'		PC1 44.4'	
Cumulative Percent Passing	D (mm)	Cumulative Percent Passing	D (mm)	Cumulative Percent Passing	D (mm)
100.00	9.500	100.00	9.500	100.00	9.500
100.00	4.750	100.00	4.750	100.00	4.750
100.00	2.000	100.00	2.000	99.65	2.000
98.31	0.850	97.80	0.850	97.19	0.850
91.96	0.425	91.07	0.425	90.92	0.425
80.55	0.180	77.64	0.180	79.61	0.180
73.16	0.106	68.76	0.106	71.30	0.106
67.80	0.075	62.35	0.075	64.71	0.075
51.40	0.032	49.37	0.031	51.71	0.032
40.39	0.021	39.81	0.020	42.01	0.021
29.37	0.012	28.67	0.012	29.09	0.013
22.03	0.009	22.30	0.009	21.01	0.009
16.52	0.006	15.93	0.006	16.16	0.007
9.18	0.003	6.37	0.003	9.70	0.003
8.00	0.002	4.84	0.002	7.48	0.002
7.34	0.001	3.98	0.001	6.46	0.001

Table B3 – (continued)

PC1 49.4'		PC1 54.4'	
Cumulative Percent Passing	D (mm)	Cumulative Percent Passing	D (mm)
100.00	9.500	100.00	9.500
100.00	4.750	100.00	4.750
95.22	2.000	96.29	2.000
90.95	0.850	90.58	0.850
81.81	0.425	81.07	0.425
63.94	0.180	62.38	0.180
52.60	0.106	50.58	0.106
44.92	0.075	43.06	0.075
33.29	0.033	32.49	0.034
25.72	0.021	24.76	0.022
18.16	0.013	18.57	0.013
15.13	0.009	13.93	0.009
9.08	0.006	12.38	0.007
3.03	0.003	7.74	0.003
3.03	0.002	5.60	0.002
3.03	0.001	4.64	0.001

Table B4 – PC1 Geologic soil color

Depth	Wet Color		Dry Color	
feet				
4.4	2.5YR 4/6		2.5YR 5/8	
9.4	2.5YR 4/8		5YR 5/8	
14.4	5YR 4/6		7.5 YR 6/6	
19.4	7.5YR 4/6		10YR 6/6	
24.4	10YR 4/6		10YR 6/6	
29.4	10YR 4/4		10YR 6/4	
34.4	10YR 4/6		10YR 6/4	
39.4	10YR 5/4		10YR 6/3	
44.4	2.5Y 4/3		2.5Y 6/4	
49.4	2.5Y 4/3		10YR 6/3	
54.4	2.5Y 4/3		2.5Y 6/3	

Table B5 – PC1 Geologic soil classification data

Depth	Gravel		Consistence			Texture
		%	stickiness	plasticity	Moist	
4.4	1 rock	< 10	slight	slight	very firm	Silty Loam
9.4	3 rocks	< 10	slight	slight	firm	Silty Loam
14.4	1 rock	< 10	slight	slight	firm	Silty Loam
19.4	10 rock	< 10	slight	slight	firm	Silty Loam
24.4	5 rocks	< 10	slight	slight	firm	Silty Loam
29.4	5 rocks	< 10	slight	slight	friable	Silty Loam
34.4	5 rocks	< 10	slight	slight	friable	Loam
39.4	5 rocks	< 10	slight	slight	friable	Loam
44.4	20 rock	< 10	slight	slight	friable	Loam
49.4	100 rocks	< 10	slight	slight	friable	Loam
54.4	100 rocks	< 10	slight	slight	friable	Loam

Table B6 – PC1 Dilatometer data output

Z (M)	THRUST (KGF)	A (BAR)	B (BAR)	C (BAR)	DA (BAR)	DB (BAR)	ZMRNG (BAR)	ZMLO (BAR)	ZMHI (BAR)	ZMCAL (BAR)	P0 (BAR)	P1 (BAR)	P2 (BAR)	U0 (BAR)	GAMMA (T/M3)	SVP (BAR)
0.3	1334	2.3	6.4		0.16	0.31	5	0	0	0	2.28	6.09		0	1.7	0.053
0.61	1905	7	19.6		0.16	0.31	5	0	0	0	6.55	19.29		0	2	0.109
0.91	2402	0	0		0.16	0.31	5	0	0	0	0.16X	-0.31		0	POI	=
1.22	1950	5.4	13		0.16	0.31	5	0	0	0	5.2	12.69		0	1.95	0.228
1.52	1913	4.5	11.6		0.16	0.31	5	0	0	0	4.33	11.29		0	1.8	0.283
1.83	1949	4.6	10.6		0.16	0.31	5	0	0	0	4.48	10.29		0	1.8	0.337
2.13	1745	2.7	8		0.16	0.31	5	0	0	0	2.62	7.69		0	1.9	0.392
2.44	1657	3.15	8.6		0.16	0.31	5	0	0	0	3.06	8.29		0	1.8	0.448
2.74	1635	2.43	7.3		0.16	0.31	5	0	0	0	2.37	6.99		0	1.9	0.503
3.05	1616	2.75	8.3		0.16	0.31	5	0	0	0	2.66	7.99		0	1.9	0.56
3.35	1565	3.5	8.5		0.16	0.31	5	0	0	0	3.43	8.19		0	1.8	0.615
3.66	1512	3.3	8.2		0.16	0.31	5	0	0	0	3.24	7.89		0	1.8	0.67
3.96	1508	2.4	7.2		0.16	0.31	5	0	0	0	2.34	6.89		0	1.9	0.724
4.27	1362	2.55	7.8		0.16	0.31	5	0	0	0	2.47	7.49		0	1.9	0.782
4.57	1438	3.25	8.7		0.16	0.31	5	0	0	0	3.16	8.39		0	1.8	0.836
4.88	1449	3.5	8.5		0.16	0.31	5	0	0	0	3.43	8.19		0	1.8	0.891
5.18	1504	3.15	8.8		0.16	0.31	5	0	0	0	3.05	8.49		0	1.8	0.944
5.49	1696	3.55	10.1		0.16	0.31	5	0	0	0	3.41	9.79		0	1.9	1
5.79	2234	2.7	10.1		0.16	0.31	5	0	0	0	2.51	9.79		0	1.9	1.056
6.1	3116	4.05	14.1		0.16	0.31	5	0	0	0	3.73	13.79		0	1.9	1.114
6.4	2644	5.1	12		0.16	0.31	5	0	0	0	4.94	11.69		0	1.8	1.169
6.71	1366	3.03	7.6		0.16	0.31	5	0	0	0	2.98	7.29		0	1.8	1.223
7.01	1172	3.55	8.1		0.16	0.31	5	0	0	0	3.51	7.79		0	1.8	1.276
7.32	1072	3.5	7.7		0.16	0.31	5	0	0	0	3.47	7.39		0	1.8	1.331
7.62	939	3.15	6.8		0.16	0.31	5	0	0	0	3.15	6.49		0	1.8	1.384
7.93	781	2.85	5.9		0.16	0.31	5	0	0	0	2.88	5.59		0	1.7	1.437
8.23	680	2.7	5.1		0.16	0.31	5	0	0	0	2.76	4.79		0	1.7	1.487
8.54	746	1.7	3.45		0.16	0.31	5	0	0	0	1.8	3.14		0	1.7	1.539
8.84	698	2.35	4.65		0.16	0.31	5	0	0	0	2.42	4.34		0	1.7	1.589
9.15	751	0	5.5		0.16	0.31	5	0	0	0	0.16X	5.19		0	1.7	1.641
9.45	1496	4.8	19.7		0.16	0.31	5	0	0	0	4.24	19.39		0	2	1.695
9.76	1564	3.9	7.7		0.16	0.31	5	0	0	0	3.89	7.39		0	1.8	1.753
10.06	1492	4.2	8.4		0.16	0.31	5	0	0	0	4.17	8.09		0	1.8	1.806
10.37	1522	4.15	8.9		0.16	0.31	5	0	0	0	4.1	8.59		0	1.8	1.861
10.67	1579	4.5	8.1		0.16	0.31	5	0	0	0	4.5	7.79		0.029	1.8	1.885
10.98	1531	4.15	7.5		0.16	0.31	5	0	0	0	4.17	7.19		0.06	1.8	1.909
11.28	1637	4.2	7.3		0.16	0.31	5	0	0	0	4.23	6.99		0.089	1.8	1.932
11.59	1636	4.1	7.1		0.16	0.31	5	0	0	0	4.13	6.79		0.12	1.8	1.957
11.89	1770	5.1	9.8		0.16	0.31	5	0	0	0	5.05	9.49		0.149	1.8	1.98
12.2	2048	3.9	7.6		0.16	0.31	5	0	0	0	3.9	7.29		0.18	1.8	2.005
12.5	2345	4.65	8.4		0.16	0.31	5	0	0	0	4.65	8.09		0.209	1.8	2.028
12.8	2500	4.9	8.9		0.16	0.31	5	0	0	0	4.88	8.59		0.238	1.8	2.052
13.11	2722	5.1	9.9		0.16	0.31	5	0	0	0	5.04	9.59		0.269	1.8	2.076
13.41	2962	5.5	10.8		0.16	0.31	5	0	0	0	5.42	10.49		0.298	1.8	2.1
13.72	1811	0	0		0.16	0.31	5	0	0	0	0.16X	-0.31		0.329	POI	=
14.02	3200	5.4	10		0.16	0.31	5	0	0	0	5.35	9.69		0.358	1.8	2.148
14.33	3647	6.5	13.3		0.16	0.31	5	0	0	0	6.34	12.99		0.389	1.95	2.174
14.63	3771	5.9	13.4		0.16	0.31	5	0	0	0	5.71	13.09		0.418	1.95	2.202
14.94	4125	7.9	16.3		0.16	0.31	5	0	0	0	7.66	15.99		0.448	1.95	2.231

Table B6 – (continued)

JOB FILE: Dissertation Research 2009																FILE NO. : Cottingham 2009-1															
LOCATION: Prosperity Church Road Site 1																															
SNDG.BY : Cottingham/Anderson																SNDG.DATE: 17 June 2008															
ANAL.BY : Cottingham																ANAL.DATE: 19 May 2009															
ANALYSIS PARAMETERS: LO RANGE = 5.00 BARS ROD DIAM. = 4.44 CM BL.THICK. = 15.0 MM SU FACTOR = 1.00																															
SURF.ELEV. = 0.00 M LO GAGE 0 = 0.00 BARS FR.RED.DIA. = 5.71 CM BL.WIDTH = 96.0 MM PHI FACTOR = 1.00																															
WATER DEPTH = 10.37 M HI GAGE 0 = 0.00 BARS LN.ROD WT. = 6.25 KGF/M DELTA-A = 0.16 BARS OCR FACTOR = 1.00																															
SP.GR.WATER = 1.000 CAL GAGE 0 = 0.00 BARS DELTA/PHI = 0.50 DELTA-B = 0.31 BARS M FACTOR = 1.00																															
MAX SU ID = 9.00 SU OPTION = MARCHETTI MIN PHI ID = 0.10 OCR OPTION = MARCHETTI KO FACTOR = 1.00																															
UNIT CONVERSIONS: 1 BAR = 1.019 KGF/CM2 = 1.044 TSF = 14.51 PSI 1 M = 3.2808 FT																															
Z	KD	ID	UD	ED	KO	SU	QD	PHI	SIGFF	PHIO	PC	OCR	M	SOIL	TYPE																
(M)				(BAR)		(BAR)	(BAR)	(DEG)	(BAR)	(DEG)	(BAR)		(BAR)																		
*****	*****	*****	*****	*****	*****	*****	*****	*****	*****	*****	*****	*****	*****	*****	*****																
0.3	42.99	1.67	0	132	0.54	513	SANDY	SILT																							
0.61	59.97	1.94	0	442	7.36	1.69	33.5	39.3	0.18	34.8	47.07	430.7	1854	SILTY	SAND																
0.91	0.18	POOR	DATA																												
1.22	22.87	1.44	0	260	2.89	1.05	40.4	39.6	0.37	36.3	13.94	61.3	853	SANDY	SILT																
1.52	15.31	1.61	0	242	1.97	0.79	42.7	39.9	0.46	37	7.82	27.7	701	SANDY	SILT																
1.83	13.29	1.3	0	201	1.74	0.79	43.5	39.3	0.55	36.7	7.26	21.5	558	SANDY	SILT																
2.13	6.68	1.94	0	176	0.92	0.39	44.5	40.2	0.64	37.9	2.27	5.8	373	SILTY	SAND																
2.44	6.83	1.71	0	181	0.99	0.46	40.4	38.7	0.73	36.5	2.91	6.5	388	SANDY	SILT																
2.74	4.71	1.95	0	160	0.73	0.32	42.5	38.9	0.82	36.9	1.72	3.4	288	SILTY	SAND																
3.05	4.74	2.01	0	185	0.76	0.36	41.1	37.9	0.91	36.1	2.04	3.6	334	SILTY	SAND																
3.35	5.58	1.39	0	165	0.9	0.49	37.2	36.4	0.98	34.6	3.12	5.1	319	SANDY	SILT																
3.66	4.84	1.44	0	161	0.82	0.44	36.5	35.9	1.06	34.2	2.75	4.1	290	SANDY	SILT																
3.96	3.24	1.94	0	158	0.62	0.29	39.5	36.4	1.15	34.9	1.61	2.2	228	SILTY	SAND																
4.27	3.16	2.03	0	174	0.64	0.3	34.9	35	1.23	33.6	1.8	2.3	248	SILTY	SAND																
4.57	3.78	1.65	0	181	0.73	0.41	35.1	34.4	1.31	33	2.53	3	285	SANDY	SILT																
4.88	3.85	1.39	0	165	0.75	0.44	34.8	33.8	1.39	32.6	2.82	3.2	259	SANDY	SILT																
5.18	3.23	1.78	0	189	0.67	0.38	37.8	34.2	1.47	33	2.32	2.5	270	SANDY	SILT																
5.49	3.4	1.87	0	222	0.68	0.43	42.4	34.5	1.57	33.5	2.6	2.6	329	SILTY	SAND																
5.79	2.38	2.89	0	252	0.49	0.29	61.7	37.2	1.69	36.4	1.5	1.4	314	SILTY	SAND																
6.1	3.35	2.7	0	349	0.57	0.47	84.1	38.6	1.81	37.9	2.28	2	533	SILTY	SAND																
6.4	4.23	1.37	0	234	0.74	0.65	65.9	36.3	1.86	35.6	3.84	3.3	389	SANDY	SILT																
6.71	2.44	1.44	0	149	0.62	0.35	34.7	31.8	1.87	31.1	2.35	1.9	169	SANDY	SILT																
7.01	2.75	1.22	0	149	0.72	0.42	27.9	29.7	1.91	28.9	3.11	2.4	183	SANDY	SILT																
7.32	2.61	1.13	0	136	0.73	0.41	25.3	28.6	1.97	27.9	3.2	2.4	159	SILT																	
7.62	2.28	1.06	0	116	0.72	0.36	22.5	27.4	2.02	26.8	3.01	2.2	119	SILT																	
7.93	2	0.94	0	94	0.73	0.32	18.9	25.7	2.06	25.1	2.94	2	83	SILT																	
8.23	1.86	0.73	0	70	0.74	0.3	16.5	24.3	2.1	23.7	2.99	2	60	CLAYEY	SILT																
8.54	1.17	0.75	0	47	0.62	0.17	20.7	26	2.21	25.6	2.03	1.3	40	CLAYEY	SILT																
8.84	1.52	0.79	0	67	0.7	0.25	18	24.5	2.25	24	2.67	1.7	57	CLAYEY	SILT																
9.15	0.1	31.44	0	175									148	SAND																	
9.45	2.5	3.57	0	526	0.69	0.49	36.3	29.6	2.53	29.4	3.73	2.2	681	SAND																	
9.76	2.22	0.9	0	121	0.65	0.44	39.3	30	2.63	29.9	3.33	1.9	120	CLAYEY	SILT																
10.06	2.31	0.94	0	136	0.68	0.48	36.6	29.2	2.69	29.1	3.71	2.1	140	SILT																	
10.37	2.2	1.1	0	156	0.66	0.46	37.9	29.2	2.77	29.3	3.63	2	156	SILT																	
10.67	2.37	0.73	0	114	0.68	0.51	38.6	29.2	2.81	29.3	3.98	2.1	118	CLAYEY	SILT																
10.98	2.15	0.74	0	105	0.66	0.46	38.2	29.1	2.84	29.2	3.66	1.9	99	CLAYEY	SILT																
11.28	2.14	0.67	0	96	0.65	0.46	41.3	29.6	2.89	29.8	3.6	1.9	89	CLAYEY	SILT																
11.59	2.05	0.66	0	92	0.64	0.44	41.7	29.6	2.92	29.8	3.49	1.8	81	CLAYEY	SILT																
11.89	2.47	0.91	0	154	0.68	0.57	43.2	29.7	2.96	29.9	4.28	2.2	169	SILT																	
12.2	1.86	0.91	0	118	0.56	0.4	54.7	31.7	3.06	31.9	2.92	1.5	100	SILT																	
12.5	2.19	0.78	0	120	0.58	0.5	61.4	32.4	3.11	32.6	3.37	1.7	115	CLAYEY	SILT																
12.8	2.26	0.8	0	129	0.58	0.53	65.4	32.8	3.16	33	3.48	1.7	128	CLAYEY	SILT																
13.11	2.3	0.95	0	158	0.57	0.54	71.6	33.3	3.22	33.6	3.5	1.7	162	SILT																	
13.41	2.44	0.99	0	176	0.58	0.59	77.8	33.8	3.27	34.1	3.7	1.8	192	SILT																	
13.72	0.18	POOR	DATA																												
14.02	2.33	0.87	0	150	0.55	0.57	85.4	34.4	3.36	34.8	3.49	1.6	155	CLAYEY	SILT																
14.33	2.74	1.12	0	231	0.59	0.71	95.6	35	3.42	35.4	4.17	1.9	281	SILT																	
14.63	2.4	1.4	0	256	0.54	0.61	101.7	35.5	3.48	35.9	3.51	1.6	285	SANDY	SILT																
14.94	3.23	1.15	0	289	0.64	0.89	105.8	35.4	3.52	35.8	5.21	2.3	400	SILT																	

APPENDIX C – Browne Road Data

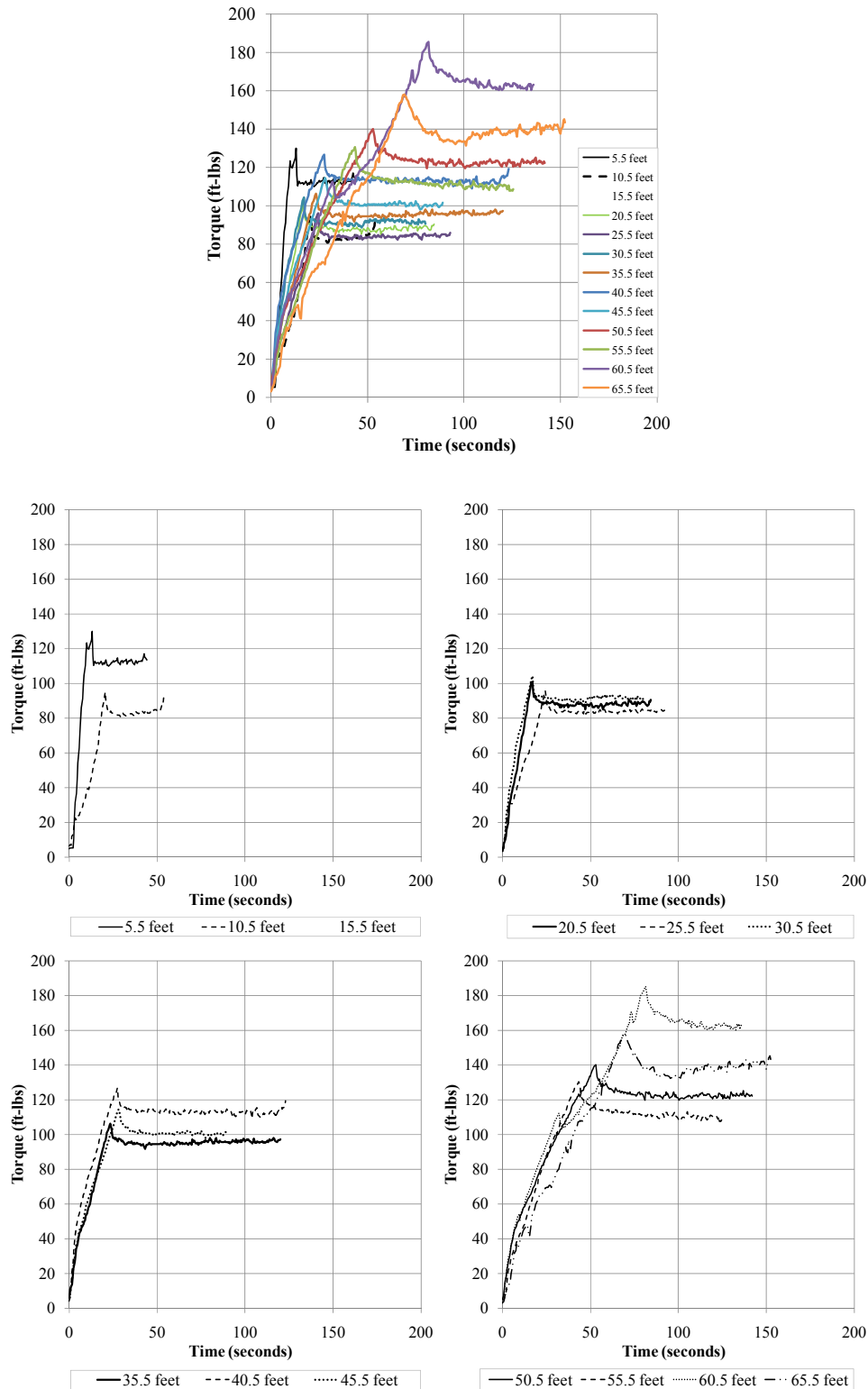


Figure C1 – BR SPT-T Torque data 1

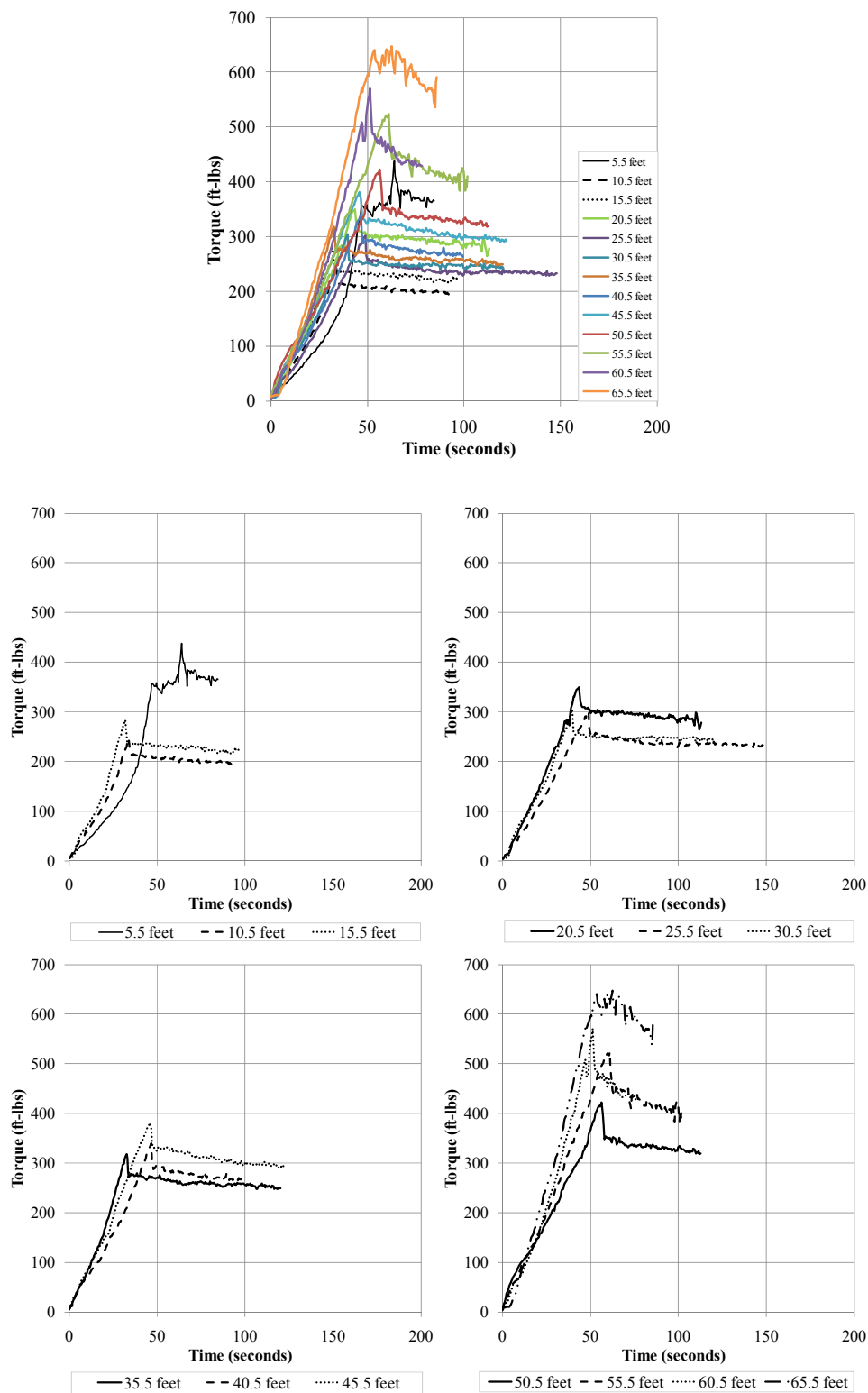


Figure C2 – BR STT-T Torque data 1

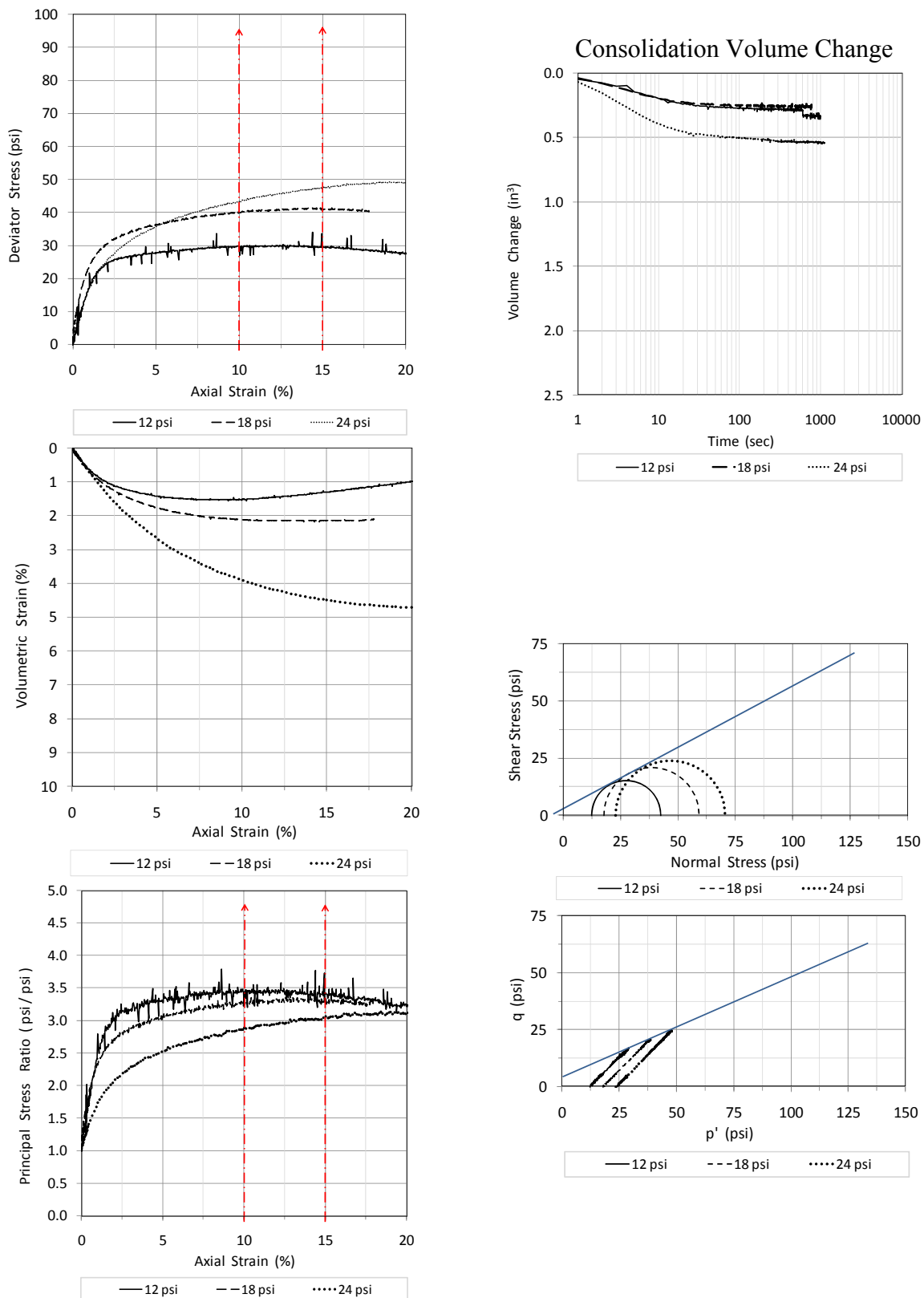


Figure C3 – BR 5.5' Triaxial data

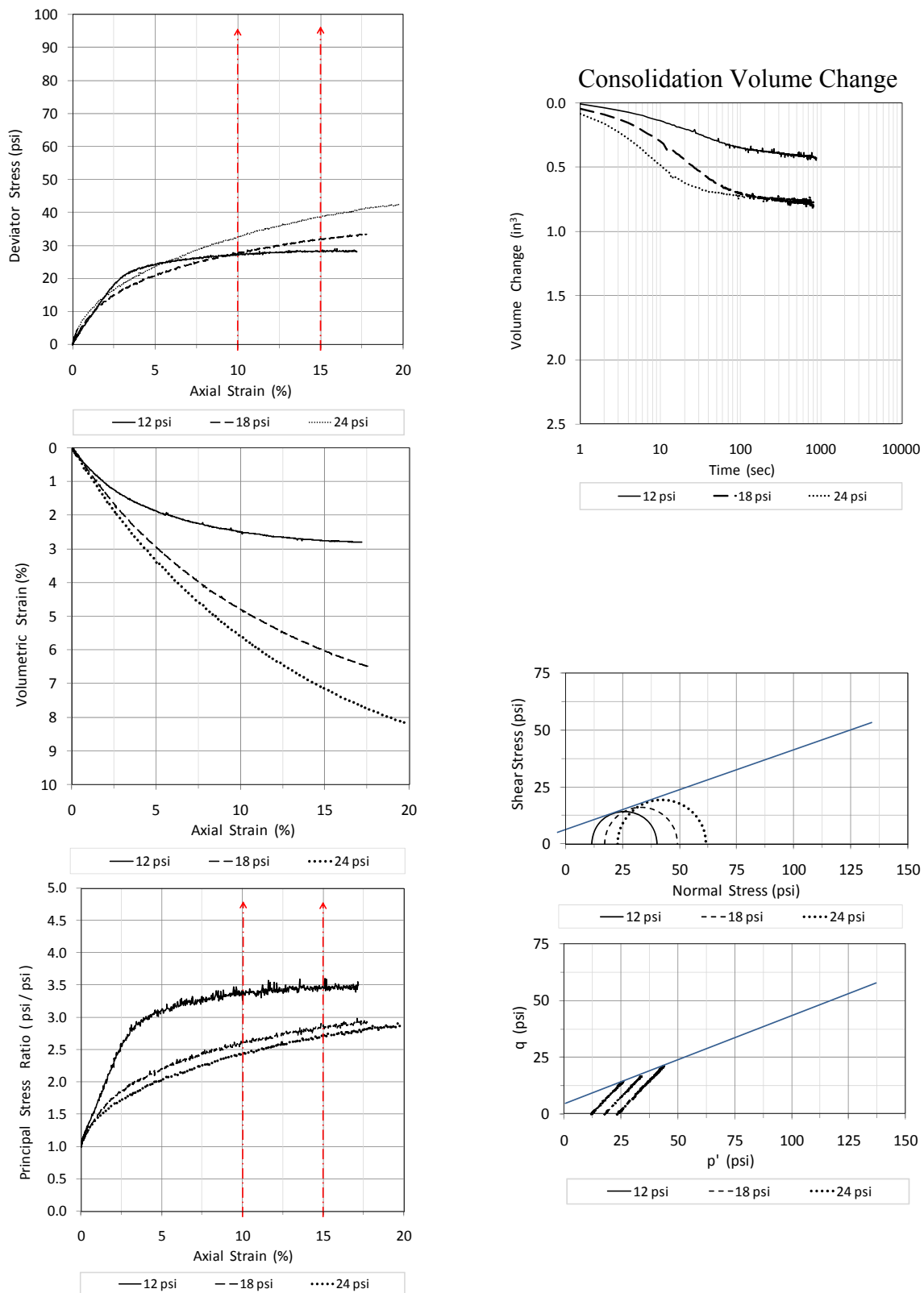


Figure C4 – BR 10.5' Triaxial data

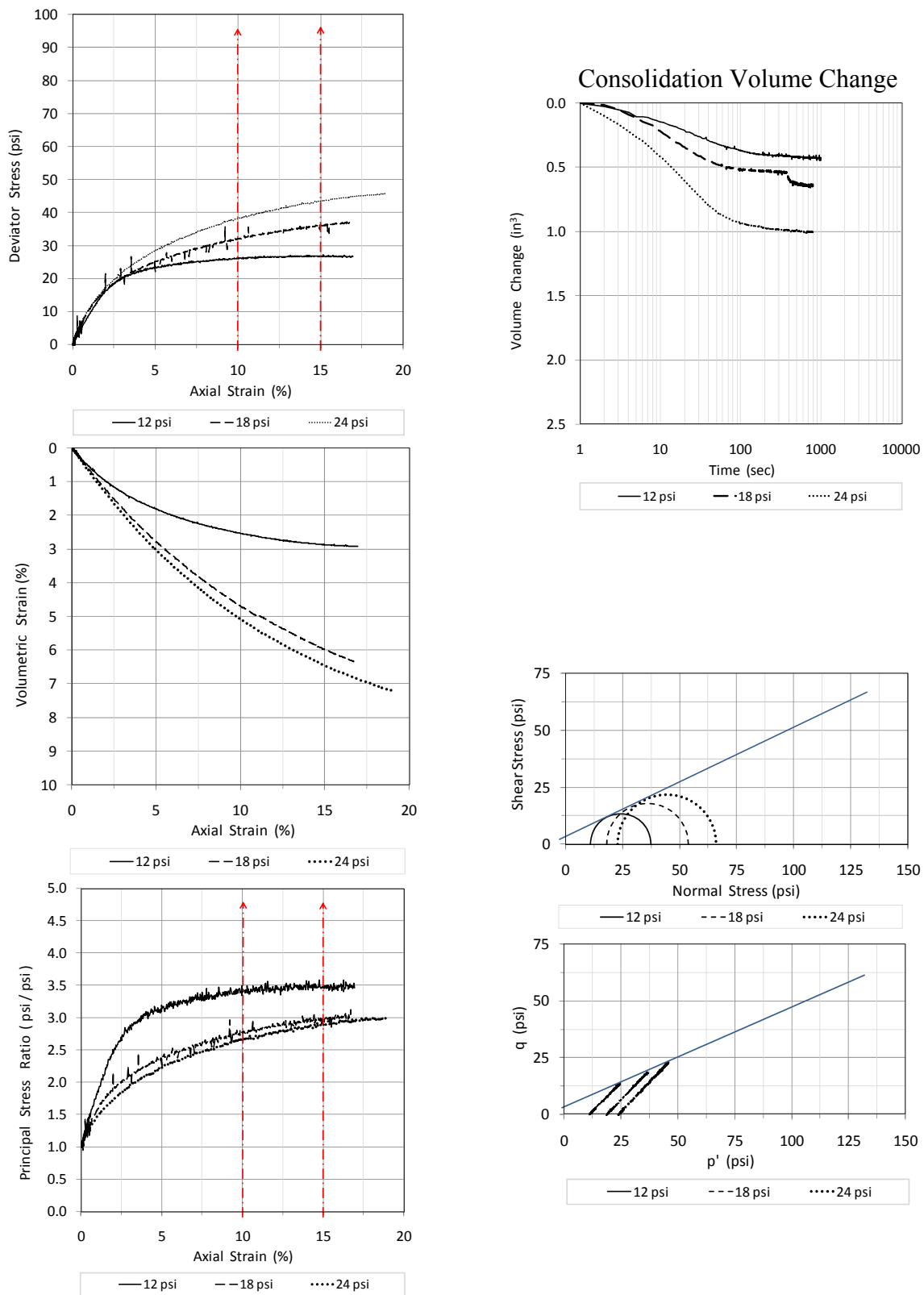


Figure C5 – BR 15.5' Triaxial data

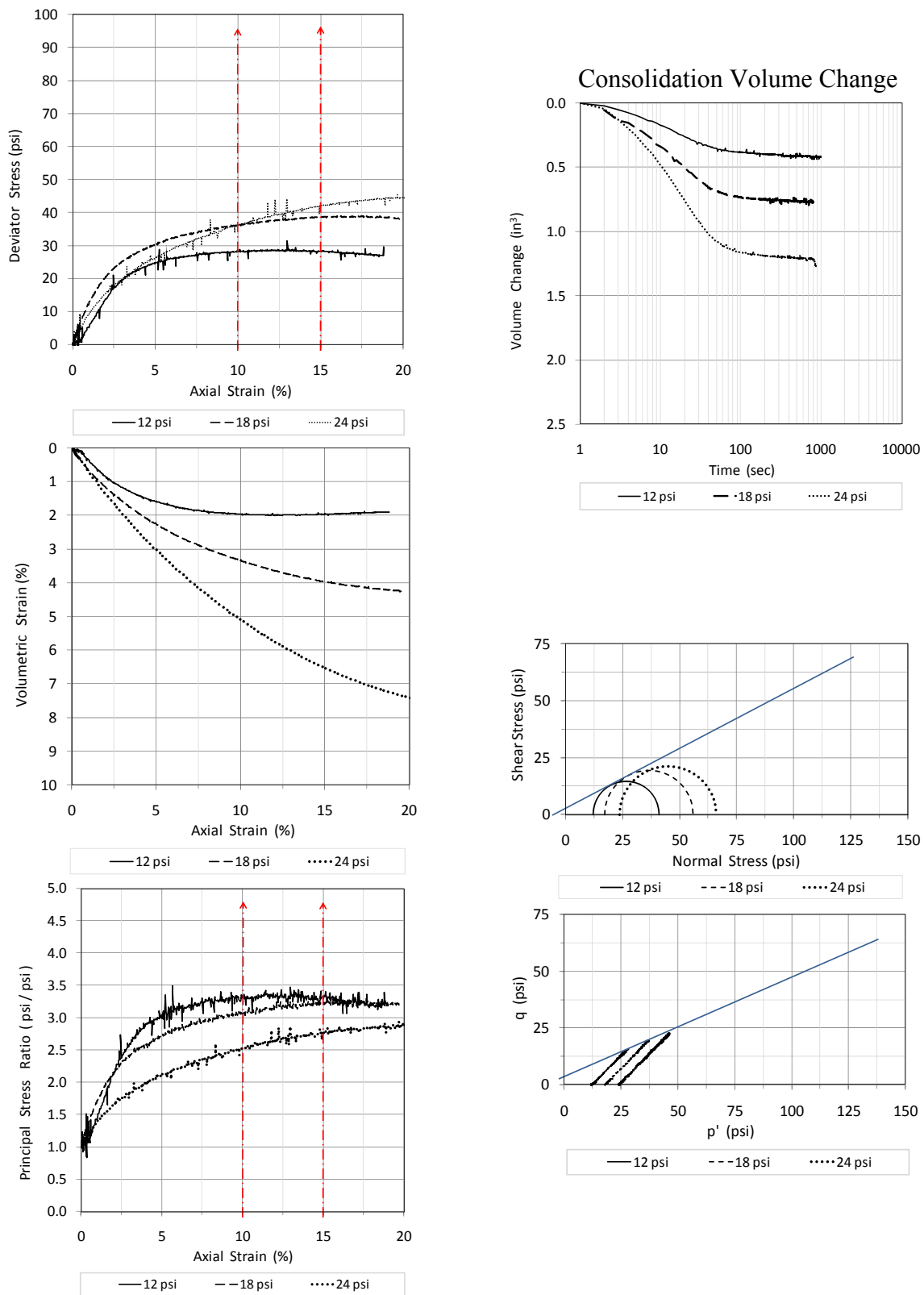


Figure C6 – BR 20.5' Triaxial data

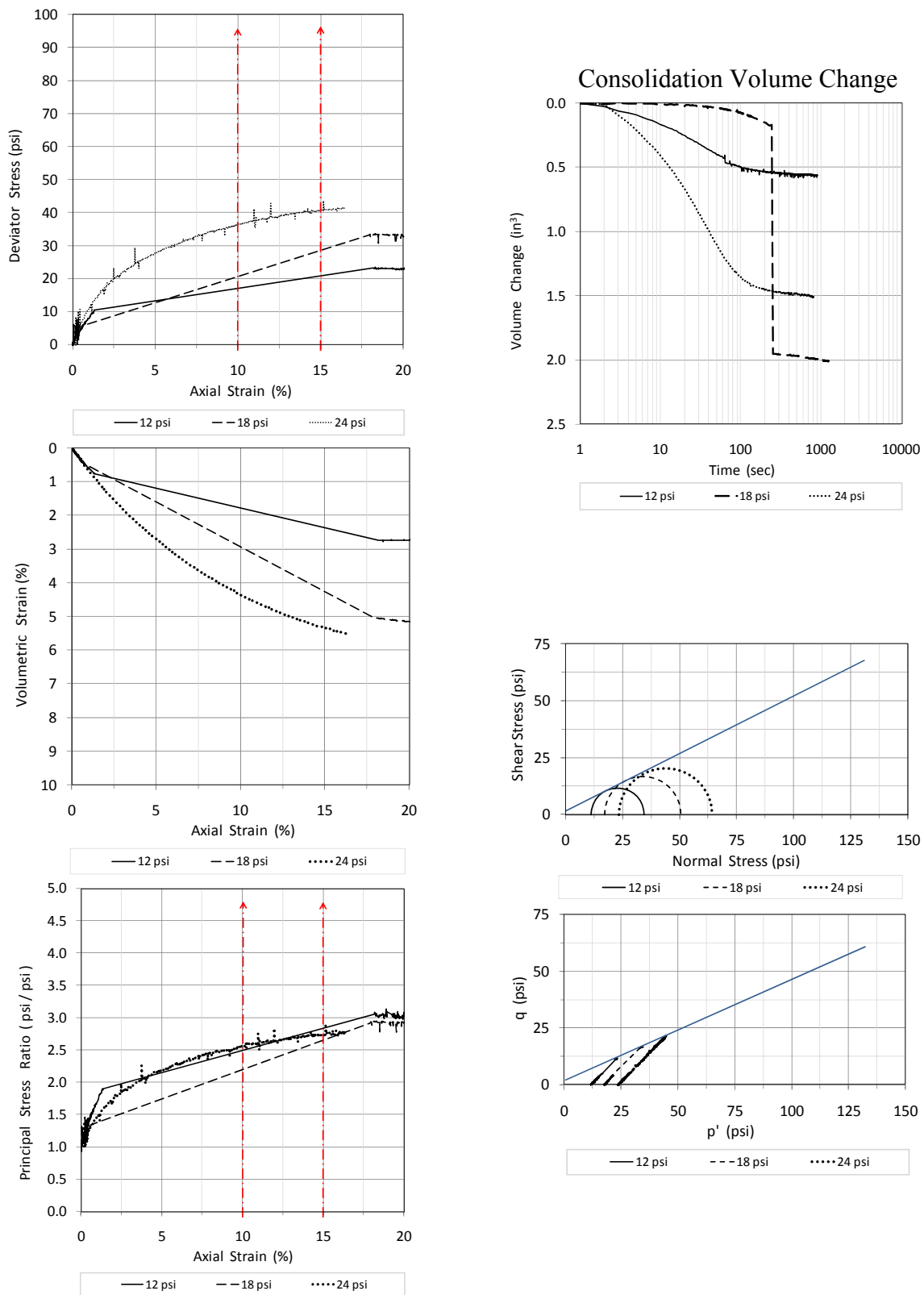


Figure C7 – BR 25.5' Triaxial data

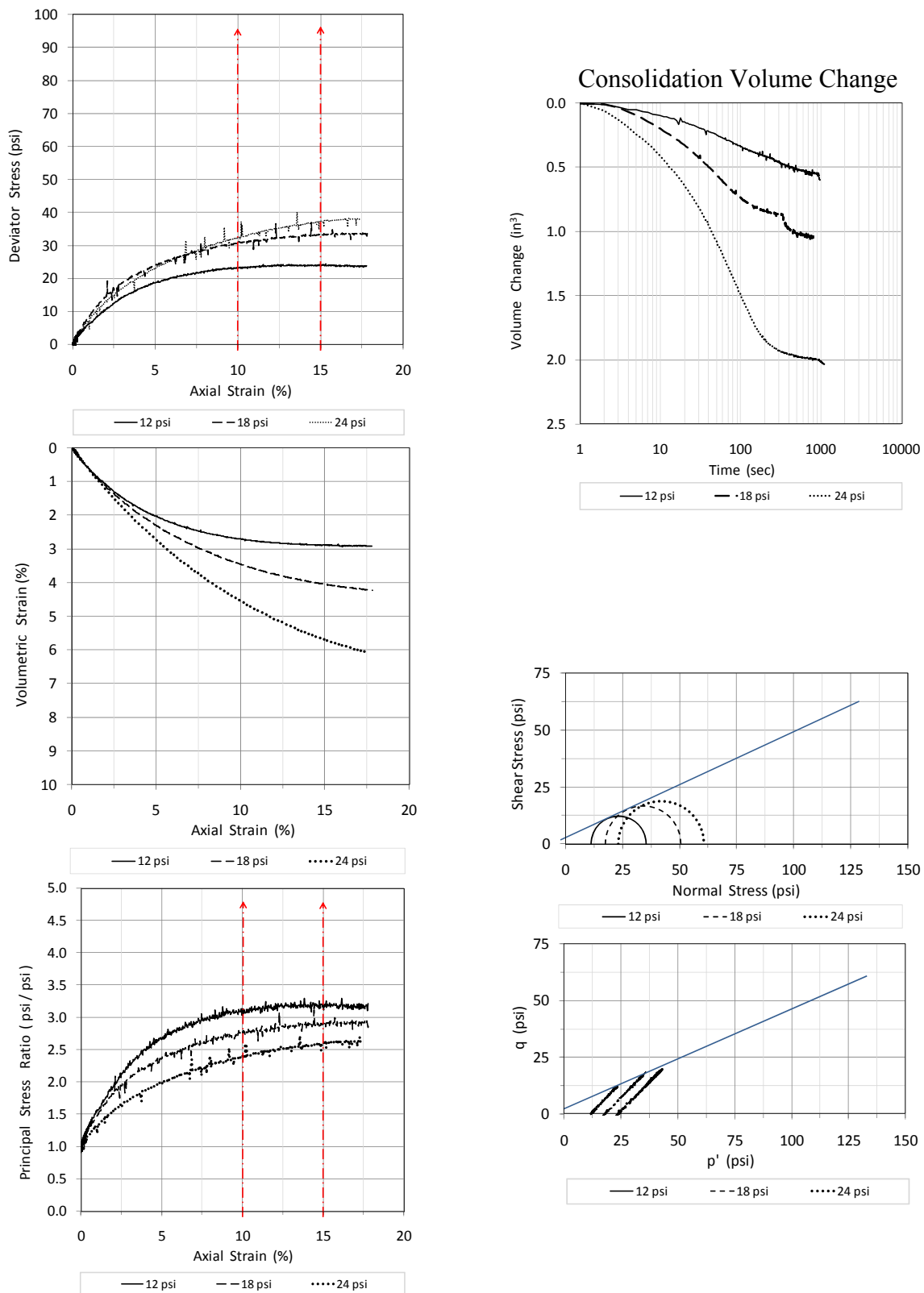


Figure C8 – BR 30.5' Triaxial data

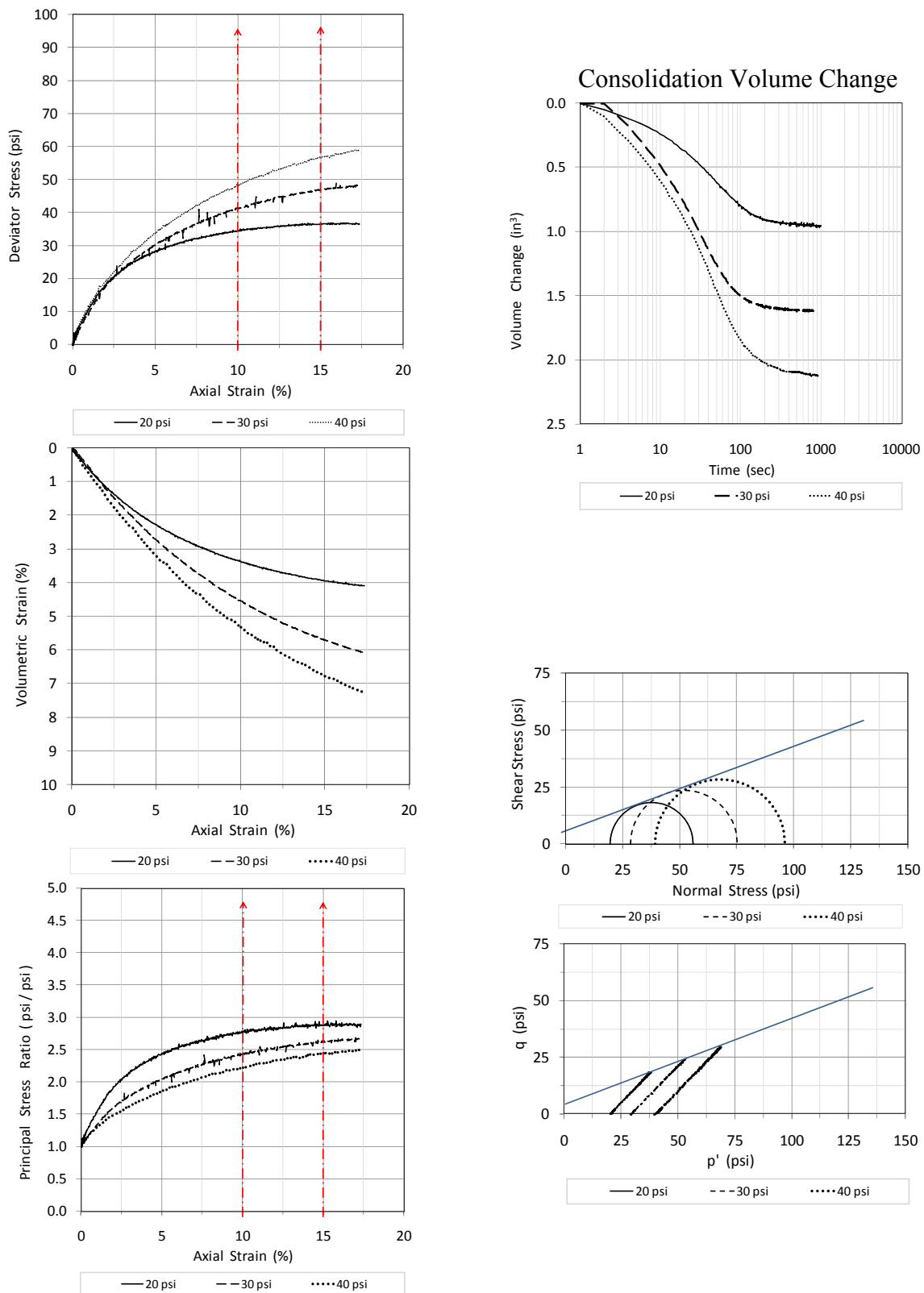


Figure C9 – BR 35.5' Triaxial data

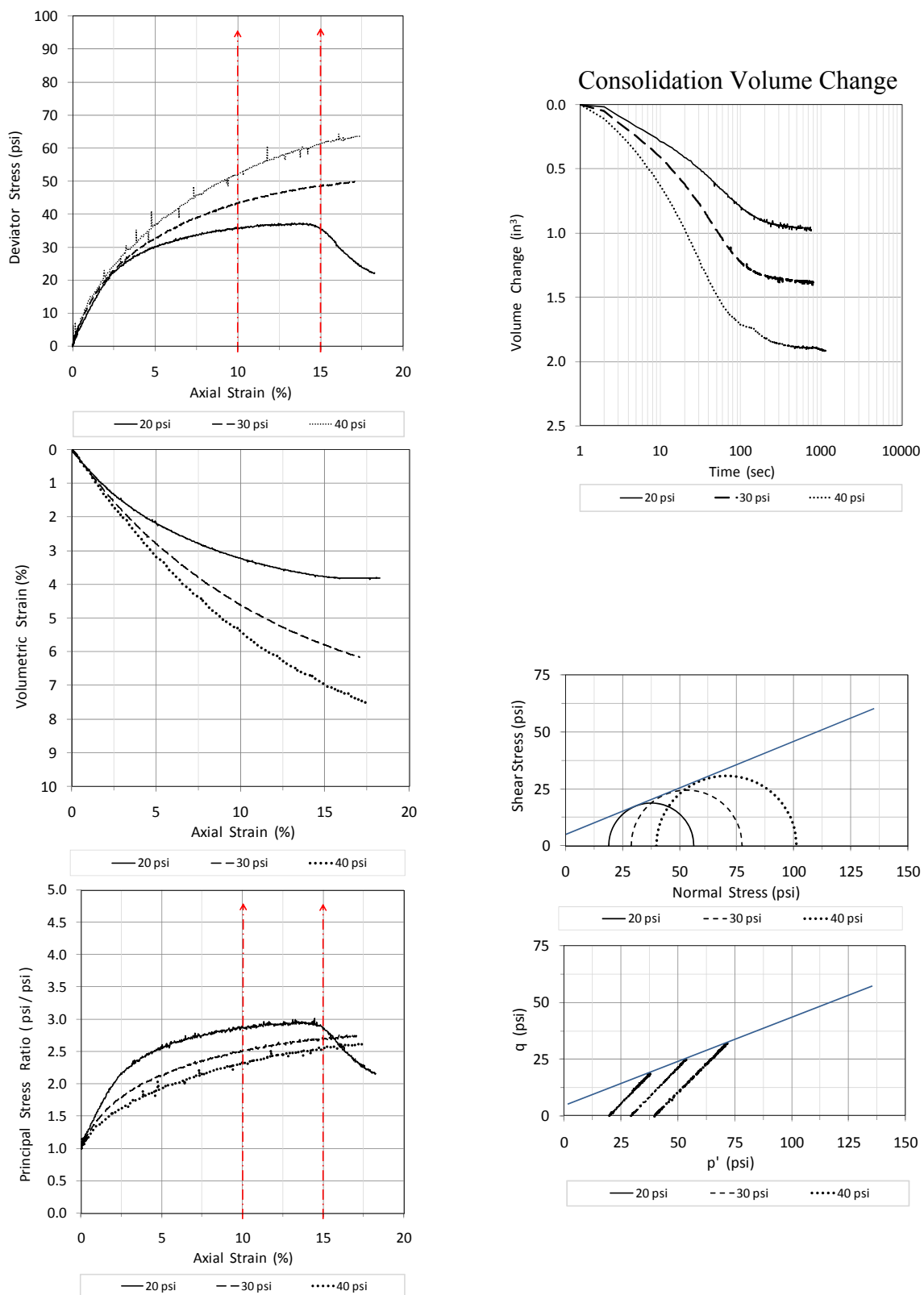


Figure C10 – BR 40.5' Triaxial data

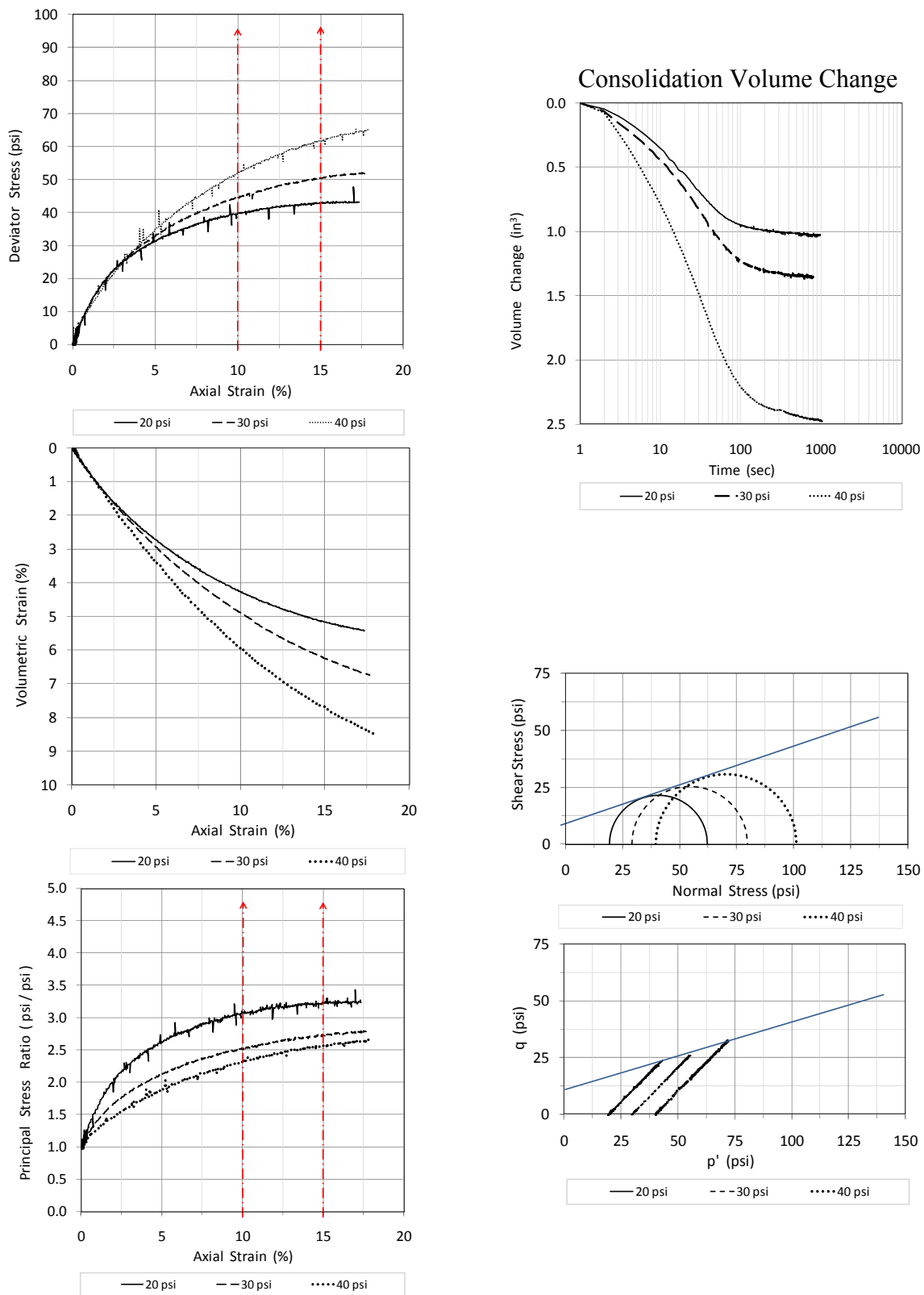


Figure C11 – BR 45.5' Triaxial data

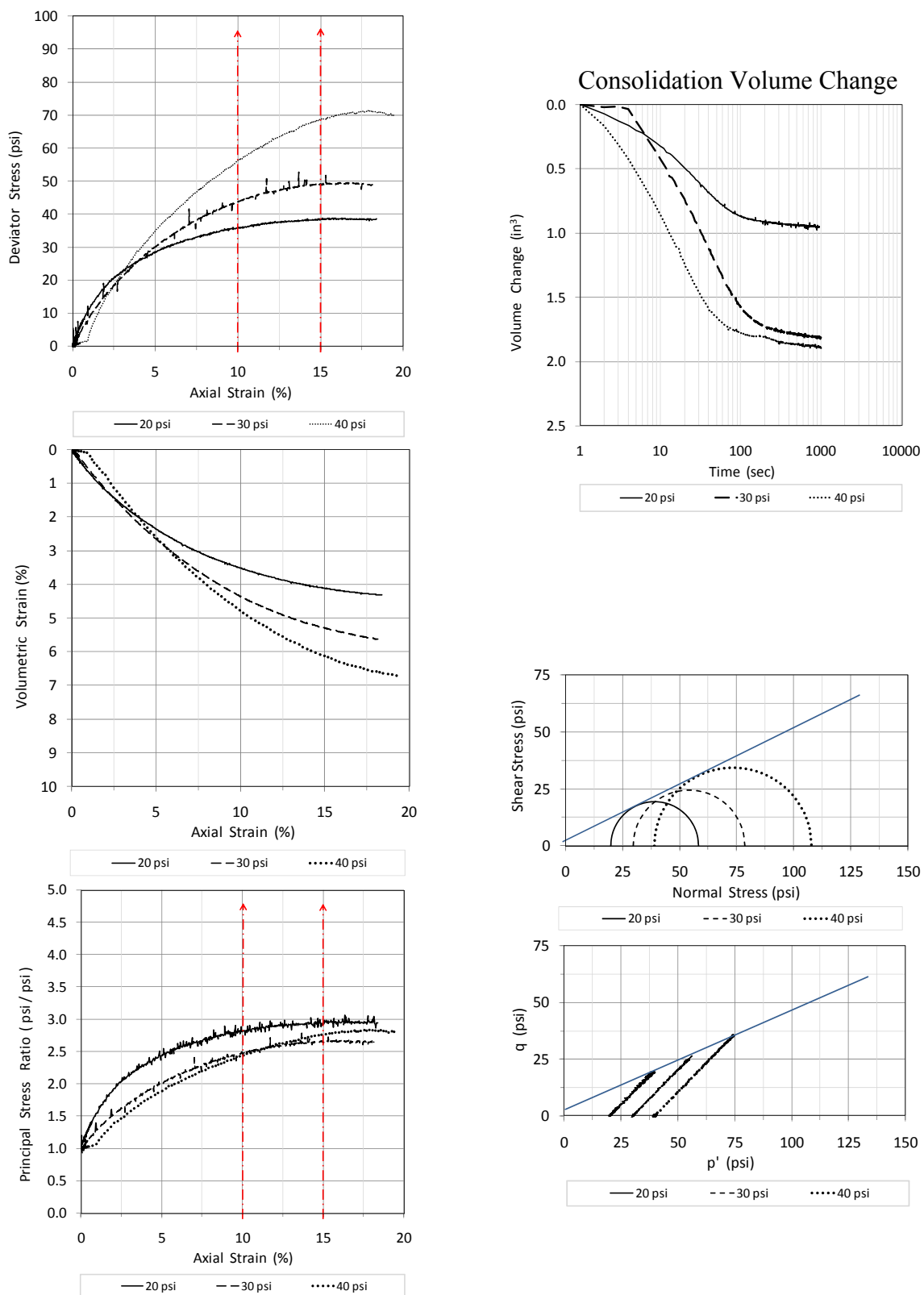


Figure C12 – BR 50.5' Triaxial data

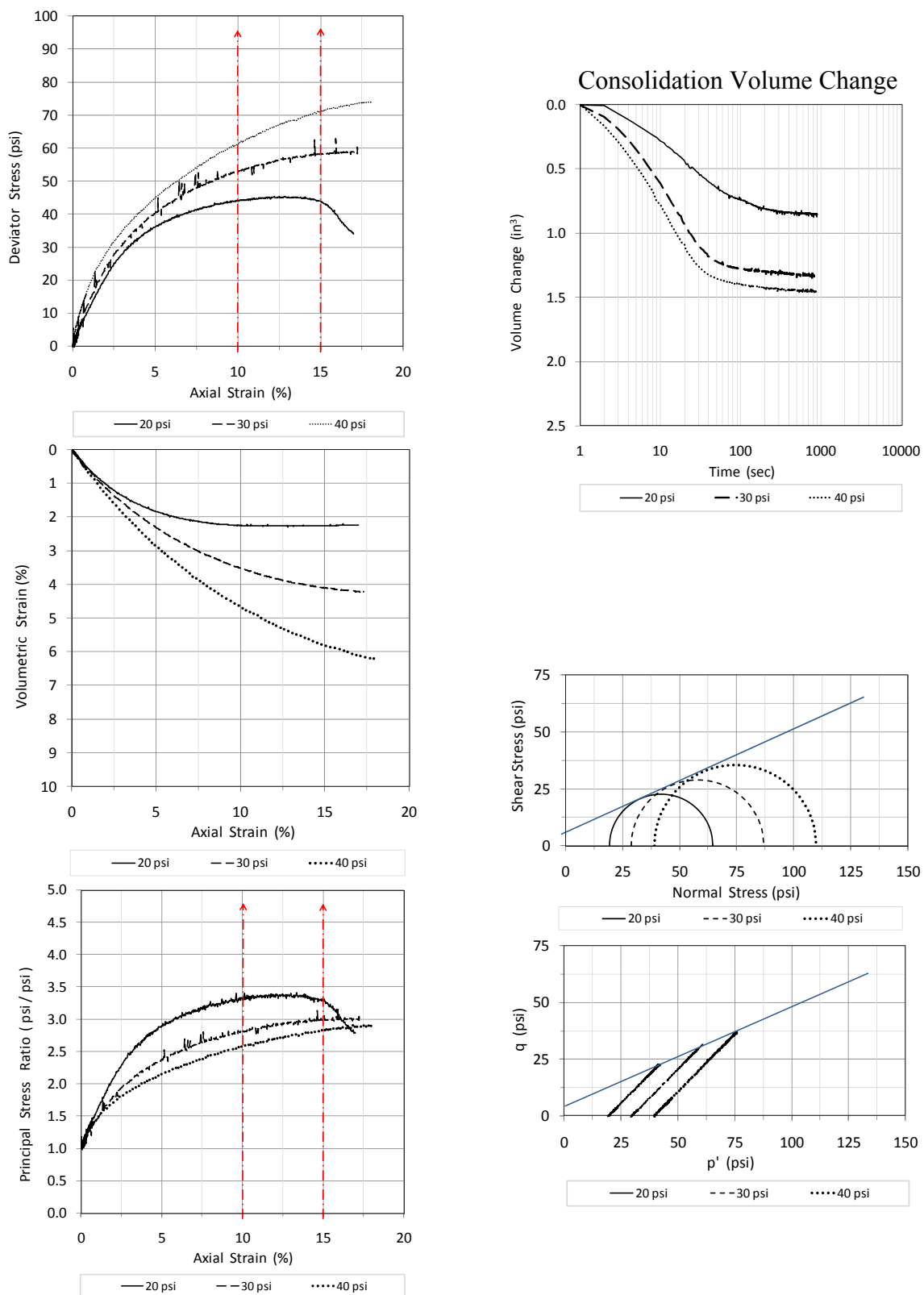


Figure C13 – BR 55.5' Triaxial data

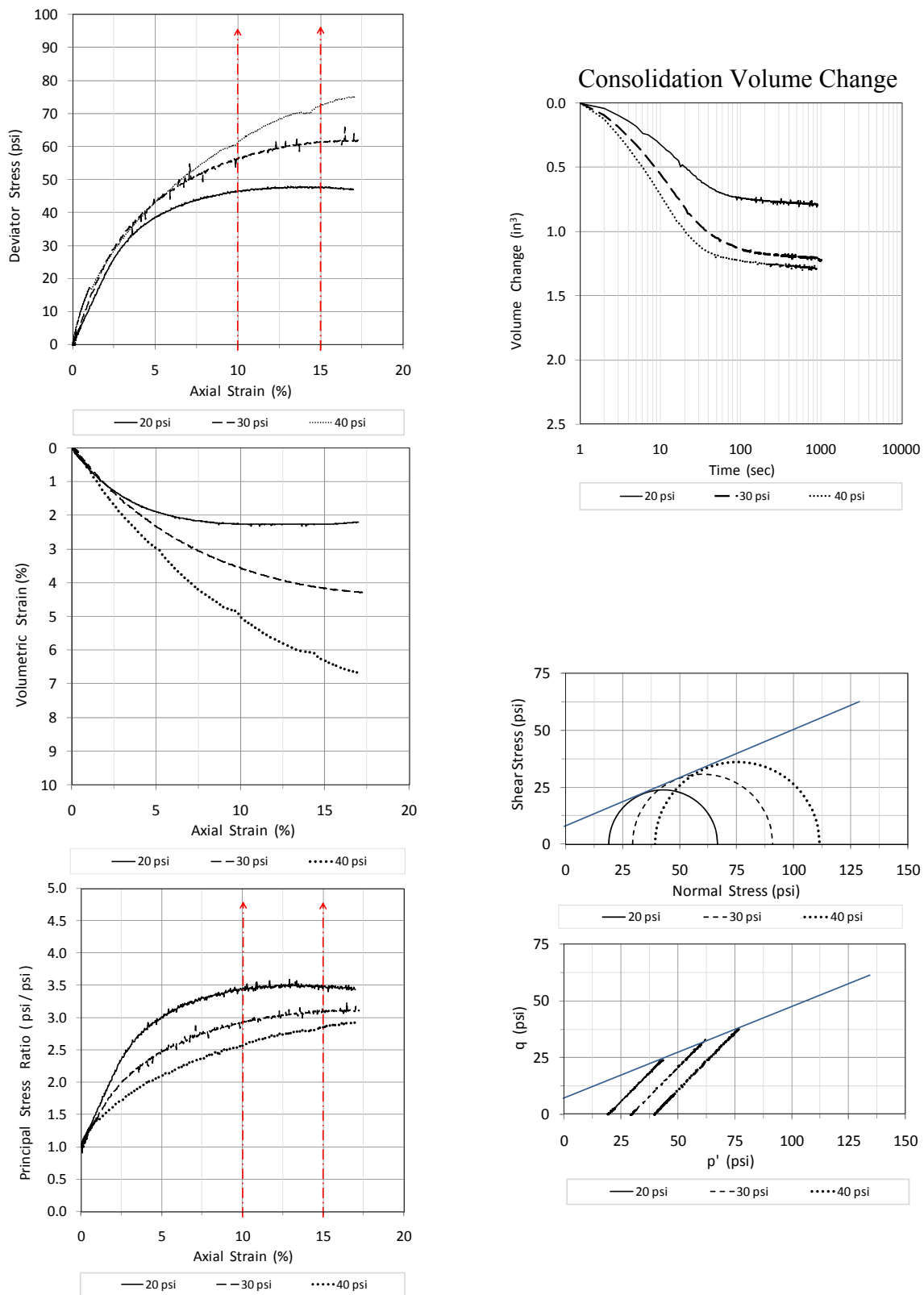


Figure C14 – BR 60.5' Triaxial data

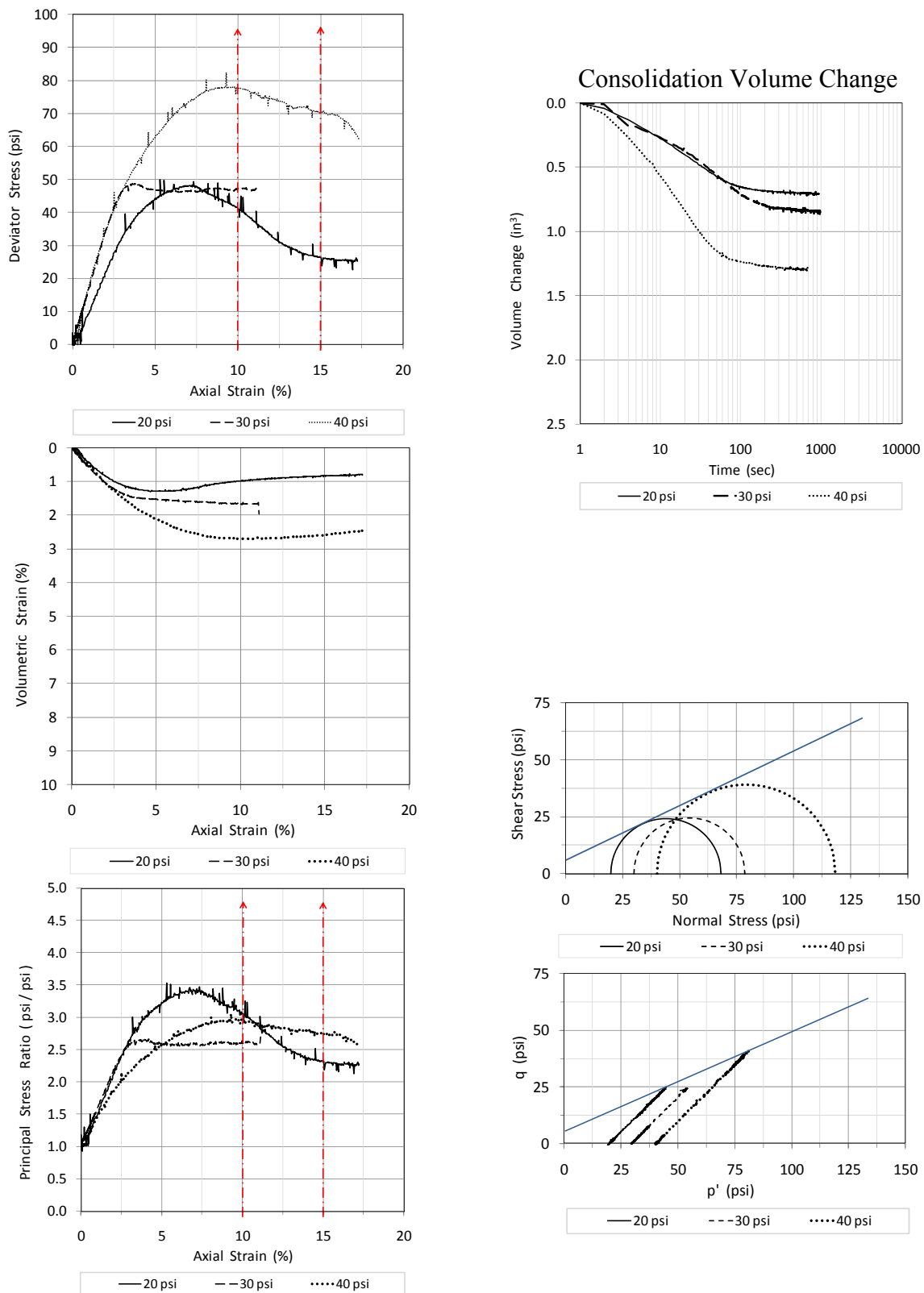


Figure C15 – BR 65.5' Triaxial data

Table C1 – BR Interface shear test data

Depth	5.5 feet	10.5 feet	15.5 feet	20.5 feet	25.5 feet
Normal Stress (psi)	Shear Stress (psi)				
10	3.111	3.153	4.313	3.201	3.264
20	6.201	7.306	7.201	6.965	6.306
30	10.528	9.688	11.313	9.278	10.924

Table C1 – (continued)

Depth	30.5 feet	35.5 feet	40.5 feet	45.5 feet	50.5 feet
Normal Stress (psi)	Shear Stress (psi)				
10	3.111	3.688	3.403	3.965	2.264
20	5.625	6.639	5.694	7.563	7.451
30	8.882	9.479	9.167	9.215	9.431

Table C1 – (continued)

Depth	55.5 feet	60.5 feet	65.5 feet
Normal Stress (psi)	Shear Stress (psi)		
10	4.354	2.986	3.819
20	7.958	6.306	7.889
30	13.028	10.111	12.507

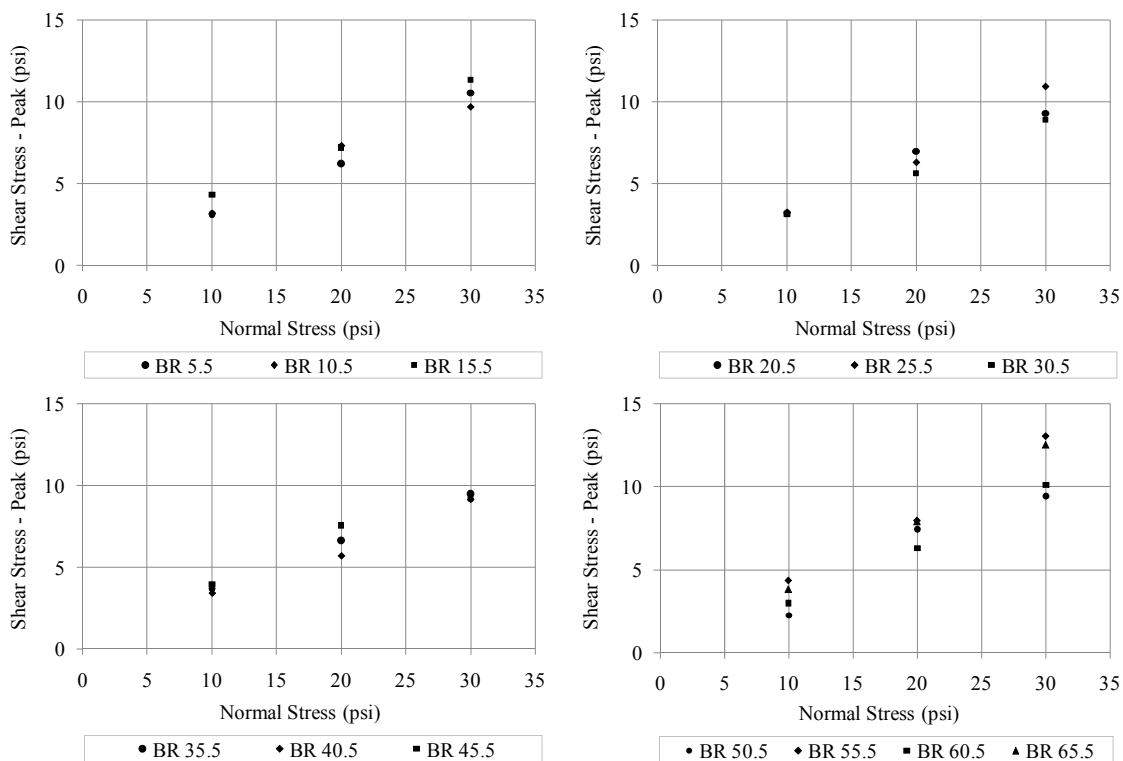


Figure C16 – BR Interface shear test data

Table C2 – BR Geotechnical soil classification data

Depth	AASHTO	USCS	LL	PL	PI	Clay Fraction
feet	Class	Class	%	%	%	% < 2 μ m
5.5	A-7-6	MH	79.3	57.3	22.1	55.9
10.5	A-5	MH	58.8	50.1	8.7	28.1
15.5	A-7-6	MH	68.7	56.8	11.9	28.2
20.5	A-5	MH	58.6	50.4	8.2	20.4
25.5	A-5	MH	60.5	50.8	9.8	24.0
30.5	A-7-6	MH	59.4	46.3	13.1	21.7
35.5	A-7-6	MH	55.0	41.8	13.1	20.4
40.5	A-5	ML	46.6	39.1	7.6	19.9
45.5	A-7-6	MH	50.4	37.8	12.6	17.3
50.5	A-5	ML	44.2	35.5	8.7	15.1
55.5	A-5	ML	45.5	37.0	8.4	16.6
60.5	A-4	ML	39.8	32.3	7.5	11.0
65.5	A-5	ML	43.1	36.2	6.9	14.4

MH - Inorganic silts, micaceous or diatomaceous fine sandy or silty soils, elastic silts
 ML - Inorganic silt and very fine sands, rocks flour, silty or clayey fine sands or clayey silts with slight plasticity

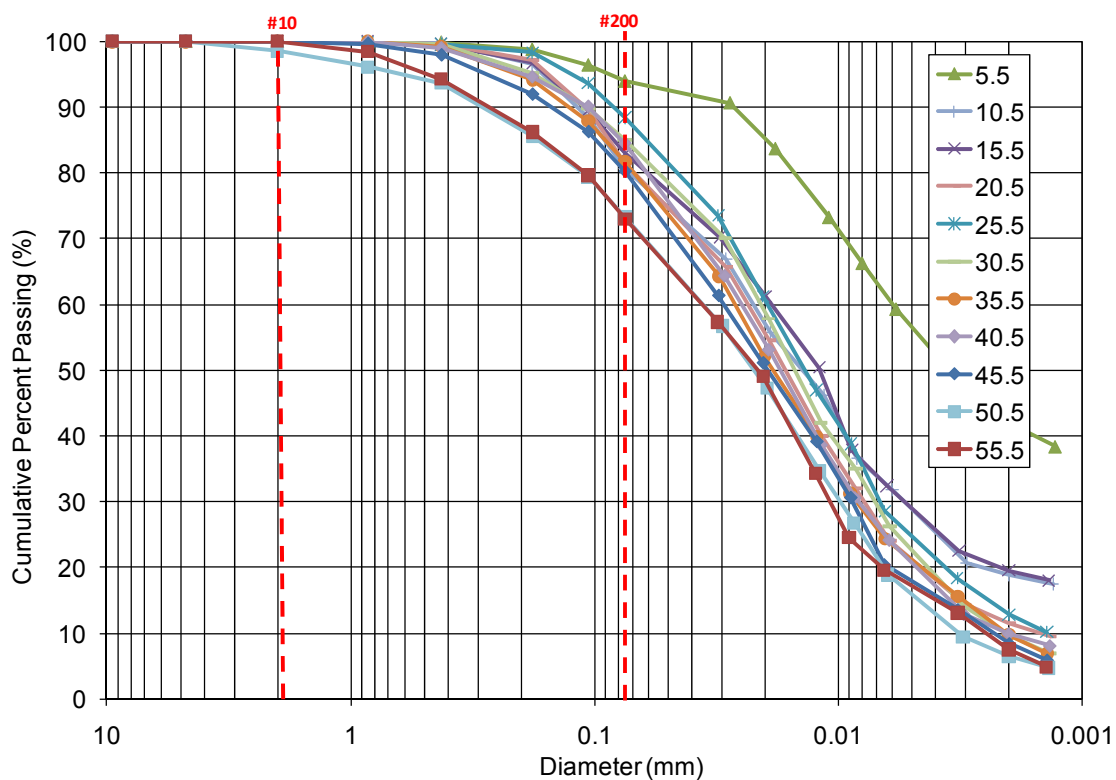


Figure C17 – BR Grain-size distribution curve

Table C3 – BR Soil classification data – grain-size distribution

BR 5.5'		BR 10.5'		BR 15.5'	
Cumulative Percent Passing	D (mm)	Cumulative Percent Passing	D (mm)	Cumulative Percent Passing	D (mm)
100.00	9.500	100.00	9.500	100.00	9.500
100.00	4.750	100.00	4.750	100.00	4.750
100.00	2.000	100.00	2.000	100.00	2.000
99.92	0.850	99.90	0.850	99.94	0.850
99.84	0.425	99.78	0.425	99.58	0.425
98.74	0.180	96.49	0.180	96.70	0.180
96.39	0.106	88.32	0.106	89.50	0.106
93.94	0.075	80.59	0.075	82.96	0.075
90.64	0.028	66.88	0.029	70.25	0.031
83.67	0.018	55.73	0.019	61.25	0.020
73.21	0.011	46.18	0.011	50.44	0.012
66.24	0.008	36.62	0.008	37.83	0.009
59.26	0.006	31.85	0.006	32.42	0.006
47.06	0.003	20.70	0.003	22.52	0.003
42.06	0.002	18.81	0.002	19.56	0.002
38.35	0.001	17.51	0.001	18.01	0.001

Table C3 – (continued)

BR 20.5'		BR 25.5'		BR 30.5'	
Cumulative Percent Passing	D (mm)	Cumulative Percent Passing	D (mm)	Cumulative Percent Passing	D (mm)
100.00	9.500	100.00	9.500	100.00	9.500
100.00	4.750	100.00	4.750	100.00	4.750
100.00	2.000	100.00	2.000	100.00	2.000
99.92	0.850	99.80	0.850	99.92	0.850
99.60	0.425	99.60	0.425	99.52	0.425
97.13	0.180	98.30	0.180	95.13	0.180
89.70	0.106	93.66	0.106	89.81	0.106
81.38	0.075	88.38	0.075	85.08	0.075
65.70	0.029	73.53	0.031	70.10	0.029
54.48	0.019	61.27	0.020	57.83	0.019
40.06	0.012	46.98	0.012	42.06	0.012
32.05	0.009	38.81	0.009	35.05	0.009
24.04	0.006	28.59	0.006	26.29	0.006
14.42	0.003	18.38	0.003	14.02	0.003
11.45	0.002	12.85	0.002	9.65	0.002
9.61	0.001	10.21	0.001	7.01	0.001

Table C3 – (continued)

BR 35.5'		BR 40.5'		BR 45.5'	
Cumulative Percent Passing	D (mm)	Cumulative Percent Passing	D (mm)	Cumulative Percent Passing	D (mm)
100.00	9.50	100.00	9.500	100.00	9.500
100.00	4.75	100.00	4.750	100.00	4.750
100.00	2.00	100.00	2.000	100.00	2.000
99.94	0.85	99.92	0.850	99.66	0.850
99.24	0.43	98.98	0.425	97.93	0.425
94.18	0.18	94.61	0.180	91.97	0.180
87.86	0.11	90.09	0.106	86.28	0.106
81.67	0.08	84.50	0.075	80.26	0.075
64.28	0.03	64.33	0.029	61.39	0.031
52.12	0.02	53.07	0.019	51.16	0.020
39.96	0.01	38.60	0.012	39.22	0.012
31.27	0.01	30.56	0.009	30.69	0.009
24.32	0.01	24.12	0.006	20.46	0.007
15.64	0.00	12.87	0.003	13.64	0.003
9.80	0.0020	9.87	0.002	8.46	0.002
6.95	0.00	8.04	0.001	5.97	0.001

Table C3 – (continued)

BR 50.5'		BR 55.5'		BR 60.5'	
Cumulative Percent Passing	D (mm)	Cumulative Percent Passing	D (mm)	Cumulative Percent Passing	D (mm)
100.00	9.500	100.00	9.500	100.00	9.500
100.00	4.750	100.00	4.750	100.00	4.750
98.47	2.000	100.00	2.000	99.29	2.000
96.14	0.850	98.46	0.850	96.56	0.850
93.63	0.425	94.26	0.425	91.46	0.425
85.59	0.180	86.24	0.180	78.70	0.180
79.47	0.106	79.64	0.106	67.58	0.106
73.25	0.075	73.03	0.075	58.36	0.075
56.75	0.030	57.31	0.031	41.43	0.032
47.29	0.020	49.12	0.020	31.87	0.021
34.68	0.012	34.39	0.012	23.90	0.012
26.80	0.009	24.56	0.009	17.53	0.009
18.92	0.006	19.65	0.007	14.34	0.006
9.46	0.003	13.10	0.003	6.37	0.003
6.46	0.002	7.56	0.002	4.33	0.002
4.73	0.001	4.91	0.001	3.19	0.001

Table C3 – (continued)

BR 65.5'	
Cumulative Percent Passing	D (mm)
100.00	9.500
100.00	4.750
99.29	2.000
95.82	0.850
89.32	0.425
76.16	0.180
65.72	0.106
57.58	0.075
45.54	0.033
35.78	0.021
26.02	0.013
20.33	0.009
17.89	0.007
10.57	0.003
6.13	0.002
4.07	0.001

Table C4 – BR Geologic soil color

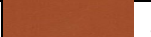
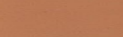
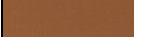

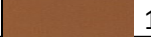
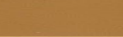
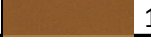
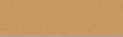
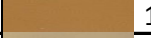

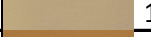

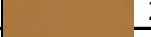
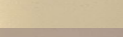

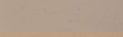


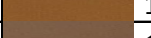







Depth feet	Wet Color		Dry Color	
5.5	5YR 5/8		5YR 6/6	
10.5	7.5YR 5/6		7.5 6/8	
15.5	7.5YR 5/6		10YR 6/6	
20.5	10YR 5/6		10YR 7/6	
25.5	10YR 6/6		10YR 7/4	
30.5	2.5Y 7/4		10YR 8/3	
35.5	10YR 6/6		2.5Y 8/3	
40.5	10YR 6/6		10YR 7/3	
45.5	10YR 5/6		10YR 7/4	
50.5	10 YR 5/6		10YR 7/3	
55.5	10YR 5/4		10YR 7/2	
60.5	7.5YR 4/6		10YR 6/3	
65.5	2.5Y 5/4		10YR 6/3	

Table C5 – BR Geologic soil classification data

Depth feet	Gravel		Consistence			Texture
		%	stickiness	plasticity	Moist	
5.5	0	0	sticky	plastic	firm	Silty Loam
10.5	0	0	sticky	plastic	friable	Silty Loam
15.5	0	0	sticky	plastic	friable	Silty Loam
20.5	0	0	sticky	plastic	friable	Silty Loam
25.5	0	0	sticky	plastic	friable	Silty Loam
30.5	0	0	sticky	plastic	friable	Silty Loam
35.5	0	0	sticky	plastic	friable	Silty Loam
40.5	0	0	sticky	plastic	friable	Silty Loam
45.5	10rocks	< 10	slight	plastic	friable	Silty Loam
50.5	60 rocks	< 10	slight	plastic	friable	Silty Loam
55.5	2 rocks	< 10	slight	plastic	friable	Silty Loam
60.5	2 rocks	< 10	slight	slight	very friable	Loam
65.5	10 rocks	< 10	slight	slight	very friable	Loam

Table C6 – BR Dilatometer data output

DILATOMETER DATA LISTING & INTERPRETATION (BASED ON THE 1988 DILATOMETER MANUAL) SNDG. NO. DMT-17																
M. Allen Cottingham																
JOB FILE: Dissertation Research 2009 FILE NO. : Cottingham 2009-1																
LOCATION: Browne Road Site 1																
SNDG.BY: Cottingham/Anderson SNDG.DATE: 7 July 2008																
ANAL.BY: Cottingham ANAL.DATE: 19 May 2009																
ANALYSIS PARAMETERS: LO RANGE = 5.00 BARS ROD DIAM. = 4.44 CM BL.THICK. = 15.0 MM SU FACTOR = 1.00																
SURF.ELEV. = 0.00 M LO GAGE 0 = 0.00 BARS FR.RED.DIA. = 5.71 CM BL.WIDTH = 96.0 MM PHI FACTOR = 1.00																
WATER DEPTH = 7.62 M HI GAGE 0 = 0.00 BARS LIN.ROD WT. = 6.25 KGF/M DELTA-A = 0.18 BARS OCR FACTOR = 1.00																
SP.GR.WATER = 1.000 CAL GAGE 0 = 0.00 BARS DELTA/PHI = 0.50 DELTA-B = 0.31 BARS M FACTOR = 1.00																
MAX SU ID = 9.00 SU OPTION = MARCHETTI MIN PHI ID = 0.10 OCR OPTION= MARCHETTI K0 FACTOR = 1.00																
UNIT CONVERSIONS: 1 BAR = 1.019 KGF/CM2 = 1.044 TSF = 14.51 PSI 1 M = 3.2808 FT																
Z	THRUST	A	B	C	DA	DB	ZMRNG	ZMLO	ZMHI	ZMCAL	P0	P1	P2	UO	GAMMA	SVP
(M)	(KGF)	(BAR)	(BAR)	(BAR)	(BAR)	(BAR)	(BAR)	(BAR)	(BAR)	(BAR)	(BAR)	(BAR)	(BAR)	(BAR)	(T/M3)	(BAR)
*****	*****	*****	*****	*****	*****	*****	*****	*****	*****	*****	*****	*****	*****	*****	*****	*****
0.3	1938	3.1	11.4		0.18	0.31	5	0	0	0	2.89	11.09		0	1.9	0.053
0.61	1616	3.85	11.2		0.18	0.31	5	0	0	0	3.69	10.89		0	1.9	0.111
0.91	1517	4.5	12.6		0.18	0.31	5	0	0	0	4.3	12.29		0	1.9	0.167
1.22	1476	7.7	14.8		0.18	0.31	5	0	0	0	7.55	14.49		0	1.95	0.225
1.52	1457	6.7	13.7		0.18	0.31	5	0	0	0	6.55	13.39		0	1.95	0.283
1.83	1337	6.4	11.9		0.18	0.31	5	0	0	0	6.33	11.59		0	1.95	0.342
2.13	1124	4.9	10.1		0.18	0.31	5	0	0	0	4.84	9.79		0	1.8	0.397
2.44	990	4.15	8.5		0.18	0.31	5	0	0	0	4.14	8.19		0	1.8	0.452
2.74	898	3.35	6.9		0.18	0.31	5	0	0	0	3.38	6.59		0	1.8	0.505
3.05	870	3.6	6.7		0.18	0.31	5	0	0	0	3.65	6.39		0	1.8	0.56
3.35	875	3.4	6.7		0.18	0.31	5	0	0	0	3.44	6.39		0	1.8	0.613
3.66	868	3.15	6.3		0.18	0.31	5	0	0	0	3.2	5.99		0	1.8	0.667
3.96	962	3.45	6.6		0.18	0.31	5	0	0	0	3.5	6.29		0	1.8	0.72
4.27	1120	3.95	7.2		0.18	0.31	5	0	0	0	3.99	6.89		0	1.8	0.775
4.57	1212	3.75	7.1		0.18	0.31	5	0	0	0	3.79	6.79		0	1.8	0.828
4.88	1211	3.3	5.9		0.18	0.31	5	0	0	0	3.37	5.59		0	1.7	0.881
5.18	1305	3.6	6.4		0.18	0.31	5	0	0	0	3.66	6.09		0	1.8	0.933
5.49	1276	4.35	6.8		0.18	0.31	5	0	0	0	4.43	6.49		0	1.8	0.988
5.79	1362	3.75	6.35		0.18	0.31	5	0	0	0	3.82	6.04		0	1.8	1.041
6.1	1354	3.4	5.7		0.18	0.31	5	0	0	0	3.49	5.39		0	1.7	1.094
6.4	1267	3.2	5.1		0.18	0.31	5	0	0	0	3.31	4.79		0	1.7	1.144
6.71	1383	3.25	5.1		0.18	0.31	5	0	0	0	3.36	4.79		0	1.7	1.196
7.01	1392	3.63	5.6		0.18	0.31	5	0	0	0	3.74	5.29		0	1.7	1.246
7.32	1492	3.6	5.7		0.18	0.31	5	0	0	0	3.7	5.39		0	1.7	1.298
7.62	1630	3.75	5.7		0.18	0.31	5	0	0	0	3.86	5.39		0	1.7	1.348
7.93	1679	4.13	6.1		0.18	0.31	5	0	0	0	4.24	5.79		0.03	1.7	1.369
8.23	1724	4.4	6.6		0.18	0.31	5	0	0	0	4.49	6.29		0.06	1.8	1.391
8.54	1806	3.1	5.3		0.18	0.31	5	0	0	0	3.19	4.99		0.09	1.7	1.414
8.84	1868	3.45	5.9		0.18	0.31	5	0	0	0	3.53	5.59		0.12	1.7	1.434
9.15	2069	4.15	6.1		0.18	0.31	5	0	0	0	4.26	5.79		0.15	1.7	1.456
9.45	2155	4.05	6.3		0.18	0.31	5	0	0	0	4.14	5.99		0.18	1.7	1.476
9.76	2360	3.95	5.6		0.18	0.31	5	0	0	0	4.07	5.29		0.21	1.7	1.498
10.06	2473	4.2	6.15		0.18	0.31	5	0	0	0	4.31	5.84		0.239	1.7	1.518
10.37	2455	4.3	6.4		0.18	0.31	5	0	0	0	4.4	6.09		0.27	1.7	1.539
10.67	2703	4.5	6.9		0.18	0.31	5	0	0	0	4.58	6.59		0.299	1.8	1.562
10.98	2752	4.35	7.1		0.18	0.31	5	0	0	0	4.42	6.79		0.33	1.8	1.586
11.28	2960	4.75	8.3		0.18	0.31	5	0	0	0	4.78	7.99		0.359	1.8	1.609
11.59	3092	4.75	7.6		0.18	0.31	5	0	0	0	4.81	7.29		0.39	1.8	1.634
11.89	3199	4.63	7.7		0.18	0.31	5	0	0	0	4.68	7.39		0.419	1.8	1.657
12.2	3260	4.45	7.1		0.18	0.31	5	0	0	0	4.52	6.79		0.449	1.8	1.682
12.5	3312	5.7	9.6		0.18	0.31	5	0	0	0	5.71	9.29		0.479	1.8	1.705
12.8	3344	5.7	10.1		0.18	0.31	5	0	0	0	5.68	9.79		0.508	1.8	1.729
13.11	3479	5.1	10		0.18	0.31	5	0	0	0	5.06	9.69		0.539	1.8	1.753
13.41	3462	5.2	10.9		0.18	0.31	5	0	0	0	5.12	10.59		0.568	1.8	1.777

Table C6 – (continued)

DILATOMETER DATA LISTING & INTERPRETATION (BASED ON THE 1988 DILATOMETER MANUAL) SNDG. NO. DMT-17															
M. Allen Cottingham															
JOB FILE: Dissertation Research 2009 FILE NO. : Cottingham 2009-1															
LOCATION: Browne Road Site 1															
SNDG.BY : Cottingham/Anderson SNDG.DATE: 7 July 2008															
ANAL.BY : Cottingham ANAL.DATE: 19 May 2009															
ANALYSIS PARAMETERS: LO RANGE = 5.00 BARS ROD DIAM. = 4.44 CM BL.THICK. = 15.0 MM SU FACTOR = 1.00															
SURF.ELEV. = 0.00 M LO GAGE 0 = 0.00 BARS FR.RED.DIA. = 5.71 CM BL.WIDTH = 96.0 MM PHI FACTOR = 1.00															
WATER DEPTH = 7.62 M HI GAGE 0 = 0.00 BARS LIN.ROD WT. = 6.25 KGF/M DELTA-A = 0.18 BARS OCR FACTOR = 1.00															
SP.GR.WATER = 1.000 CAL GAGE 0 = 0.00 BARS DELTA/PHI = 0.50 DELTA-B = 0.31 BARS M FACTOR = 1.00															
MAX SU ID = 9.00 SU OPTION = MARCHETTI MIN PHI ID = 0.10 OCR OPTION = MARCHETTI K0 FACTOR = 1.00															
UNIT CONVERSIONS: 1 BAR = 1.019 KGF/CM2 = 1.044 TSF = 14.51 PSI 1 M = 3.2808 FT															
Z	KD	ID	UD	ED	K0	SU	QD	PHI	SIGFF	PHIO	PC	OCR	M	SOIL	TYPE
(M)				(BAR)		(BAR)	(BAR)	(DEG)	(BAR)	(DEG)	(BAR)		(BAR)		
*****	*****	*****	*****	*****	*****	*****	*****	*****	*****	*****	*****	*****	*****	*****	*****
0.3	54.52	2.84	0	285		0.73							1168	SILTY	SAND
0.61	33.28	1.95	0	250	4.05	0.82	35	42	0.18	37.9	12.96	117	909	SILTY	SAND
0.91	25.79	1.86	0	277	3.24	0.9	30.5	39.5	0.27	35.7	13.01	78	942	SILTY	SAND
1.22	33.51	0.92	0	241	4.3	1.68	20.4	34.3	0.35	30.5	37.69	167.3	878	SILT	
1.52	23.18	1.04	0	237	3.05	1.33	22.9	34.9	0.44	31.6	21.4	75.7	782	SILT	
1.83	18.51	0.83	0	183	2.51	1.21	20.8	33.8	0.53	30.7	17.12	50.1	563	CLAYEY	SILT
2.13	12.2	1.02	0	172	1.76	0.84	19.4	33.5	0.62	30.6	8.84	22.3	461	SILT	
2.44	9.15	0.98	0	141	1.41	0.67	18.1	32.7	0.7	30.1	6.04	13.4	339	SILT	
2.74	6.69	0.95	0	111	1.12	0.5	17.9	32.4	0.78	30	3.93	7.8	234	SILT	
3.05	6.52	0.75	0	95	1.13	0.54	16.7	31.1	0.85	28.9	4.39	7.8	196	CLAYEY	SILT
3.35	5.61	0.86	0	102	1.02	0.49	17.6	31.1	0.93	29	3.77	6.2	196	CLAYEY	SILT
3.66	4.79	0.87	0	97	0.93	0.44	18.2	30.9	1.01	28.9	3.24	4.9	170	CLAYEY	SILT
3.96	4.85	0.8	0	97	0.93	0.48	20.2	31.1	1.09	29.3	3.54	4.9	171	CLAYEY	SILT
4.27	5.15	0.73	0	101	0.95	0.56	23.4	31.6	1.18	30	4.08	5.3	184	CLAYEY	SILT
4.57	4.57	0.79	0	104	0.87	0.51	26.8	32.2	1.27	30.8	3.54	4.3	178	CLAYEY	SILT
4.88	3.83	0.66	0	77	0.78	0.44	28.1	32.3	1.35	31	2.91	3.3	117	CLAYEY	SILT
5.18	3.93	0.66	0	84	0.79	0.48	30.1	32.4	1.43	31.2	3.19	3.4	130	CLAYEY	SILT
5.49	4.49	0.46	0	71	0.89	0.6	27.4	31.1	1.5	29.9	4.31	4.4	120	SILTY	CLAY
5.79	3.67	0.58	0	77	0.77	0.49	31.6	32	1.59	31	3.29	3.2	113	SILTY	CLAY
6.1	3.19	0.54	0	66	0.71	0.43	32.6	32	1.67	31	2.87	2.6	88	SILTY	CLAY
6.4	2.89	0.45	0	51	0.69	0.4	30.7	31.3	1.74	30.4	2.75	2.4	63	SILTY	CLAY
6.71	2.81	0.42	0	50	0.67	0.4	34.1	31.7	1.82	31	2.71	2.3	59	SILTY	CLAY
7.01	3	0.42	0	54	0.71	0.45	33.4	31.2	1.89	30.5	3.14	2.5	68	SILTY	CLAY
7.32	2.85	0.46	0	59	0.68	0.44	36.5	31.6	1.98	31	3.01	2.3	71	SILTY	CLAY
7.62	2.86	0.4	0	53	0.67	0.46	40.2	32.1	2.06	31.6	3.07	2.3	65	SILTY	CLAY
7.93	3.07	0.37	0	54	0.69	0.52	40.7	32	2.09	31.5	3.42	2.5	70	SILTY	CLAY
8.23	3.19	0.4	0	62	0.71	0.55	41.4	32	2.13	31.5	3.65	2.6	83	SILTY	CLAY
8.54	2.2	0.58	0	62	0.56	0.35	47.9	33.2	2.19	32.8	2.27	1.6	59	SILTY	CLAY
8.84	2.38	0.6	0	71	0.58	0.39	48.9	33.2	2.22	32.8	2.52	1.8	73	CLAYEY	SILT
9.15	2.82	0.37	0	53	0.63	0.49	52.7	33.5	2.26	33.2	3.09	2.1	64	SILTY	CLAY
9.45	2.68	0.47	0	64	0.61	0.47	55.8	33.9	2.3	33.6	2.9	2	74	SILTY	CLAY
9.76	2.58	0.32	0	42	0.58	0.45	62.2	34.6	2.35	34.4	2.71	1.8	47	CLAY	
10.06	2.68	0.38	0	53	0.59	0.48	65	34.8	2.39	34.6	2.86	1.9	61	SILTY	CLAY
10.37	2.68	0.41	0	59	0.59	0.49	64.4	34.6	2.41	34.4	2.92	1.9	68	SILTY	CLAY
10.67	2.74	0.47	0	70	0.58	0.51	71.3	35.3	2.46	35.1	2.96	1.9	82	SILTY	CLAY
10.98	2.58	0.58	0	82	0.56	0.48	73.5	35.4	2.51	35.3	2.76	1.7	91	SILTY	CLAY
11.28	2.74	0.73	0	111	0.57	0.53	78.7	35.8	2.55	35.6	2.98	1.8	132	CLAYEY	SILT
11.59	2.71	0.56	0	86	0.56	0.52	82.7	36	2.59	35.9	2.92	1.8	100	SILTY	CLAY
11.89	2.57	0.64	0	94	0.54	0.5	86.6	36.3	2.64	36.2	2.74	1.7	104	CLAYEY	SILT
12.2	2.42	0.56	0	79	0.52	0.47	89.2	36.5	2.68	36.4	2.55	1.5	82	SILTY	CLAY
12.5	3.07	0.68	0	124	0.61	0.64	86.8	35.9	2.71	35.9	3.61	2.1	161	CLAYEY	SILT
12.8	2.99	0.79	0	142	0.6	0.63	88	36	2.74	36	3.54	2	182	CLAYEY	SILT
13.11	2.58	1.02	0	161	0.53	0.53	94.4	36.5	2.8	36.5	2.87	1.6	185	SILT	
13.41	2.56	1.2	0	190	0.54	0.53	93.9	36.4	2.83	36.4	2.91	1.6	220	SANDY	SILT

APPENDIX D – Prosperity Church Road Site 2 Data

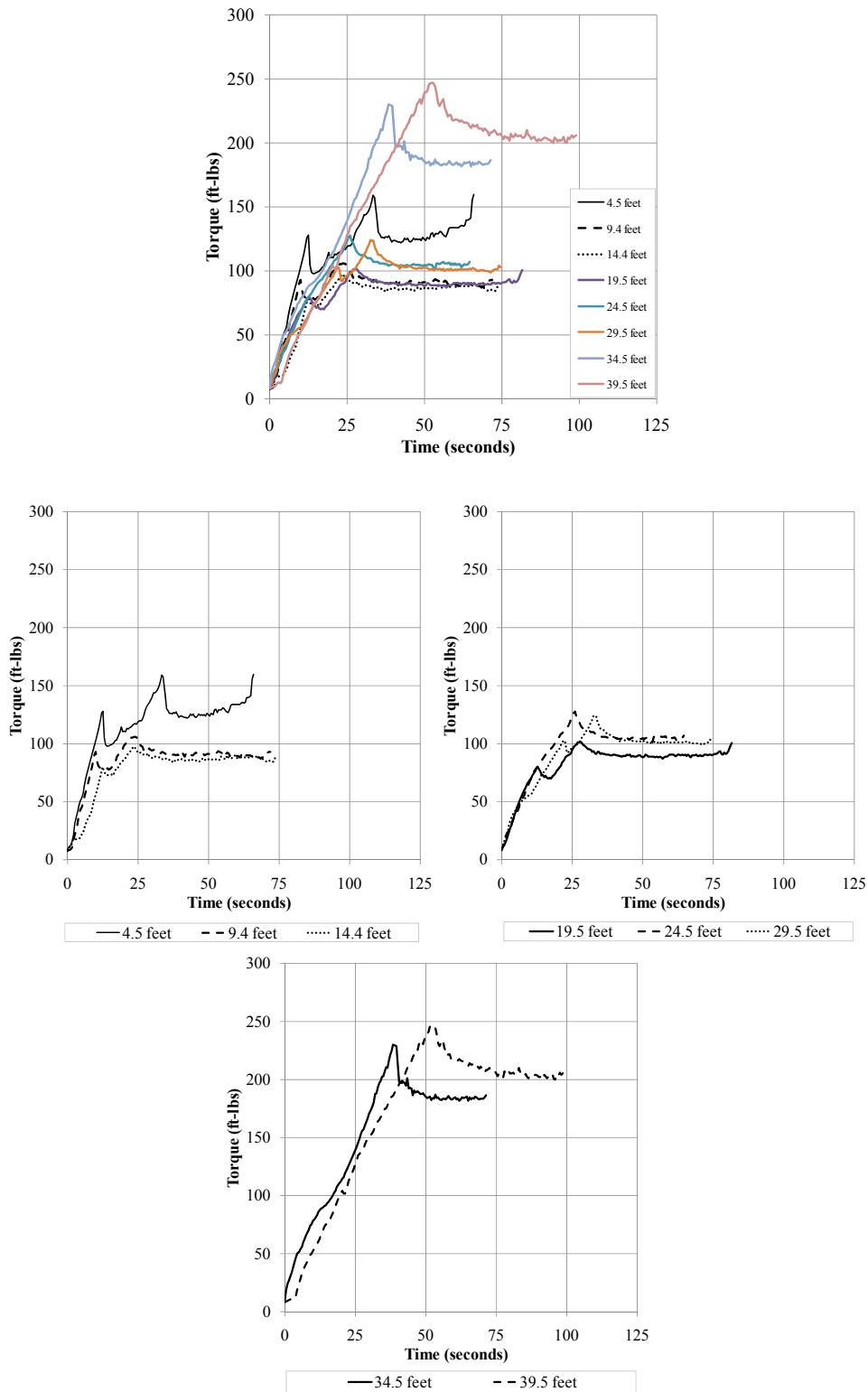


Figure D1 – PC2 SPT-T Torque data

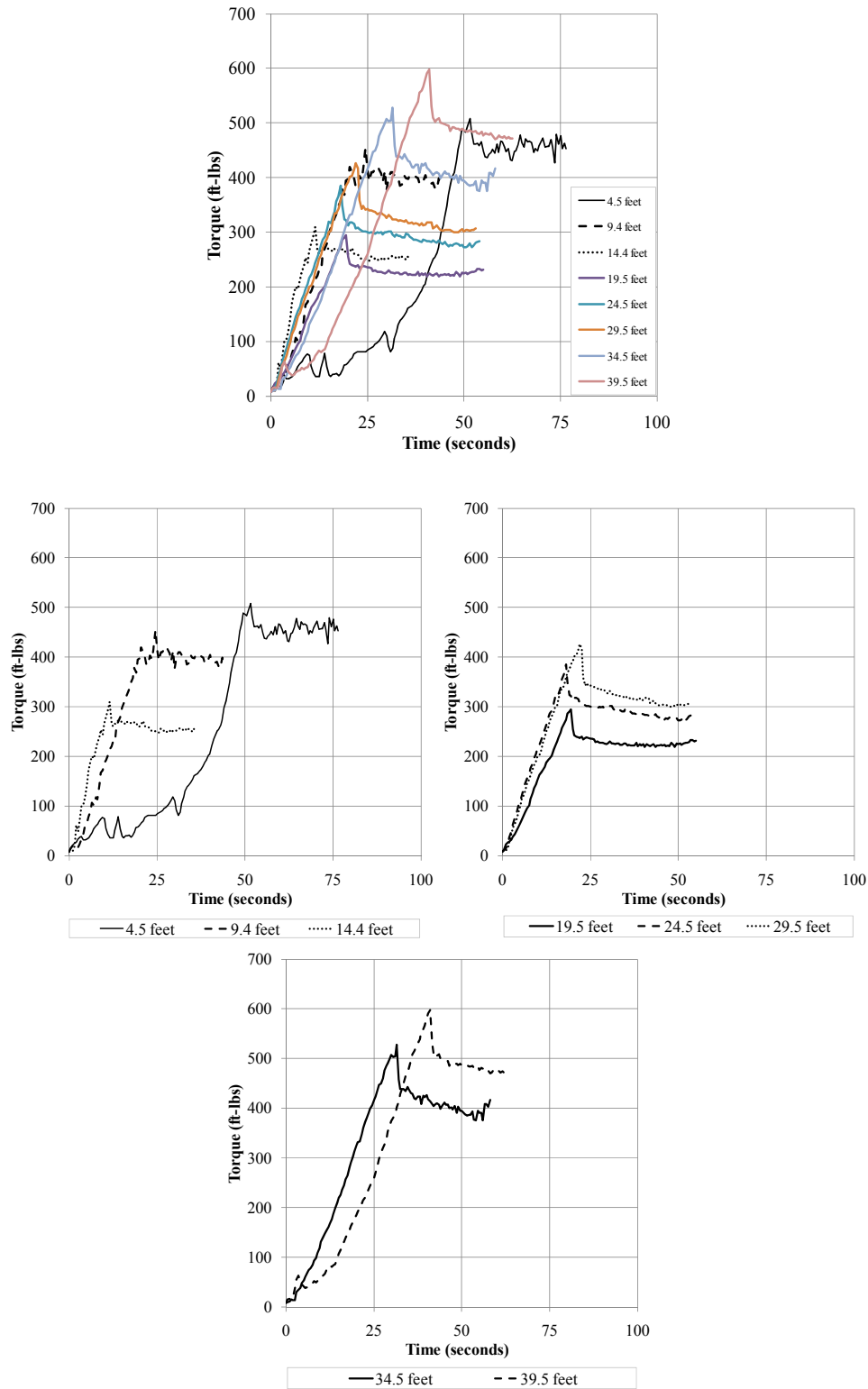


Figure D2 – PC2 STT-T Torque data

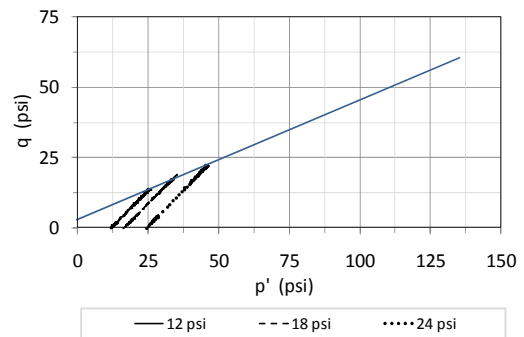
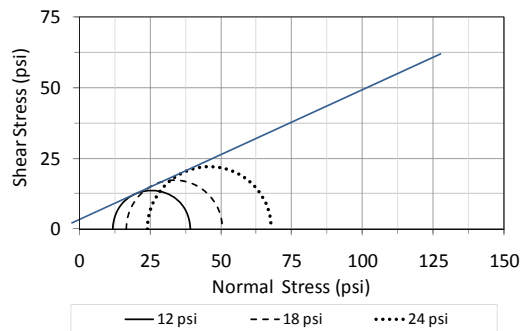
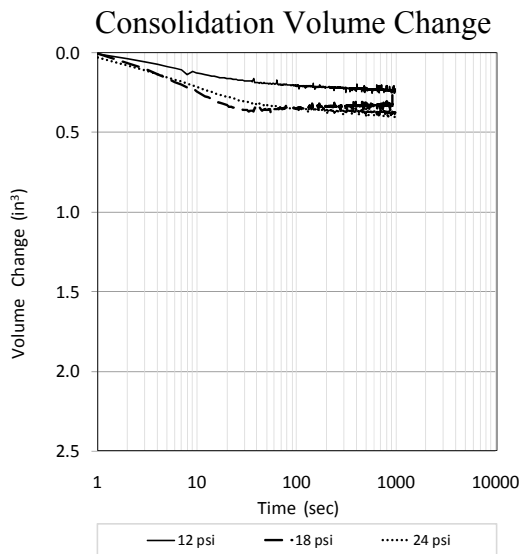
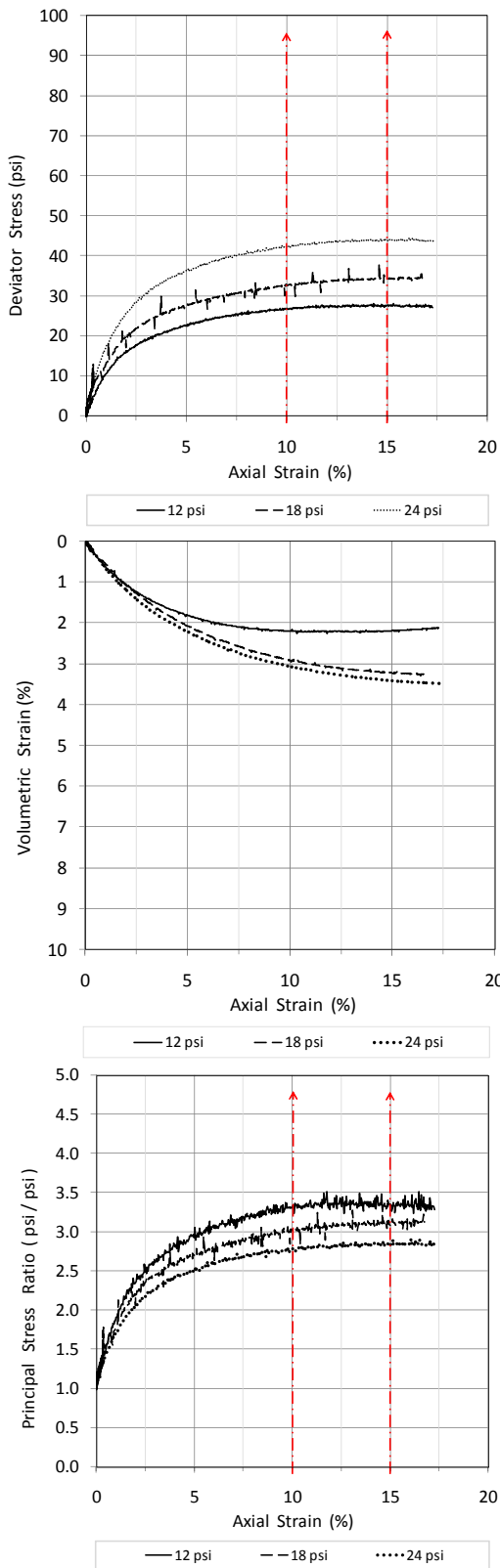


Figure D3 – PC2 4.5' Triaxial data

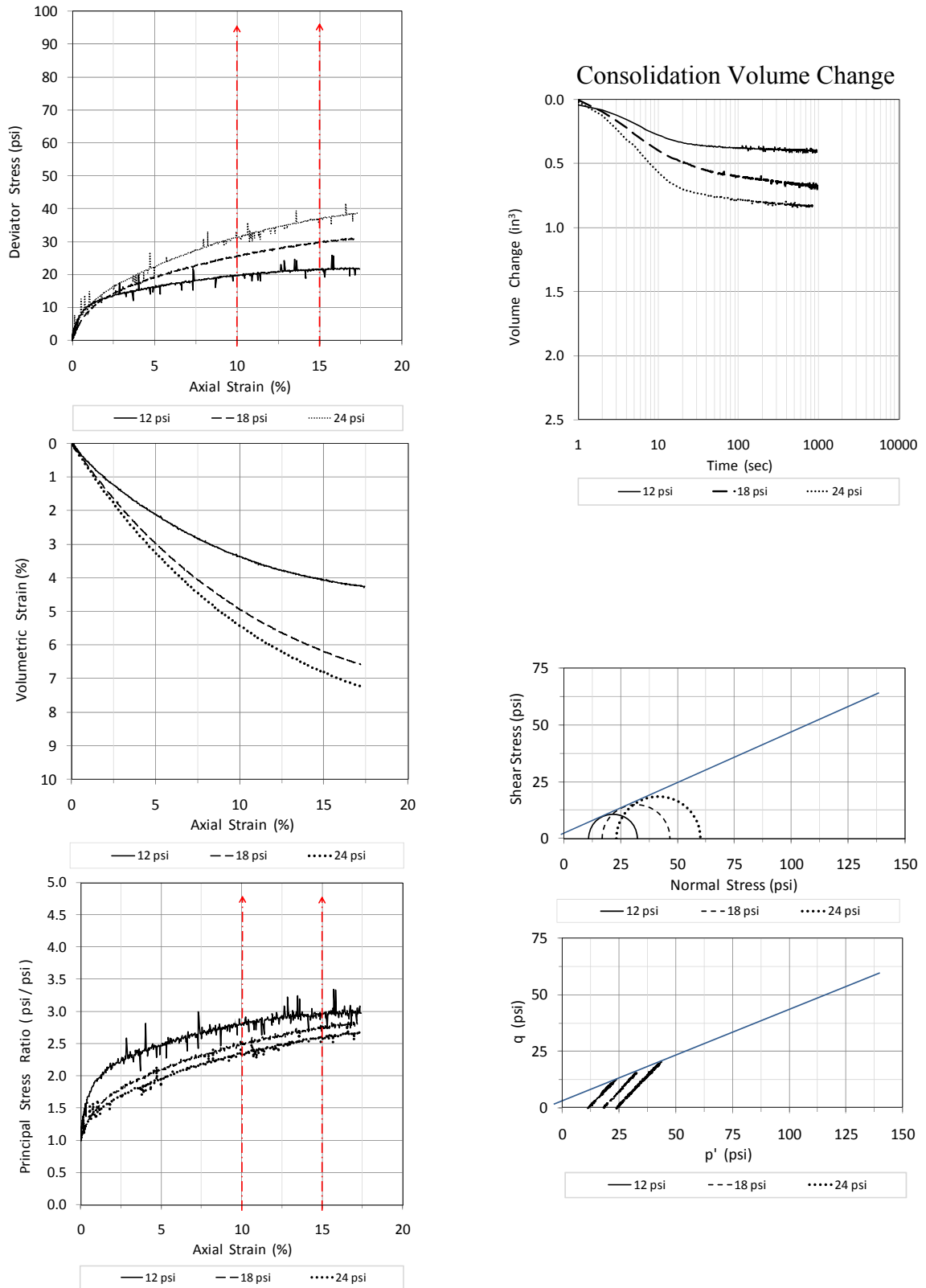


Figure D4 – PC2 9.4' Triaxial data

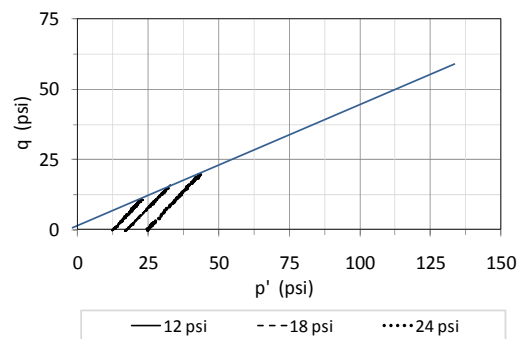
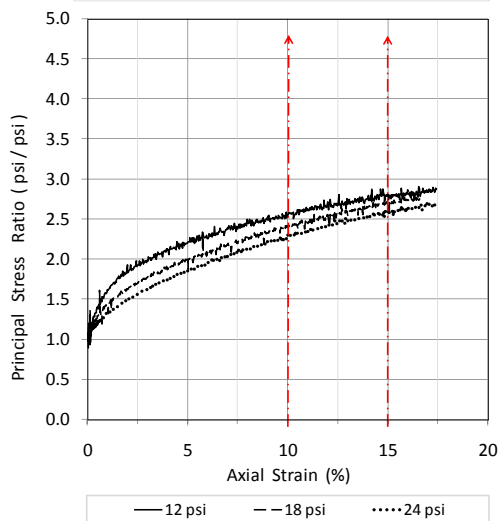
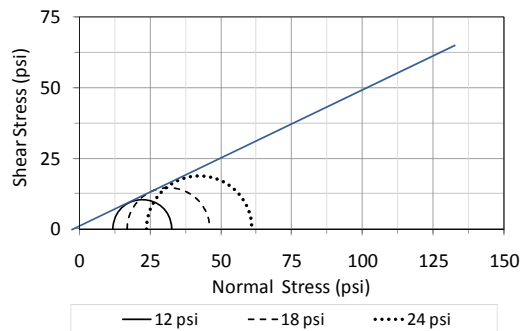
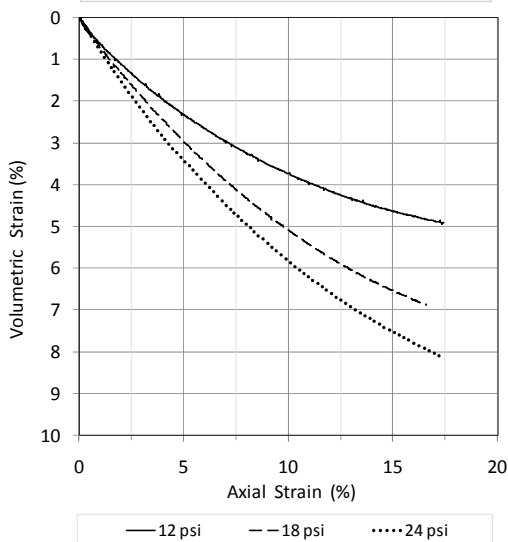
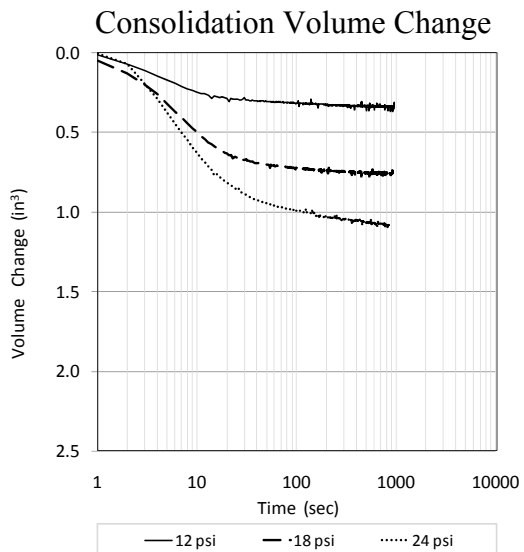
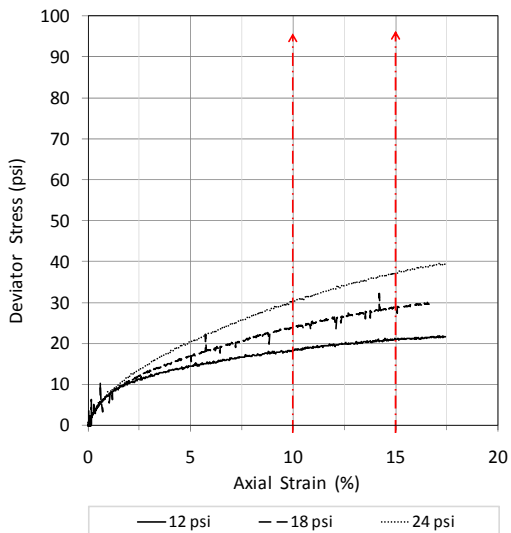


Figure D5 – PC2 14.4' Triaxial data

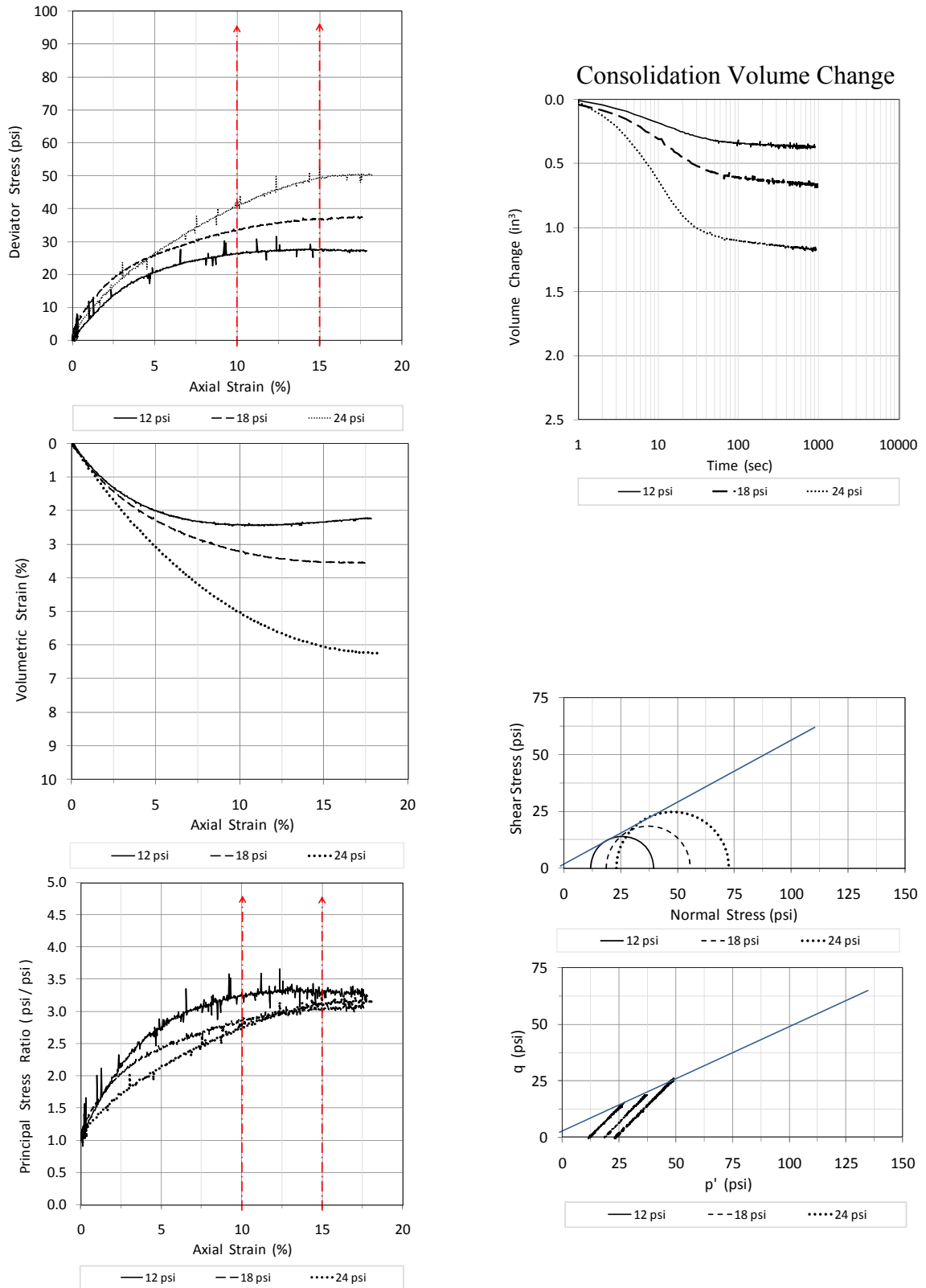


Figure D6 – PC2 24.5' Triaxial data

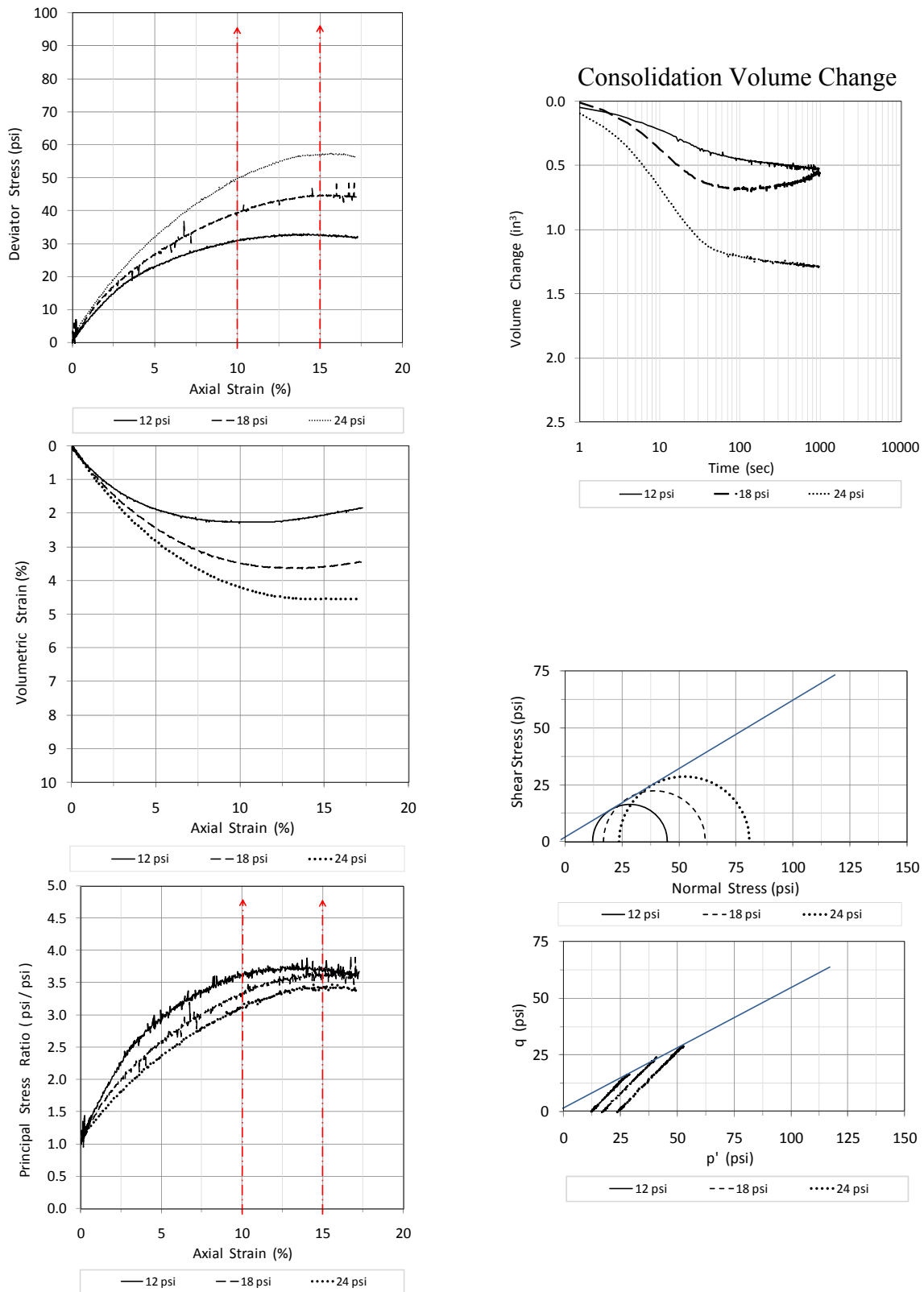


Figure D7 – PC2 29.5' Triaxial data

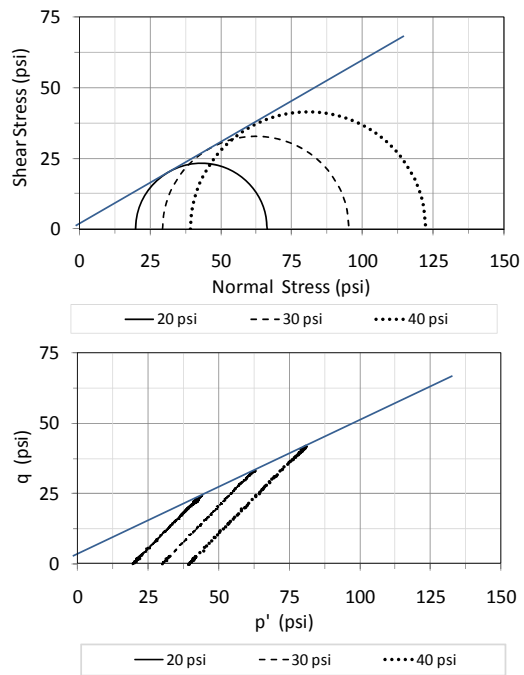
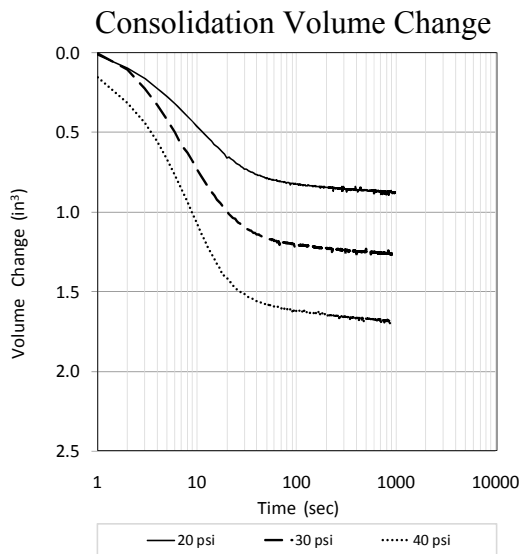
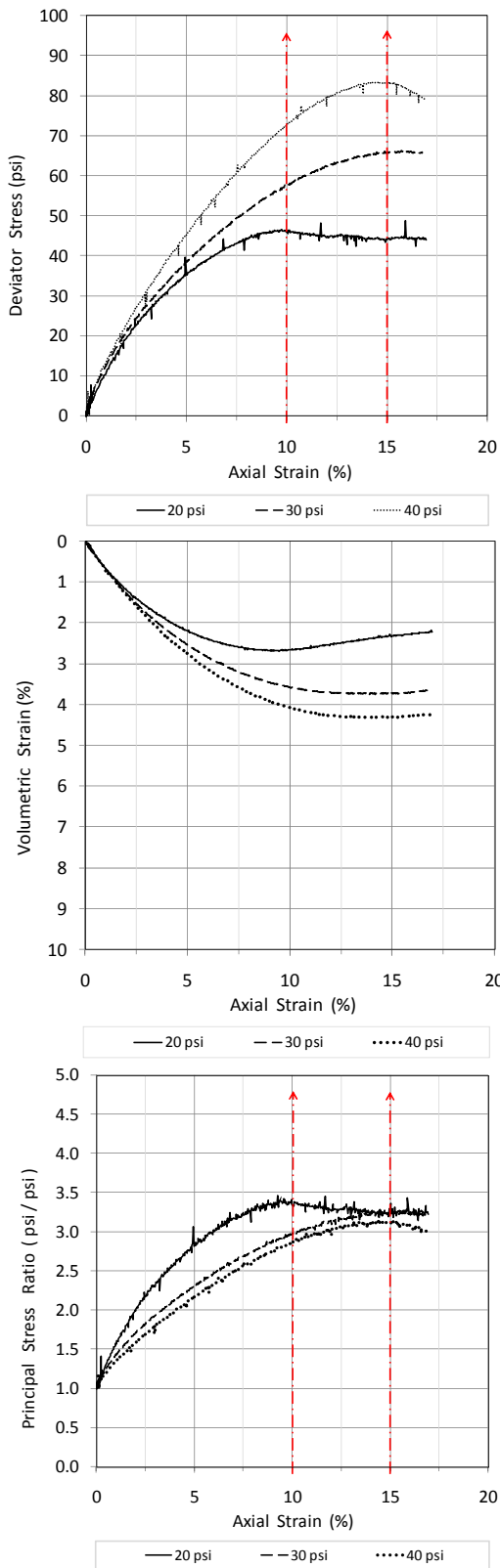


Figure D8 – PC2 34.5' Triaxial data

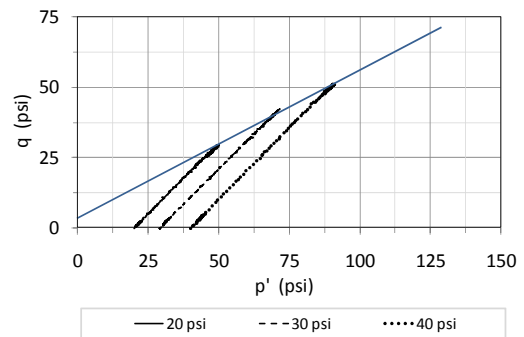
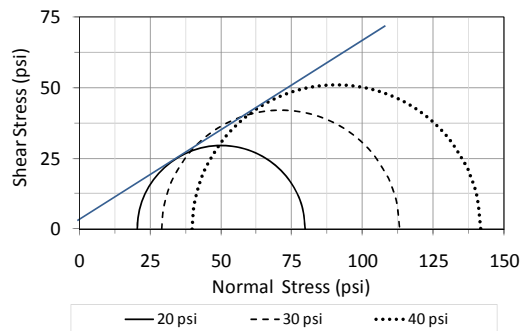
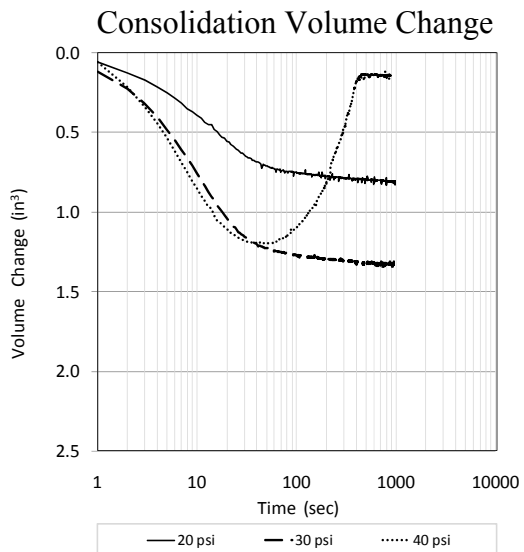
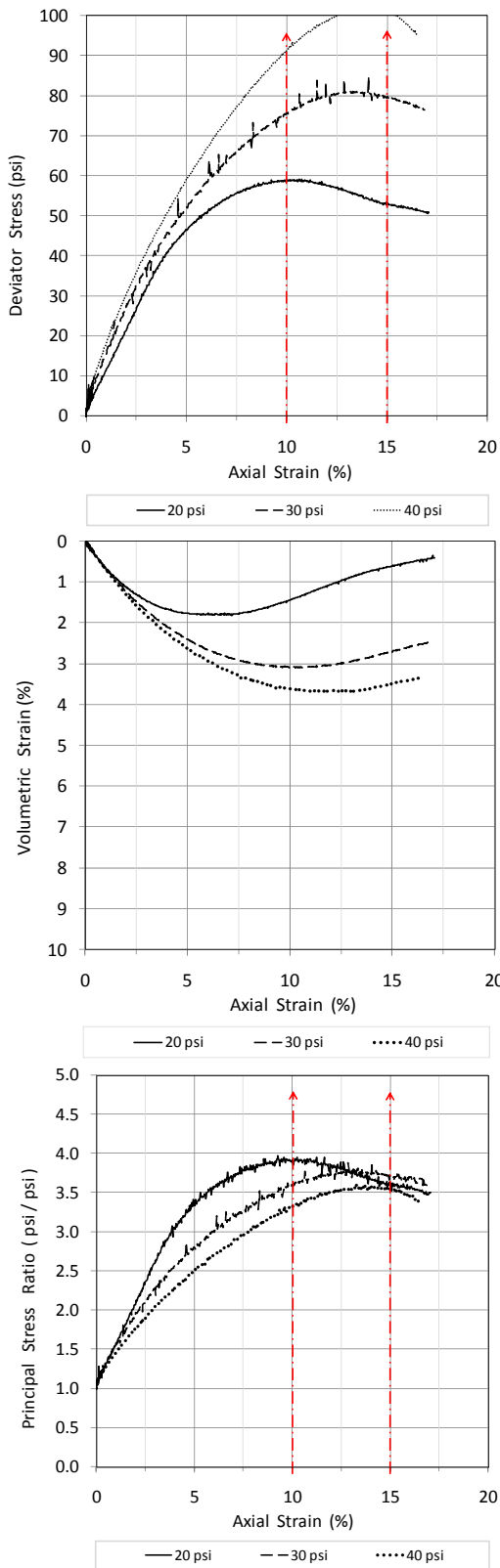


Figure D9 – PC2 39.5' Triaxial data

Table D1 – PC2 Interface shear test data

Depth	4.5 feet	9.4 feet	14.4 feet	19.4 feet	24.5 feet
Normal Stress (psi)	Shear Stress (psi)				
10	2.438	2.847	3.819		3.701
20	5.903	6.639	7.250		8.229
30	8.597	10.299	12.688		11.896

Table D1 – (continued)

Depth	29.5 feet	34.5 feet	39.5 feet
Normal Stress (psi)	Shear Stress (psi)		
10	4.688	4.438	5.264
20	8.604	9.160	10.528
30	12.271	14.882	14.806

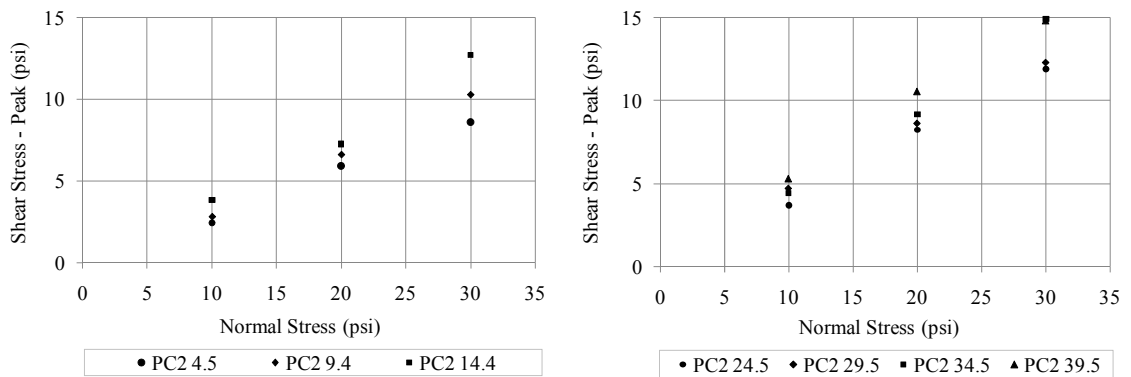


Figure D10 – PC2 Interface shear test data

Tables D2 – PC2 Geotechnical soil classification data

Depth	AASHTO	USCS	LL	PL	PI	Clay Fraction
feet	Class	Class	%	%	%	% < 2 μ m
4.5	A-5	MH	52.7	44.4	8.4	25.8
9.4	A-5	ML	45.3	38.5	6.8	21.9
14.4	A-5	ML	42.6	36.9	5.7	11.4
19.5	A-5	ML	41.5	35.6	5.9	11.3
24.5	A-4	ML	38.6	33.1	5.5	10.5
29.5	A-5	SM	42.6	36.0	6.6	10.4
34.5	A-4	SM	38.4	33.5	5.0	8.0
39.5	A-4	SM	33.9	30.9	3.0	5.2

MH - Inorganic silts, micaceous or diatomaceous fine sandy or silty soils, elastic silts
 ML - Inorganic silt and very fine sands, rocks flour, silty or clayey fine sands or clayey silts with slight plasticity
 SM - Silty-Sands, sand-silt mixtures – Non-plastic fines or fines with low plasticity

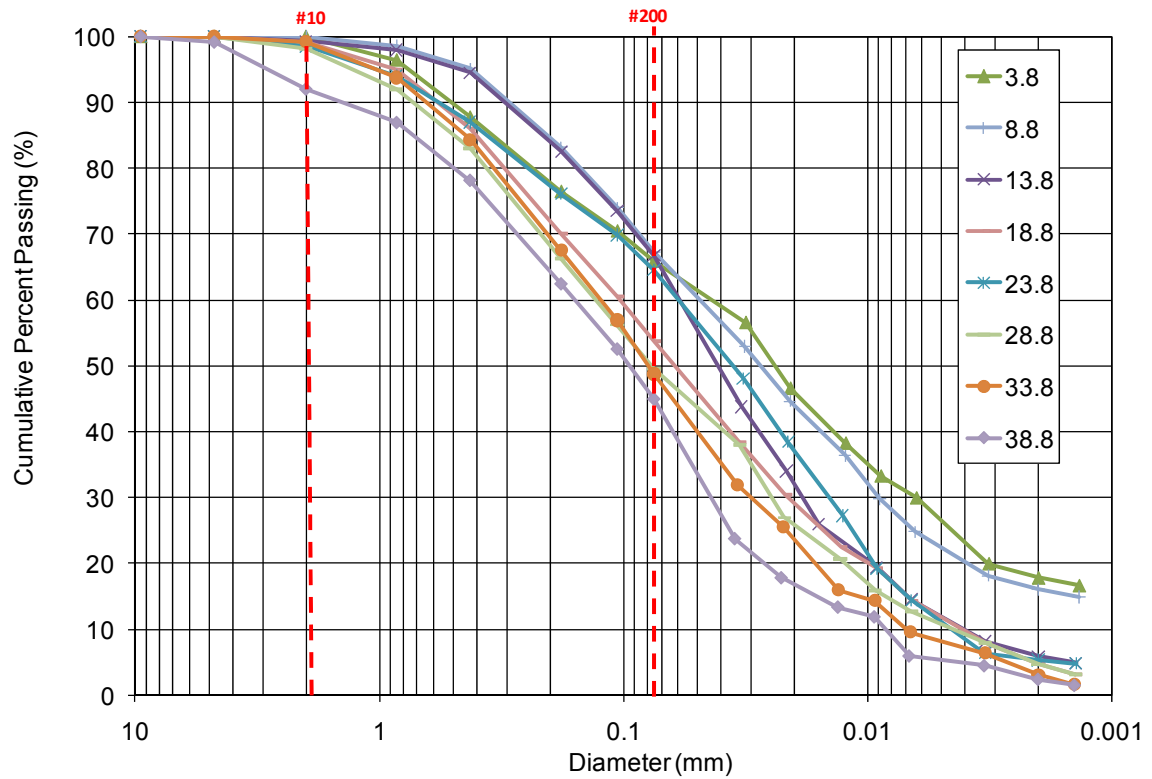


Figure D11 – PC2 Grain-size distribution curve

Table D3 – PC2 Soil classification data – grain-size distribution

PC2 3.8'		PC2 8.8'		PC2 13.8'	
Cumulative Percent Passing	D (mm)	Cumulative Percent Passing	D (mm)	Cumulative Percent Passing	D (mm)
100.00	9.5000	100.00	9.5000	100.00	9.5000
100.00	4.7500	100.00	4.7500	100.00	4.7500
100.00	2.0000	99.98	2.0000	99.33	2.0000
96.43	0.8500	98.65	0.8500	98.01	0.8500
87.75	0.4250	95.13	0.4250	94.51	0.4250
76.47	0.1800	83.14	0.1800	82.60	0.1800
70.48	0.1060	74.00	0.1060	73.52	0.1060
65.91	0.0750	67.23	0.0750	66.79	0.0750
56.59	0.0316	52.92	0.0319	43.76	0.0329
46.60	0.0207	44.65	0.0208	34.04	0.0215
38.28	0.0123	36.38	0.0124	25.93	0.0159
33.29	0.0088	29.77	0.0089	19.45	0.0092
29.96	0.0063	24.81	0.0064	14.59	0.0066
19.97	0.0032	18.19	0.0032	8.10	0.0033
17.81	0.0020	16.02	0.0020	5.88	0.0020
16.64	0.0014	14.88	0.0014	4.86	0.0014

Table D3 – (continued)

PC2 18.8'		PC2 23.8'		PC2 28.8'	
Cumulative Percent Passing	D (mm)	Cumulative Percent Passing	D (mm)	Cumulative Percent Passing	D (mm)
100.00	9.5000	100.00	9.5000	100.00	9.5000
100.00	4.7500	100.00	4.7500	100.00	4.7500
99.16	2.0000	98.51	2.0000	98.15	2.0000
95.04	0.8500	94.07	0.8500	92.07	0.8500
86.01	0.4250	87.03	0.4250	83.02	0.4250
70.10	0.1800	76.13	0.1800	66.26	0.1800
60.53	0.1060	69.92	0.1060	56.24	0.1060
53.68	0.0750	64.59	0.0750	49.57	0.0750
38.44	0.0335	48.10	0.0323	38.07	0.0335
30.43	0.0217	38.48	0.0212	26.97	0.0220
22.42	0.0129	27.26	0.0127	20.62	0.0130
19.22	0.0092	19.24	0.0092	15.86	0.0093
14.42	0.0066	14.43	0.0066	12.69	0.0066
8.01	0.0033	6.41	0.0033	7.93	0.0033
4.71	0.0020	5.31	0.0020	4.66	0.0020
3.20	0.0014	4.81	0.0014	3.17	0.0014

Table D3 – (continued)

PC2 33.8'		PC2 38.8'	
Cumulative Percent Passing	D (mm)	Cumulative Percent Passing	D (mm)
100.00	9.5000	100.00	9.5000
100.00	4.7500	99.14	4.7500
99.21	2.0000	92.00	2.0000
93.76	0.8500	86.92	0.8500
84.36	0.4250	78.15	0.4250
67.53	0.1800	62.45	0.1800
56.91	0.1060	52.54	0.1060
48.79	0.0750	44.96	0.0750
31.93	0.0342	23.76	0.0350
25.54	0.0221	17.82	0.0226
15.96	0.0132	13.36	0.0132
14.37	0.0093	11.88	0.0094
9.58	0.0067	5.94	0.0068
6.39	0.0033	4.45	0.0033
3.07	0.0020	2.39	0.0020
1.60	0.0014	1.48	0.0014

Table D4 – PC2 Geologic soil color

















Depth feet	Wet Color		Dry Color	
4.5	7.5YR 5/8		5YR 6/8	
9.4	5YR 6/8		7.5YR 7/8	
14.4	10YR 7/6		7.5YR 8/6	
19.4	10YR 6/6		10YR 8/4	
24.5	10YR 7/6		10YR 8/6	
29.5	10YR 6/6		7.5YR 8/6	
34.5	2.5Y 6/6		10YR 8/4	
39.5	2.5Y 6/6		10YR 7/6	

Table D5 – PC2 Geologic soil classification data

Depth feet	Gravel		Consistence			Texture
	#	%	stickiness	plasticity	Moist	
4.5	0 rock	0	sticky	plastic	firm	Silty Clay Loam
9.4	1 rock	< 10	slight	slight	firm	Silty Loam
14.4	50 rock	< 10	slight	slight	friable	Loam
19.4	100 rock	< 10	slight	slight	friable	Loam
24.5	100 rocks	< 10	slight	slight	friable	Loam
29.5	< 100 rocks	< 10	slight	slight	friable	Loam
34.5	< 100 rocks	< 10	slight	no	friable to very friable	Loam
39.5	< 200 rocks	< 10	no	no	very friable	Sandy Loam

Table D6 – PC2 Dilatometer data output

DILATOMETER DATA LISTING & INTERPRETATION (BASED ON THE 1988 DILATOMETER MANUAL) SNDG. NO. DMT-17

M. Allen Cottingham

JOB FILE: Dissertation Research 2009 FILE NO. : Cottingham 2009-1

LOCATION: Prosperity Church Road Site 2

SNDG.BY : Cottingham/Anderson SNDG.DATE: 17 March 2009

ANAL.BY : Cottingham ANAL.DATE: 19 May 2009

ANALYSIS PARAMETERS: LO RANGE = 5.00 BARS ROD DIAM. = 4.44 CM BL.THICK. = 15.0 MM SU FACTOR = 1.00
 SURF.ELEV. = 0.00 M LO GAGE 0 = 0.00 BARS FR.RED.DIA. = 5.71 CM BL.WIDTH = 96.0 MM PHI FACTOR = 1.00
 WATER DEPTH = 7.93 M HI GAGE 0 = 0.00 BARS LIN.ROD WT. = 6.25 KG/M DELTA-A = 0.18 BARS OCR FACTOR = 1.00
 SP.GR.WATER = 1.000 CAL GAGE 0 = 0.00 BARS DELTA/PHI = 0.50 DELTA-B = 0.52 BARS M FACTOR = 1.00
 MAX SU ID = 9.00 SU OPTION = MARCHETTI MIN PHI ID = 0.10 OCR OPTION = MARCHETTI K0 FACTOR = 1.00
 UNIT CONVERSIONS: 1 BAR = 1.019 KG/CM2 = 1.044 TSF = 14.51 PSI 1 M = 3.2808 FT

Z (M)	THRUST (KGF)	A (BAR)	B (BAR)	C (BAR)	DA (BAR)	DB (BAR)	ZMRNG (BAR)	ZMLO (BAR)	ZMHI (BAR)	ZMCAL (BAR)	P0 (BAR)	P1 (BAR)	P2 (BAR)	U0 (BAR)	GAMMA (T/M3)	SVP (BAR)
*****	*****	*****	*****	*****	*****	*****	*****	*****	*****	*****	*****	*****	*****	*****	*****	*****
0.3	585	1.7	4.75		0.18	0.52	5	0	0	0	1.76	4.23		0	1.7	0.053
0.61	1149	3.65	0		0.18	0.52	5	0	0	0	3.83X	-0.52		0		
0.91	1347	6.9	13.1		0.18	0.52	5	0	0	0	6.8	12.58		0	1.95	0.162
1.22	1525	8.1	0		0.18	0.52	5	0	0	0	8.28X	-0.52		0		
1.52	1902	7.9	0		0.18	0.52	5	0	0	0	8.08X	-0.52		0		
1.83	2321	7.4	0		0.18	0.52	5	0	0	0	7.58X	-0.52		0		
2.13	2380	6.1	0		0.18	0.52	5	0	0	0	6.28X	-0.52		0		
2.44	2213	7.1	14.1		0.18	0.52	5	0	0	0	6.96	13.58		0	1.95	0.455
2.74	2114	6.2	14.3		0.18	0.52	5	0	0	0	6.01	13.78		0	1.95	0.512
3.05	1949	5.9	12.3		0.18	0.52	5	0	0	0	5.79	11.78		0	1.95	0.572
3.35	1980	5.6	13.6		0.18	0.52	5	0	0	0	5.41	13.08		0	1.95	0.629
3.66	1971	4.4	10.4		0.18	0.52	5	0	0	0	4.32	9.88		0	1.8	0.686
3.96	1428	3.4	7.7		0.18	0.52	5	0	0	0	3.4	7.18		0	1.8	0.739
4.27	1265	3.1	7.2		0.18	0.52	5	0	0	0	3.11	6.68		0	1.8	0.794
4.57	1467	3.2	8.3		0.18	0.52	5	0	0	0	3.16	7.78		0	1.8	0.847
4.88	1337	3	7.2		0.18	0.52	5	0	0	0	3	6.68		0	1.8	0.902
5.18	1339	2.65	7.1		0.18	0.52	5	0	0	0	2.64	6.58		0	1.8	0.955
5.49	1183	3.2	9.3		0.18	0.52	5	0	0	0	3.11	8.78		0	1.9	1.011
5.79	1193	3.55	8.1		0.18	0.52	5	0	0	0	3.54	7.58		0	1.8	1.065
6.1	1220	3.6	8		0.18	0.52	5	0	0	0	3.59	7.48		0	1.8	1.12
6.4	1242	3.6	7.9		0.18	0.52	5	0	0	0	3.6	7.38		0	1.8	1.173
6.71	1454	5	10.7		0.18	0.52	5	0	0	0	4.93	10.18		0	1.8	1.228
7.01	1560	4.3	9.1		0.18	0.52	5	0	0	0	4.28	8.58		0	1.8	1.281
7.32	1939	3.9	10.6		0.18	0.52	5	0	0	0	3.78	10.08		0	1.8	1.336
7.62	2245	5.8	0		0.18	0.52	5	0	0	0	5.98X	-0.52		0		
7.93	2024	4.75	11.4		0.18	0.52	5	0	0	0	4.63	10.88		0	1.8	1.443
8.23	1798	6.5	12.6		0.18	0.52	5	0	0	0	6.41	12.08		0.029	1.95	1.469
8.54	1788	6.1	12.1		0.18	0.52	5	0	0	0	6.01	11.58		0.06	1.95	1.498
8.84	2188	6.5	13.6		0.18	0.52	5	0	0	0	6.36	13.08		0.089	1.95	1.526
9.15	2370	5.8	13.3		0.18	0.52	5	0	0	0	5.64	12.78		0.12	1.95	1.555
9.45	2489	7.8	0		0.18	0.52	5	0	0	0	7.98X	-0.52		0.149		
9.76	2843	7.1	0		0.18	0.52	5	0	0	0	7.28X	-0.52		0.18		
10.06	2927	7.4	0		0.18	0.52	5	0	0	0	7.58X	-0.52		0.209		

APPENDIX E – Additional Soil Data

TABLE E1 – PC1 Shelby tube storage time

Depth (feet)	Date Collected	Date Tested		Number of days	
		TXL	INT	TXL	INT
4.4	7/12/2007	6/9/2008	2/24/2009	333	593
9.4	7/12/2007	9/27/2007		77	
14.4	7/12/2007	6/4/2008	2/22/2009	328	591
19.4	7/12/2007	9/27/2007	3/3/2009	77	600
24.4	7/12/2007	5/21/2008	2/22/2009	314	591
29.4	7/12/2007	10/23/2007	3/3/2009	103	600
34.4	7/13/2007	5/20/2008	2/22/2009	312	590
39.4	7/13/2007	11/18/2007	3/3/2009	128	599
44.4	7/13/2007	5/19/2008	2/24/2009	311	592
49.4	7/13/2007	11/26/2007	3/3/2009	136	599
54.4	7/13/2007	11/27/2007	2/24/2009	137	592

TABLE E2 – BR Shelby tube storage time

Depth (feet)	Date Collected	Date Tested		Number of days	
		TXL	INT	TXL	INT
5.5	6/17/2008	9/12/2008	2/24/2009	87	252
10.5	6/17/2008	10/7/2008	3/3/2009	112	259
15.5	6/17/2008	9/8/2008	2/25/2009	83	253
20.5	6/17/2008	9/17/2008	3/3/2009	92	259
25.5	6/17/2008	9/9/2008	2/25/2009	84	253
30.5	6/17/2008	10/8/2008	3/3/2009	113	259
35.5	6/17/2008	9/10/2008	2/28/2009	85	256
40.5	6/17/2008	10/8/2008	3/4/2009	113	260
45.5	6/17/2008	9/11/2008	3/1/2009	86	257
50.5	6/17/2008	9/16/2008	3/4/2009	91	260
55.5	6/17/2008	9/15/2008	3/1/2009	90	257
60.5	6/17/2008	10/9/2008	3/4/2009	114	260
65.5	6/17/2008	9/15/2008	3/3/2009	90	259

TABLE E3 – PC2 Shelby tube storage time

Depth (feet)	Date Collected	Date Tested		Number of days	
		TXL	INT	TXL	INT
4.5	3/12/2009	3/28/2009	4/21/2009	16	40
9.4	3/16/2009	3/29/2009	4/21/2009	13	36
14.4	3/16/2009	3/29/2009	4/21/2009	13	36
19.4	3/16/2009				
24.5	3/12/2009	3/30/2009	4/21/2009	18	40
29.5	3/12/2009	3/31/2009	4/22/2009	19	41
34.5	3/12/2009	4/1/2009	4/22/2009	20	41
39.5	3/12/2009	4/1/2009	4/22/2009	20	41

Table E4 – PC1 Soil collected and remaining

Depth	Soil Collected	Soil Remaining
feet	inch	inch
4.4	24	4
9.4	24	0
14.4	24	0
19.4	24	1
24.4	24	3
29.4	24	1
34.4	24	3
39.4	24	3
44.4	18	2
49.4	14	2
54.4	24	1

Table E5 – BR Soil collected and remaining

Depth	Soil Collected	Soil Remaining
feet	inch	inch
5.5	26	4
10.5	26	2
15.5	24	1
20.5	24	2.5
25.5	24	2
30.5	24	2.5
35.5	24	2.5
40.5	24	3
45.5	24	2.5
50.5	24	3
55.5	24	1.5
60.5	24	3.5
65.5	24	1

Table E6 – PC2 Soil collected and remaining

Depth	Soil Collected	Soil Remaining
feet	inch	inch
4.5	24	1
9.4	24	0
14.4	24	1
19.4	8	8
24.5	24	3
29.5	24	2
34.5	24	2
39.5	24	2

APPENDIX F – Triaxial Test Quick Reference List and Datasheets

1. Equipment Preparation
 - a. Triaxial Chamber, Pressure board, Load Frame, Computer (Labview)
 - b. O-rings, Saturated porous stones, Filter papers, Membranes, Filter strips
- 2. Measure height of porous stones, filter paper, end caps**
3. Saturate the tubing *and attach tubing to burettes (may not be necessary)*
4. Prepare membrane in undisturbed membrane stretcher
5. Prepare specimen
 - a. Cut Shelby tube in cutter frame with pipe cutter – 6” length
 - b. Trim specimen inside of the 6” Shelby tube piece
 - c. Extrude vertically
- 6. Collect and weigh sample for water content (i.e. end of tube)**
- 7. Measure weight of the specimen**
8. Place specimen on base plate
9. Install membrane over specimen using membrane stretcher, o-rings, and spares
10. Apply small pore vacuum to check for leaks
- 11. Measure diameter & height of porous stones, filter paper, end caps, and specimen**
12. Install chamber, top plate, and tightening rods
13. Insert locking piston into and in contact with the top specimen cap and LOCK DOWN
14. Fill chamber with water allowing to vent
15. Attach chamber pressure tubing and apply small amount of pressure
16. Vacuum saturation, if necessary
17. Back pressure saturation
 - a. **Measure initial pore pressure burette readings for volume change**
 - i. *Situate the level high because water is going into the specimen*
 - b. Open top and bottom burette valves of pore pressure
 - c. Raise the chamber and burette regulators together up (Based on ASTM)
- 18. Measure height change “due to back pressure saturation”**
19. Consolidation (Run approx 15 minutes)
 - a. Isolate sample by closing top and bottom valves to pore pressure
 - b. Connect the “Volume Change Device” and allow to equalize
 - i. *Check that VCD arm is high or low (Range →)*
 - c. Set the chamber and pore pressures to desired value (test settings)
 - d. *Situate the pore pressure burettes low, since water is removed from sample*
 - i. **Measure top and bottom burettes values**, as a verification back-up

- e. Initiate Labview program (ETriaxVol.vi and MTriaxVol.vi)
- f. Open the top and bottom burette valves (Drainage will occur)

20. Measure height change “due to consolidation”

21. Shearing the specimen

- a. Determine and enter the loading rate (mm/min) - *[0.254 mm/min]*
- b. Open or close pore pressure valves based on drained or undrained test
- c. *Check that VCD arm is high or low*
- d. Note VCD and Burette values**
- e. *TARE and Zero Labview values*
- f. *Set Labview time step to 1 sec – After 2-3 minutes, set time step to 10 sec*
- g. Initiate the Labview program (ETriaxVol.vi and MTriaxVol.vi)
- h. Press “START (GO)” on the load frame
- i. Stop at 1 inch, unless...

22. Equipment cleanup

23. “B” value test

- a. Isolate sample by closing chamber valves to pore pressure
- b. Measure initial chamber and pore pressures
- c. Raise the chamber burette pressure a set increment (~5-10 psi)
- d. Measure final chamber and pore pressures – Allow time to stabilize
 - i. Pore pressure shouldn’t fall based on ASTM
- e. Lower the chamber burette pressure back to original value
- f. Open top and bottom burette valves
- g. Calculate the “B” value
- h. NOTE: Leave valves open if saturating over time

24. Height Change Measurement

- a. Place chamber into load frame
- b. Raise chamber until load begins to raise (~5-10 lbs)
- c. Unlock loading piston (Load will jump to ~ 14 lbs)
- d. Adjust displacement gage
- e. Zero displacement gage - TARE
- f. Raise chamber until load raised to ~ 20 lbs
- g. Record displacement
- h. Lock loading piston (lower cell?)

25. Overnight checks

- a. Correct valves open/closed
- b. Burette water levels correct
- c. VCD is high or low
- d. Leaks

Name of tester(s): _____		Bore Hole # <input style="width: 50px;" type="text"/>	
Date of test: _____		Depth (ft) <input style="width: 50px;" type="text"/>	
Notes: _____		Tube length (in) <input style="width: 50px;" type="text"/>	

Height (inch)		w/o Sample	w/ Sample	Triaxial Machine No. <input style="width: 50px;" type="text"/>
	N	<input style="width: 50px;" type="text"/>	<input style="width: 50px;" type="text"/>	
Platen(s)	S	<input style="width: 50px;" type="text"/>	<input style="width: 50px;" type="text"/>	EFFECTIVE STRESS (psi) <input style="width: 50px;" type="text"/>
Porous disk(s)	E	<input style="width: 50px;" type="text"/>	<input style="width: 50px;" type="text"/>	Pore Pressure (psi) <input style="width: 50px;" type="text"/>
Filter paper(s)	W	<input style="width: 50px;" type="text"/>	<input style="width: 50px;" type="text"/>	Chamber Pressure (psi) <input style="width: 50px;" type="text"/>
	average =	<input style="width: 50px;" type="text"/>	<input style="width: 50px;" type="text"/>	

Diameter (inch)		Top		t50 (min) <input style="width: 50px;" type="text"/>
+		Middle	<input style="width: 50px;" type="text"/>	Test Rate (mm/min) <input style="width: 50px;" type="text"/>
		Bottom	<input style="width: 50px;" type="text"/>	0.254mm/min; t50 < X
		Membrane	YES - NO <input style="width: 50px;" type="text"/>	

Weight of sample (grams)				Load at start (lbs) <input style="width: 50px;" type="text"/>
Weight_Sample + Misc. =	<input style="width: 50px;" type="text"/>	(Before)		ΔH BPS (inch) <input style="width: 50px;" type="text"/>
Weight_Misc = plastic /stone/?	<input style="width: 50px;" type="text"/>			ΔH Consol. (inch) <input style="width: 50px;" type="text"/>
Weight_Pan =	<input style="width: 50px;" type="text"/>	(After)		ΔV BPS (inch) <input style="width: 50px;" type="text"/>
Weight_Pan + wet sample =	<input style="width: 50px;" type="text"/>			ΔV Consol. (inch) <input style="width: 50px;" type="text"/>
Weight_Pan + dry Sample =	<input style="width: 50px;" type="text"/>			ΔV Shear (inch) <input style="width: 50px;" type="text"/>

Water Contents	Description -->			
	Can ID -->			
Weight_Can (g) =				
Weight_Can + Wet sample (g) =				
Weight_Can + Dry sample (g) =				

B-Value	Pore	Chamber	Pore	Chamber
Before	<input style="width: 50px;" type="text"/>	<input style="width: 50px;" type="text"/>	Before	<input style="width: 50px;" type="text"/>
After	<input style="width: 50px;" type="text"/>	<input style="width: 50px;" type="text"/>	After	<input style="width: 50px;" type="text"/>
		B = <input style="width: 50px;" type="text"/>		B = <input style="width: 50px;" type="text"/>

B-Value	Pore	Chamber	Pore	Chamber
Before	<input style="width: 50px;" type="text"/>	<input style="width: 50px;" type="text"/>	Before	<input style="width: 50px;" type="text"/>
After	<input style="width: 50px;" type="text"/>	<input style="width: 50px;" type="text"/>	After	<input style="width: 50px;" type="text"/>
		B = <input style="width: 50px;" type="text"/>		B = <input style="width: 50px;" type="text"/>

Figure F1 – Datasheet for triaxial test – Page 1/2

Name of tester(s): _____ Bore Hole #

Date of test: _____ Depth (ft)

Notes: _____ Tube length (in)

Failure : Bulging / Mohr Coulomb

Notes	Date	Time	Burette Readings		u (psi)	σ_v
			Top	Bottom		
Beginning BPS						
End BPS						

	Date	Time	Small	Large	VCD (mV)	VCD (cc)
Beginning Consolidation						
End Consolidation						
Beginning Shear						
End Shear						

Notes:

Figure F2 – Datasheet for triaxial test – Page 2/2

APPENDIX G – Interface Shear Box Drawing

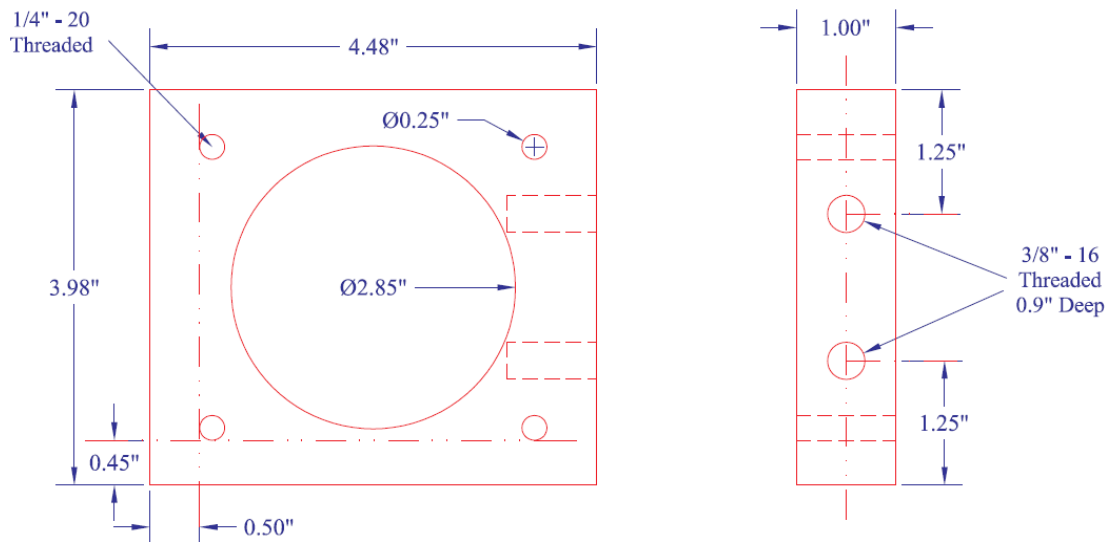


Figure G1 – Top half of interface shear box (Aluminum)

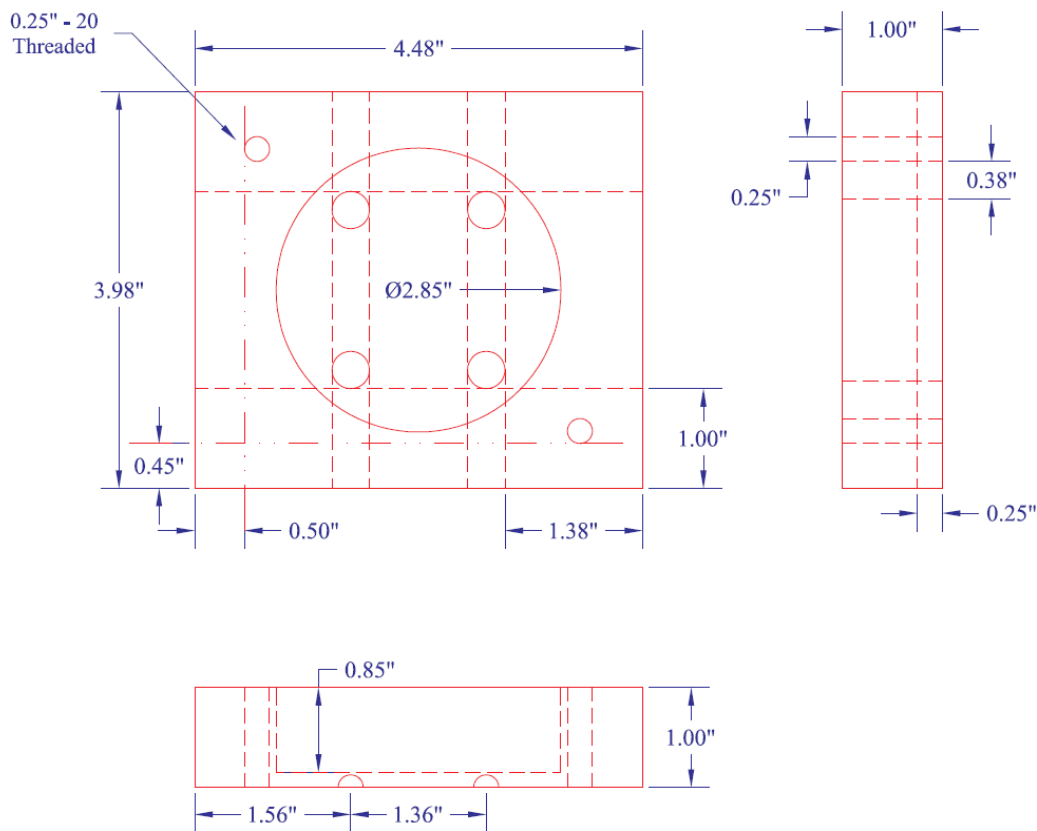


Figure G2 – Bottom half of interface shear box (Aluminum)

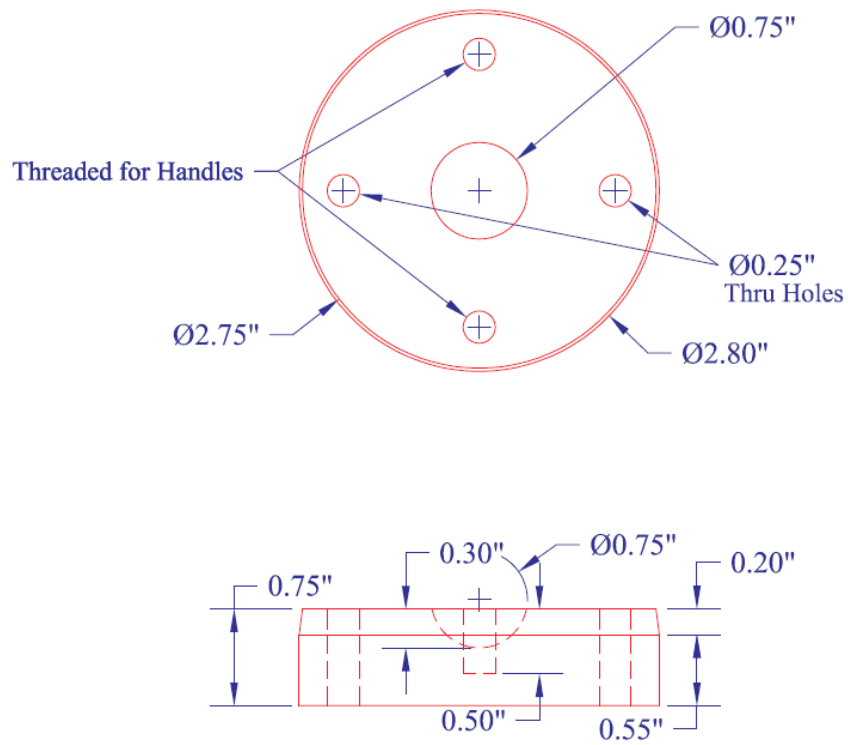


Figure G3 – Cover plate of interface shear box (Aluminum)

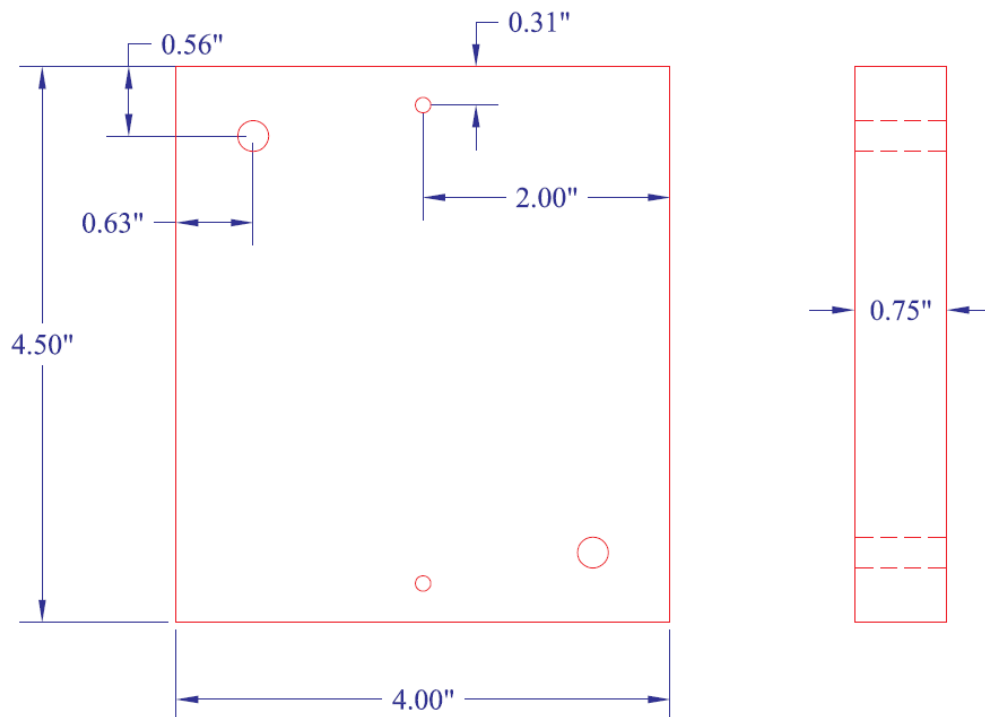


Figure G4 – Steel block to mimic split-spoon sampler

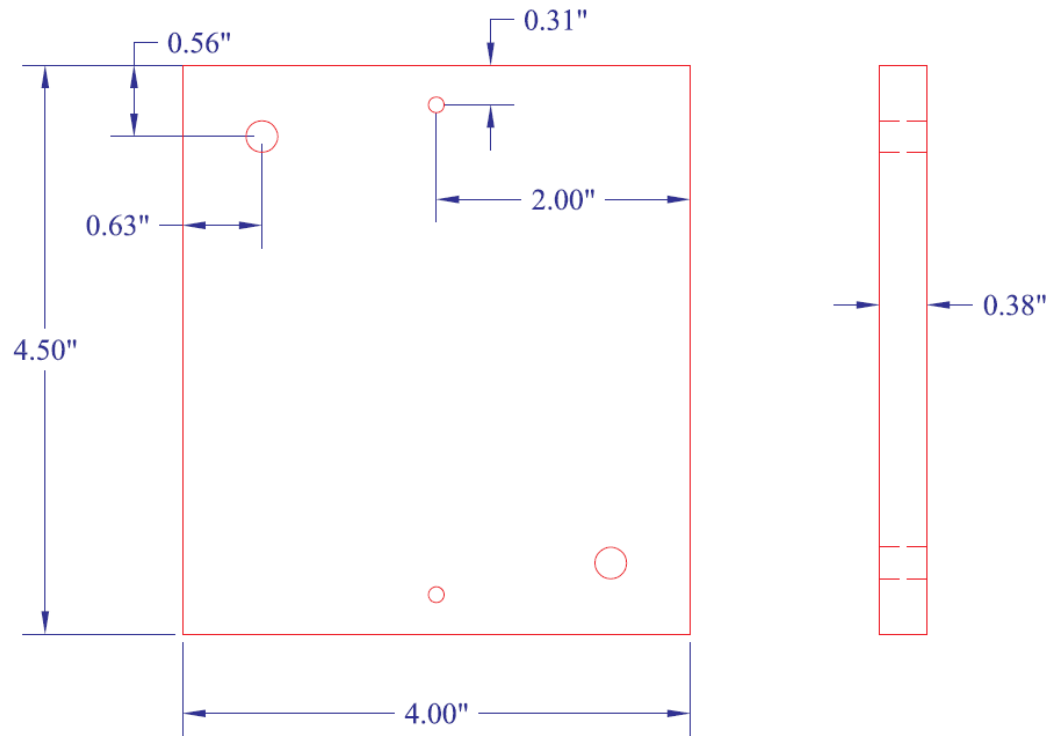


Figure G5 – Galvanized sheet metal to mimic Shelby tube sampler

APPENDIX H – Interface Shear Box Roughness Graphs

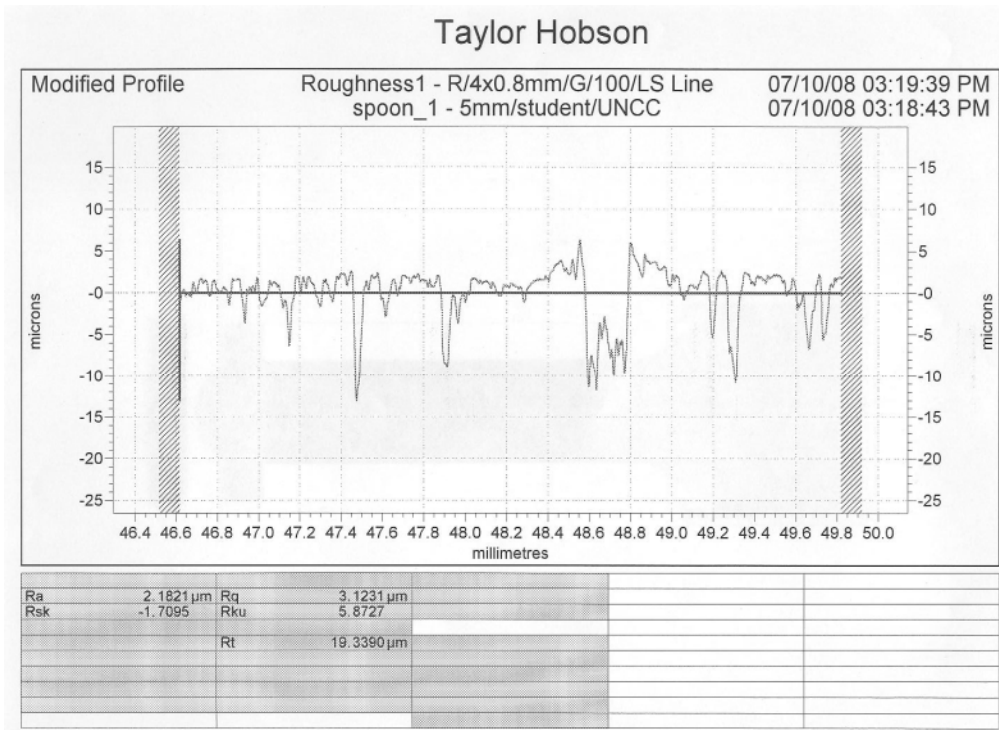


Figure H1 – New split-spoon roughness graph 1

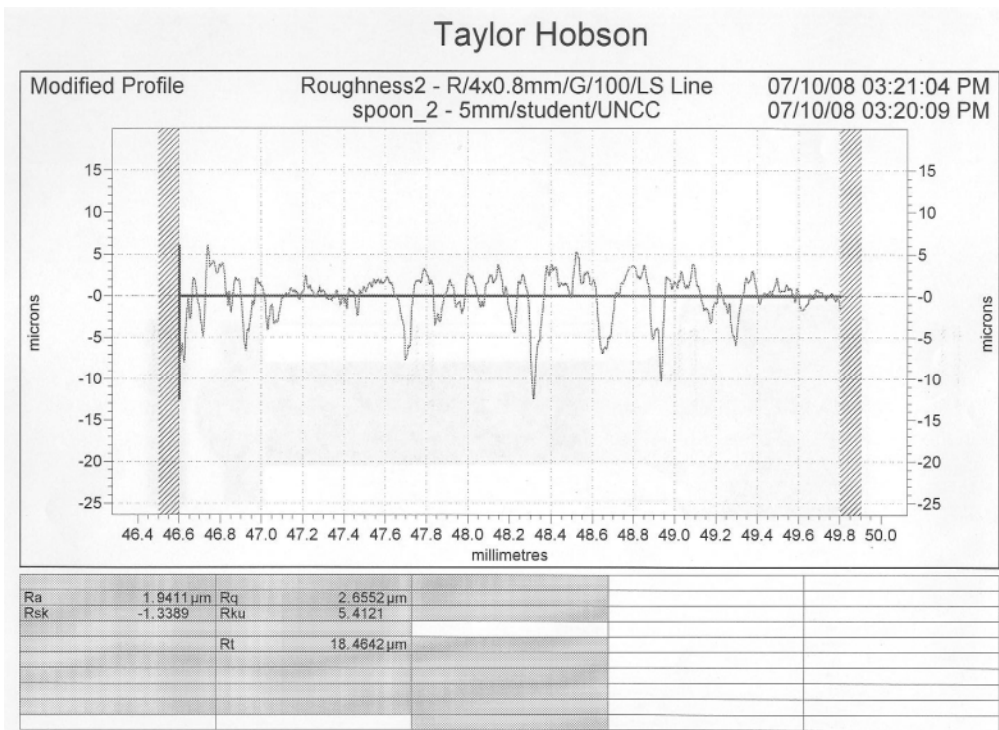


Figure H2 – New split-spoon roughness graph 2

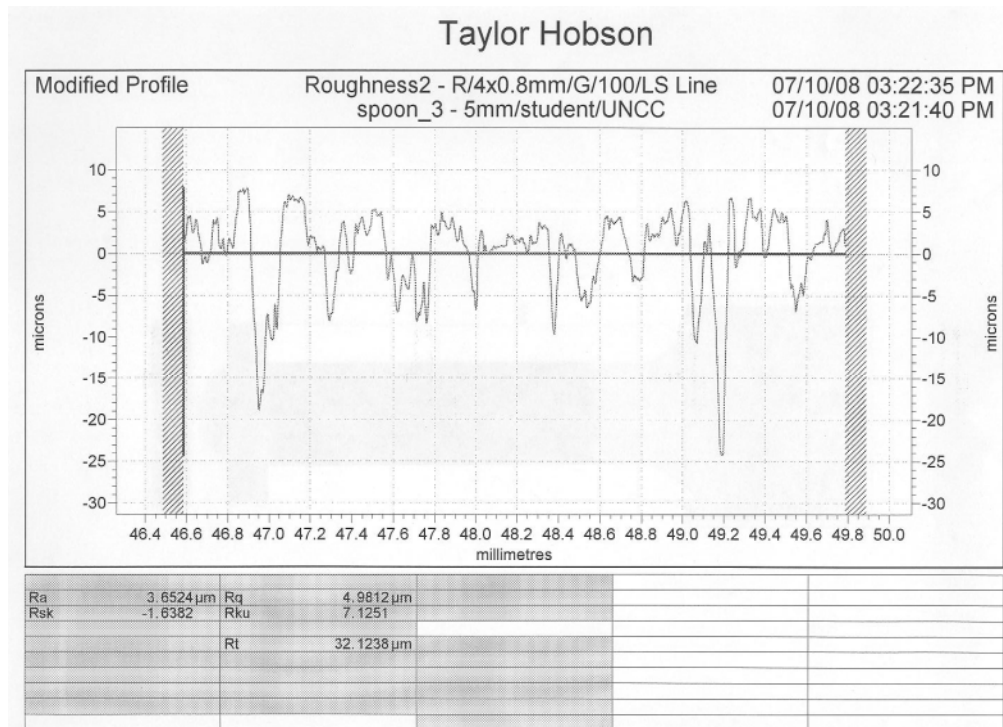


Figure H3 – New split-spoon roughness graph 3

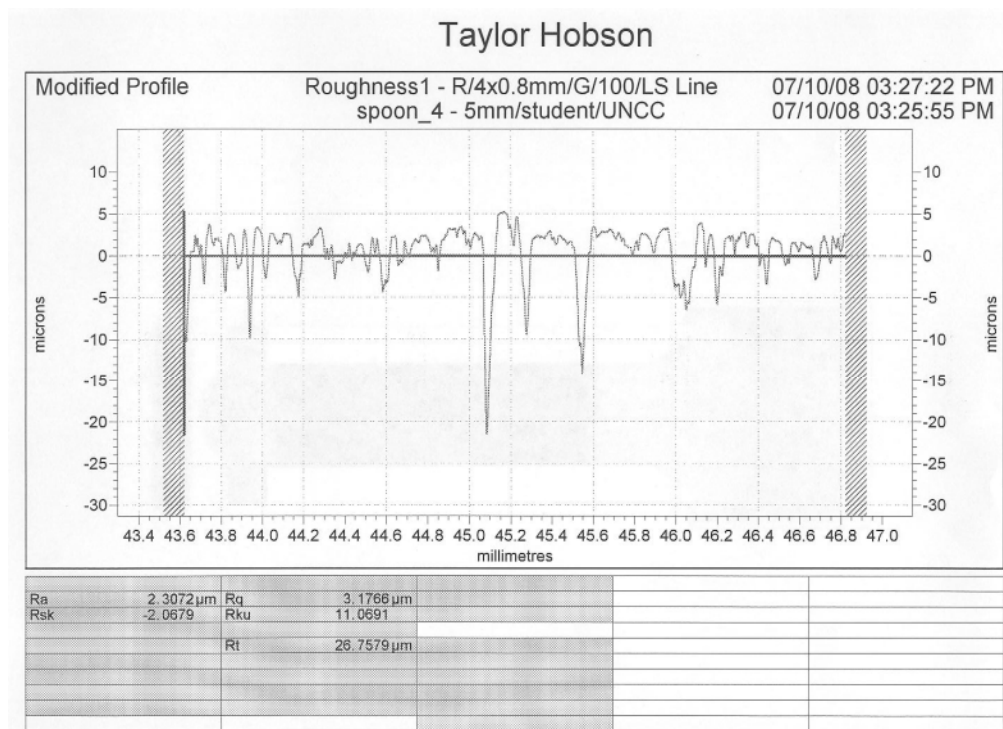


Figure H4 – New split-spoon roughness graph 4

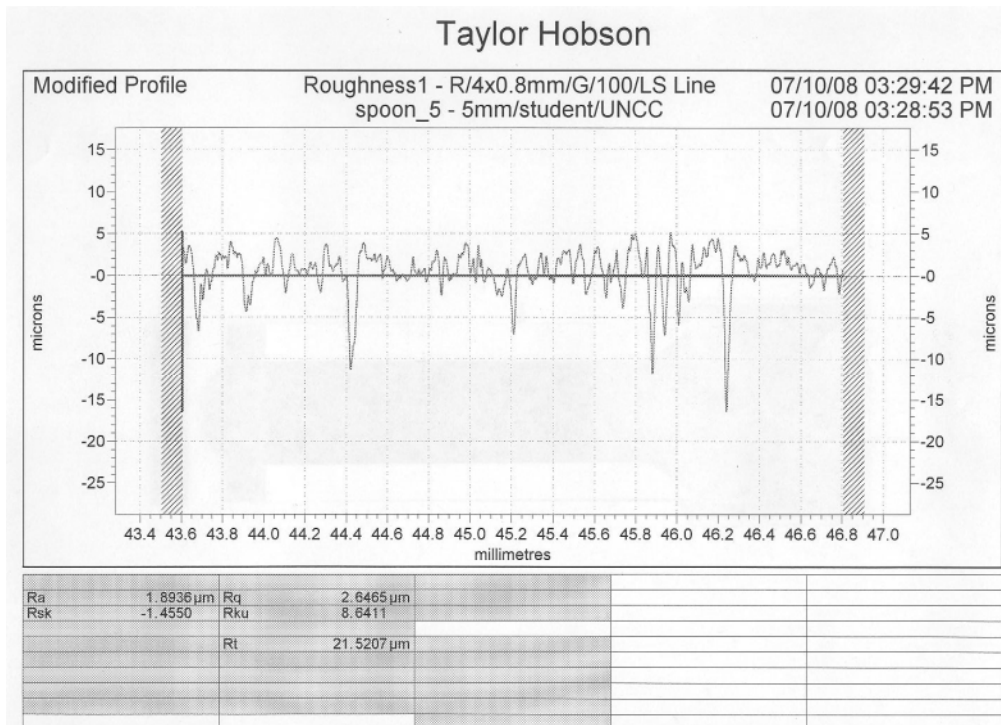


Figure H5 – New split-spoon roughness graph 5

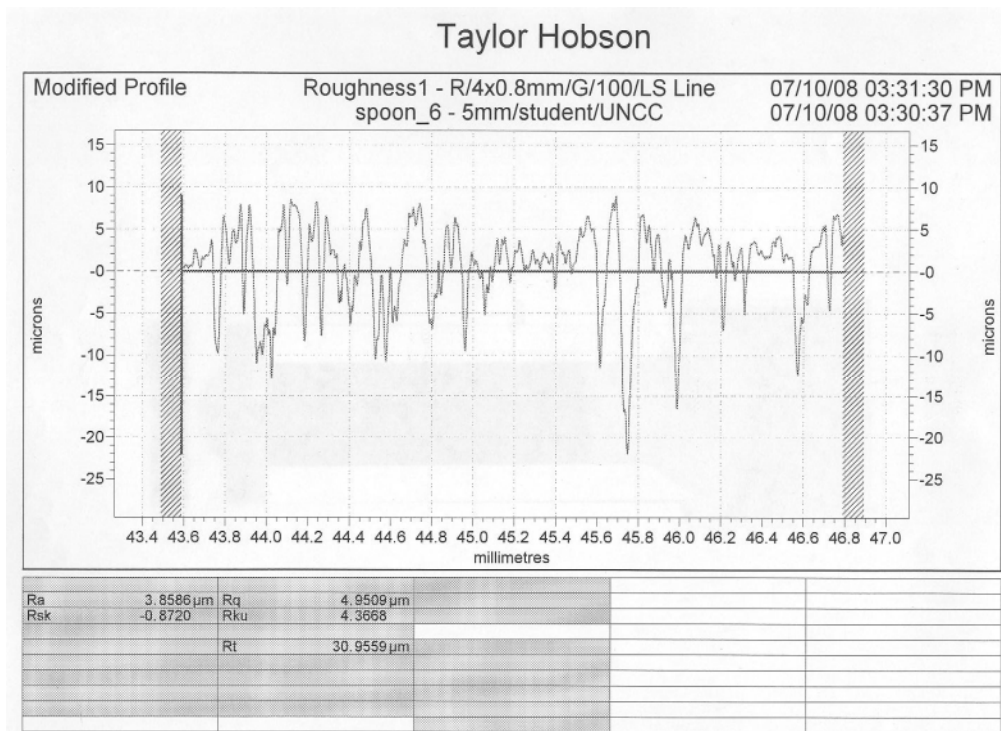


Figure H6 – New split-spoon roughness graph 6

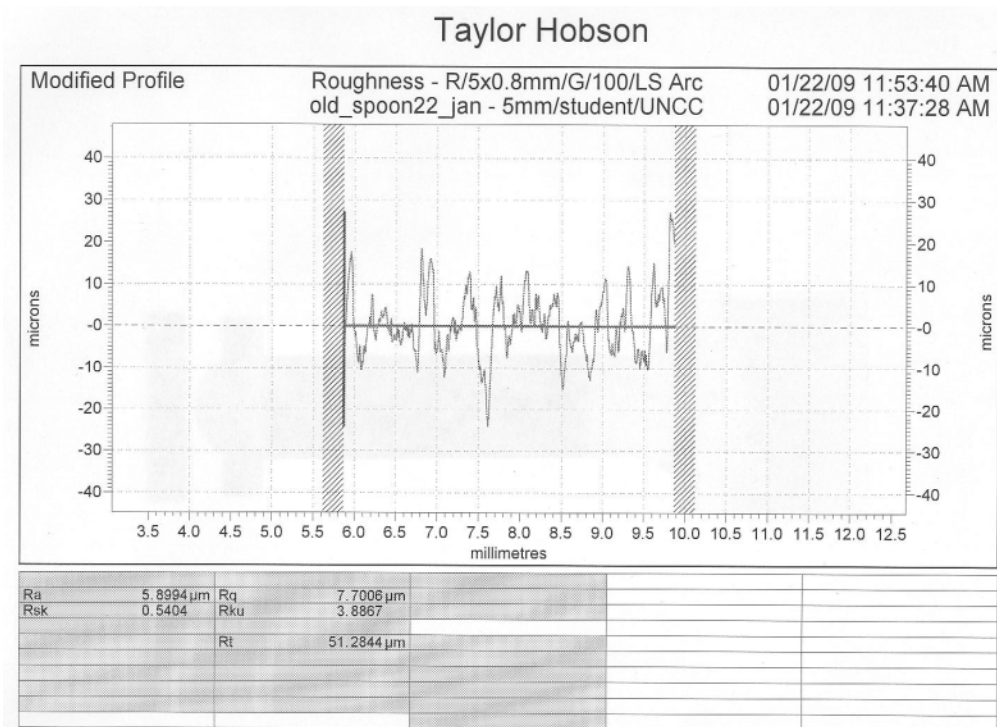


Figure H7 – Old split-spoon roughness graph 1

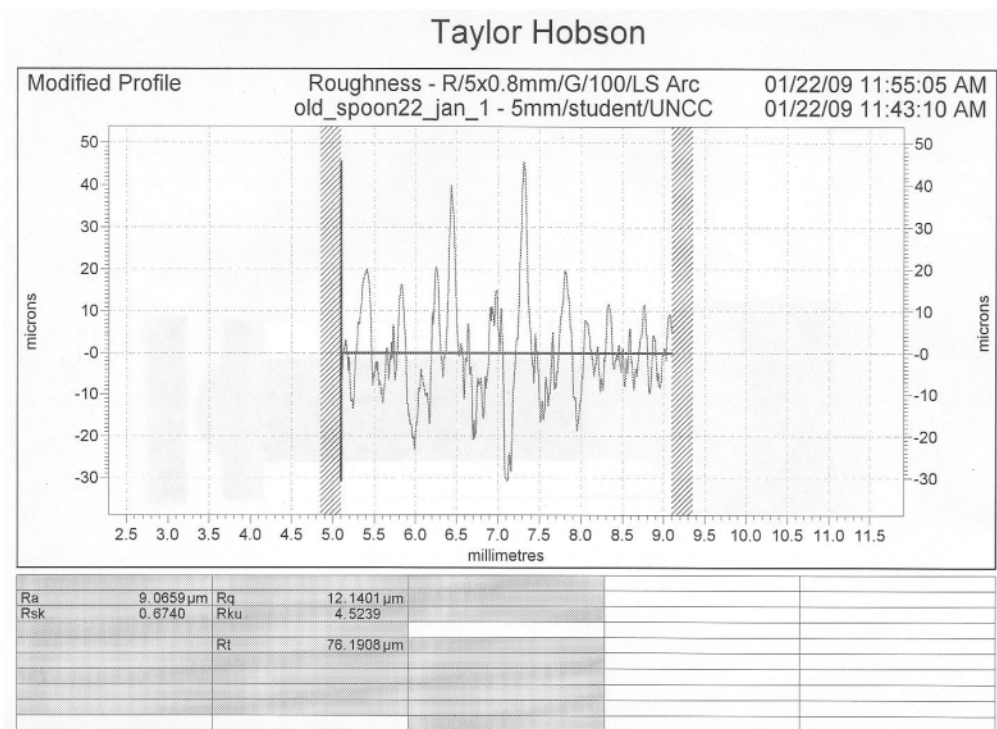


Figure H8 – Old split-spoon roughness graph 2

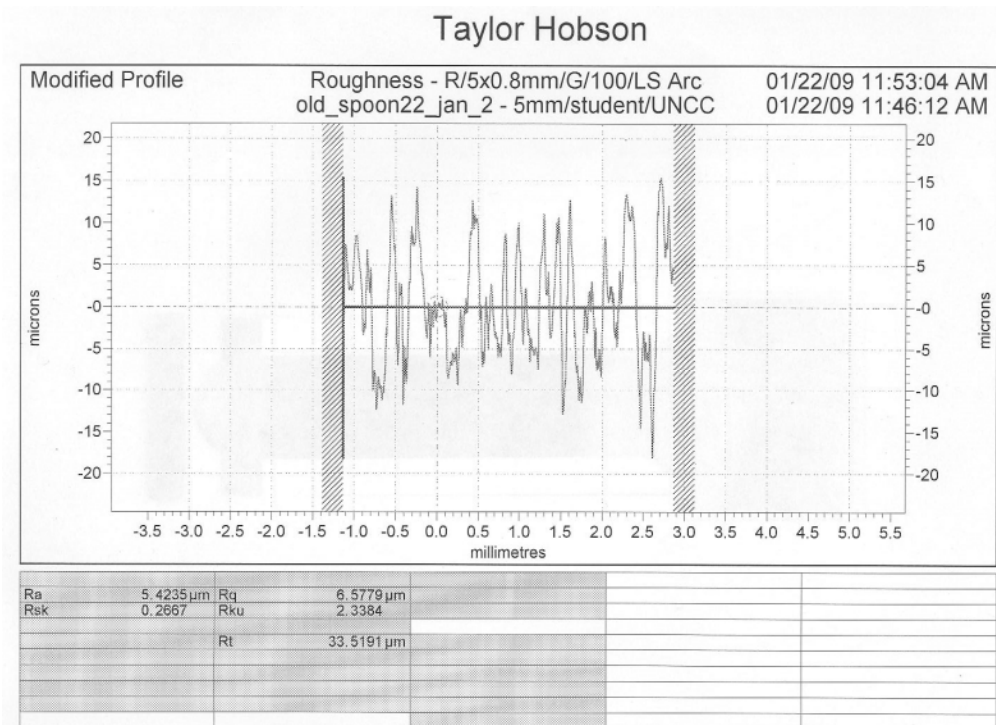


Figure H9 – Old split-spoon roughness graph 3

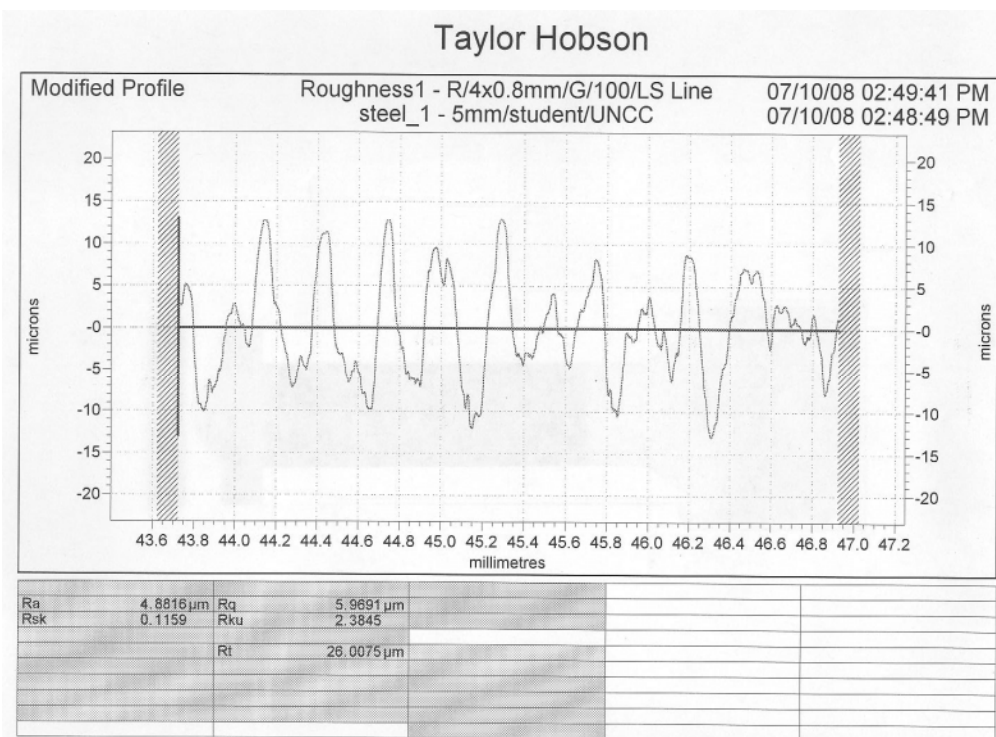


Figure H10 – Steel block roughness graph 1

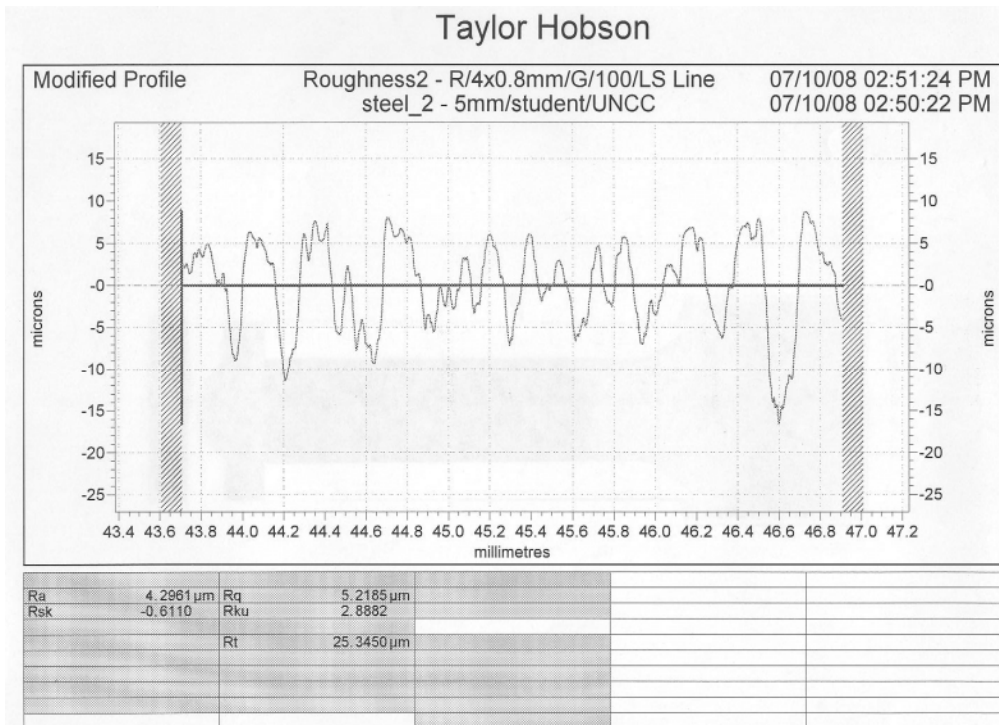


Figure H11 – Steel block roughness graph 2

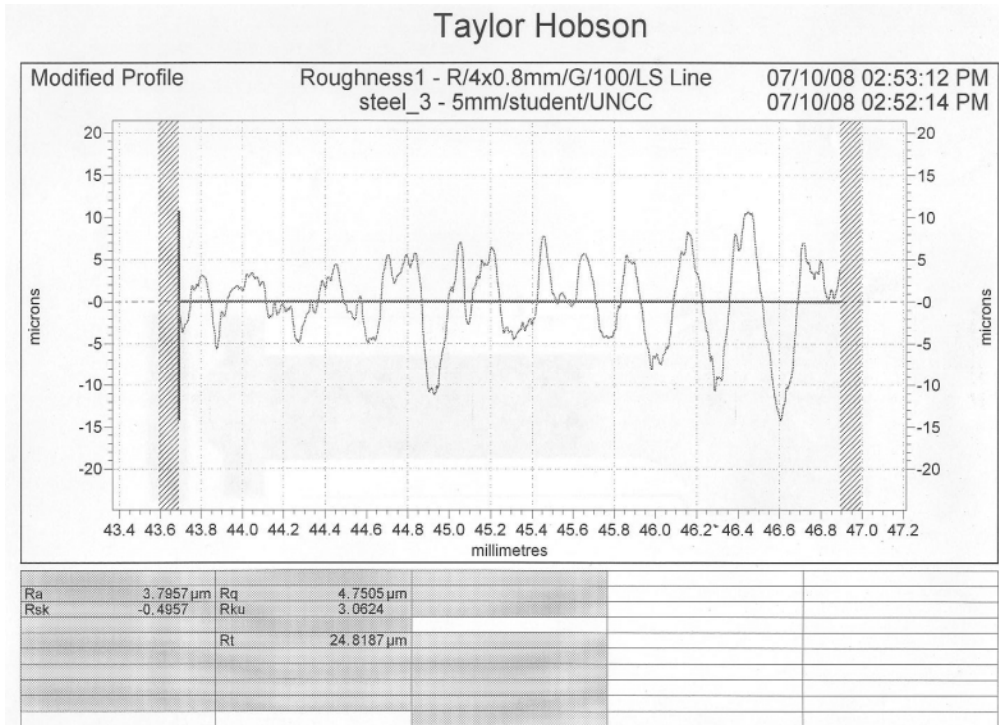


Figure H12 – Steel block roughness graph 3

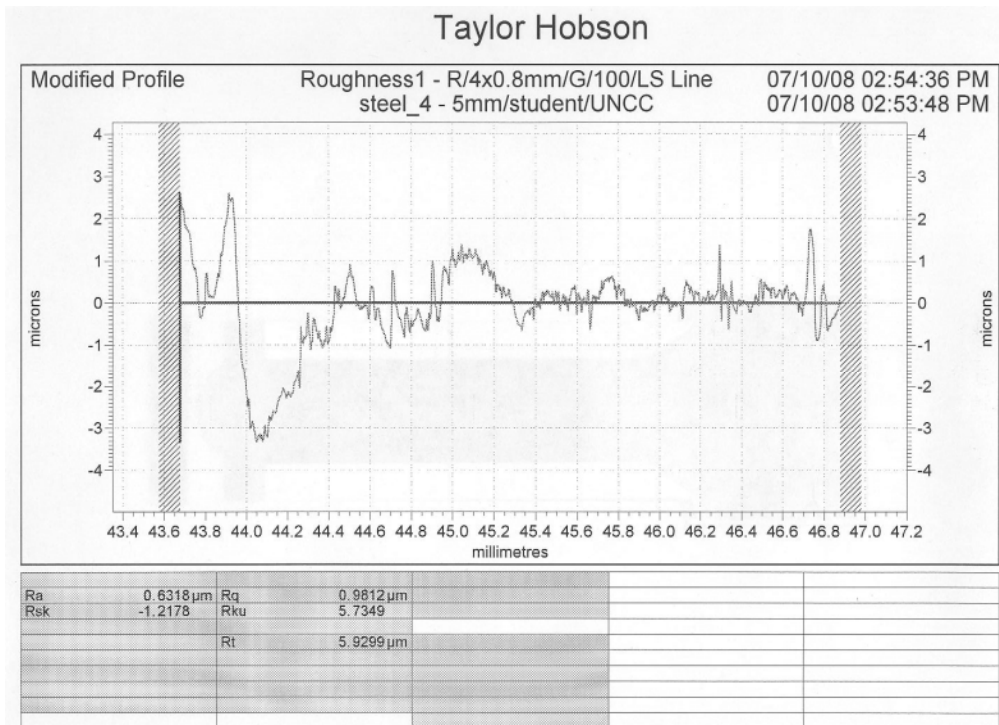


Figure H13 – Steel block roughness graph 4

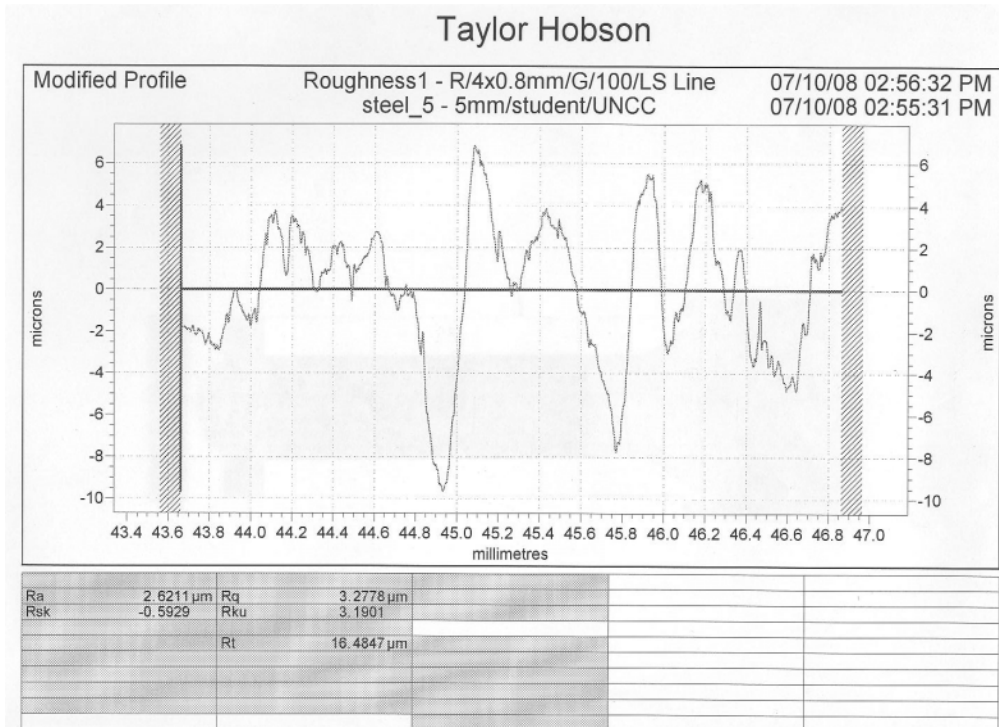


Figure H14 – Steel block roughness graph 5

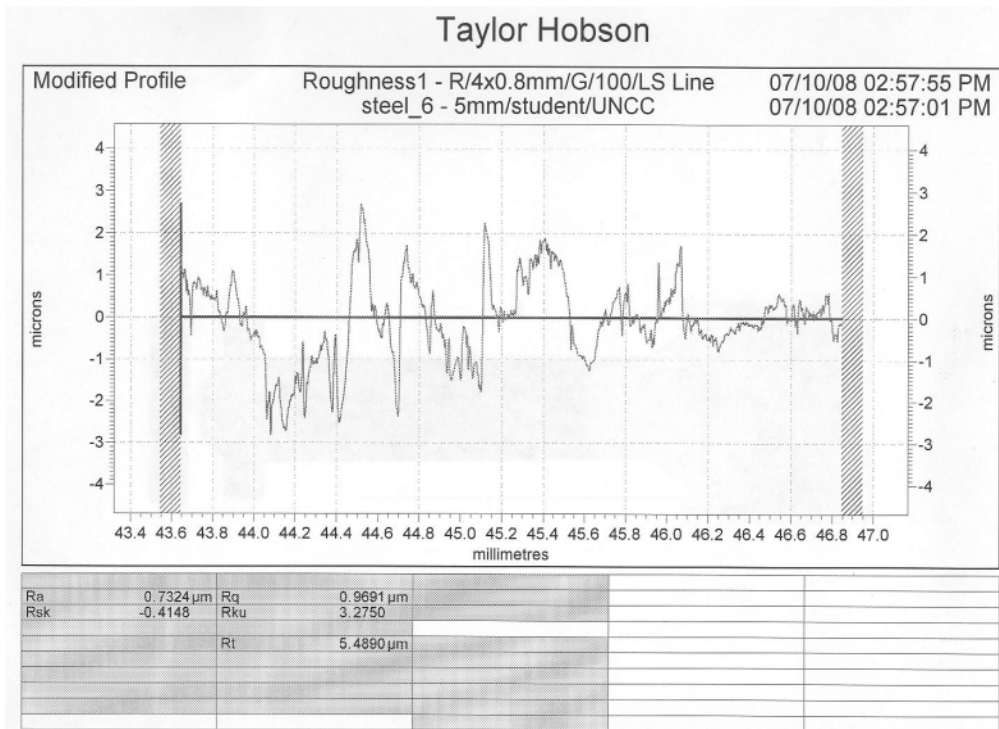


Figure H15 – Steel block roughness graph 6

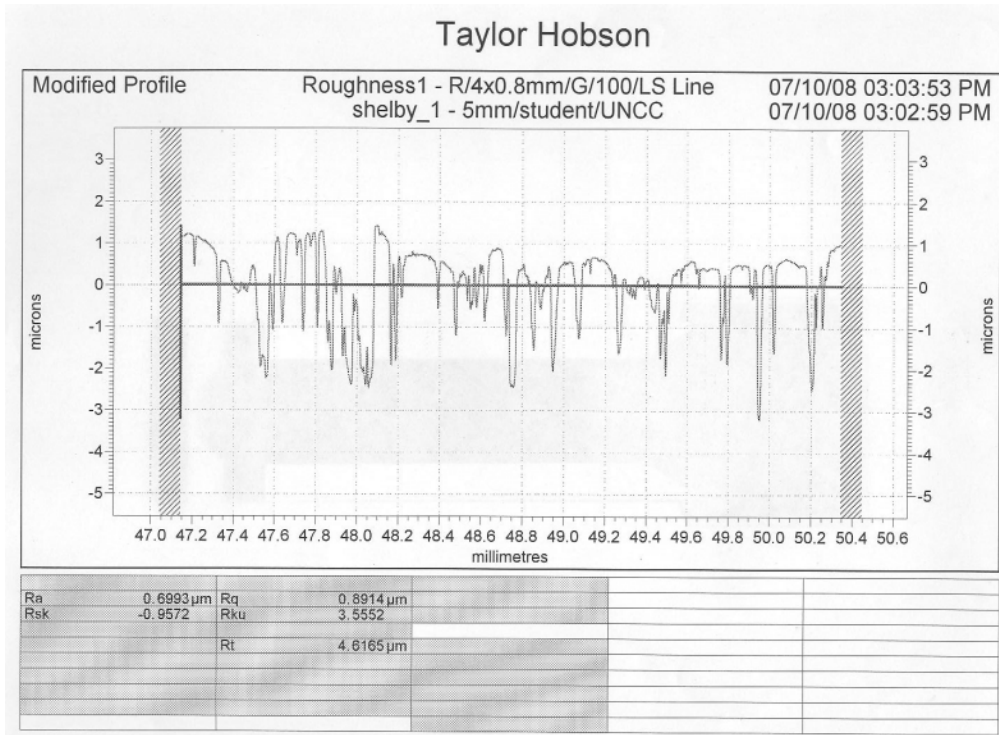


Figure H16 – Shelby tube roughness graph 1

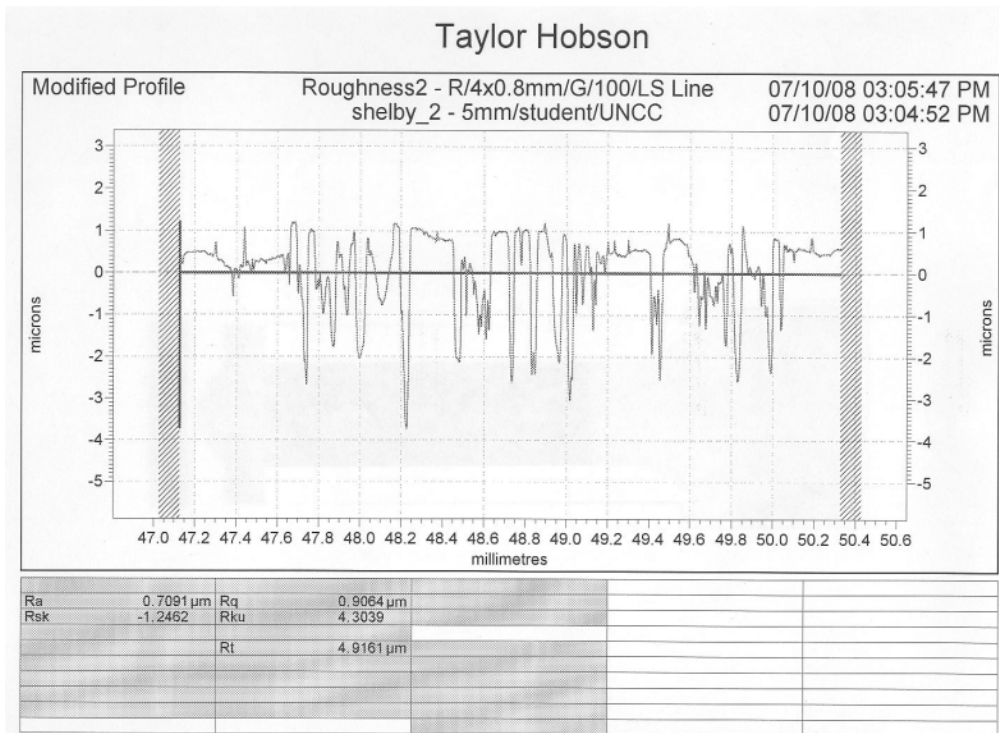


Figure H17 – Shelby tube roughness graph 2

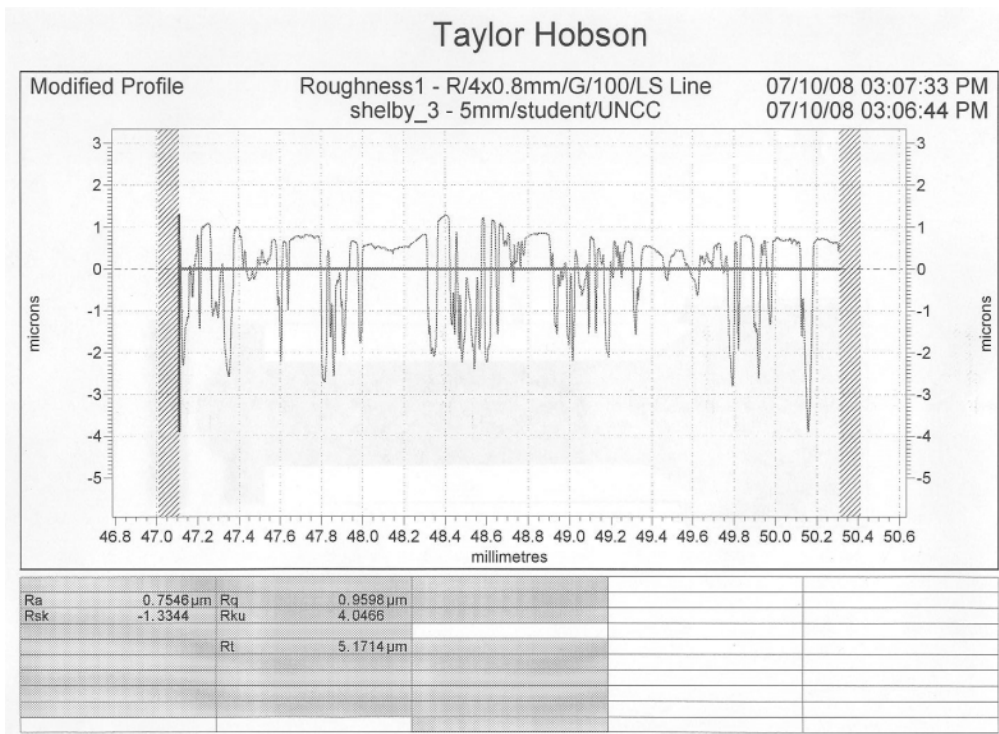


Figure H18 – Shelby tube roughness graph 3

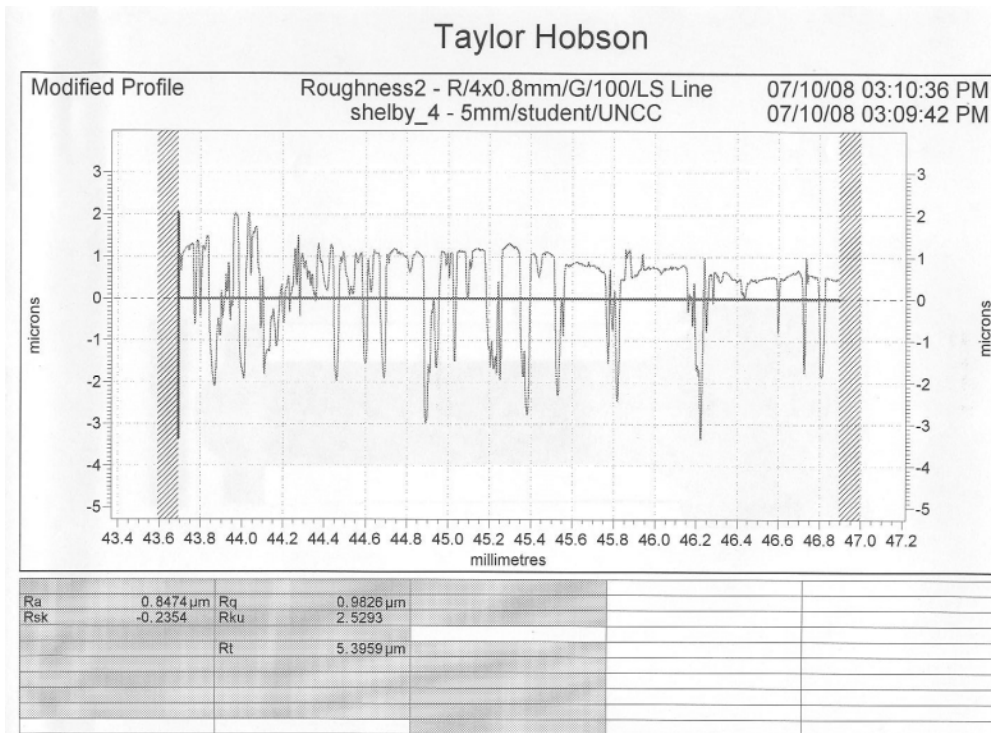


Figure H19 – Shelby tube roughness graph 4

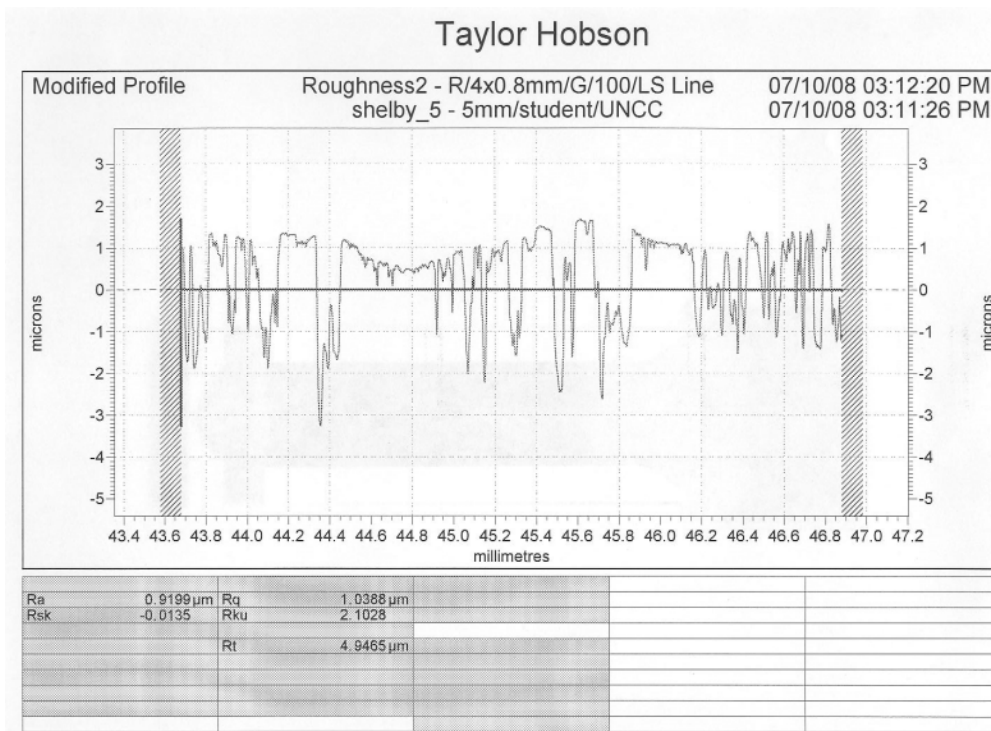


Figure H20 – Shelby tube roughness graph 5

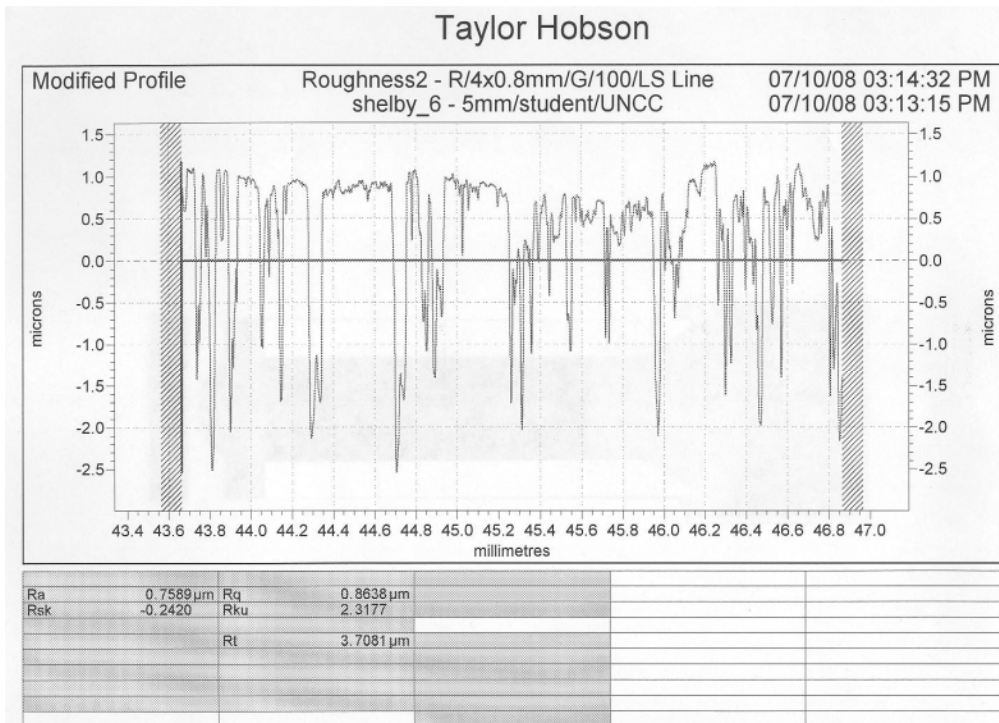


Figure H21 – Shelby tube roughness graph 6

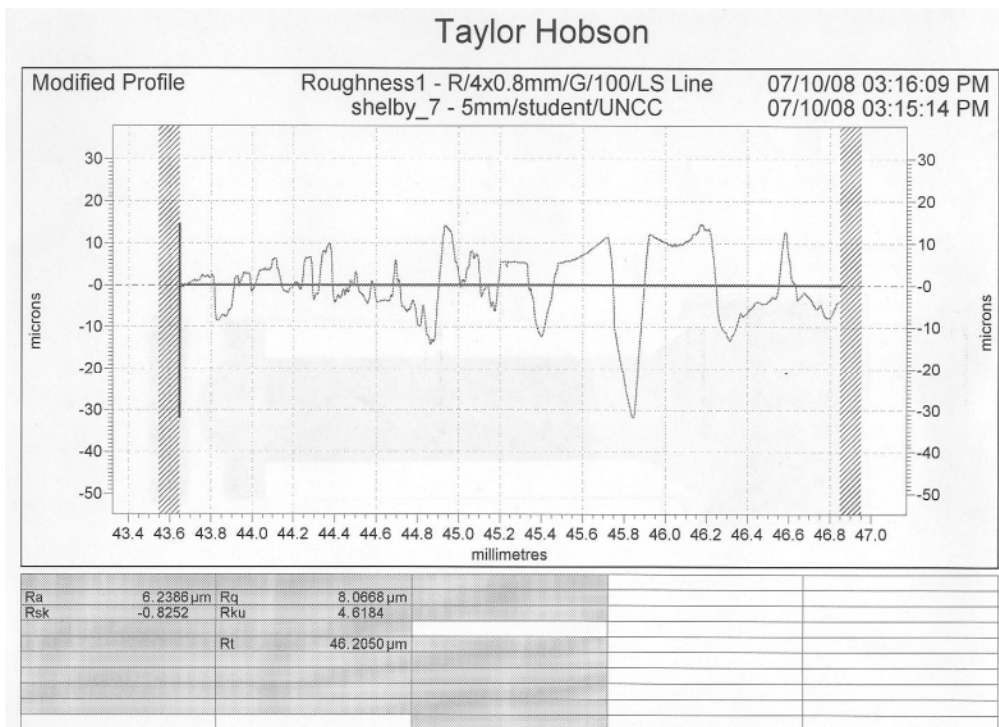
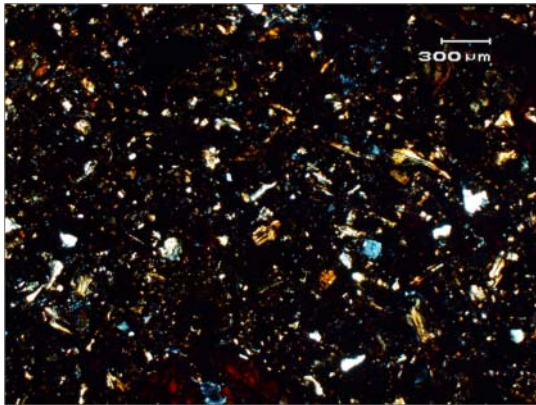
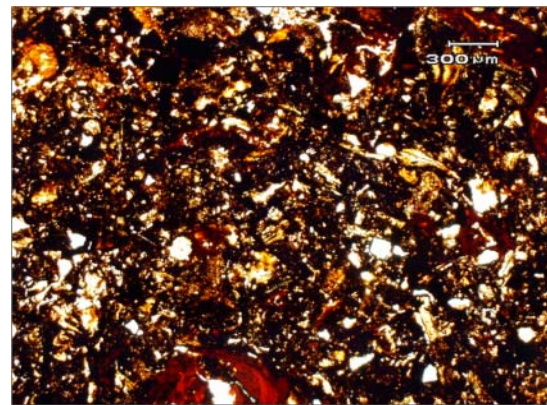


Figure H22 – Shelby tube roughness graph 7

Appendix I – Geologic Petrographic Analysis

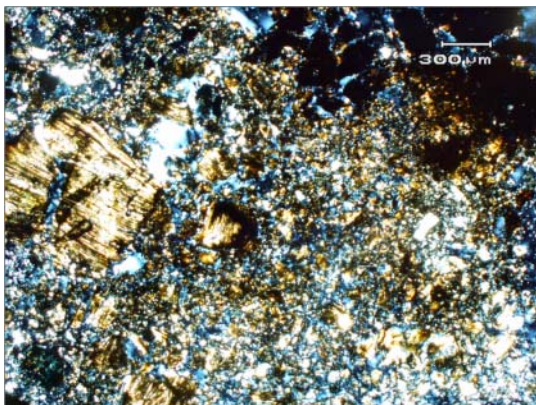


(a) Cross polarized light (CP)

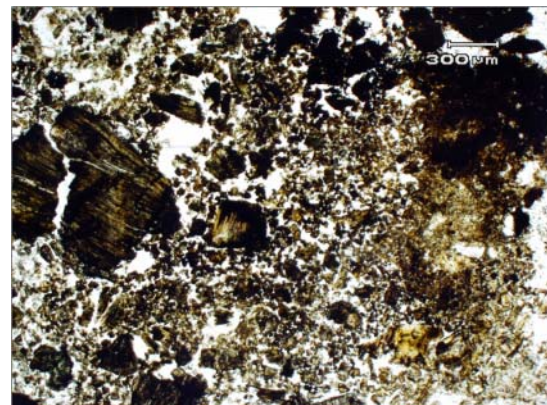


(b) Plain polarized light (PP)

Figure I1 – PC1 4.4' UND – 2 X magnification

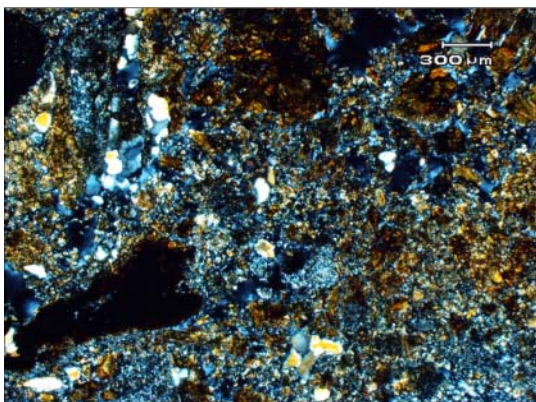


(a) Cross polarized light (CP)

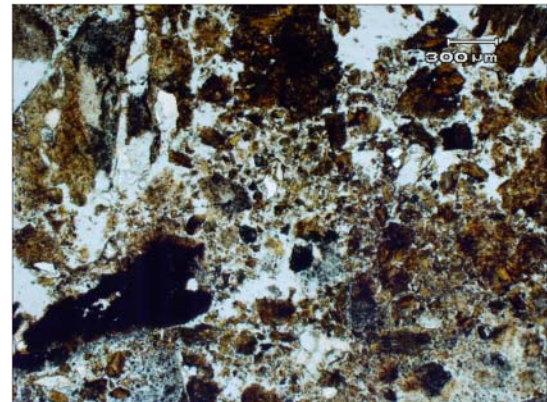


(b) Plain polarized light (PP)

Figure I2 – PC1 14.4' UND – 2 X magnification

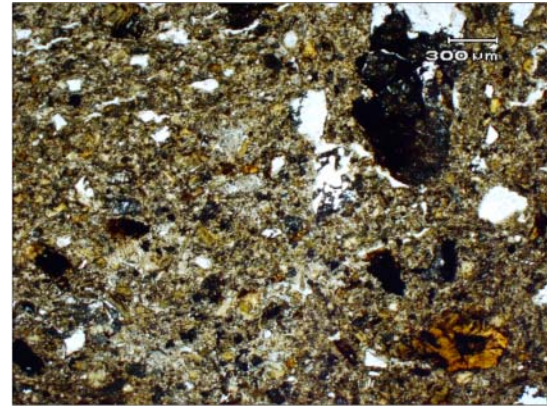
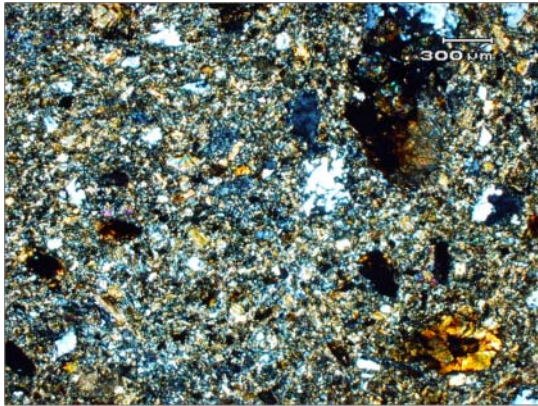


(a) Cross polarized light (CP)

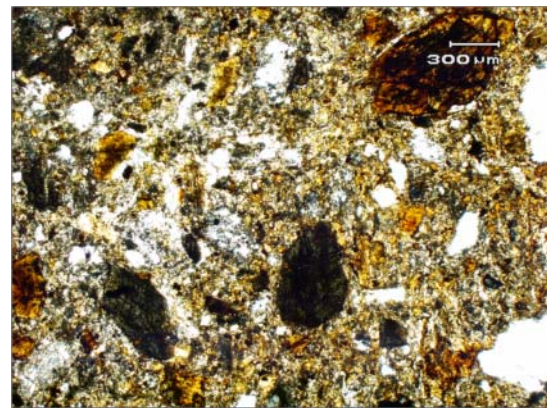
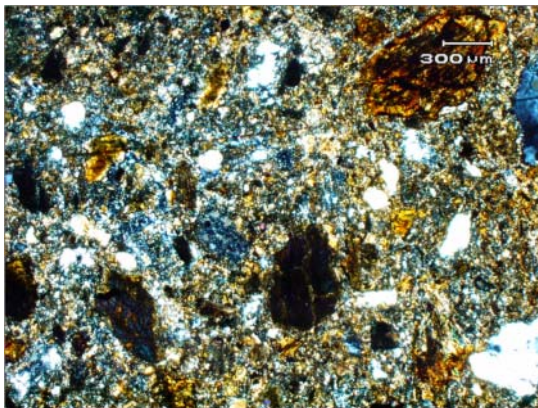


(b) Plain polarized light (PP)

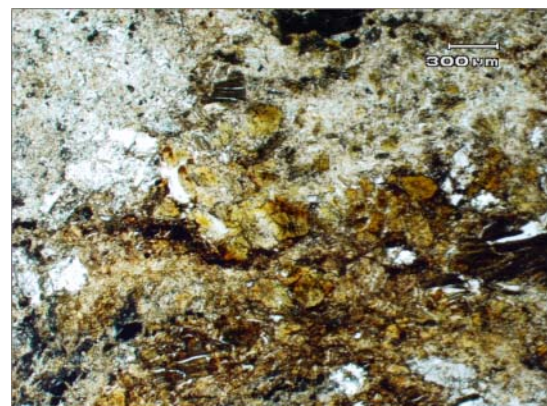
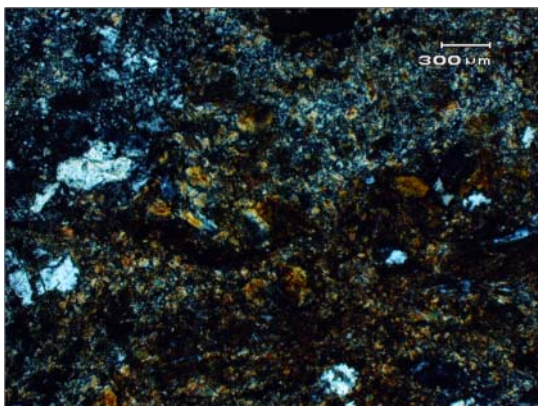
Figure I3 – PC1 24.4' UND – 2 X magnification



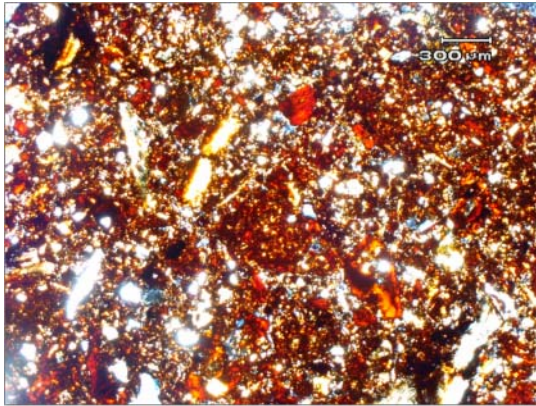
(a) Cross polarized light (CP) **(b) Plain polarized light (PP)**
Figure I4 – PC1 34.4' UND – 2 X magnification



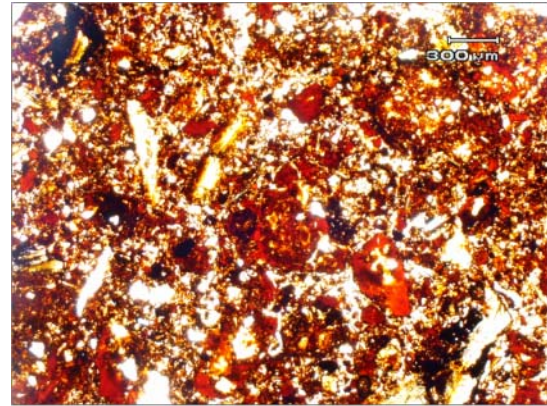
(a) Cross polarized light (CP) **(b) Plain polarized light (PP)**
Figure I5 – PC1 44.4' UND – 2 X magnification



(a) Cross polarized light (CP) **(b) Plain polarized light (PP)**
Figure I6 – PC1 54.4' UND – 2 X magnification

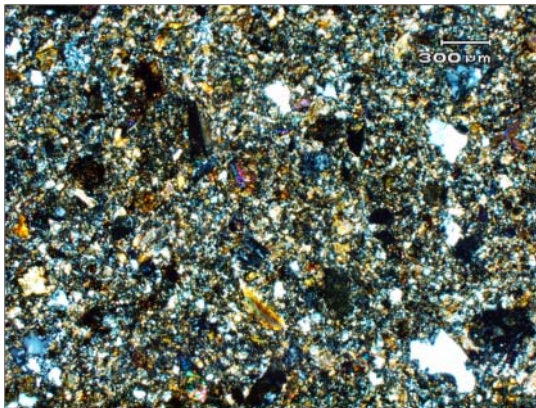


(a) Cross polarized light (CP)

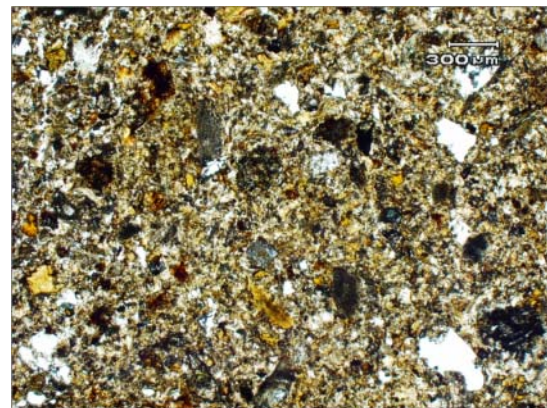


(b) Plain polarized light (PP)

Figure I7 – PC1 4.4' REM – 2 X magnification

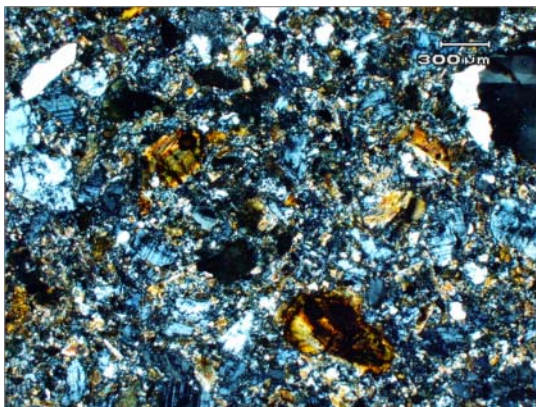


(a) Cross polarized light (CP)

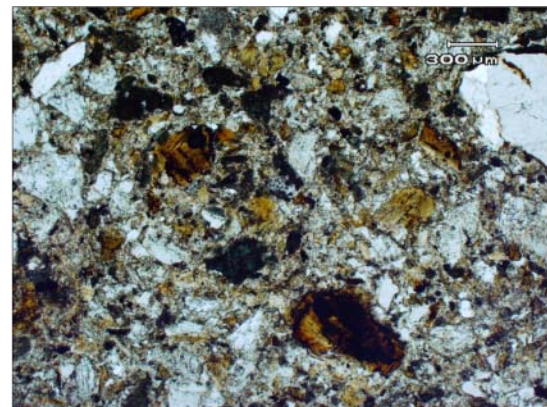


(b) Plain polarized light (PP)

Figure I8 – PC1 24.4' REM – 2 X magnifications



(a) Cross polarized light (CP)



(b) Plain polarized light (PP)

Figure I9 – PC1 54.4' REM – 2 X magnifications

APPENDIX I – Geologic petrographic analysis

Table II – PC1 Undisturbed (UND) residual soil – Petrographic analysis summary

4.4' UND	Minerals Present	Zircon
		Quartz – Unaltered anhedral to subhedral 0.2-2.0 mm
		Hemetite - Euhedral, ~0.5 mm
	Groundmass	Consists of disaggregated clay minerals and very fine grained quartz as well as what I believe to be organic material
	Clay blebs	Large, displaying preferred orientation of mineral grains and appearing to conform to original mineral grain boundaries
14.4' UND	Minerals Present	Quartz – Unaltered, anhedral to subhedral, 0.5-2.0 mm.
		Biotite – Anhedral, 1.0-1.5 mm, altering to chlorite.
		Hemetite – Euhedral, 0.5-2.0 mm
		Hornblende – Anhedral, ~1mm
	Chlorite – micro crystalline (0.01-0.1 mm)	
Groundmass	Consists of disaggregated clay minerals and very fine grained quartz, hornblende, biotite and chlorite	
Clay blebs	Large particles displaying preferred orientation of mineral grains and appearing to conform to original mineral grain boundaries	
Quartz	Grains are heavily fractured with many showing infiltration and wedging along fractures by clay minerals	
Notes	-Hornblende and Biotite grains show alteration. -Overall rock matrix appears to be much more cohesive and intact than that of PC 4.4 UND	
24.4' UND	Minerals Present	Quartz – Unaltered anhedral to subhedral 0.2-2.0 mm
		Biotite – Sub to Euhedral 0.5-1.5 mm
		Titanaugite – Fractured, anhedral, 0.1-1.0 mm
		Hemetite – Euhedral 0.5-1.0 mm
	Hornblende – Anhedral, ~1.0 mm	
Groundmass	Consists of disaggregated clay minerals and very fine grained quartz, hornblende, biotite, titanaugite and chlorite	
Clay blebs	Large, displaying preferred orientation of mineral grains and appearing to conform to original mineral grain boundaries	
Quartz	Grains are heavily fractured with many showing infiltration and wedging along fractures by clay minerals	
Notes	-Hornblende and Biotite grains show alteration -Overall rock matrix appears to be much more cohesive and intact than that of PC 4.4 UND	

Table I1 – (continued)

34.4' UND	Minerals Present	Quartz – Sub-Anhedral, 0.5-1.5 mm		
		Hemetite – sub-euhedral 0.5-2.0 mm		
		Olivine – Anhedral, heavily fractured 1.0-2.0 mm		
		Plagioclase Feldspar – Extensively altered/serisitized obliterating original grain shape		
		Hornblende – Subhedral 1.0-2.0mm		
34.4' UND	Minerals Present	Titanaugite – Subhedral ~1.0mm		
		Biotite – Euhedral 0.5-2.0mm		
		Chlorite		
		Groundmass	Consists of disaggregated clay minerals and very fine grained quartz, hornblende, biotite, titanaugite and chlorite	
		Clay blebs	Large, displaying preferred orientation of mineral grains and appearing to conform to original mineral grain boundaries	
34.4' UND	Minerals Present	Quartz	Grains in this sample show far less infiltration by clay minerals along fractures than samples from higher strata	
		Notes	-Hornblende, Biotite and Chlorite grains show alteration -Voids and cavities in plagioclase often filled with fine grained clays -Overall rock matrix appears to be much more cohesive and intact than that of PC 4.4 UND	
		44.4' UND	Minerals Present	Quartz – Unaltered sub-anhedral, 0.5-2.0 mm
				Hornblende – subhedral 1.0-2.0 mm
				Biotite – Sub-euhedral, 0.25-1.5 mm
Titanaugite – anhedral, fractured, 0.1 – 2.0 mm				
Plagioclase Feldspar - heavily altered 0.01-0.5 mm				
44.4' UND	Minerals Present	Olivine - anhedral		
		Chlorite – anhedral, fractured		
		Hemetite – euhedral 0.5-2.0 mm		
		Garnet – euhedral, 1.0 mm		
		Groundmass	Consists of disaggregated clay minerals and very fine grained quartz, hornblende, biotite, titanaugite ,chlorite and incompletely serisitized plagioclase	
44.4' UND	Minerals Present	Clay blebs	Large, displaying preferred orientation of mineral grains and appearing to conform to original mineral grain boundaries	
		Quartz	Grains in this sample show far less infiltration by clay minerals along fractures than samples from higher strata	
		Notes	-Hornblende, Biotite and Chlorite grains show alteration -Voids and cavities in plagioclase often filled with fine grained clays -Overall rock matrix appears to be much more cohesive and intact than that of PC 4.4 UND -Despite identical point count results, more plagioclase appears to be present in this sample than in PC 34.4 UND	

Table I1 – (continued)

54.4' UND	Minerals Present	Quartz – Unaltered sub-anhedral, 0.5-2.0 mm
		Plagioclase Feldspar - heavily altered 0.01-1.0 mm
		Titanaugite – anhedral, fractured, 0.1 – 2.0 mm
		Hornblende – subhedral 1.0-2.0 mm
		Hemetite – euhedral 0.5-2.0 mm
		Olivine - anhedral
		Garnet – euhedral, 1.0 mm
		Biotite – Sub-euhedral, 0.25-1.5 mm
		Chlorite – anhedral, fractured
	Groundmass	Consists of disaggregated clay minerals and very fine grained quartz, hornblende, biotite, titanaugite ,chlorite and incompletely serisitized plagioclase
Clay blebs	Large, displaying preferred orientation of mineral grains and appearing to conform to original mineral grain boundaries	
Quartz	Grains in this sample show far less infiltration by clay minerals along fractures than samples from higher strata	
Notes	<ul style="list-style-type: none"> -Hornblende, Biotite and Chlorite grains show alteration -Voids and cavities in Plagioclase often filled by fine grained clays -Plagioclase noticeably more abundant than in PC 34.4 UND or PC 44.4 UND -Overall rock matrix appears to be much more cohesive and intact than that of PC 4.4 UND 	

Table I2 – PC1 Remolded (REM) residual soil – Petrographic analysis summary

4.4' REM	Minerals Present	Quartz – Anhedral 0.1 – 0.5 mm
		Hemetite – Euhedral 0.5 – 1.0 mm
		Biotite – Subhedral 0.25-0.5 mm
	Groundmass	Consists of disaggregated clay minerals and very fine grained quartz as well as what I believe to be organic material
	Clay blebs	Display preferred orientation of mineral grains and appearing to conform to original mineral grain boundaries.
	Quartz	Grains in particular seem to have been broken into smaller pieces.
Notes	<p>-Clay blebs are smaller and less plentiful than those in UND samples.</p> <p>-Overall matrix is less compact and cohesive than PC 4.4 UND despite similar mineralogy.</p> <p>-Grain to grain relations are looser than those of PC 4.4 UN with more interstitial pore space.</p> <p>-Generally more fine grained than PC 4.4 UND.</p>	
24.4' REM	Minerals Present	Quartz – Anhedral 0.1-0.5 mm
		Hornblende – Sub-Euhedral 0.25–2.0 mm
		Titanaugite – subhedral 0.1-0.2 mm
		Olivine – Sub-Euhedral 0.5-2.0 mm
		Chlorite – Sub-Anhedral 0.2-1.0 mm
	Groundmass	consisting of disaggregated clay minerals and very fine grained quartz, hornblende, biotite, titanaugite and chlorite.
Clay blebs	Large particles displaying preferred orientation of mineral grains and appearing to conform to original mineral grain boundaries.	
Quartz	Grains in particular seem to have been broken into smaller pieces.	
Notes	<p>-Matrix is tightly packed with very little interstitial pore space.</p> <p>-Clay blebs are smaller and less plentiful than those in UND samples.</p> <p>-Generally more fine grained than PC 24.4 UND.</p>	
54.4' REM	Minerals Present	Quartz – Anhedral 0.1-0.5 mm
		Hornblende – Sub-Euhedral 0.25–2.0 mm
		Hemetite – Euhedral 0.25-1.5 mm
		Chlorite – Sub-Anhedral 0.2-1.0 mm
		Biotite – Heavily altered
		Titanaugite – Sub-Anhedral 0.1-0.2 mm many smaller fragments
		Plagioclase Feldspar – Heavily sericitized with fine grained clays filling voids
	Groundmass	Consistsof disaggregated clay minerals and very fine grained quartz, hornblende, biotite, titanaugite, chlorite and plagioclase feldspar.
	Clay blebs	Large, displaying preferred orientation of mineral grains and appearing to conform to original mineral grain boundaries.
	Quartz	Grains in particular seem to have been broken into smaller pieces.
Notes	<p>-Clay blebs are smaller and less plentiful than those in un-remixed samples (few larger than 0.3 mm).</p> <p>-Matrix is tightly packed with very little interstitial pore space.</p> <p>-Generally more fine grained than PC 24.4 UND.</p>	

APPENDIX J – PC1 Remolded Triaxial Shear Test Data

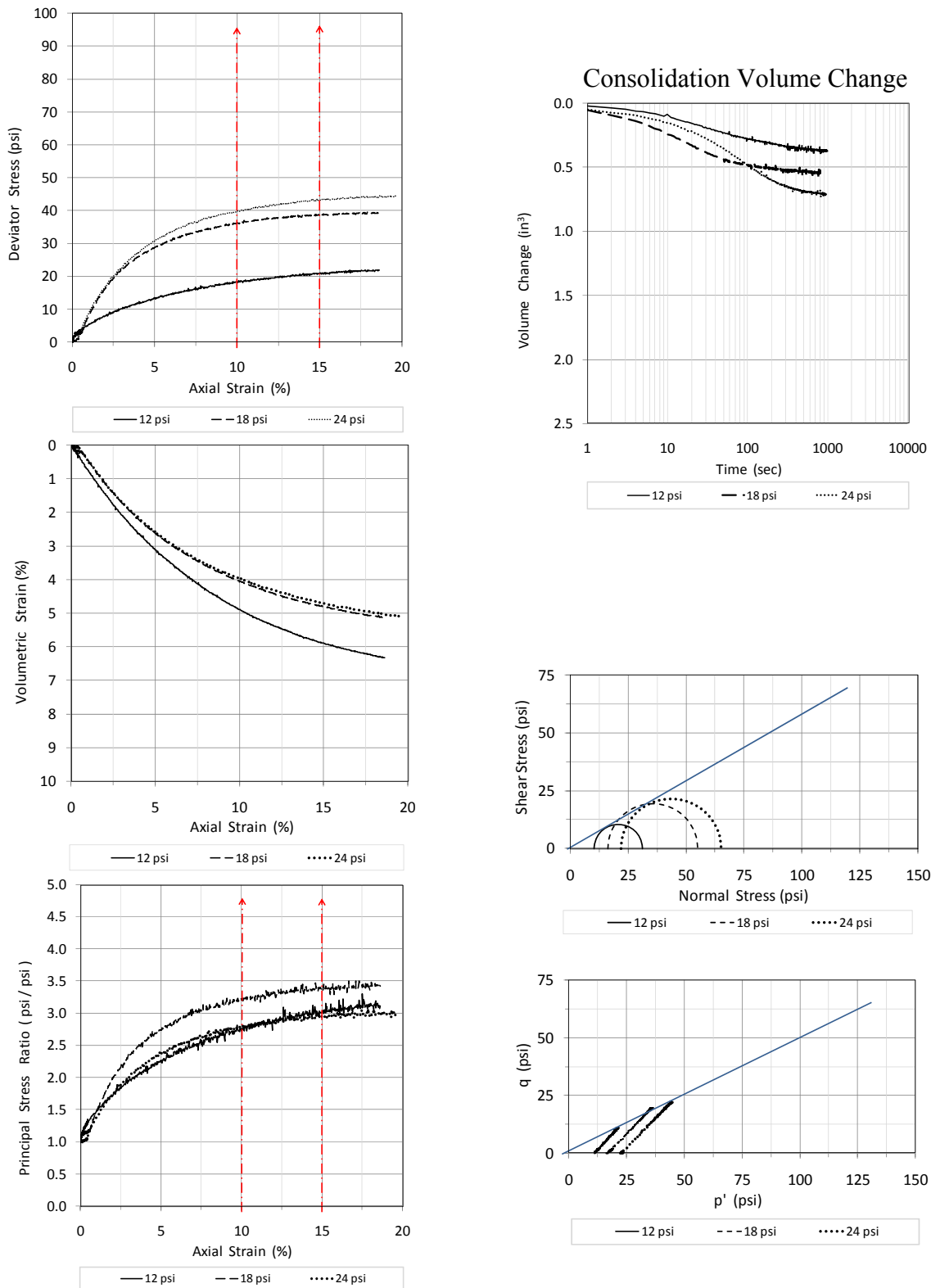


Figure J1 – PC1 4.4' REM – Remolded triaxial data

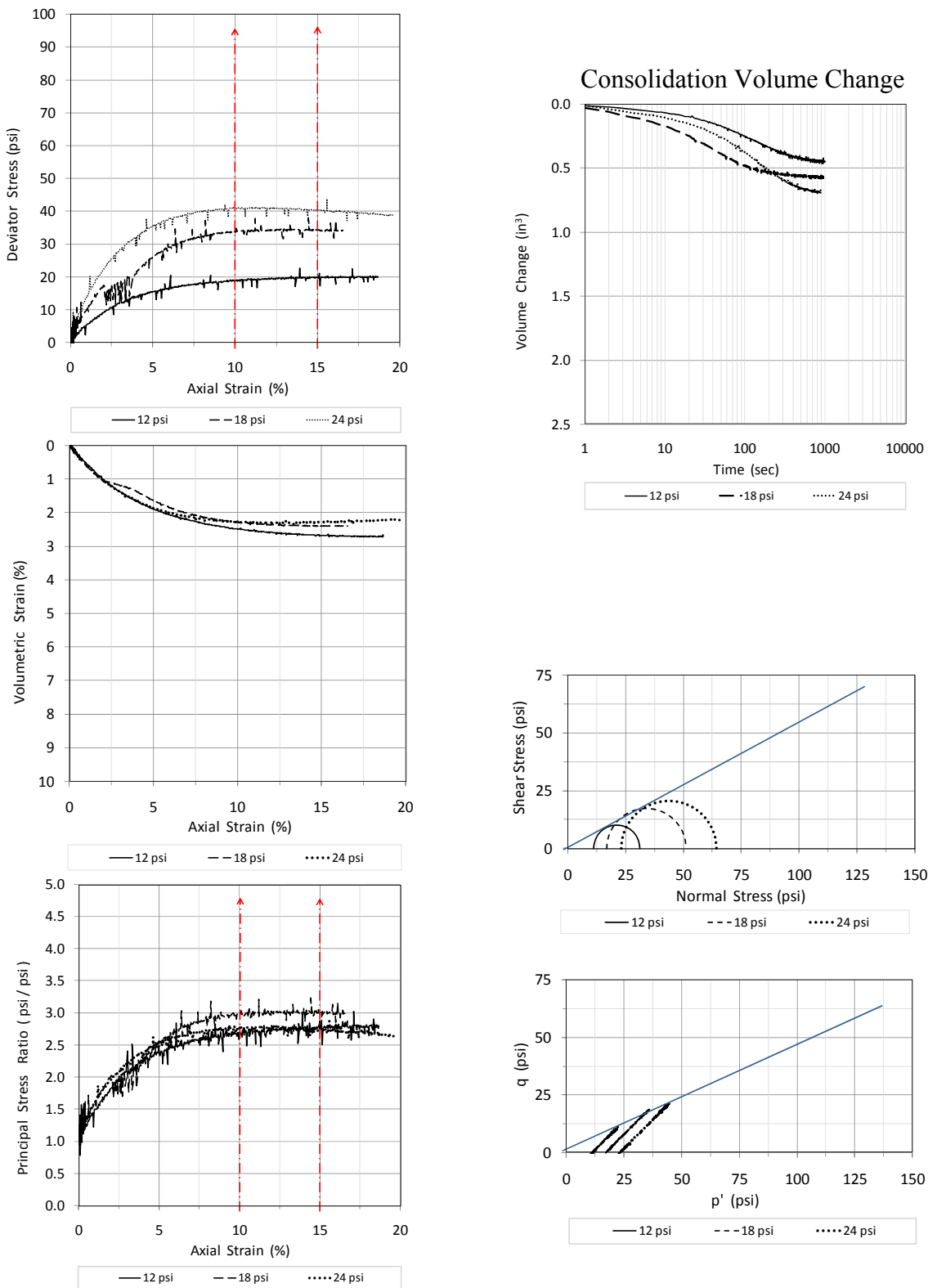
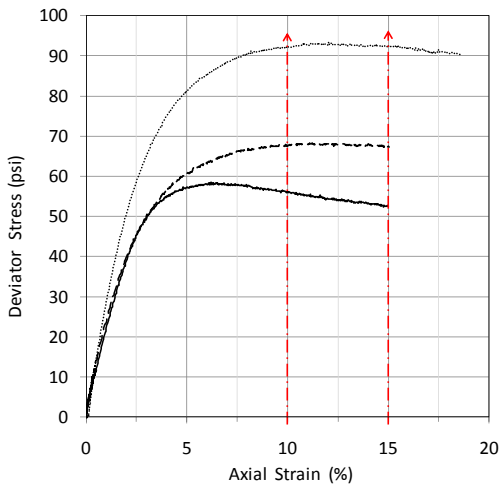
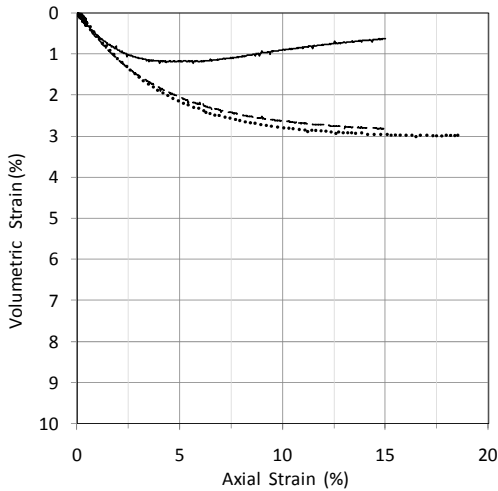


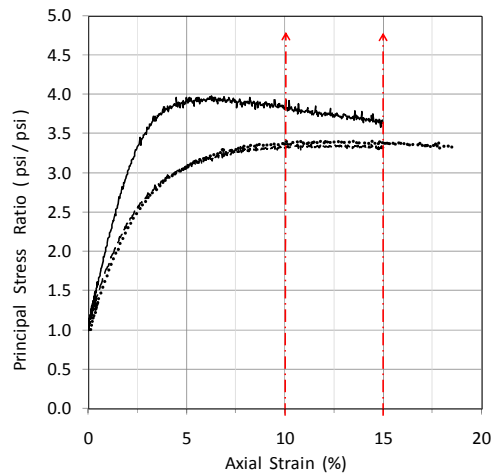
Figure J2 – PC1 24.4' REM – Remolded triaxial data



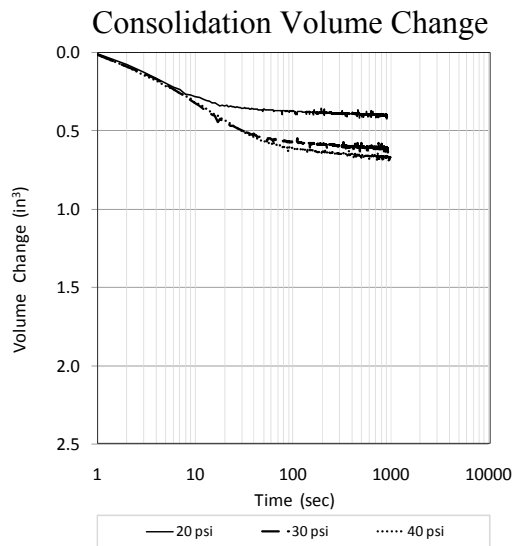
— 20 psi - - 30 psi 40 psi



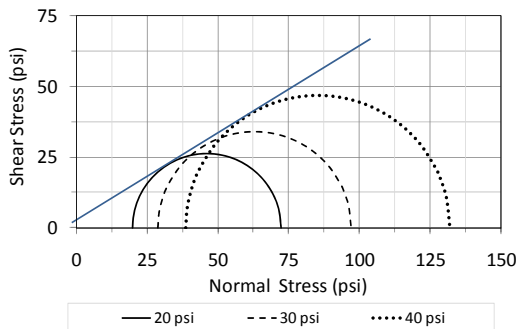
— 20 psi - - 30 psi 40 psi



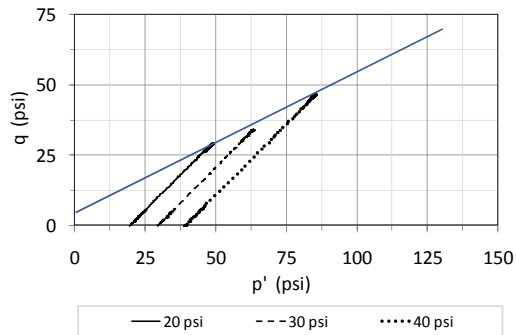
— 20 psi - - 30 psi 40 psi



— 20 psi - - 30 psi 40 psi



— 20 psi - - 30 psi 40 psi



— 20 psi - - 30 psi 40 psi

Figure J3 – PC1 54.4' REM – Remolded triaxial data